Lecture Notes in Civil Engineering

Sanjay Kumar Shukla
Sudhirkumar V. Barai
Ankur Mehta *Editors*

Advances in Sustainable Construction Materials and Geotechnical Engineering

Select Proceedings of TRACE 2018

Springer

Lecture Notes in Civil Engineering

Volume 35

Lecture Notes in Civil Engineering (LNCE) publishes the latest developments in Civil Engineering - quickly, informally and in top quality. Though original research reported in proceedings and post-proceedings represents the core of LNCE, edited volumes of exceptionally high quality and interest may also be considered for publication. Volumes published in LNCE embrace all aspects and subfields of, as well as new challenges in, Civil Engineering. Topics in the series include:

- Construction and Structural Mechanics
- Building Materials
- Concrete, Steel and Timber Structures
- Geotechnical Engineering
- Earthquake Engineering
- Coastal Engineering
- Hydraulics, Hydrology and Water Resources Engineering
- Environmental Engineering and Sustainability
- Structural Health and Monitoring
- Surveying and Geographical Information Systems
- Heating, Ventilation and Air Conditioning (HVAC)
- Transportation and Traffic
- Risk Analysis
- Safety and Security

To submit a proposal or request further information, please contact the appropriate Springer Editor:

– Mr. Pierpaolo Riva at pierpaolo.riva@springer.com (Europe and Americas);
– Ms. Swati Meherishi at swati.meherishi@springer.com (India);
– Ms. Li Shen at li.shen@springer.com (China);
– Dr. Loyola D'Silva at loyola.dsilva@springer.com (Southeast Asia and Australia/NZ).

Indexed by Scopus

More information about this series at http://www.springer.com/series/15087

Sanjay Kumar Shukla · Sudhirkumar V. Barai · Ankur Mehta
Editors

Advances in Sustainable Construction Materials and Geotechnical Engineering

Select Proceedings of TRACE 2018

Springer

Editors
Sanjay Kumar Shukla
Edith Cowan University
Joondalup, WA, Australia

Sudhirkumar V. Barai
Indian Institute of Technology Kharagpur
Kharagpur, West Bengal, India

Ankur Mehta
Arkade Infra
Hisar, India

ISSN 2366-2557 ISSN 2366-2565 (electronic)
Lecture Notes in Civil Engineering
ISBN 978-981-13-7479-1 ISBN 978-981-13-7480-7 (eBook)
https://doi.org/10.1007/978-981-13-7480-7

This Springer imprint is published by the registered company Springer Nature Singapore Pte Ltd.
The registered company address is: 152 Beach Road, #21-01/04 Gateway East, Singapore 189721, Singapore

Preface

In recent years, the civil engineering profession has been focusing on various environmental concerns, sustainable developments and safety of structures subjected to natural hazards and environmental impacts. The Second International Conference on "Trends and Recent Advancement in Civil Engineering (TRACE)" was organized by the Department of Civil Engineering, Amity University, Uttar Pradesh, Noida, India, on 23 and 24 August 2018.

TRACE 2018 focused on advances and rapid evolution of various areas of civil engineering. The conference witnessed participation and presentation of research papers (reviews and original articles) from academia, industry experts and researchers from R&D centres from India and abroad. The conference proceedings have been classified under the following five book titles:

- *Advances in Sustainable Construction Materials and Geotechnical Engineering*
- *Advances in Transportation Engineering*
- *Advances in Structural Engineering and Rehabilitation*
- *Advances in Energy and Built Environment*
- *Advances in Water Resources Engineering and Management*

This book titled *Advances in Sustainable Construction Materials and Geotechnical Engineering* covers various review and research papers on recent Advances in Sustainable Construction Materials and Geotechnical Engineering. In total, 25 papers have been selected for publication as included in this book. The papers related to sustainable construction materials include the utilization of various industrial by-products such as paper industry sludge, glass powder, metakaolin, chopped fibres, waste tyres, fly ash, blast furnace slags and recycled coarse aggregates used as addition and/or replacement of conventional construction materials for the construction industry. Some papers are also related to the development of innovative construction technology, such as geopolymer technology as an alternative to conventional construction applications. Such efforts not only alleviate the disposal problems of industrial by-products but also make the construction industry more sustainable. On the other hand, the papers from geotechnical engineering are related to the study of the effect of various parameters and

numerical analysis on laterally loaded piles and also the improvement of soil subgrade utilizing plastic wastes, municipal solid wastes, fly ash, etc. It is believed that this book will be highly useful for a fairly wide spectrum of people, including researchers, field engineers, industry managers and civil engineering students.

We would like to thank Ms. Swati Mehershi, Dr. Akash Chakraborty, Ms. Rini Christy and the whole Springer team, for their full support and cooperation at various stages of the preparation and production of this book.

Perth, Australia — Sanjay Kumar Shukla
Kharagpur, India — Sudhirkumar V. Barai
Hisar, India — Ankur Mehta

Acknowledgements

The conference was organized to fulfil the vision of Honourable Dr. Ashok K Chauhan, Founder President of Ritnand Balved Education Foundation (RBEF), and under the able leadership of Honourable Dr. Atul Chauhan, Chancellor, Amity University, Uttar Pradesh, Noida, India. I am honoured to organize this prestigious conference which connected the world's foremost industries with the topmost academia.

I express my sincerest thanks to all the lead speakers and authors of original research papers for their contribution. I also express my thanks to all the reviewers for their cooperation in the review process. I am happy to express my deep sense of gratitude to our publication sponsor Springer for publishing the conference proceedings.

I express my warm gratitude towards all our sponsors: academic partners: Liverpool John Moores University, UK, and National University of Malaysia; industry partner: Defence Infrastructure Planning and Management (DIPM) Council of India; knowledge partners: Institution of Civil Engineers (ICE), Indian Association of Structural Engineers (IAStuctE), Women in Science and Engineering (WiSE), Indian Geotechnical Society (IGS) and Indian Buildings Congress (IBC); platinum sponsor: Ministry of Water Resources, River Development and Ganga Rejuvenation; gold sponsor: J K Cement Ltd.; supporting sponsor: Bentley, HEICO, VCL Group, BL Goel & Co., Subham Builders, Innovative Construction and Consultants, Satya Sai Builders and Contractors Pvt. Ltd. and Megde India Projects OPC Pvt. Ltd.

Finally, I compliment my team for their hard work and enthusiasm to make TRACE a success story. I am confident that TRACE 2018 will allow exciting and meaningful conversations, partnerships and collaborations in construction technology and infrastructure growth.

Dr. Ankur Mehta
Organizing Secretary, TRACE 2018

Contents

About the Editors

Dr. Sanjay Kumar Shukla is the Founding Editor-in-Chief of International Journal of Geosynthetics and Ground Engineering, and the Founding Research Group Leader of the Geotechnical and Geoenvironmental Engineering Research Group at the School of Engineering, Edith Cowan University, Perth, Australia, He is also the Distinguished/Adjunct Professor of Civil Engineering at Fiji National University, Fiji, VIT University, Vellore, Chitkara University, Himachal Pradesh, and VR Siddhartha Engineering College, Vijayawada, India. He graduated in 1988 with a first-class degree with distinction in Civil Engineering from BIT Sindri, India. He earned his MTech in Civil Engineering (Engineering Geology) in 1992 and Ph.D. in Civil Engineering (Geotechnical Engineering) in 1995 from the Indian Institute of Technology Kanpur, India. He has over 22 years of experience in teaching, research and consultancy in the field of Civil (Geotechnical) Engineering. He has authored more than 220 research papers and technical articles, including over 130 journal publications. He is also author/co-author/editor of 11 books, including 7 textbooks, and 12 book chapters. His books titled 'Core Principles of Soil Mechanics' and 'Core Concepts of Geotechnical Engineering' are popular textbooks in the core geotechnical engineering courses worldwide.

Dr. Sudhirkumar V. Barai is a professor in the Department of Civil Engineering at the Indian Institute of Technology, Kharagpur specializing in structural engineering. He obtained his Ph.D. from the Indian Institute of Science, Bangalore. He completed his bachelor's and master's in civil engineering from M S University of Baroda. He was a postdoctoral fellow at the Department of Solid Mechanics, Materials and Structures, Tel Aviv University. He was also Erskine Visiting Fellow at the University of Canterbury, Christchurch, and a visiting scientist at the National University of Singapore. His research interests include computational intelligence applications, structural health monitoring and concrete technology. He has published more than 200 articles in leading national and international journals and conferences.

Dr. Ankur Mehta is working as Director at his consultancy firm Arkade Infra in Hisar (Haryana). Prior to this, he worked as Assistant Professor in the Civil Engineering Department at Amity University, Noida (U.P.) and also as Deputy Manager at National Council of Cement and Building Materials under the Ministry of Commerce and Industry, Govt. of India. He obtained his Ph.D. from Thapar University, Patiala in 2017 after completing his M.Tech. in Structural Engineering from the same university. His primary research interests are sustainable materials, utilisation of waste materials in concrete, retrofitting of structures through various techniques, and supplementary cementitious materials. He has authored around 10 research papers in reputed journals along with a few book chapters. He is also a Chartered Structure Engineer as Life Member of Institution of Structural Engineers Pune (India), an Associate Member of Institution of Engineers (India).

Development of Geopolymer Concrete for Sustainable Infrastructures

Rohan Jethwani, Mohit Singh Thakur and Satadru Das Adhikary

Abstract This research is based on the development of sustainable concrete which would replace the conventional concrete. This special type of concrete is called as geopolymer concrete (GPC). Ordinary Portland cement (OPC) is generally utilised as a primary binder material for casting of concrete around the world. But, it is well known that generation of OPC adversely affects the environment. Thus, researchers and scientists are looking for alternative binder from industrial by-product. One of these by-product are fly ash (FA) and ground granulated blast furnace slag (GGBS) which can used in the presence of alkaline activator to develop GPC. The fly ash is the by-product of thermal power plant, and GGBS is the by-product of steel-manufacturing plant. The combined solution of sodium hydroxide (NaOH) and sodium silicate (Na_2SiO_3) is usually used as alkaline activators. The objective of this paper is to develop GPC under ambient curing condition by using locally available materials nearby IIT (ISM) Dhanbad, for sustainable infrastructures. Emphasis has been given towards ambient curing so that the developed GPC can be applicable to the general practical application. Various mechanical properties such as compressive strength, split tensile strength and flexural strength are mainly taken into consideration. Research outcome reveals that FA-GGBS-based GPC could able to provide comparable mechanical properties to that of conventional concrete and has the potential for wider application in civil infrastructures.

Keywords Geopolymer concrete · Fly ash · GGBS · Sodium hydroxide · Sodium silicate and strength

R. Jethwani (✉) · M. S. Thakur · S. Das Adhikary
Department of Civil Engineering, Indian Institute of Technology (ISM) Dhanbad, Dhanbad, Jharkhand, India
e-mail: rohanjethwani10@gmail.com

M. S. Thakur
e-mail: mst2301@gmail.com

S. Das Adhikary
e-mail: satadru@iitism.ac.in; 2009satadru@gmail.com

S. Kumar Shukla et al. (eds.), *Advances in Sustainable Construction Materials and Geotechnical Engineering*, Lecture Notes in Civil Engineering 35,
https://doi.org/10.1007/978-981-13-7480-7_1

1 Introduction

The biggest trending problem of today's world is global warming which is caused majorly due to the emission of greenhouse gases in the nature. It is well known that there is a huge amount of emissions of CO_2 due to the production of ordinary Portland cement (OPC). The production of OPC and construction of structures are hazardous to the environment with respect to emission of the greenhouse gases. As OPC is used as a binding material in major construction activities, this is on the major contributor to the emission of harmful gases. To reduce the emissions of gases, major amount of industrial by-products from the steel plant and thermal power plant such as fly ash (FA) and GGBS can be used for the development of eco-friendly concrete which can be used for civil infrastructures. As disposal of these by-products would cause hazard to the environment, thus these by-products can be used effectively for developing sustainable concrete. One such type of sustainable concrete is geopolymer concrete (GPC).

'Geopolymer' the term was coined by Joseph Davidovits in [1]. The raw materials used for geopolymer are of geological origin, and the structure is akin to polymeric chain structure. Moreover, the term 'geopolymer' is usually used to designate an amorphous alkali aluminosilicate. The crystalline polymeric structures consist of Si–O–Al bonds. The reaction between the binders and alkaline activators plays a major role in the formation of GPC. Various binders such as fly ash (FA), ground granulated blast furnace slag (GGBS), red mud and metakaolin can be used for the development of GPC. Previous research reveals that the curing at high temperatures is required for the fast polymerisation of GPC, but the addition of some proportion of GGBS with FA reduces this curing temperature to the ambient temperature. As both the raw materials used for the formation of GPC are by-products of industries, they help in protecting the environment by reducing the use of OPC and also preventing the need for heat curing. This also helps in the ease of practical application of the GPC which makes it easier to apply in future developments of civil infrastructures [2–4].

The strength of geopolymer concrete depends on various parameters such as composition of the binding materials, type of alkaline activators, concentration of the alkaline activators used, curing temperature, curing time, Si–Al ratio and sodium-based compounds. The curing temperature primarily contributes to the enhancement of the polymerisation process which helps in the development of strength properties, i.e. as the curing temperature is increased, there is a significant increase in the polymerisation process which gives more strength to the GPC. As the application of heat (oven curing) [5–8] is not possible during the construction of large size structures, ambient curing would be the feasible option for practical application in cast-in-situ construction. From the previous studies, it has been found that the factors influencing the properties of the geopolymer concrete are the optimum proportion of the GGBS used as it enhances the strength properties but has a drawback that it reduces the workability and the setting times of the GPC. A naphthalene-based superplasticizer can be used to improve the workability of the FA-GGBA-based geopolymer con-

crete [9]. GPC performs better than OPC in aggressive environments. Due to various excellent properties, GPC is a promising candidate as an alternative to conventional concrete for developing sustainable infrastructures.

2 Research Significance

Till date, there is limited information available in the literature on proper mix design as well as about the optimum proportion of the FA and GGBS for the development of GPC. Thus to determine the proportion of FA, GGBS and alkaline solution, this research is carried out. GPC has shown excellent properties in terms of strength and durability as compared to that of conventional concrete. Thus to ensure the use of GPC around us in day-to-day life, this research is carried out and various tests are performed on the samples made of GPC and comparison is done with conventional concrete. It has a huge potential in replacing the conventional concrete for future sustainable infrastructures. This research mainly emphasises on the performance evaluation of GPC with 100% replacement to OPC with FA and GGBS under ambient-curing conditions. Further research has been initiated to assess the structural application of this developed GPC at IIT (ISM) Dhanbad.

3 Experimental Investigations

This section provides the details of materials used for the development of GPC, preparation of alkaline solutions, mix proportioning, casting and curing of cube, cylinder and plain concrete beams and test results. The aim of this experimental programme is to determine the fresh and hardened properties of developed GPC. The materials used in this research are as follows:

(1) **Fly ash**
Fly ash (FA) is the by-product that can be obtained during the electricity production at thermal power plant. The fly ash used in the following research was obtained from Maithon Power Limited, Dhanbad, Jharkhand, India. As per IS 3812 (Indian Standard) Part 1 2013 [10], FA can be classified into categories such as calcareous and siliceous FA. In the present study, the calcareous FA has been used.

(2) **GGBS**
GGBS is the by-product obtained from the manufacturing of steel. The GGBS used in this study was obtained from the Owndust India Pvt. Ltd., Kolkata, West Bengal, India. The role of GGBS in this study is that it is used as the major binding material by replacing the OPC and providing good strength and flexural properties to the GPC. Table 1 shows the chemical comparison of the OPC, fly ash and GGBS.

Table 1 Comparison of chemical comparison of cement, fly ash and GGBS

OPC	Percentage	Fly ash	Percentage	GGBS	Percentage
CaO	60–65	CaO	0.5–1	CaO	35–40
SiO_2	17–25	SiO_2	50–55	SiO_2	30–35
Al_2O_3	3–8	Al_2O_3	30–35	Al_2O_3	15–20
Fe_2O_3	0.5–6	Fe_2O_3	5–6	Fe_2O_3	2.5–5
MgO	0.5–4	MgO	0.5–1	MgO	5–10
$Na_2O + K_2O$	0.5–1.3	$Na_2O + K_2O$	0.5–1	$Na_2O + K_2O$	–
TiO_2	0.1–0.4	TiO_2	1–3	TiO_2	–
P_2O_5	0.1–0.2	P_2O_5	0.5–1	P_2O_5	–
SO_3	1–2	SO_3	0.5–1	SO_3	0.25–1

(3) **Fine Aggregate**
Fine aggregate used in current study has been collected from the nearby river and has specific gravity of 2.65. Fine aggregates are conforming to zone III.

(4) **Coarse Aggregate**
Coarse aggregate used in current study has specific gravity of 2.8. Coarse aggregate that has been used of is nominal size of 20 mm.

(5) **Superplasticizer**
Super plasticizer collected from JBS Associate Dhanbad, it is sulphonated naphthalene formaldehyde.

3.1 Preparation of Alkaline Activator Liquid Solution

Activator liquid is prepared using NaOH flakes. Figure 1 shows the NaOH flakes and Fig. 2 shows the Na_2SiO_3. In the present case of study 10-M (Molar) solution of NaOH is being prepared using 400 g of NaOH flakes per litre of water. This process is exothermic in nature; hence to protect plastic buckets from getting melted, Fig. 3 shows the process of mixing. Once the heat is evolved, Na_2SiO_3 has been added to make alkaline solution. Figure 4 shows the water bath of the mix to reduce the heat generation.

3.2 pH Test of Solution

To check the acidity or basicity of the solution, pH test has been performed using universal pH paper. Figure 5 shows the universal pH paper. The change of colour can be observed of pH paper as shown in Fig. 6. The pH of solution is in the range of 8.5–9. Hence, the solution is basic in nature.

Fig. 1 NaOH flakes

Fig. 2 Na_2SiO_3 solution

3.3 Casting and Curing

Casting of GPC is similar to that of conventional concrete. At first, aggregate has been mixed and after that FA and GGBS have been mixed, till complete mix becomes grey in colour. After that, alkaline solution has been added along with superplasticizer. To obtain flowable GPC, 4% of superplasticizer dose has been used in the present study. The needle vibrator has been used to remove the air voids for the concrete as shown in Fig. 7. Ambient curing has been done. The term ambient curing means curing done in the presence of sunlight without water. Figure 8 shows the ambient

Fig. 3 Preparation of alkaline liquid

Fig. 4 Water bath

Fig. 5 pH paper

Fig. 6 pH test

curing process of concrete samples. In this process, sunlight is required to activate the polymerisation process of the geopolymer.

3.4 Mix Design

The mix design has been prepared according to IS 10262:2000 [11], but the procedure of preparation of mix design has not been given in any code; so, the mix design has been prepared as the method suggested by Subhash et al. [12] and Anuradha et al. [13].

Fig. 7 Needle vibrator

Fig. 8 Ambient curing

Table 2 Mix proportion

S. No.	Mix type	Cement (kg)	GGBS (kg)	Fly ash (kg)	Coarse aggregate (kg)	Fine aggregate (kg)	Alkaline solution (kg)	Super plasticizer (kg)	Water/cement ratio	AAS/binder ratio	Water replacement (%)
1	Mix 1	350	Nil	Nil	1120	855	160	7.7	0.45	Nil	20
2	Mix 2	Nil	226	226	935	900	206	7.7	Nil	0.45	20

Fig. 9 Slump test

Fig. 10 Compressive strength test

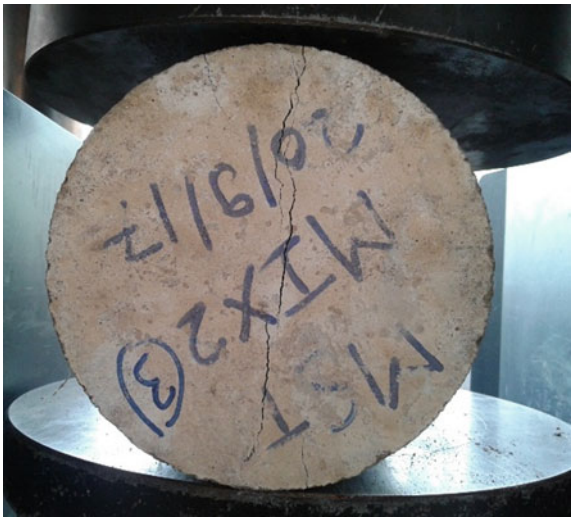

Fig. 11 Split tensile test

Fig. 12 Flexural test

Table 3 Test result

Mix	Strength	14 days (MPa)	28 days (MPa)
Mix-1	Compressive	18	33
Mix-2	Compressive	21	29.86
Mix-1	Split tensile	0.91	1.44
Mix-2	Split tensile	0.81	1.35
Mix-1	Flexural	Not available	3.53
Mix-2	Flexural	Not available	2.33

For the preparation of mix design, the specific gravity of cement has been replaced by the GGBS and FA, and water has been replaced by alkaline solution. In the present study, the total binder material consists of 50% FA and 50% GGBS. In conventional concrete (Mix-1), water/cement (W/C) ratio was maintained to 0.45, similarly in GPC (Mix-2) alkaline-activator-solution-to-binder ratio (AAS/B) was kept to 0.45. Table 2 shows the mix proportion of various constituents for conventional concrete and GPC.

The investigation aims at finding the fresh state and hardened state properties of the GPC. The grade of concrete used in this study was GPC 25. For the fresh properties of the concrete, slump test has been performed to check the workability of conventional concrete and GPC. Figure 9 shows the slump test. The GPC was a flowable range of concrete. Cube specimens of size 150 × 150 × 150 mm, cylinder size of 150 mm diameter and 150 mm height and beam 150 × 150 × 700 mm were cast and cured and then taken into testing for compressive strength, split tensile strength, flexural strength, respectively. To test the compressive strength of concrete, test has been done as per IS 516 (1959) [14], compression testing machine of 3000 kN has been used with loading rate of 5150 N/s. Figure 10 shows the compression testing of cube sample. To test the split tensile strength of concrete, test has been conducted as per IS 5816 (1999) [15] with loading rate of 1713 N/s. Figure 11 shows the split tensile test of cylinder sample. To test the flexural strength of concrete, test has been conducted as per IS 516 (1959) [14], the flexural testing machine used was of 1000 kN capacity, rate of loading used was 66.67 N/s. Figure 12 shows the flexural testing of plain concrete beam sample.

3.5 Test Result

Table 3 shows the comparative strength evaluation of conventional concrete (Mix-1) and GPC (Mix-2) at 14 and 28 days in terms of compressive, split tensile and flexural. It is observed that GPC almost provides similar compressive, split tensile and flexural strength as that of conventional concrete at various ages after casting. Moreover, GPC shows good slump values which would satisfy the workability criteria and would be applicable to various construction sectors. Thus, the developed GPC under ambient curing could satisfy both the workability and strength criteria and can be very useful for cast-in-situ construction as no special curing procedures would be required.

4 Conclusions

In the present study, efforts have been driven towards the development of geopolymer concrete (GPC) by replacing OPC 100% by using industrial by-products such as FA and GGBS. The objective is to develop the GPC in such a way that no special curing (i.e., heat curing) would be required so that the GPC could be applicable to cast-in-situ

construction. From that motivation, cubes, cylinder and plain concrete beam made of conventional concrete and GPC were prepared and cured under ambient temperature to evaluate and compare their fresh and hardened properties. The fresh and hardened properties of the conventional concrete and GPC show similar properties. GPC sets faster as compared to the conventional concrete; hence, the moulds can be demoulded earlier than that of conventional concrete. Thus, this study as a whole will solve two problems at a time. One is the usage of FA and GGBS as construction and building materials and reduces the problem of disposal of fly ash and GGBS. Another one is the reduction of OPC consumption in concrete production through the complete replacement of OPC with FA and GGBS which indirectly helps in the reduction of CO_2 emission to the environment.

Acknowledgements This research is supported by TEQIP-III (MRP) which is gratefully acknowledged. The authors wish to acknowledge the support of Maithon Power Limited (Jharkhand, India) for providing of fly ash and JBS Associates (Dhanbad, Jharkhand, India) for supplying the superplasticizer and Owndust India (Kolkata, India) for supplying GGBS.

References

1. Davidovits J (1984) Synthetic mineral polymer compound of the silicoaluminate family and preparation process. US Patent, 4472199
2. Hardjito D, Wallah SE, Sumajouw DMJ, Rangan BV (2004) On the development of fly ash-based geopolymer concrete. ACI Mater J 101(6):467–472
3. Pradip N, Prabir KS (2014) Effect of GGBFS on setting, workability and early strength properties of fly ash geopolymer concrete cured in ambient condition. Constr Build Mater 66:163–171
4. Manjunatha GS, Radhakrishna KV, Sasalatti VM (2014) Strength characteristics of open air cured geopolymer concrete. Trans Ind Ceram Soc 73(2):149–156
5. Chawla A et al (2017) Effect of curing conditions on compressive strength of fly ash-ground granulated blast furnace slag based geopolymer concrete. Int J Emerg Technol Adv Eng (UGC Approved List of Recommended Journal) 7. E-ISSN 2250–2459
6. Deb PS, Nath P, Sarker PK (2014) The effects of ground granulated blast-furnace slag blending with fly ash and activator content on the workability and strength properties of geopolymer concrete cured at ambient temperature. Mater Des 62(2014):32–39
7. Nath P, Sarker PK (2014) Effect of GGBFS on setting, workability, and early strength properties of fly ash geopolymer concrete cured in ambient condition. Constr Build Mater 130(2017):22–31
8. Pradip N, Prabir KS (2014) Effect of GGBFS on setting, workability and early strength properties of fly ash geopolymer concrete cured in ambient condition. Constr Build Mater 66(2014):163–171
9. Goriparthi MR, Rao GTD (2017) Effect of fly ash and GGBS combination on mechanical and durability properties of GPC. Adv Concr Constr 5(4):313–330
10. IS (Indian Standard) 3812 Parts 1 2013 pulverized fuel ash—specification part 1 for use as pozzolana in cement, cement mortar and concrete
11. IS (Indian Standard) 10262 (2009) Guidelines for concrete mix design proportioning
12. Patankar SV, Jamkar SS, Ghugal YM (2013) Effect of water-to-geopolymer binder ratio on the production of fly ash based geopolymer concrete. J Adv Technol Civ Eng 2(1):79–83
13. Anuradha R, Sreevidya V, Venkatasubramani R, Rangan BV (2012) Modified guidelines for geopolymer concrete mix design using Indian Standard. Asian J Civ Eng (Build Hous) 13(3):353–364

14. IS (Indian Standard) 516 (1959) Method of tests for strength of concrete
15. IS (Indian Standard) 5816 (1999) Method of test splitting tensile strength of concrete

Feasibility of Using Paper Industry Sludge Containing Calcium Carbonate in Manufacturing Bricks

Brij Bhushan, Upasana Grover, Siby John and Varinder S. Kanwar

Abstract Bricks have been regarded as one of the most durable and strongest building materials used throughout history. In this study, an attempt has been made to study the behavior of bricks manufactured using waste material like paper industry waste sludge. The objective of this work is to study the stabilization and solidification of industry sludge and then to study the engineering behavior of brick made from it. This paper presents an experimental investigation performed to check the feasibility of using paper sludge waste to reduce the quantity of clay, as there is a greater shortage of clay in many parts of the world. To begin, XRF characterization of paper sludge has been carried out. The bricks were prepared by paper sludge with varying compositions, with reduced quantity of clay from 10 to 50%. After performing various tests, it has been observed that these waste material bricks are lightweighted, sound, corrosion resistant, and strong in compression.

Keywords Bricks · Industrial waste material · Paper industry sludge · Lightweight material · Compressive strength

1 Introduction

Brick is one of the most widely used conventional building materials around the world. Bricks are manufactured from a variety of materials such as clay, lime, sand, concrete, and natural stone. Clay bricks are manufactured by shaping suitable clay to rectangular units of standard size. There may be variations in composition and properties by mixing the clays from different locations. Some of the important char-

B. Bhushan · U. Grover
Chitkara University, Solan, Himachal Pradesh, India

S. John
Department of Civil Engineering, PEC University of Technology, Chandigarh, India

V. S. Kanwar (✉)
Department of Civil Engineering, Chitkara University, Solan, Himachal Pradesh, India
e-mail: vc@chitkarauniversity.edu.in; varinderkanwar@gmail.com

S. Kumar Shukla et al. (eds.), *Advances in Sustainable Construction Materials and Geotechnical Engineering*, Lecture Notes in Civil Engineering 35,
https://doi.org/10.1007/978-981-13-7480-7_2

acteristics of bricks that make it popular building material are its high economical cost, high compressive strength, and good durability. Conservation of resources and minimization of pollution are two main problems that the world is facing. There is an increase in demand of bricks, which is resulting in the escalation of its cost in India. This problem can be tackled by using some waste material to replace some part of the primary component which in turn can also solve the disposal problem of the waste material. This will reduce the cost of brick and will also help in economizing the resources. One such material is paper industry sludge, which is produced in a great amount on an everyday basis.

Lime sludge generated from paper mill, sugar mill, and soda ash industries, etc., contains lime as calcium carbonate. All sludge contains some deleterious constituents/contaminants, which come from the process through which they are generated, e.g., the paper mill sludge contains free alkalies up to 2%. The presences of these deleterious contaminants restrict their bulk utilization in making cement and related building materials. The study has revealed that sludge from paper industry can be utilized up to 74% (dry basis) as a component of raw mix for the manufacturing of cement clinker. In addition to this, about 30% (dry basis) lime sludge can also be utilized for the manufacturing of masonry cement. Paper mill sludge containing high inorganic fraction can be utilized in the production of building materials. Due to its combustion matrix, it can be used in the brick industry.

Pitroda et al. [1] conducted an experimental study for the innovative use of hypo sludge in concrete formulations as a supplementary cementitious material was tested as an alternative to traditional concrete. The cement has been replaced by waste paper sludge accordingly in the range of 0% (without hypo sludge), 10, 20, 30, and 40% by weight for M-25 and M-40 mix. Concrete mixtures were produced, tested, and compared in terms of strength with conventional concrete. These tests were carried out to evaluate the mechanical properties like compressive strength up to 28 days and split strength for 56 days were taken. As a result, the compressive strength increased up to 10% by the addition of hypo sludge and the further increase in hypo sludge reduces the strength gradually.

Srinivasan et al. [2] experimentally investigated the strength of concrete and optimum percentage of the partial replacement by replacing cement via 10, 20, 30, 40, 50, 60, and 70% of hypo sludge. A mix M25 grade was designed as per Indian Standard method and the same was used to prepare the test samples. Based on the limited experimental investigation concerning the compressive and splitting tensile strength of concrete, it was observed that compressive strength of the concrete increased when the percentage of replacement is increased up to 40% and beyond this, as the replacement increased, compressive strength decreased. Replacement of cement with this waste hypo sludge material provides maximum compressive strength at 30% replacement. The split tensile strength decreased when the percentage of the replacement is increased.

Solanki and Pitroda [3] studied the flexural strength of beams for M 20 grade of concrete by partial replacement of cement with fly ash and hypo sludge in concrete. Based on experimental investigations in respect of flexural strength of concrete by partially replacement of cement with fly ash and hypo sludge, it was observed that

Table 1 Physical properties of material used

Material	Specific gravity	Fineness modulus
Paper sludge	1.89	1.44

flexural strength of the concrete increases up to 11.08%, when 20% replacement of cement by fly ash is increased and flexural strength of the concrete increases up to 8.91%, when 10% replacement of cement by fly ash is increased.

Balwaik and Raut [4] studied the compressive, split tensile strength and flexural strength by replacement of cement with waste paper sludge in the range of 5–20% by weight for M-20 and M-30 mix. As a result, the compressive, splitting tensile strength and flexural strength increased up to 10% addition of waste paper pulp and further increase in waste paper reduces the strength gradually.

From the above literature, it can be concluded that the incorporation of papermaking residues in brick manufacturing is technically viable. Therefore, no additional waste management procedures should be necessary when compared with normal construction and demolition residues. As a consequence, this method may be an alternative waste management route for these papermaking residues, avoiding their landfill and giving some value to the lime-rich-containing materials.

2 Materials and Methods

2.1 Materials Used

Materials used in the study were locally procured. The paper sludge was taken from a local paper manufacturing unit. The clay soil was also taken from a nearby locally based brick kiln. The sludge was kept in containers. It was available in powdered form. The physical properties of sludge were as per Table 1. The chemical composition was calculated from XRF tests. The chemical composition of the sludge is given in Table 2.

2.2 Mixing and Proportions

All the materials of brick, i.e., clay and sludge were mixed in the desired proportion. The sample prepared from all these mixes were compared and tested for several strength parameters. Figure 1 shows pictures of bricks while mixing and formation.

Mix proportions of several mixes are as given in Table 3.

Table 2 Chemical composition of paper sludge

Composition	Percentage (%)
O	44.74
Ca	37.34
C	11.70
Si	4.25
Na	0.86
Mg	0.50
K	0.21
P	0.10
S	0.09
Fe	0.06
Cl	0.06
Al	0.05
Sr	0.01
Mn	0.0038
Cu	0.0030
Ni	0.0030
Zn	0.0027

Fig. 1 Figures of bricks while mixing and formation (researcher getting the soil mixed with the sludge and thereafter formation of bricks out of it)

Table 3 Mix proportions of trial mixes

S. No.	Die	Sand (kg)	Sludge (kg)	Sludge (%)	Identity
1	Akm	80	0	0	A1
2	Akm	72	8	10	A2
3	Akm	64	16	20	A3
4	Sk	56	24	30	A4
5	Sk	48	32	40	A5
6	Sk	40	40	50	A6

Table 4 Weight of bricks

S. No.	Brick type	Weight (kg)
1	A1	3.104
2	A2	2.555
3	A3	2.431
4	A4	2.228
5	A5	1.956
6	A6	1.769

Table 5 % age water absorption after 24 h

S. No.	Brick type	Initial weight	Weight after 24 h	% age increase in weight after water absorption
1	A1	3.111	3.386	8.83
2	A2	2.546	2.873	12.86
3	A3	2.373	2.826	19.11
4	A4	2.239	2.845	27.07
5	A5	1.890	2.608	37.97
6	A6	1.819	2.670	46.80

2.3 Weight of the Brick After Formation

The average dry weight of each category of brick was found out to get the desired standard weight. The average weight of each type is given in Table 4.

2.4 Water Absorption

The bricks of each type were dipped in a water tank and water absorption was found out on a period of 24 h. Table 5 shows the weight of each type and the percentage of water absorption after standard time.

2.5 Compressive Strength

The bricks casted were tested for compressive tests by firstly curing the bricks for a day and then putting a mixture of cement mortar in the ratio of 1:3 in the frog section. The bricks were then covered with a damp jute bag for a day and then bricks were cured for 3 days. After drying, the compressive strength was tested in UTM. Table 6 shows the compressive strength of bricks.

Table 6 Compressive strength of bricks

S. No.	Bricks type	Load at failure (kN)	Compressive strength (N/mm^2)
1	A1	402.5	23.50
2	A2	290.7	17
3	A3	205.2	12
4	A4	119.7	7
5	A5	76.95	4.5
6	A6	59.85	3.5

Table 7 Efflorescence of bricks

S. No.	Brick type	Efflorescence
1	A1	Nil
2	A2	Nil
3	A3	Nil
4	A4	Nil
5	A5	Slight
6	A6	Slight

Table 8 Soundness of bricks

S. No.	Brick type	Soundness
1	A1	Satisfactory
2	A2	Satisfactory
3	A3	Satisfactory
4	A4	Satisfactory
5	A5	Not satisfactory
6	A6	Not satisfactory

2.6 Efflorescence Test

The bricks were tested for efflorescence by placing them in a tray in the vertical position and adding water in it. Then physical examination was done. Table 7 shows the results for efflorescence.

2.7 Soundness Test

Two bricks of the same type were taken and strike against each other. If it does not break and a metallic ringing sound forms, then the bricks were sound. Table 8 shows the details of the soundness of samples.

Table 9 pH test of bricks

S. No.	Brick type	Fresh water	7 days	21 days	28 days
1	A1	7.3	7.31	7.55	8.62
2	A2	7.3	7.42	7.56	8.63
3	A3	7.3	7.48	7.58	8.65
4	A4	7.3	7.53	7.75	8.79
5	A5	7.3	7.71	7.85	8.85
6	A6	7.3	7.84	7.85	8.85

Table 10 Conductivity test of bricks

S. No.	Brick type	7 days	21 days	28 days
1	A1	0.901	0.960	0.990
2	A2	0.921	0.933	1.009
3	A3	0.998	0.999	1.012
4	A4	1.215	1.430	1.527
5	A5	1.220	2.480	2.615
6	A6	1.410	2.528	2.622

2.8 Water-Related Tests

The bricks were dipped into separate containers for a period of 28 days and the water in which the bricks were dipped was tested and compared to fresh water before dipping. The comparison was done on certain parameters like pH, conductivity, turbidity, hardness, and the amount of chlorides.

2.9 pH Test

pH of water in which bricks were dipped was tested for a period of 7 days, 21 days, and 28 days and compared with fresh water. Table 9 shows the value for pH test.

2.10 Conductivity Test

Samples prepared were also tested for conductivity for a period of 7 days, 21 days, and 28 days. Table 10 shows the conductivity of samples.

Table 11 Hardness test of bricks

S. No.	Brick type	7 days	21 days	28 days
1	A1	400	575	875
2	A2	625	875	1300
3	A3	725	912.5	1400
4	A4	1200	1580	2250
5	A5	1375	1925	2250
6	A6	1525	2040	2800

Table 12 Chlorides test of bricks

S. No.	Brick type	7 days	21 days	28 days
1	A1	34.97	59.98	66.64
2	A2	44.98	74.47	79.97
3	A3	49.98	79.95	84.47
4	A4	54.97	81.97	89.48
5	A5	64.97	84.98	91.98
6	A6	79.96	106.48	110.47

2.11 Hardness Test

Hardness of water in which bricks were dipped was tested for a period of 7 days, 21 days, and 28 days. Table 11 shows the value for the hardness test.

2.12 Chloride Test

Chloride of water in which bricks were dipped was tested for a period of 7 days, 21 days, and 28 days. Table 12 shows the value for chlorides test.

3 Results and Discussions

The results and properties of various mixes tested are shown below.

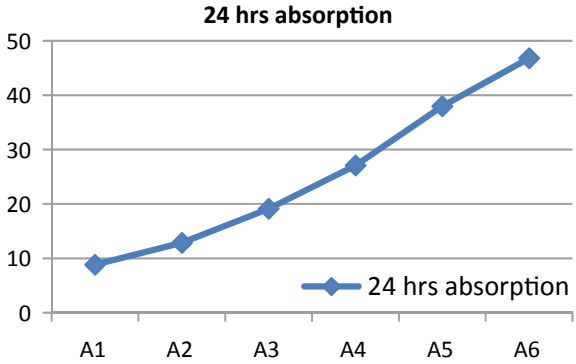

Fig. 2 % age water absorption after standard time

3.1 Weight

The weight results show that all the bricks are light in weight as compared to the standard brick A1, which does not contain any sludge. Therefore, all bricks are lightweighted bricks, which have an advantage in construction.

3.2 Water Absorption

According to the Indian standards, water absorption for the class I and class II bricks should not be more than 20% after 24 h immersion. The result of water absorption shows that the samples A1, A2, and A3 have absorption under standard value and hence acceptable. But the rest of the samples have a greater amount of water absorption. Figure 2 shows the comparison of initial and final weights and percentage of water absorption, respectively.

3.3 Compressive Strength

The result of compressive strength shows that the compressive strength of brick can be increased on addition of sludge to a limited quantity of 10 and 20% only. The compressive strength of brick decreased with the addition of more than 20% sludge. Figure 3 shows the comparative study of compressive strength test results of various mixes.

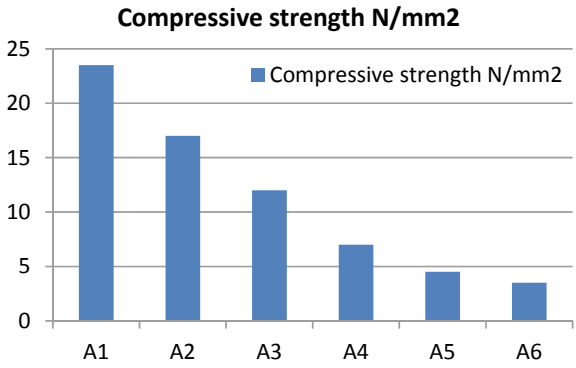

Fig. 3 Compressive strength of bricks

3.4 Efflorescence Test

According to Indian Standard Code, when there is no perceptible deposit, the efflorescence is NIL but there is slight efflorescence when 10% of the exposed area has a thin deposit of salts. In our specimens, samples with 0, 10, and 20% sludge have nil efflorescence but the rest have slight efflorescence.

3.5 Soundness Test

A brick is sound only if it does not break and a ringing sound is produced. The bricks with 10 and 20% are proved to be sound enough for construction.

3.6 pH Test

According to Indian standards, the samples with greater pH have a low risk of corrosion. So, all our samples have a pH greater than 7 and thus are less prone to corrosion. Figure 4 shows a chart of pH value of different samples at different days.

3.7 Conductivity Test

The tests performed shows that brick specimen A1 without any sludge and specimen A2 and A3 with sludge have conductivity less than 1 which is required by Indian Standard. Hence these bricks are acceptable to use. Figure 5 shows the comparison of conductivity of different samples.

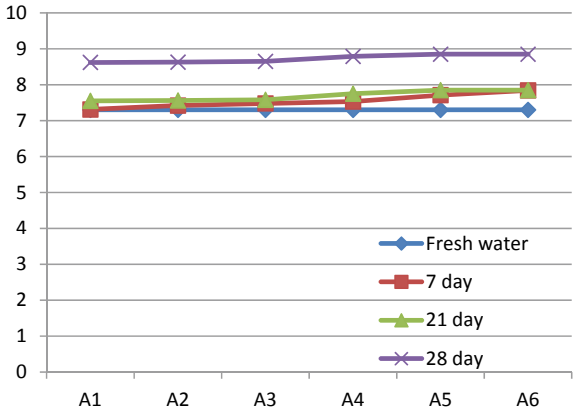

Fig. 4 pH test of bricks

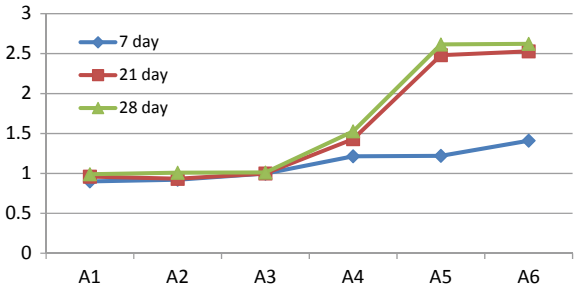

Fig. 5 Conductivity test of bricks

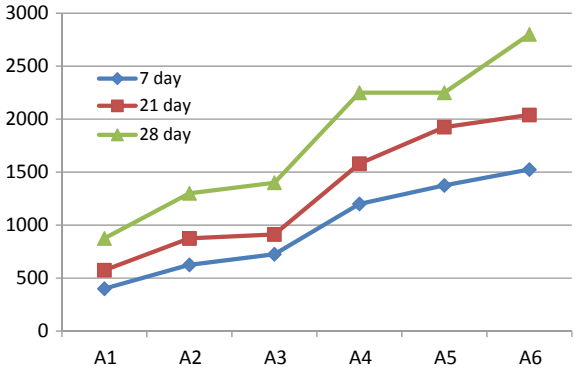

Fig. 6 Hardness test of water soaked bricks

3.8 Hardness Test

When compared to A1, we see that sample A2 and A3 have an almost same hardness which is near to A1 and thus are acceptable. Figure 6 shows the hardness test results of water in which bricks were soaked.

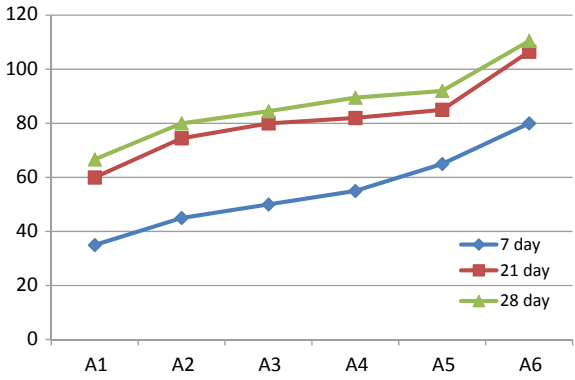

Fig. 7 Chlorides test of bricks

3.9 Chloride Test

The chloride tests show the corrosion-prone chances of the bricks. Low values usually are less prone to corrosion. We see that A2 and A3 have lower values of corrosion than the sample brick A1. So, sample A2 and A3 are acceptable. Figure 7 shows the chloride content of various specimens.

4 Conclusion

Following conclusions can be drawn from this research:

- The paper sludge can be utilized as an additive in the form of powder in the production of bricks up to 20% of replacement of soil (clay).
- Lightweight materials are formed as we keep increasing the amount the sludge in brick.
- Compressive strength holds well if sludge is added up to 20%, further increasing the percentage of sludge in bricks will lead to a decrease in the compressive strength of bricks.
- Addition of sludge in bricks leads to well sound bricks provided a limited amount of sludge is added.
- Addition of sludge in bricks leads to negligible efflorescence in it provided a limited amount of 20% is added.
- With the addition of 20% of sludge, there is lower chloride content and higher pH content than the specimen without sludge, which means resistance to corrosion.

Acknowledgements Authors are thankful to the Himachal Pradesh State Council of Science Technology and Environment for providing the financial assistance to carry out this research.

References

1. Pitroda J, Zala LB, Umrigar FS (2013) Innovative use of paper industry waste (hypo sludge) in design mix concrete. Int J Adv Eng Technol IJAET IV(I):31–35
2. Srinivasan R, Sathiya K, Palanisamy M (2010) Experimental investigation in developing low cost concrete from paper industry waste. Bull Inst Polytech
3. Solanki JV, Pitroda J (2013) Study of modulus of elasticity of concrete with partial replacement of cement by hypo sludge waste from paper industry. Glob Res Anal 2(1). ISSN 2277–8160
4. Balwaik SA, Raut SP (2011) The use of paper-mill pulp in concrete formulations. Int J Eng Res Appl (IJERA) 717–725

Experimental Investigations on Fly Ash Geopolymer Mortar

Sanghamitra Jena and Ramakanta Panigrahi

Abstract The industrial waste which is rich in silica and alumina activated with alkaline activators such as sodium silicate (NS) or potassium silicate combined with sodium hydroxide (NH) or potassium hydroxide forms geopolymer cement. The present investigation aims to utilize the fly ash in an innovative way that is to activate it using alkaline activators. The use of environmentally friendly cement can reduce greenhouse effect, solve disposal problems, and improve waste utilization. The main objective of this study was to investigate the effects of activator and curing conditions on the compressive strength and microstructure of alkali-activated fly ash mortar or geopolymer mortar. Two different activators were used to activate the binder such as NS and NH solutions. Six separate mixes were designed with different NaOH concentrations (8M–18M). Furthermore, the effect of the solution-to-binder ratio on the compressive strength (CS) of fly ash (FA) geopolymer mortar (GPM) was investigated. The outcome of the present study revealed that the compressive strength was found to be enhanced with NaOH concentration up to 14M, and after that, this strength reduced. Further, the compressive strength was increased up to solution-to-binder ratio of 0.6, and beyond that, this strength decreased. Heat-cured specimen was more strengthened than ambient-cured specimen.

Keywords Fly ash · Alkali activator · Compressive strength · Scanning electron microscope

S. Jena (✉) · R. Panigrahi
Department of Civil Engineering, Veer Surendra Sai University of Technology, Burla, Sambalpur, Odisha, India
e-mail: sanghamitrajena1987@gmail.com

R. Panigrahi
e-mail: ramakanta.p@rediffmail.com

S. Kumar Shukla et al. (eds.), *Advances in Sustainable Construction Materials and Geotechnical Engineering*, Lecture Notes in Civil Engineering 35,
https://doi.org/10.1007/978-981-13-7480-7_3

1 Introduction

Productions of construction materials such as concrete are indirectly affecting the environment. The main constituent of concrete is cement, which generates more amounts of wastes as well as causes environmental pollution. One tonne of cement produces nearly about one tonne of CO_2. Therefore, our main challenge is to produce sustainable geopolymer concrete using environmentally friendly cement such as the utilization of activated industrial wastes. The main challenge is to reduce cement consumption and production of high-strength innovative materials.

FA-based geopolymer concrete (GPC) consists of fly ash, sand, and coarse aggregate with alkaline solutions such as NS and NH. It can control the greenhouse effect of the environment [1]. The reduction in the CO_2 ultimately reduces the temperature of the earth. This cause compels to develop cementitious material which can replace the cement totally. Fly ash is one type of aluminosilicate solid waste material which was commonly used for the preparation of geopolymer concrete. Lloyd [2] found that the mixes activated with silicate activator are more homogeneous than that of activated with sodium hydroxide activator and improved compressive strength. Kotwal et al. [3] found the CS of the FA GPM using limestone sand as fine aggregate with different curing temperatures. It was observed that the CS was increased by 83% as the temperature was increased from 30 to 45 °C, but the strength was decreased by 33% at temperature 55 °C. Okoye et al. [4] observed the mechanical properties of blended FA and silica fume GPC. It was found that the FA GPC with silica fume possesses excellent compressive strength as well as durability properties with no alkali–aggregate reaction. Reddy et al. [5] studied the behavior of the FA GPC in the marine environment. It was found that 7 days' and 28 days' compressive strength of control concrete was 65 and 41% lower than the GPC, respectively. Here, the failure occurred only in the interfaces of aggregate and paste. Topark-Ngarm et al. [6] conducted the setting time and the CS test of the FA GPC. It was reported that the strength was increased at a high temperature than the ambient temperature. Boonserm et al. [7] observed that the CS of the FA GPM combined with bottom ash in different percentages. It was found that the CS of the bottom ash GPM was 46% lesser in strength than that of the FA GPM. Waste gypsum was used as an additive in this GPM. Chindaprasirt et al. [8] investigated the compressive strength of coarse lignite high-calcium FA GPM. It was observed that the CS of 15M specimen was more than that of 10 and 20M.

The current study aims to investigate the properties of the FA GPM cured under elevated temperature and room temperature. The compressive strength of mortar with different solution-to-binder ratios was determined. Moreover, the microstructural examination of the mixes was carried out by scanning electron microscope (SEM) and energy-dispersive spectroscopy (EDS) measurements.

2 Experimental Program

2.1 Materials and Mix Design

The FA was collected from thermal power corporation Hindalco (Burla, Sambalpur, Odisha, India) confirming to class F as per ASTM C 618. The specific gravity of the FA was 2.44. It was used as binder in the geopolymer mortar. River sand was utilized as natural fine aggregate. Sieve analysis was done for particle size distribution as per IS 383:1970. NH and NS were used as alkaline activators to perform geopolymerization. Solutions were prepared with different NaOH concentrations or molarity (M). M stands for the molar weight of NaOH which is 40 g. For the preparation of 1M NaOH solution, 40 g of NaOH flakes was added in one liter of water. Similarly, in 8M solution, $8 \times 40 = 320$ g of NaOH flakes was added in one liter of water. In this study, six mixes were prepared separately by taking different molarity, such as 8, 10, 12, 14, 16, and 18M. Na_2SiO_3-to-NaOH ratio was constant, i.e., 2.5, and the solution-to-binder ratio was fixed for all mixes, i.e., 0.5. Some amount of extra water is added only to increase workability. Also, another parameter was checked, i.e., increase of solution-to-binder ratio. 0.4, 0.45, 0.5, 0.6, and 0.7 are different solution-to-binder ratios. Heat curing in the oven and ambient curing in the room temperature are the two types of curing methods that were adopted for measuring the strength of the GPM.

2.2 Mixing Method and Casting of Specimen

NH flakes (98% purity) and locally available NS solution (SiO_2/Na_2O equal to 2.21) were used as alkaline activators. The required concentration of NH solution was prepared by mixing NH pellets in the potable water. This solution was kept in room temperature for 24 h to cool down. Then, sodium silicate solution was mixed with sodium hydroxide solution prior to mix with the fly ash and sand mixture. $70.5 \times 70.5 \times 70.5$ mm size cube specimens were prepared for the CS test.

2.3 Curing of the Specimen

These specimens were removed after 24 h of its casting. Then, those specimens were kept in a hot air oven at 70 °C for 24 h [9]. After 24 h, those were removed and kept in the room temperature until the day of testing. But for the specimens which were to be tested with ambient curing, those specimens were demolded after 24 h of its casting and kept in the room temperature for the test in a required day. Table 1 gives the elemental analysis of the FA obtained by energy-dispersive spectroscopy (EDS).

Table 1 Elemental analysis of fly ash obtained by EDS

Element	Weight %	Atomic %
C	23.04	32.40
O	47.17	49.75
Mg	0.10	0.08
Al	0.22	0.14
Si	28.92	17.37
S	0.22	0.11
K	0.33	0.15
Total	100	100

Table 2 Physical properties of fine aggregate

Properties	Value
Fineness modulus	3.14
Zone	II
Specific gravity	2.74
Water absorption	1.6%

Table 3 Mix proportion of GPM

Mix symbol	NaOH concentration (M)	Na_2SiO_3/NaOH	*w*/*b* ratio	Fly ash (kg/m^3)	Fine aggregate (kg/m^3)
GPM1	8	2.5	0.17	110	330
GPM2	10	2.5	0.17	110	330
GPM3	12	2.5	0.17	110	330
GPM4	14	2.5	0.17	110	330
GPM5	16	2.5	0.17	110	330
GPM6	18	2.5	0.17	110	330

GPM Geopolymer mortar

Table 2 gives the physical properties of fine aggregate. Mix proportions were given in Table 3. Figure 1 shows the image of sodium hydroxide flakes.

3 Results and Discussion

3.1 Effect of NH Concentration on Compressive Strength

The variation of the CS with respect to different molarity is shown in Fig. 2.

Fig. 1 NH flakes

Fig. 2 Variation of the CS in different NH concentrations

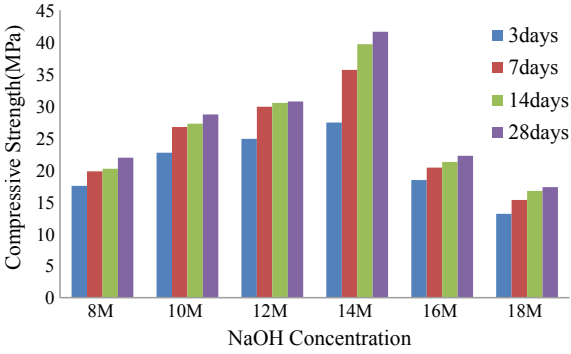

Figure 2 shows that the CS was increased as the NaOH concentration was increased. But optimum strength was achieved in 14M specimen for all the days of curing. 3, 7, 14, and 28 days' compressive strength was increased with the increased molarity up to 14M. Leaching of silica and alumina was increased at high NaOH concentrations. This could be due to the increased geopolymerization from 8 to 14M. But at 16 and 18M, the strength was decreased about 50 and 61%, respectively, than 14M due to the increased viscosity of activator. This could be due to the formation of precipitation of aluminosilicate gel from a high concentration of OH^- ions with a high NaOH concentration. It was also noticed by Aliabdo et al. [1]. The variation in the compressive strength in different solution-to-binder ratios is shown in Fig. 3.

3.2 Effect of Solution-to-FA Ratio on Compressive Strength

Figure 3 shows that the CS of the GPM was increased by 43% as the solution-to-binder ratio was increased from 0.4 to 0.6, and then, the effect was reversed. A fall in the strength was noticed as the ratio increased to 0.7. But this strength was 34% higher than that of the strength observed in ratio of 0.4. 28 days' compressive strength was varied from 25.39 to 36.27 MPa, when the solution-to-FA ratio was increased from 0.4 to 0.6. The same type of increment in strength occurred from 3 to 28 days.

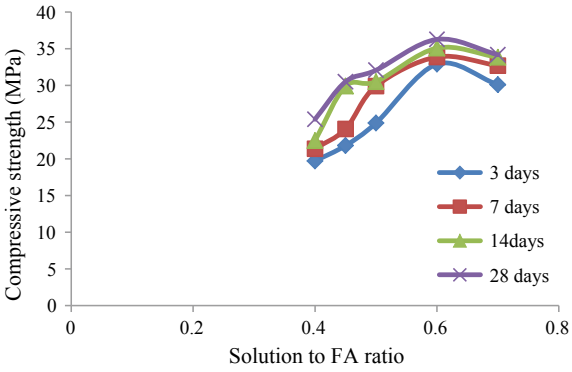

Fig. 3 Variation of the CS in different solution-to-FA ratios

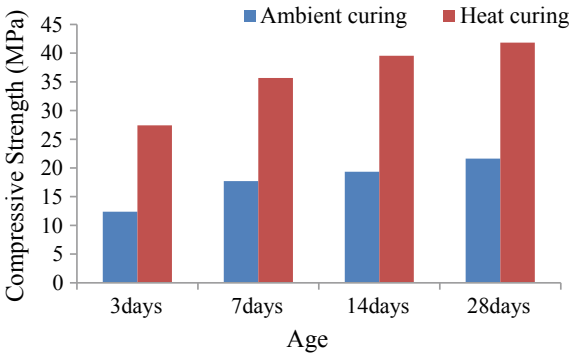

Fig. 4 Variation in the CS in different curing processes

This strength was decreased by 7%, when the ratio was increased up to 0.7. It was also found by Aliabdo et al. [1].

3.3 Effect of Curing Process on Compressive Strength

Hydration process is the exothermic reaction. Internally heat is produced as the reaction starts in cement paste. But geopolymerization process is endothermic reaction. Here, no internal heat is produced. Therefore, some amount of external heat is required to perform the geopolymerization in a better way. The variation in the CS with respect to curing process is shown in Fig. 4.

Figure 4 shows that the compressive strength was increased nearly about two times in case of heat curing than that of ambient curing. This could be due to the external heat. This was also observed in the previous study [10]. It was observed that the CS of heat-cured specimen was 27.42 MPa, whereas the CS of ambient-cured specimen was 12.38 MPa in 3 days. It was increased up to 28 days, i.e., 41.54 MPa in case of elevated temperature and 21.63 MPa for room temperature.

3.4 Microstructural Analysis

The SEM of the geopolymer mortar with solution-to-binder ratios of 0.45, 0.5, and 0.6 is shown in Figs. 5, 6, and 7, respectively.

Above three microstructure images of the geopolymer mortar show that the increased ratio of alkaline to binder increases the viscosity, which binds the other materials to form a compacted mass. Alkaline-to-binder ratio of 0.6 of the specimen shows denser medium than that of 0.5 and also 0.5 of the specimen shows denser medium than that of 0.45.

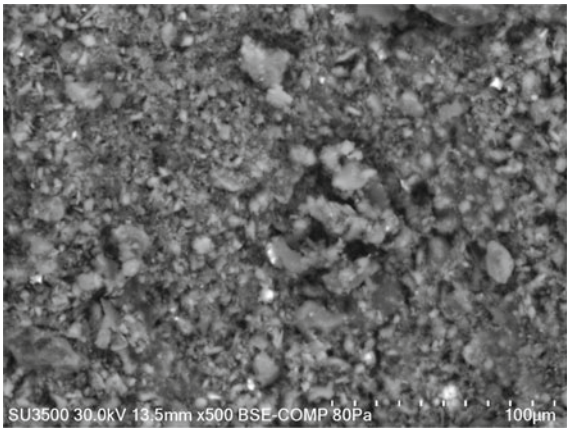

Fig. 5 SEM of geopolymer mortar with solution-to-binder ratio of 0.45

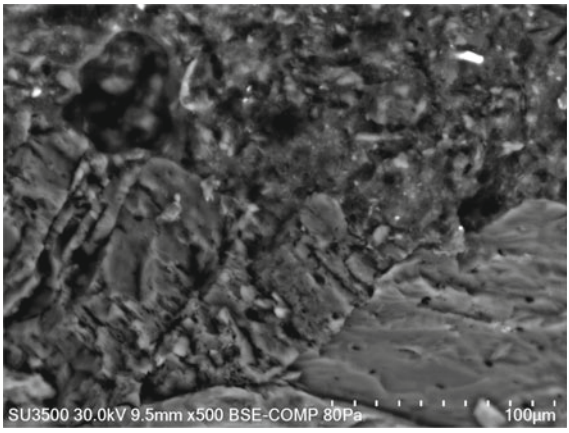

Fig. 6 SEM of geopolymer mortar with solution-to-binder ratio of 0.5

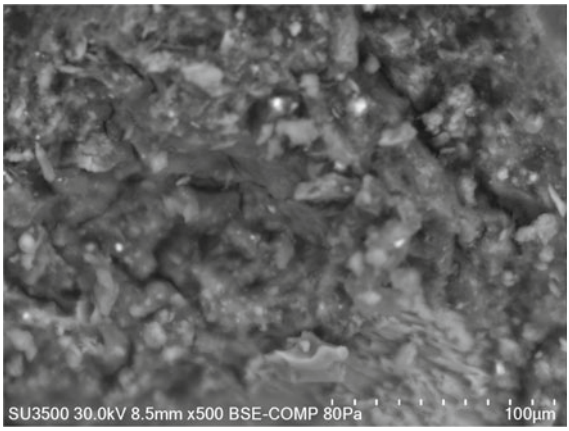

Fig. 7 SEM of geopolymer mortar with solution-to-binder ratio of 0.6

4 Conclusion

The present work deals with a detailed investigation, including both experimental study and microstructural study using the SEM. The following observations were obtained from the results and discussion which are reported below.

1. The CS of the FA GPM was increased when the molarity was increased up to 14M, and after that, it was decreased.
2. The compressive strength of the fly ash geopolymer mortar was increased when the solution-to-binder ratio was increased up to 0.6, and then, it was slightly decreased.
3. The external heat in heat curing performed best to produce more compressive strength than in case of ambient curing.
4. The microstructure of geopolymer mortar with varying solution to binder ratios shows that higher the ratio offers more compactnees and denser media.

Appendix

1. Table 1. Elemental analysis of fly ash
2. Table 2. Physical properties of fine aggregate
3. Table 3. Mix proportions of geopolymer mortar
4. Fig. 1. Sodium hydroxide flakes
5. Fig. 2. Variation of the CS in different NH concentrations
6. Fig. 3. Variation of the CS in different solution-to-FA ratios
7. Fig. 4. Variation in the CS in different curing processes
8. Fig. 5. SEM of geopolymer mortar with solution-to-binder ratio of 0.45

9. Fig. 6. SEM of geopolymer mortar with solution-to-binder ratio of 0.5
10. Fig. 7. SEM of geopolymer mortar with solution-to-binder ratio of 0.6

References

1. Aliabdo AA, Elmoaty MA, Salem HA (2016) Effect of water addition, plasticizer and alkaline solution constitution on fly ash based geopolymer concrete performance. Constr Build Mater 121:694–703. https://doi.org/10.1016/j.conbuildmat.2016.06.062
2. Lloyd RR, Provis JL, van Deventer JS (2009) Microscopy and microanalysis of inorganic polymer cements. 1: Remnant fly ash particles. J Mater Sci 44(2):608–619. https://doi.org/10.1007/s10853-008-3077-0
3. Kotwal AR, Kim YJ, Hu J, Sriraman V (2009) Characterization and early age physical properties of ambient cured geopolymer mortar based on class C fly ash. Int J Concr Struct Mater 9(1):35–43. https://doi.org/10.1007/s40069-014-0085-0
4. Okoye FN, Durgaprasad J, Singh NB (2016) Effect of silica fume on the mechanical properties of fly ash based geopolymer concrete. Ceram Int 42:3000–3006. https://doi.org/10.1016/j.ceramint.2015.10.084
5. Reddy DV, Edouard JB, Sobhan K (2012) Durability of fly ash-based geopolymer structural concrete in the marine environment. J Mater Civ Eng 25(6):781–787. https://doi.org/10.1061/(ASCE)MT.1943-5533.0000632
6. Topark-Ngarm P, Chindaprasirt P, Sata V (2014) Setting time, strength, and bond of high-calcium fly ash geopolymer concrete. J Mater Civ Eng 27(7):04014198. https://doi.org/10.1061/(asce)mt.1943-5533.0001157
7. Boonserm K, Sata V, Pimraksa K, Chindaprasirt P (2012) Improved geopolymerization of bottom ash by incorporating fly ash and using waste gypsum as additive. Cem Concr Compos 34:819–824. https://doi.org/10.1016/j.cemconcomp.2012.04.001
8. Chindaprasirt P, Jaturapitakkul C, Chalee W, Rattanasak U (2009) Comparative study on the characteristics of fly ash and bottom ash geopolymers. Waste Manag 29:539–543. https://doi.org/10.1016/j.wasman.2008.06.023
9. Albitar M, Visintin P, Ali MMS, Drechsler M (2015) Assessing behaviour of fresh and hardened geopolymer concrete mixed with class-F fly ash. KSCE J Civ Eng 19(5):1445–1455. https://doi.org/10.1007/s12205-014-1254-z
10. Part WK, Ramli M, Cheah CB (2015) An overview on the influence of various factors on the properties of geopolymer concrete derived from industrial by-products. Constr Build Mater 77:370–395. https://doi.org/10.1016/j.conbuildmat.2014.12.065
11. IS 383:1970 Indian standard code “specification for coarse and fine aggregates from natural sources for concrete”

Three-Dimensional Numerical Modeling of Underground Powerhouse Complex of 720 MW Mangdechhu Hydroelectric Project, Bhutan

Arvind Kumar Mishra and Iqrar Ahmed

Abstract The underground powerhouse complex of Mangdechhu Hydroelectric Project (MHEP) comprises of a 155-m-long, 23-m-wide, and 41-m-high machine hall cavern and a 135.5-m-long, 18-m-wide, and 23-m-high transformer hall cavern. The engineering design, support system, and excavation methodology of the caverns were designed based on the geological data obtained from surface and subsurface investigations during detailed project report stage investigations, using two-dimensional elastoplastic finite element analysis by Phase^2 software. However during the excavation of the caverns, a shear zone of 1–1.5 m thickness with associated fracture zone of 1.5–3 m thickness on either side was encountered. In view of the changed geological scenario, the excavation methodology and support system designed based on two-dimensional analysis appeared inadequate as such progressive three-dimensional discontinuum numerical modeling analysis using 3DEC software was undertaken to optimize the excavation methodology, sequence, and support system. The models were updated at various stages of the excavation using the encountered and anticipated geological conditions, rock mass properties, and instrumentation data to simulate the rock mass behavior during the excavation, to analyze the stress changes and associated displacements in the caverns for particular excavation stage, and to evolve a safe excavation methodology, sequence, and support system prior to benching to next level, while simultaneously revalidating the installed support system. The overall stability of the caverns was also determined after the complete excavation. By the aid of numerical modeling results, the excavation methodology, sequence, and support system were optimized and the excavation of the caverns was successfully completed within the schedule.

Keywords Numerical modeling · Excavation methodology · Support system · Phase^2 · 3DEC

A. K. Mishra · I. Ahmed (✉)
Mangdechhu Hydroelectric Project Authority, Trongsa Dzongkhag, Bhutan
e-mail: iqrar_a@hotmail.com

S. Kumar Shukla et al. (eds.), *Advances in Sustainable Construction Materials and Geotechnical Engineering*, Lecture Notes in Civil Engineering 35,
https://doi.org/10.1007/978-981-13-7480-7_4

1 Introduction

The underconstruction 720 MW Mangdechhu Hydroelectric Project (MHEP) is located in Trongsa District of Central Bhutan. The project is in advance stage of construction and is scheduled for commissioning by May 2019. The project comprises of 112-m-high concrete gravity dam, 13.521-km-long head race tunnel, 152-m-deep surge shaft, two pressure shafts of stepped configuration, an underground powerhouse complex comprising of machine hall and transformer hall caverns along with appurtenant structures, and a 1.333-km-long tail race tunnel. The underground powerhouse complex comprises of a 155-m-long, 23-m-wide, and 41-m-high machine hall cavern, a 135.5-m-long, 18-m-wide, and 23-m-high transformer hall cavern, four bus ducts of 43 m length each connecting both the caverns, four circular penstocks of 2.5 m diameter to feed the turbines, four D-shaped draft tubes to convey water to the tail race tunnel for releasing it back into the river, and a 3-m-diameter and 235-m-long drainage gallery behind the machine hall cavern.

The engineering design, support system, and excavation methodology of the caverns were designed based on the two-dimensional elastoplastic finite element analysis by Phase^2 software using geological data obtained from surface and subsurface investigations during detailed project report stage investigations. However during the excavation of the caverns, a shear zone of 1–1.5 m thickness with associated fracture zone of 1.5–3 m thickness on either side was encountered. In view of the changed geological scenario, the excavation methodology and support system designed based on two-dimensional analysis appeared inadequate as such the project authority approached National Institute of Rock Mechanics (NIRM), Bengaluru, to conduct progressive three-dimensional discontinuum numerical modeling analysis using 3DEC software to optimize the excavation methodology, sequence, and support system.

2 Geological Setup of the Powerhouse Area

The powerhouse complex is housed within the Cheka Formation of Higher Himalayan Crystallines. The underground powerhouse complex is located below a spur in between two streams with a maximum superincumbent cover of 180 m. The Mangdechhu River flowing toward the western side is about 350 m away from the powerhouse complex. The rock mass is represented by quartzite with bands of mica schist and intrusive pegmatite and amphibolite. The foliation dips toward south and southwest in the outcrops exposed along the road, whereas in the stream cuttings on both the sides of the powerhouse spur westerly direction foliation dips are observed indicating broad open fold plunging toward the river [1].

3 Design Analysis of the Caverns

Phase^2, a two-dimensional elastoplastic finite element program, was used for evaluating stresses and displacement around the caverns to determine the optimum thickness of the rock pillar between the two caverns and also to evaluate the design support system. The rock mass was assumed to be homogeneous, isotropic, and elastic–plastic material. The analysis was aimed to determine the width of the rock pillar to place the two caverns as close as possible in order to reduce the length and hence cost of the bus bars that link the generators to the transformers, while also avoiding unfavorable stress distribution and yielding in the rock pillar between the two caverns and to have a sufficient undisturbed (unyielding) zone after excavation.

Four models with rock pillar widths of 30, 35, 40, and 45 m were analyzed with two different cases of input parameters. The details of the two cases of input parameters are given in Table 1. Rock cover of 200 m thickness was taken above the caverns. Both the caverns were excavated simultaneously in the model. Gravitational loading was considered for rock pillar analysis. For all the four models in both the cases, yield zone, strength factor, and total displacement were evaluated. The evaluated parameters are given in Table 2.

After determining the safe thickness of the rock pillar analysis of support system was undertaken. Based on the stress distribution and extent of plastic zone around the caverns as a result of excavation, support system for the crown and walls of the caverns was estimated and analyzed in Phase^2 program. Based on the analysis support system comprising of steel fiber reinforced shotcrete and rock bolts was finalized. The design support system incorporated in the construction drawings is given in Table 3.

Table 1 Input parameters used for the analysis in Phase^2 software

Parameters	Case-I	Case-II	Remarks
UCS σ_{ci} (MPa)	75	100	
Hoek–Brown constant m_i	18	18	
Geological strength index (GSI)	46	54	Measured in exploratory drift [2]
Disturbance factor (D)	0.7	0.7	As suggested by Hoek [2]
Modulus of deformation (GPa)	11	11	
In situ stress ratio (K) = (σ_{H}/σ_{v})	1.76	1.76	

Table 2 Evaluated parameters obtained after the analysis in Phase^2 software

Parameters obtained after the analysis	Thickness of rock column between the caverns							
	30 m		35 m		40 m		45 m	
	Case-I	Case-II	Case-I	Case-II	Case-I	Case-II	Case-I	Case-II
Yield zone	Zone of overstress extends across the pillar	Stress zone overlaps across the pillar	Stress zone overlaps, but zone of overstress extends 10.5 m	Stress zone overlaps across the pillar	Stress fields are independent undisturbed zone = 2.3 m	Stress fields are independent undisturbed zone = 14 m	Stress fields are independent undisturbed zone = 17.8 m	Stress fields are independent undisturbed zone = 18 m
Strength factor	<1	<1	<1	<1	>1	>1	>1	>1
Total displacement (mm)	42	37.5	40	35	38	35	36	33

Table 3 Suggested support system for machine hall and transformer hall caverns

Support system	Crown	Walls
Machine hall cavern		
Shotcrete	200-mm-thick SFRS	150-mm-thick SFRS
Rock bolts	36 mm dia. 7.5 m long @ 3 m C/C and 36 mm dia. 9 m long @ 3 m C/C	36 mm dia. 12 m long @ 3 m C/C, along the downstream wall and 36 mm dia. 9 m long @ 3 m C/C on the upstream walls
Transformer hall cavern		
Shotcrete	200-mm-thick SFRS	150-mm-thick SFRS
Rock bolts	36 mm dia. 7.5 m long @ 1.5 m C/C	36 mm dia. 9 m long @ 1.5 m C/C, along both the walls

4 Encountered Geological Conditions and Need of Re-evaluation of Support System and Stability

The rock mass encountered during the excavation of the caverns was represented by moderately jointed, strong quartzite with intercalated schist bands of 1–5 cm thickness intruded by randomly oriented pegmatite and amphibolite. Both the caverns were traversed by a shear/fracture zone of 5–8 m thickness, with attitude of N 30°E–S 30°W dipping 10–24° due to N 60°W. This shear/fractured zones intercepted both the upstream and downstream walls of the caverns along the long axis and also cutting across them (Fig. 1a–e). The mean attitude of foliation recorded along the caverns was N 28°W–S 28°E dipping 33° due to S 62°W. Apart from foliation, the rock mass was traversed by three other prominent sets of discontinuities along with some randomly oriented joints.

The presence of a shear/fracture zone, cutting along and across the caverns and large size of the caverns, necessitated the re-evaluation of the support system, excavation methodology, and sequence along with monitoring and analysis of the behavior of the rock mass during the course of the excavation. As such, progressive 3D stress analysis of the powerhouse caverns along with monitoring of the caverns by the aid of geotechnical instrumentation was undertaken. The predicted behavior of rock mass as inferred from 3D stress analysis was regularly compared with the observed behavior as recorded by geotechnical instrumentation to optimize excavation methodology and sequence along with the optimization and validation of the support system [1, 3–6].

5 Three-Dimensional Numerical Analysis of the Caverns

Three-dimensional stress analyses of the caverns were undertaken by NIRM, Bengaluru, using 3DEC software. Based on the geological conditions encountered during the excavation of the caverns and appurtenant structures, a three-dimensional

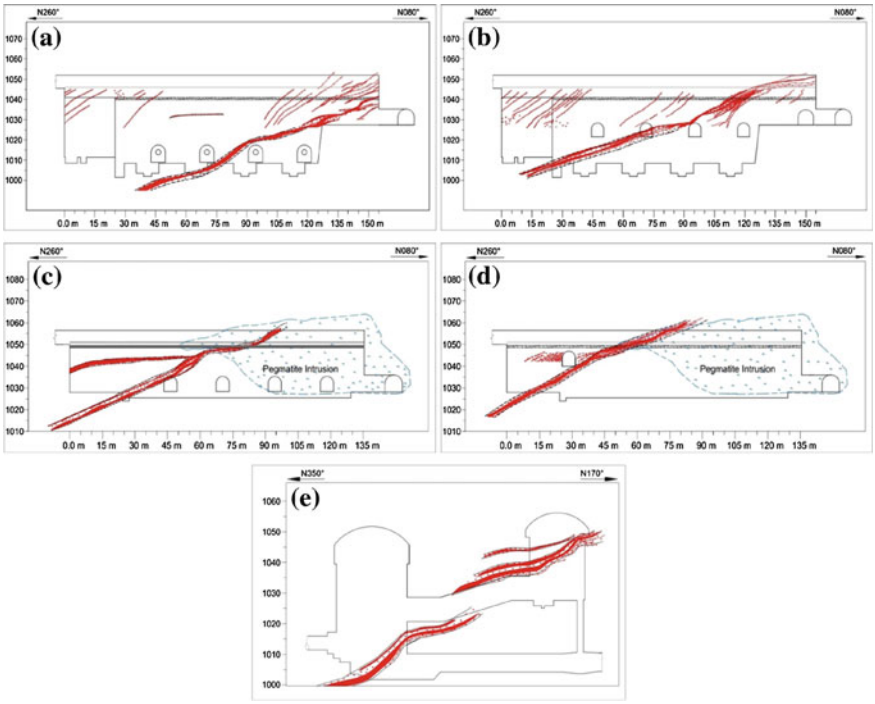

Fig. 1 Geological section showing the disposition of the shear zone along **a** upstream wall, **b** downstream wall of powerhouse cavern, **c** upstream wall, **d** downstream wall of transformer hall cavern, and **e** across the caverns

numerical model in 3DEC software comprising of powerhouse cavern, transformer hall cavern, bus ducts, and other excavations was prepared (Fig. 2). To simulate a realistic behavior of the rock mass in 3DEC model, the prevailing in situ stress along with the in situ geotechnical parameters of the rock mass and engineering properties of the rocks was determined and was used as input parameters. In situ stress conditions were measured by hydrofracturing method in accordance with the method suggested by Cornet [7], while the geotechnical parameters, viz. in situ deformability and elasticity, were determined by plate load test [8], and in situ shear strength parameters were evaluated by direct shear test method [9] in class-III type of rock mass and in shear zone. The physicomechanical properties of the rocks were determined by testing various types of rock samples collected from exploratory boreholes [10]. The determined parameters are given in Tables 4, 5, 6, and 7, respectively.

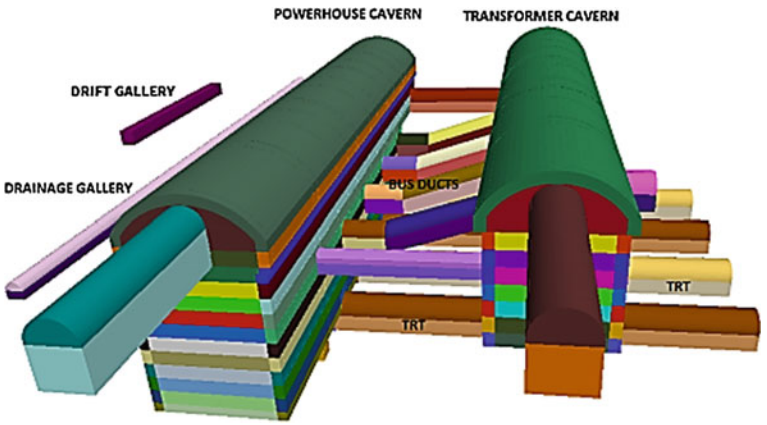

Fig. 2 3D model showing various components of the powerhouse complex

Table 4 Summary of in situ stress measurement results

Principal stresses	
Vertical stress (σ_v) in MPA (calculated with an overburden of 180 m and density of rock 2.7 gm/cc)	4.76 MPa
Maximum horizontal principal stress (σ_H)	8.38 ± 0.6496 MPa
Minimum horizontal principal stress (σ_h)	5.59 ± 0.4331 MPa
Maximum horizontal principal stress direction	N 70°
$K = (\sigma_H + \sigma_h)/2/\sigma_v$	1.47
$K = (\sigma_H/\sigma_v)$	1.76

Table 5 Summary of plate load test

In situ deformability parameters	Class-III	Shear zone
Modulus of deformability of rock mass (E_m) in GPa	2.01–3.99	0.46–1.24
Modulus of elasticity of rock mass (E_{em}) in GPa	2.31–5.24	0.49–1.36

Table 6 Summary of in situ direct shear test results

Loading condition	Rock mass category	Cohesion (C) MPA	Angle of internal friction (ϕ) degrees
Peak shear parameters	Class-III rock mass	0.375	35.8
	Shear zone	0.354	25.6
Residual shear parameters	Class-III rock mass	0.274	34.2
	Shear zone	0.231	25.3

Table 7 Physicomechanical properties of different types of rocks of underground caverns

Properties	Rock type		
	Pegmatite	Quartzite	Pegmatite from shear zone
Density (kg/m^3)	2590–2605	2642–2646	2586
UCS (MPa)	114–143	237	40
Young's modulus (GPa)	38.5–45.5	67	12
Poisson's ratio	0.32	0.17	0.49
Tensile strength (MPa)	6.08	10.64	–

5.1 3DEC Analysis

Three-dimensional analyses of the caverns were undertaken using 3DEC software, which is a three-dimensional numerical program based on the distinct element method for discontinuum modeling [11]. 3DEC software simulates the response of discontinuous media (such as a jointed rock mass) subjected to either static or dynamic loading. The discontinuous medium is represented as an assemblage of discrete blocks. The discontinuities are treated as boundary conditions between blocks; large displacements along discontinuities and rotations of blocks are allowed. Individual blocks behave as either rigid or deformable material. Deformable blocks are subdivided into a mesh of finite difference elements, and each element responds according to a prescribed linear or nonlinear stress–strain law. The relative motion of the discontinuities is also governed by linear or nonlinear force–displacement relations for the movement in both the normal and shear directions. 3DEC has several built-in material behavior models, for both the intact blocks and the discontinuities that permit the simulation of response, representative of discontinuous geologic or similar materials. 3DEC is based on a Lagrangian calculation scheme that is well-suited to model the large movements and deformations of a blocky system [11, 12].

For the analysis of the stress response of the rock during and after excavation, a three-dimensional model of the caverns and appurtenant structures was prepared and geological conditions encountered during the excavation were incorporated in it (Fig. 3). The excavation was simultaneously carried out in the powerhouse and transformer hall caverns. The actual sequence as adopted during the excavation was modeled in the analysis (refer Fig. 4 and Table 8). The support system was optimized and validated during progressive analysis. The support system incorporated in the analysis is given in Table 9.

The rock mass properties for the model were determined from the Geological Strength Index (GSI) determined along the caverns as suggested by Hoek [2] and modified by Hoek and Brown [13], Hoek et al. [14], Sonmez and Ulusay [15], and Marinos and Hoek [16] and the data obtained from laboratory and in situ testing of the rock mass in accordance with the method suggested by Hoek et al. [17] and Hoek and Diederiches [18]. The rock mass properties incorporated in the analysis are given in Table 10.

Table 8 Benching sequence adopted for simulation of 3DEC numerical modeling

Stage-I	Excavation of crown (up to El. 1044 in MCH (P1, P2, and P3) and El. 1048.6 in THC (T1, T2, and T3))
Stage-II	Bench-I, El. 1044–1041 m in MHC (P4, P5, and P6) and El. 1048.6–1045 m in THC (T4, T5, and T6)
Stage-III	Bench-II, El. 1038–1035 m in MHC (P7) and El. 1045–1042 m in THC (T7)
Stage-IV	Bench-III, El. 1038–1035 m in MHC (P8) and El. 1042–1039 m in THC (T8)
Stage-V	Bench-IV, El. 1035–1032 m in MHC (P9) and El. 1039–1036 m in THC (T9)
Stage-VI	Bench-V, El. 1032–1029 m in MHC (P10) and El. 1036–1033 m in THC (T10)
Stage-VII	Bench-VI, El. 1029–1026 m in MHC (P11) and El. 1033–1030 m in THC (T11)
Stage-VIII	Bench-VII, El. 1026–1023 m in MHC (P12) and El. 1030–1028 m in THC (T12)
Stage-IX	Bench-VIII, El. 1023–1020 m in MHC (P13) and bus ducts near THC
Stage-X	Bus ducts near MHC (P14)
Stage-XI	Bench-IX, El. 1020–1017 m in MHC (P15)
Stage-XII	Bench-X, El. 1017–1014 m in MHC (P16)
Stage-XIII	Bench-XI, El. 1014–1011 m in MHC (P17)
Stage-XIV	Bench-XII, El. 1011–1009 m in MHC (P18), along with turbine pits (P19)
Stage-XV	Excavation of penstocks, TRT manifolds, and drainage gallery (P20)

Table 9 Support system used for numerical analysis

Support system	Crown	Walls
Machine hall cavern		
Shotcrete	250-mm-thick SFRS	250-mm-thick SFRS
Rock bolts	36 mm dia. 7.5 m long @ 3 m C/C, 36 mm dia. 9 m long @ 3 m C/C, 36 mm dia. 12 m long @ 3 m C/C	36 mm dia. 12 m long @ 1.5 m C/C, along u/s and d/s wall and 36 mm dia. 7.5 m long @ 1.5 m C/C on gable end walls
Ribs	ISMB 350 @ 0.5 C/C from RD 0 to 35 and 100 to 155 m	
Transformer hall cavern		
Shotcrete	250-mm-thick SFRS	250-mm-thick SFRS
Rock bolts	36 mm dia. 7.5 m long @ 1.5 m C/C	36 mm dia. 9 m long @ 1.5 m C/C, along u/s and d/s wall and 36 mm dia. 7.5 m long @ 1.5 m C/C on gable end walls
Ribs	ISMB 350 @ 0.5 C/C from RD 0 to 20 and 60 to 120 m	

Table 10 Rock mass properties used for preparing model for 3DEC analysis

Rock mass type	UCS (MPa)	GSI	E_i (MPa)	m_b	s	a	C (MPa)	ϕ	E_m (MPa)
Quartzite	237	45	67,000	2.805	0.002	0.508	1.911	58.52	14,984.5
Pegmatite	128	45	42,000	4.067	0.002	0.508	1.549	57.38	9393.3
Schist	50	30	33,750	0.821	0.0004	0.522	0.597	37.39	2746.68
Shear zone/fracture zone	40	–	–	–	–	–	0.354	25.6	850

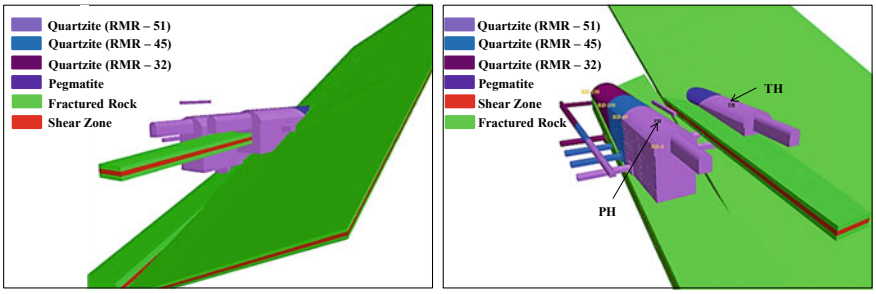

Fig. 3 3D model of the caverns showing the disposition of the shear and fracture zones

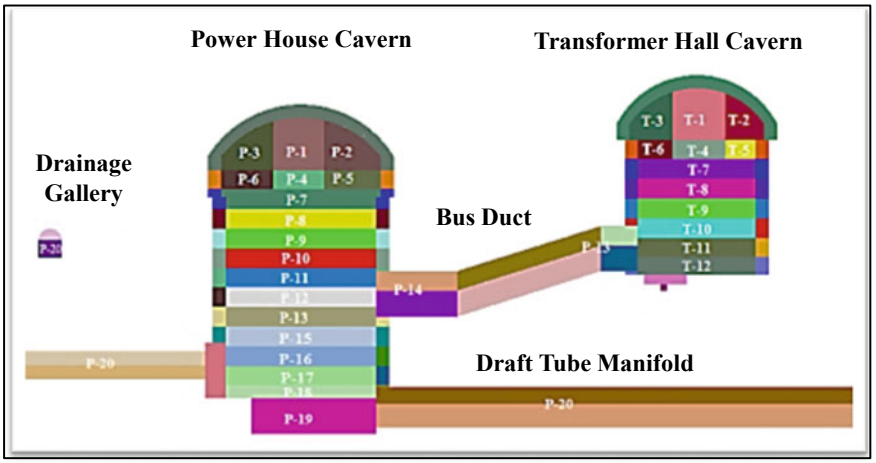

Fig. 4 Schematic section showing the excavation sequence adopted and incorporated in the model study

Based on the laboratory normal and shear stiffness data and the prevailing stress levels around the caverns, the following joint stiffness and joint shear strength parameters were calculated and used in the model.

- Joint normal stiffness: 50 GPa/m
- Joint shear stiffness: 0.6 GPa/m
- Joint cohesion: 0 MPa
- Joint friction: 40°.

5.2 Results of 3DEC Analysis

The three-dimensional numerical model was simulated with the input parameters and excavation sequence as discussed above. The behavior of the rock mass was evaluated based on the analysis by computing deformations at every 10 m RD and at different elevations as a function of excavation sequence, and corresponding factor of safety, using three-dimensional Hoek and Brown yield criteria as suggested by Melkoumian et al. [19]. The results of progressive analysis incorporating encountered and projected geological conditions carried out during the excavation of the caverns were discussed by Mishra et al., in 2015, 2016, and 2017 [1, 3–6]. In the current paper, the results of the final analysis incorporating the actual encountered geological conditions, excavation sequence as adopted, and the actual installed support system are discussed.

Displacements: The displacements at the crown of machine hall and transformer hall caverns are shown in Fig. 5a, b, while for the walls and floor, they are shown in Fig. 6a, b. The displacement at the center of the crown of the machine hall cavern varied from 3.1 mm (at RD 150 m) to 9.4 mm (at RD 70 and 80 m). Along the upstream side of crown, the displacements varied from 3.9 mm (at RD 150 m) to 11.2 mm (at RD 70 m), while along the downstream side of crown, it varied from 3.7 mm (at RD 150 m) to 8.8 mm (at RD 70 and 80 m). Along transformer hall cavern, the displacements varied from 5.5 mm (at RD 130 m) to 8.1 mm (at RD 90 m) at center crown, while along the upstream and downstream sides of crown, it varied from 4.8 mm (at RD 130 m) to 6.8 mm (at RD 10 m) and 5.8 mm (at RD 130 m) to 9.43 mm (at RD 90 m), respectively.

Along the upstream and downstream walls of powerhouse cavern, the magnitude of displacement varied from 7.75 mm (at RD 150 m, El. 1039.36 m) to 28.03 mm (at RD 80 m, El. 1031.06 m) and 8.15 mm (at RD 150 m, El. 1039.6 m) to 26.61 mm (at RD 70 m, El. 1039.4 m), respectively. The displacement along the upstream wall of transformer hall cavern varied from 13.71 mm (at RD 70 m, El. 1043.9 m) to

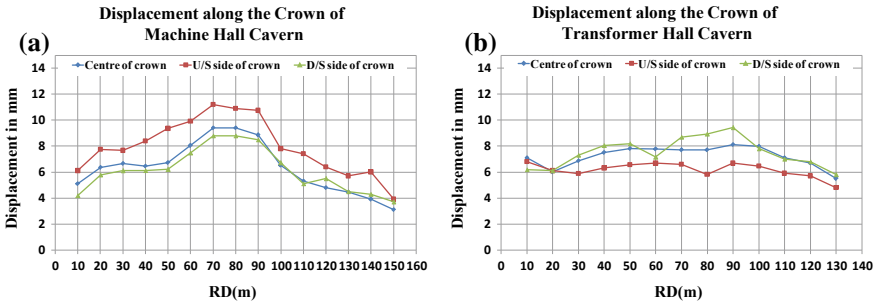

Fig. 5 Computed deformations along the crown of **a** machine hall cavern and **b** transformer hall cavern

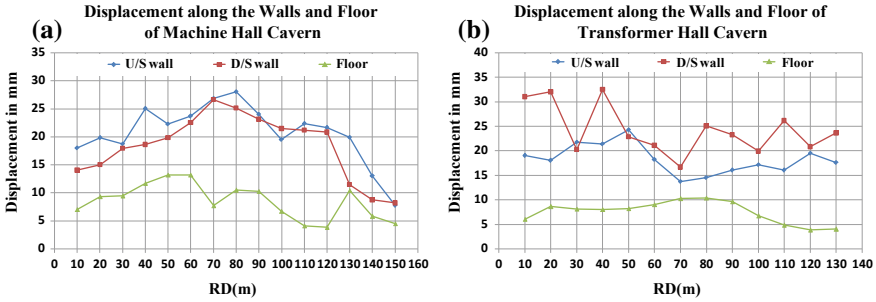

Fig. 6 Computed deformations along the walls and floor of **a** machine hall cavern and **b** transformer hall cavern

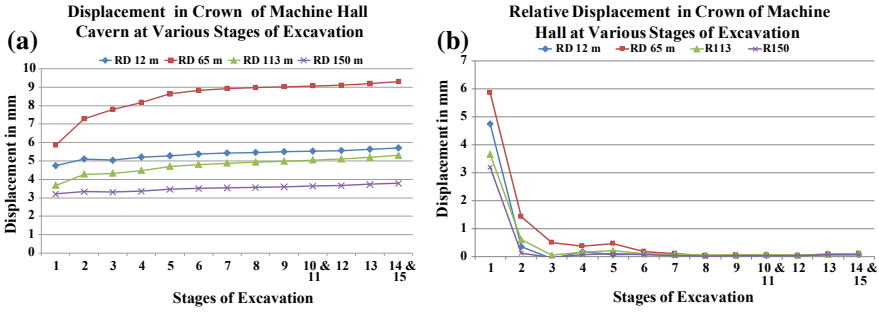

Fig. 7 Deformations along the crown of machine hall cavern **a** cumulative and **b** relative, at various stages of the excavation

24.3 mm (at RD 50 m, El. 1048.54 m), while that along the downstream wall varied from 16.63 mm (at RD 70 m, El. 1043 m) to 32.5 mm (at RD 40 m, El. 1048.4 m).

Displacements at Various Stages of the Excavation: The displacement inside the crown and walls of the caverns was obtained from the 3DEC analysis at the point of anchor/sensor of the installed MPBX (4, 7, 10 m in crown and 7, 14, 20 m along the walls). The three components of deformation, i.e., X-displacement (strike trending N 170°–350°), Y-displacement (strike trending N 080°–260°), and Z-displacement (trending vertical) at each stage of excavation, were obtained from the model analysis. The total deformation was computed as a resultant of these three components. For crown of machine hall cavern, deformations with various stages of the excavation were computed at RD 12, 65, 113, and 150 m, while for transformer hall cavern, they were obtained at RD 13, 55, 84 and 125 m. For the upstream and downstream walls of machine hall cavern, deformations were determined at RD 12, 65, 112, and 140 m at EL. 1039 m and at RD 12, 65, and 140 at El. 1029 m. For transformer hall cavern wall, deformations were computed for RD 13, 55, and 125 m at El. 1038.5. The graphical representation of deformations along the crown and walls of both the caverns is depicted in Figs. 7, 8, 9, 10, and 11.

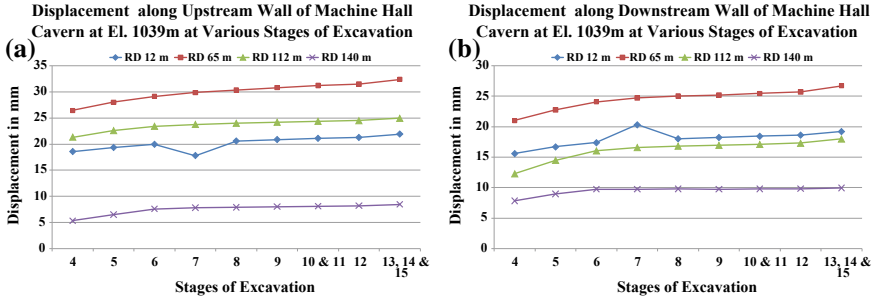

Fig. 8 Deformations along **a** upstream wall and **b** downstream wall, at El. 1039 m at various stages of the excavation

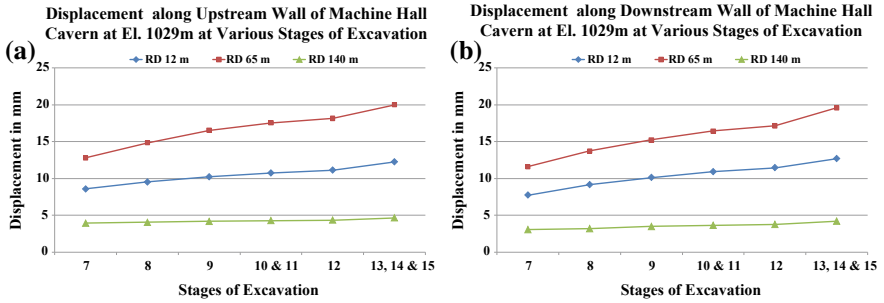

Fig. 9 Deformations along **a** upstream wall and **b** downstream wall, at El. 1029 m at various stages of the excavation

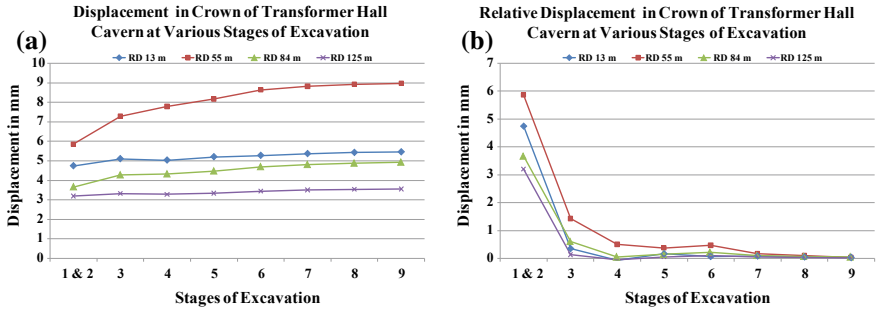

Fig. 10 Deformations along the crown of transformer hall cavern **a** cumulative and **b** relative, at various stages of the excavation

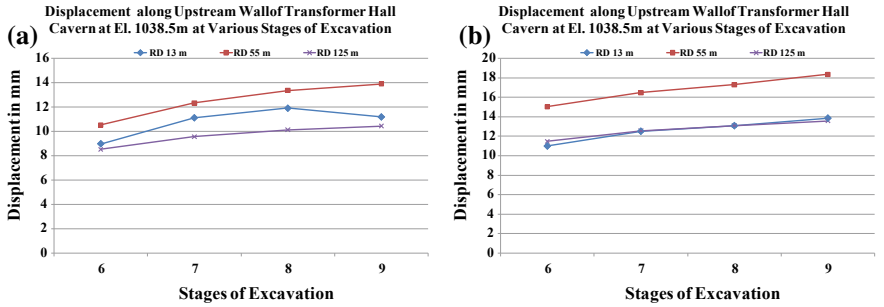

Fig. 11 Deformations along **a** upstream wall and **b** downstream wall, at El. 1038.5 m at various stages of the excavation

Displacements along Machine Hall Cavern: The deformations computed from the model studies along the crown of machine hall cavern at various stages of the excavation at the location of installed instruments are shown in Fig. 7a, b. Maximum deformation was obtained at RD 65 m, where a cumulative displacement of 9.3 mm was obtained after the complete excavation of the caverns. At RD 12, 113, and 150 m, the order of total deformations was 5.7, 5.3, and 3.78 mm, respectively. Higher deformations were obtained during the excavation of the crown part of the cavern, i.e., Stage-I and Stage-II. The gradually rising deformations were obtained till the excavation of the cavern up to El. 1029 m, i.e., up to Stage-VI after which the deformations tend to stabilize and followed an almost horizontal trend (Fig. 7a, b). The relative deformations after the excavation of Stage-VI were generally less than 0.1 mm.

Displacement obtained from the analysis along the upstream and downstream walls of the machine hall cavern at El. 1039 m is shown in Fig. 8a, b. Along the walls also maximum displacements were obtained at RD 65 m, where total displacements of 32.38 mm were obtained along the upstream wall and 26.69 mm along the downstream wall. Maximum deformations were observed to occur during the excavation from El 1038 to 1029 m, i.e., Stage-IV to VI, after which the deformations followed an almost horizontal trend. Displacements along the walls at El. 1029 m are depicted in Fig. 9a, b. Here also maximum deformations were observed at RD 65 m, where a deformation of 19.98 mm was obtained for the upstream wall and 19.58 mm for the downstream wall. Most of the deformations were observed during benching between El. 1029 and 1020 m.

Along the crown and walls of the machine hall cavern, maximum deformations were obtained at RD 65 m. In this regard, it is pertinent to mention that this location lies almost at the center of the area between rigid supports, i.e., steel rib support. As such, the higher deformations at this location were in general accordance with the stress distribution pattern of underground opening.

Displacements along Transformer Hall Cavern: Along the crown of transformer hall cavern, maximum cumulative deformation of 8.97 mm was obtained at RD 55 m after the complete excavation of the cavern. The deformations obtained at RD 13, 84,

and 125 m were of the order of 5.46, 4.93, and 3.56 mm, respectively (Fig. 10a, b). Maximum deformations were obtained during the excavation of the crown (Stage-I and Stage-II), i.e., excavation between El. 1056.5 and 1045 m, while deformation trend at RD 13, 84, and 125 m followed a horizontal trend after the excavation of the cavern up to El. 1043 (Stage-III). The deformations at RD 55 followed a gradually rising trend up to the excavation of Stage-VI, i.e., benching up to El. 1033 m.

The graphical representation of displacements for the wall of the transformer hall cavern at El. 1038.5 m is depicted in Fig. 11a, b. Here also maximum deformation along both the walls was obtained at RD 55 m, where a displacement of 13.91 mm was computed for the upstream wall and 18.37 mm for the downstream wall. Along the walls, maximum deformations were obtained during benching between El. 1036 and 1033 m, i.e., excavation of Stage-VI. The deformations along both the walls showed a gradually rising trend till the complete excavation of the cavern.

Factor of Safety: The model was considered to be elastoplastic with yielding of rock mass at failure. Three-dimensional principal stresses were obtained from the model after the final stage of excavation. These stresses along with strength parameters (m_b, s, a) were incorporated into 3DEC to obtain factor of safety (FoS) contours (Fig. 12) at every 10 m RD for the model by using FISH programming in 3DEC code, using the three-dimensional Hoek and Brown yield criterion as proposed by Melkoumian et al. [19] for the analysis of failure state.

The FoS plots revealed that the shear/fracture zone had low values (less than 1) indicating a failure in that zone. The pillar between the powerhouse and transformer hall cavern showed increased FoS due to the stitching of the bus duct with cross bolts in comparison with the model without cross-stitching them, though it did not have any significant impact on the FoS of the shear zone. However, it did not influence the overall stability of the caverns. The rock mass in the blast zone shows FoS close to 1. The rock mass beyond the blasting zone was found to have factor of safety of more than 2. In view of the low FoS obtained for the shear zone, longer rock bolts of 18 m length were used in the shear zone along with extensive grouting by the aid of 20-m-deep holes.

Performance of Support System: The performance of the installed support system was evaluated by obtaining the failure state of the rock bolts as shown in Fig. 13. It was observed that at some places, the bolts have reached the yield load of the rock bolts (shown in red color in Fig. 13). The cables installed along the crane beam and cross bolts installed to stitch the rock pillar between bus ducts have a positive effect on the behavior of the rock mass (stress distribution). The axial force distribution in cable anchors at crane beam and cross-stitching rock bolts along bus ducts is shown in Fig. 14. The axial force distribution in the steel ribs at the crown of machine hall and transformer hall caverns is shown in Fig. 15. The steel rib support is attributed toward the proper redistribution of the stress along the crown affected by the shear zone and other weak features. The same was also confirmed by instrumentation observation, where complete cessation of deformation was observed after the installation of steel rib support [4].

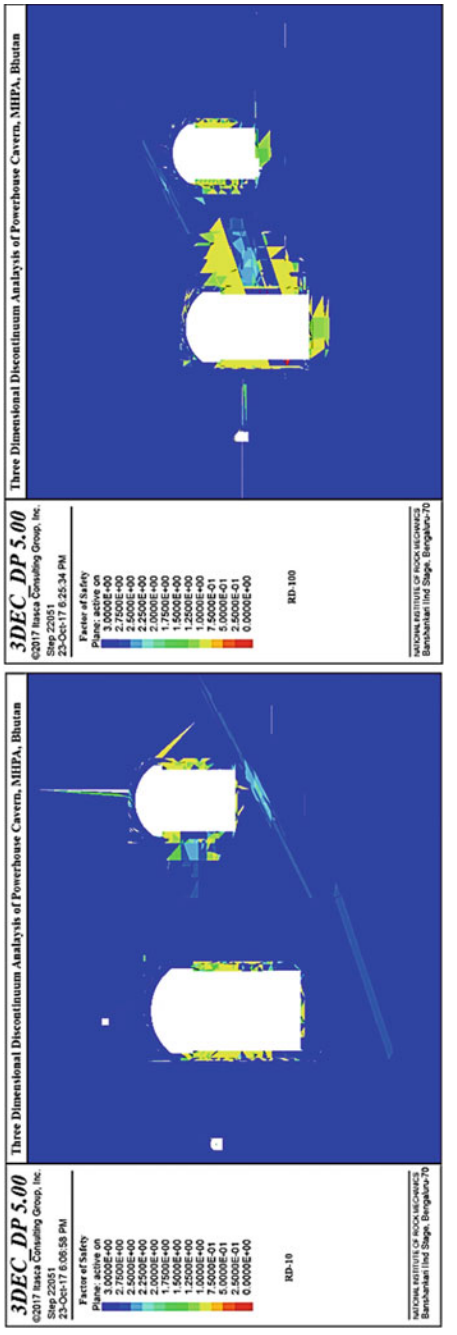

Fig. 12 Factor of safety contours at RD 10 and 100 m

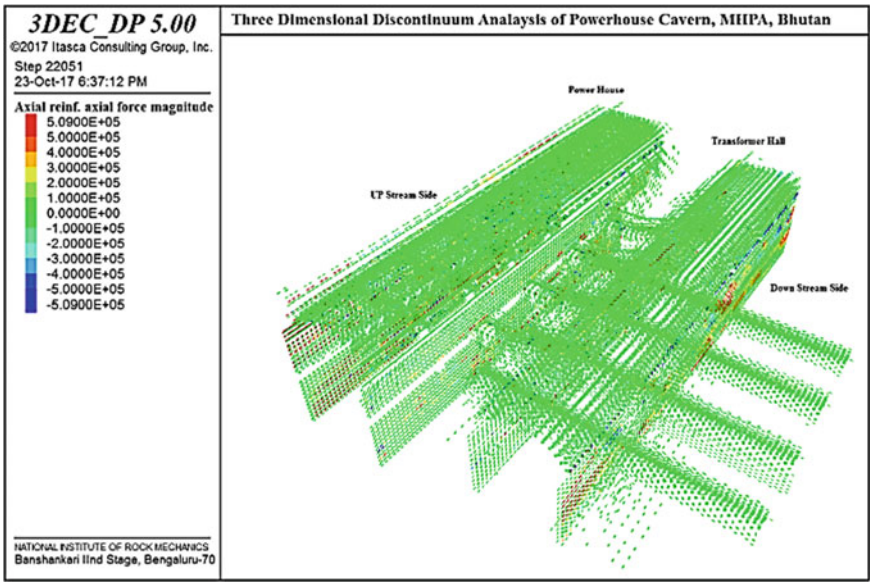

Fig. 13 State of rock bolts in the caverns

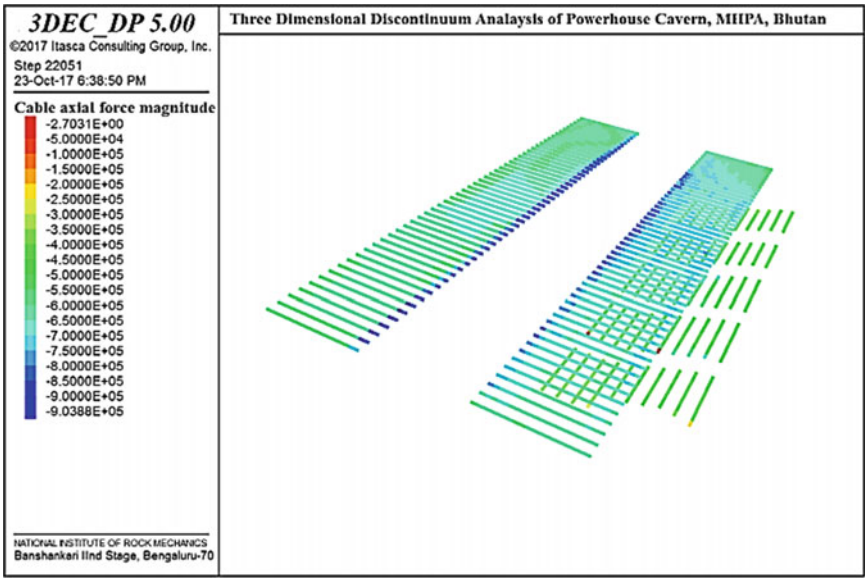

Fig. 14 Axial stress distribution in the cable anchors at crane beam and cross bolts along the bus ducts

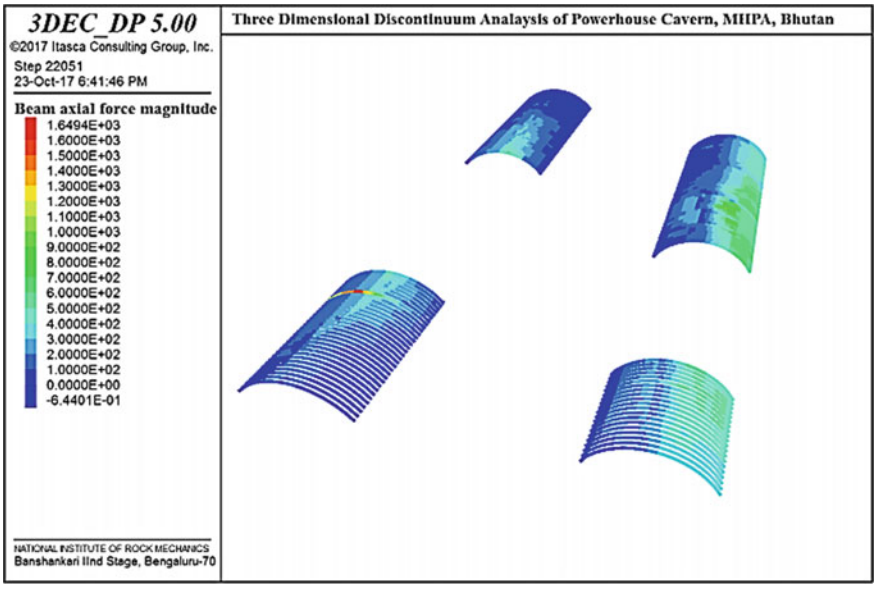

Fig. 15 Axial stress distribution in the steel ribs installed along the crown of the caverns

5.3 Comparison of 3DEC Modeling Results with Instrumentation

To monitor the behavior of the rock mass during the course of the excavation of the caverns, an elaborate and systematic geotechnical instrumentation program was implemented at the site. The data was regularly collected and analyzed. The observed deformations were regularly compared with the results of numerical analysis [4, 6]. The deformations obtained after the complete excavation of the caverns by 3DEC analysis are compared with those observed by installed MPBX along the crown and walls of the caverns and are discussed below.

Comparison of observed deformation with computed deformation along the crown of the caverns: The vertical component of deformation (Z-deformation) was obtained from the model at each sensor depth, i.e., 4, 7, and 10 m of installed MPBX, from which the relative deformation between two sensor depths was calculated and the total surfacial deformation was computed as the sum of the total deformation between various depths. Instrument data was analyzed to determine the observed deformation between two sensors, and the total observed surfacial deformation was computed as the sum of the deformation observed at various depths. The comparisons of observed deformations along the crown of machine hall and transformer hall caverns are given in Tables 11 and 12, respectively. The observed deformations along the crown of both the caverns were generally less than those computed from the numerical analysis, except at RD 113 m of machine hall cavern and at RD 12 m

Table 11 Comparison of observed deformation with computed deformations along the crown of machine hall cavern

Displacement in mm								
Depth	RD 12 m		RD 65 m		RD 113 m		RD 150 m	
	3D model	Inst. data	3D model	Inst. data	3D model	Inst. data	3D model	Inst. data
At crown	5.48	0.5	9.24	7.3	5.17	12.9	3.71	1.6
Between crown and 4 m	1.56	2.3	3.18	8.5	1.31	6.7	1.19	2.7
Between 4 and 7 m	3.69	−0.3	6.06	−3.9	3.86	−0.1	2.52	−0.5
Between 7 and 10 m	0.23	−1.5	0	2.7	0	6.3	0	−0.6

of transformer hall cavern, where higher deformations were observed as compared to computed displacements. This variation is attributed to delay in the installation of steel rib support at these chainages. In model simulation, the support system was installed concurrently to excavation; however, the steel rib support in actual was provided at least after nine to ten months of the excavation. It is also pertinent to mention that maximum deformation at these chainages was observed during the period between excavation and installation of the support system. After the installation of steel ribs along these chainages, deformations were completely arrested [4].

Comparison of observed deformation with computed deformation along the walls of the cavern: The horizontal component (X-component) of deformation along strike trending N 170°–350° was compared with the observed displacement recorded by installed MPBX along the upstream and downstream walls of the caverns. The comparison of both the walls of the caverns is discussed below.

Comparison of Observed Deformation with Computed Deformation along the Walls of the Machine Hall Cavern: The displacement observed and obtained from the model study along the upstream and downstream walls of the cavern at El. 1039 and 1029 m is summarized in Tables 13, 14, 15, and 16. The displacements recorded along the upstream wall at both the levels were generally lower than those obtained from the analysis, while along the downstream wall, the observed deformations were higher than the calculated deformations. The variation along the upstream wall may be attributed to delay in the installation of instruments, which are generally installed after three to four days of the excavation, and some part of the deformation was lost during that period. The higher displacement along the downstream walls may be due to the variation of the geological conditions (attitude of shear, its thickness, pinching and swelling nature of the weak feature, localized variation in geotechnical

Table 12 Comparison of observed deformation with computed deformations along the crown of transformer hall cavern

Displacement in mm								
Depth	RD 13 m		RD 55 m[a]		RD 84 m		RD 125 m	
	3D model	Inst. data	3D model	Inst. data	3D model	Inst. data	3D model	Inst. data
At crown	6.98	18.1	7.89	7.9	6.9	9.7	6.18	11.2
Between crown and 4 m	3.45	16.3	2.19	8.2	1.19	−0.5	1.38	8.1
Between 4 and 7 m	3.53	−1.3	2.66	−1.2	4.15	7.5	4.80	−0.5
Between 7 and 10 m	0	3.1	3.04	0.9	1.56	2.7	0	3.6

[a]Deformation computed at 5 m, 10 and 5 m and surface and 5 m

Table 13 Comparison of observed deformation with computed deformations along the upstream wall at El. 1039 m

Displacement in mm								
Depth	RD 12 m		RD 65 m		RD 113 m		RD 140 m	
	3D model	Inst. data	3D model	Inst. data	3D model	Inst. data	3D model	Inst. data
At crown	21.7	–	32.31	4.3	24.96	22.4	8.29	7.7
Between crown and 7 m	16.89	–	23.33	2.5	18.95	5.2	4.93	7.9
Between 7 and 14 m	4.74	–	8.78	1.6	5.91	15.7	3.54	−0.7
Between 14 and 20 m	0.07	–	0.2	0.2	0.1	1.5	−0.18	0.5

properties of rock mass and rock, and groundwater conditions) inside the wall which may not be accurately projected into the model.

Comparison of Observed Deformation with Computed Deformation along the Walls of Transformer Hall Cavern: Along the walls of the transformer hall cavern, instruments (MPBX) were installed at RD 13, 55, and 125 m at El. 1038.5 m. The comparison of calculated and observed displacements along both the walls of the cavern at El. 1038.5 m is summarized in Tables 17 and 18. The recorded displacements

Table 14 Comparison of observed deformation with computed deformations along the downstream wall at El. 1039 m

Displacement in mm								
Depth	RD 12 m		RD 65 m		RD 113 m		RD 140 m	
	3D model	Inst. data	3D model	Inst. data	3D model	Inst. data	3D model	Inst. data
At crown	18.98	32.9	26.59	32.8	17.92	18	9.89	−33.7
Between crown and 7 m	13.78	29.1	20.60	6.3	12.25	9.9	5.14	−4.1
Between 7 and 14 m	3.66	−0.6	3.73	25.9	2.77	7.7	4.04	−2.1
Between 14 and 20 m	1.54	4.4	2.26	0.6	2.90	0.4	0.71	−27.5

Table 15 Comparison of observed deformation with computed deformations along the upstream wall at El. 1029 m

Depth	RD 12 m		RD 65 m		RD 140 m	
	3D model	Inst. data	3D model	Inst. data	3D model	Inst. data
At crown	12.06	−39.7	19.89	10.7	3.65	4.6
Between crown and 7 m	6.03	0.5	9.12	7.7	0.27	3.6
Between 7 and 14 m	5.77	−0.6	10.53	1.6	3.4	−2.5
Between 14 and 20 m	0.26	−39.6	0.24	1.4	−0.02	3.5

Table 16 Comparison of observed deformation with computed deformations along the downstream wall at El. 1029 m

Depth	RD 12 m		RD 65 m		RD 140 m	
	3D model	Inst. data	3D model	Inst. data	3D model	Inst. data
At crown	12.49	32.55	19.48	53.1	1.53	−21.4
Between crown and 7 m	6.33	16.25	9.92	38.0	−0.17	−0.8
Between 7 and 14 m	3.82	13.6	6.12	0.7	1.16	2.2
Between 14 and 20 m	2.34	2.7	3.44	14.4	0.54	−22.8

Table 17 Comparison of observed deformation with computed deformations along the upstream wall of transformer hall

Depth	RD 13 m		RD 55 m		RD 125 m	
	3D model	Inst. data	3D model	Inst. data	3D model	Inst. data
At crown	10.96	0.9	13.9	2.2	10.14	4.1
Between crown and 7 m	7.47	0.4	10.18	1.3	6.2	3.1
Between 7 and 14 m	1.26	0.5	1.3	−0.3	2.64	1.3
Between 14 and 20 m	2.23	0.0	2.42	1.2	1.3	−0.3

Table 18 Comparison of observed deformation with computed deformations along the downstream wall of transformer hall

Depth	RD 13 m		RD 55 m		RD 125 m	
	3D model	Inst. data	3D model	Inst. data	3D model	Inst. data
At crown	13.77	5.6	18.21	1.4	13.49	3.7
Between crown and 7 m	7.3	1.5	10.81	1.3	7.16	1.6
Between 7 and 14 m	6.47	1.8	4.65	−0.5	6.33	−0.2
Between 14 and 20 m	0.0	2.3	2.75	0.6	0.0	2.3

were much less than those obtained from the numerical simulations. This may be attributed either to delay in the installation of instruments or the variation in geological conditions inside the walls which might have not been precisely projected into the numerical model.

6 Conclusion

Stress analysis of the underground powerhouse caverns of the Mangdechhu Hydroelectric Project was carried out at various stages of the excavation of the caverns to optimize the support system and excavation methodology. The recommendations based on the analysis were implemented during the construction of the caverns. The models were regularly updated based on the encountered geological conditions. The observed behavior of the rock mass in response to excavation was compared with the simulated response. 3DEC modeling results correlated well with the instrumentation data to a large extent. Deviation in some areas may be attributed to localized variation in prevailing geological conditions and strength of the rock mass and difference between the actual excavation time and the time of installation of the instruments.

The final three-dimensional model analyses well simulated the response of the rock mass surrounding the caverns with respect to change in stress conditions as a result of excavation. The model results showed that the support system provided along the caverns in form of shotcrete, rock bolts, steel ribs, cable anchors, and cross bolts between the bus ducts was adequate and enhanced the stability of the structures. With adequate support system, the factor of safety was more than 1 in most of the excavated area of the caverns. Some isolated areas in the blast-affected zone and major part of the shear zone had factor of safety of less than 1. However, these zones of low strength-to-stress ratio do not influence the overall stability of the caverns; the same was also confirmed by the instrumentation observations which did not show any alarming trends. Both the numeric model simulation and geotechnical instrumentation observation complimented each other and confirmed the stability of the caverns.

Acknowledgements The authors are thankful to the Director and Scientist of Numerical Modelling Division of National Institute of Rock Mechanics, Bengaluru, for conducting the analysis and providing valuable suggestions which helped in the optimization of the support system and excavation methodology of the caverns. I. Ahmed specially acknowledges the efforts of Mr. Sripad R. Naik, Head of Numerical Modelling Division, NIRM, for extending all the cooperation toward the finalization of the manuscript.

References

1. Mishra AK, Punetha P, Ahmed I (2017) Engineering design and construction of underground power house caverns of Mangdechhu Hydro-Electric Project (720 MW). In: Bhutan proceedings of the world tunnel congress 2017, Norway, pp 1073–1082
2. Hoek E (1994) Strength of rock and rock masses. ISRM News J 2(2):4–16
3. Mishra AK, Baidhya G, Punetha P, Krishna L, Ahmed I (2015) Numerical modeling and re-evaluation of support system while excavating underground cavern in weak rock. Spec Publ J Eng Geol 902–917
4. Mishra AK, Baidya G, Punetha P, Ahmed I, Krishna L (2015) Geotechnical instrumentation and monitoring of excavation of underground power house caverns of Mangdechhu Hydro-Electric Project. Spec Publ J Eng Geol 918–934
5. Mishra AK, Chaudhary RK, Punetha P (2016) Recent advances in rock engineering, advances in excavation, design and support methods: a case study of Mangdechhu project (Trongsa) Central Bhutan. In: Proceedings of recent advances in rock engineering (RARE 2016), Bengaluru, India, pp 67–76
6. Mishra AK, Chaudhary RK, Punetha P, Ahmed I (2017) Numerical modelling a tool to evaluate stability and support system of large underground caverns: a case study of underground power house caverns of Mangdechhu Hydro-Electric Project, Bhutan. In: Proceedings of INDOROCK 2017: 7th Indian rock conference, New Delhi, India, pp 442–455
7. Cornet FH (1986) Stress determination from hydraulic tests on pre-existing fractures—the HTPF method. In: Proceedings of international symposium rock stress and rock stress measurements. CENTEK Publications, Lulea, pp 301–311
8. ISRM (1979) Suggested methods for determining in situ deformability of rock. Int J Rock Mech Min Sci Geomech Abs 16(3):195–214
9. ISRM (1974) International society for rock mechanics, commission on standardization of laboratory tests: suggested methods for determining shear strength

10. International Society for Rock Mechanics (1981) Rock characterization, testing and monitoring. In: Brown ET (ed) ISRM suggested methods. Pergoman, Oxford, p 221
11. Anon (2013) 3-DEC version 5 manual. Itasca Consulting Group, Inc. USA
12. Ren LX, Kai N (2013) Research of an slope under rainfall and deep excavation conditions with UDEC. In: Applied mechanics and material, vol 353. pp 756–760
13. Hoek E, Brown E (1997) Practical estimates of rock mass strength. Int J Rock Mech Min Sci 34(8):1165–1186
14. Hoek E, Marinos V, Benissi M (1998) Application of Geological Strength Index (GSI) classification for very weak and sheared rock masses. The case of Athena schist formation. Bull Eng Geol Environ 57:151–160
15. Sonmez H, Ulusay R (1999) Modifications to the Geological Strength Index (GSI) and their applicability to stability of slopes. Int J Rock Mech Min Sci 36:743–760
16. Marinos P, Hoek E (2001) Estimating the geotechnical properties of heterogeneous rock mass such as flysh. Bull Eng Geol Environ 65:129–142
17. Hoek E, Carranza-Torres CT, Corkum B (2002) Hoek and Brown failure criterion-2002 edition. In: Proceedings of the fifth North American rock mechanics symposium, Toronto, Canada, vol 1, pp 267–273
18. Hoek E, Diederichs MS (2006) Empirical estimation of rock mass modulus. Int J Rock Mech Min Sci 43:203–215
19. Melkoumian N, Priest SD, Hunt SP (2009) Further development of the three-dimensional Hoek-Brown yield criterion. J Rock Mech Rock Eng 42(6):835–847

Enhancement of Sustainable Mortar by Using Fine Glass Powder

Anand B. Zanwar and Yogesh D. Patil

Abstract The amounts of waste glass have expanded after some time because of quick industrialization. Moreover, the majority of times has not reused this waste. Concrete is the most generally utilized development element, and the large measure of natural assets is needed to produce concrete. In this way, it is essential to examine the feasibility of reusing of material waste glass as ingredients during the production of mortar. This work describes the aftereffects of an examination directed to evaluate the likelihood of using waste glass powder (WGP) obtained from glass industries, as partial substitution of cement. The objective was to examine the effect of WGP on the fresh properties of mortar. The WGP replacement content is considered as 0, 10, 20, 30, and 40% by weight of cement. Based on the outcome, it is found that WGP shows pozzolanic characteristics. By using 20% WGP in the mortar, it was concluded that compressive strength increases by around 11%. This result indicates that the WGP has good pozzolanic reactivity. However, when the WGP replacement level increases, the setting time of cement mix decreases.

Keywords Fresh properties · Waste glass powder (WGP) · Cement replacement · Flowability · Compressive strength

1 Introduction

Concrete is a remarkable and critical auxiliary material in mankind's history. As composed by Brunauer and Copeland the [1], "Man expends no material aside from water in such huge amounts." It is presumed that with the advancement of human progress, concrete will keep on being a popular development material later on. The present-day cement industry, likewise, presents numerous ecological issues, for example, contamination, squander dumping, the outflow of hazardous gases, consumption of particular assets, and so forth.

A. B. Zanwar (✉) · Y. D. Patil
S V National Institute of Technology, Surat, India
e-mail: anandzanwar143@gmail.com

S. Kumar Shukla et al. (eds.), *Advances in Sustainable Construction Materials and Geotechnical Engineering*, Lecture Notes in Civil Engineering 35,
https://doi.org/10.1007/978-981-13-7480-7_5

Similarly, as industrialization quickly expanding and standard living are changing, the amounts of modern squanders have additionally expanded. To manage this circumstance, much consideration has been given toward the advancement of numerous kinds of development materials from industrial squanders [2]. Likewise, a few sorts of new waste are presently utilized as a part of assembling of an eco-accommodating element which supplants the conventional materials. Recycled materials in development are among the most alluring choices on account of vast amount, low-quality necessity, and broad of development. Among different kinds of modern waste, glass is viewed as the most reasonable substitute for a cementitious material because of its physical and chemical attributes [3, 4].

Being shapeless and containing a vast amount of silicate, the soda–lime glass may be used as cementitious material when it has a smaller particle size. Also, it shows the pozzolanic activity [5, 6]. The glass powder indicates pozzolanic activity at a particle size of around 300 μm. However, the WGP shows the maximum 90 days compressive strength than fly ash when a size of WGP is less than 100 μm [5, 7, 8].

As per the past investigations, it seems that the utilization of WGP in concrete production had logical inconsistencies in the available test outcomes. These logical inconsistencies included fresh properties of cement altered with WGP.

For fresh properties concern, Khatib [9] demonstrated that there was an efficient increment in the slump when WGP content in the blend increased. However, author did not discuss the size dissemination of utilized WGP. Aliabdo [10] declared not only the increase in the WGP increases the slump, but also that there is such a significant influence of WGP on the setting time of cement. Chikhalikar [11] explored the attributes of SFRC cement containing 600 μm WGP. The author states that the increase in concrete workability seen is maximum at about 40% WGP as cement substitution. Nasar [12] used processed 15 μm WGP and came about that workability is seems to be increased with an increase in process WGP.

On the contrary, Vandhiyan [13] discussed the utilization of WGP which negatively affects solid workability. Lu [14] explored that WGP increases the setting time. Subsequently, it is essential to think about the impact of WGP on the fresh properties of mortar when it is a substitution to cement.

2 Experimental Methods

2.1 Materials

Quartz sand is free from silt and a particle size is less than 2 mm as per IS 650:1991 [15] specification limits. The sieve size of sand conforms to IS 460 (Part 1):1985 [16]. The used ordinary Portland cement of grade 53 conforms to BIS 12269:1987 [17] is used. The used WGP had particle size finer than 18 μm and specific gravity of 2.25 in this investigation work. The chemical composition of Portland cement (PC)

Table 1 Chemical composition of used materials by XRF

	Cement	WGP
SiO_2	20.6	80.84
Al_2O_3	4.8	1.10
Fe_2O_3	3.5	0.04
CaO	64	7.50
MgO	0.1	0.38
K_2O	3.4	0.30
Na_2O	0.3	9.64
SO_3	0.3	0.20
Loss on ignition		0.8

Table 2 Proportions of different mortar mixes

Mix	Cement: WGP: Sand	W/cm
53C-0	1:0:3	0.35
53C-10	0.9:0.1:3	0.35
53C-20	0.8:0.2:3	0.35
53C-30	0.7:0.3:3	0.35
53C-40	0.6:0.4:3	0.35

and WGP is described in Table 1. The particle size of WGP is calculated by Blaine's air permeability method. For mixing and curing process, the potable water is used.

2.2 Experimental Parameters

In this research work, the fresh properties of mortar are discussed. This investigation includes Pozzolanic effect, setting time, flowability, and compressive strength.

This research presented the effects of WGP as a substituent to cement in the mortar is presented and considered 28 days compressive strength is considered. All the mixes are prepared with water–cementitious ratio of 0.35. For all the work the 0, 10, 20, 30, and 40% WGP replacement of cement is taken. Mix proportions of studied mortar mix is shown in Table 2. It ought to be noticed that control mortar has not contained the WGP as a perspective blend, and remaining mix proportioned with 10, 20, 30, and 40% of cement substituted by WGP obtained separately (namely as M-10%WGP, M-20%WGP, M-30%WGP, and M-40%WGP).

3 Results and Discussions

3.1 Consistency, Setting Time, and Soundness

The primary tests are performed to find the performance of cement. These tests include setting time, soundness, and compressive tests for the mortar. By calculating the water requirement for standard consistency, estimate the value of setting time and soundness. Figure 1 demonstrates the estimation of water necessity using the Vicat test method with various WGP cement substitution stages. When the replacement ratio of WGP increases, linear increment in water requirement is observed as shown in Fig. 1. Each 10% increase in the WGP cement substitution linearly increases in water requirement by approximately 7%. This behavior due to the finer size of the WGP is compared to the cement particle. Due to the increase in the surface area of the particle, the requirement of water increases.

The outcome of WGP toward initial and final setting time is described in Fig. 2. When a percentage of WGP level increases, it is seen that the setting time goes on decreases. The initial and final setting time linearly decreases compared to cement around 10 and 7.5%. The values of setting time satisfy the conditions of ASTM C 150 [18] and BIS 4031 (Part 5) [19].

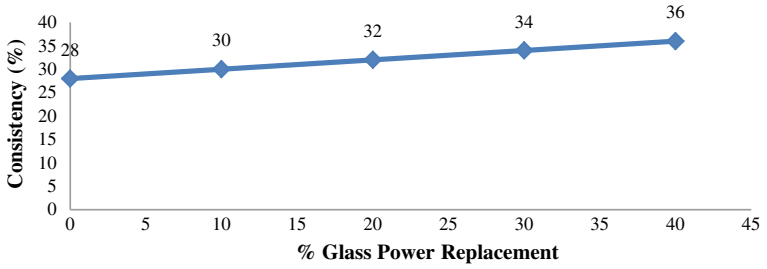

Fig. 1 Consistency for cement pastes altered by WGP as a cement substitute

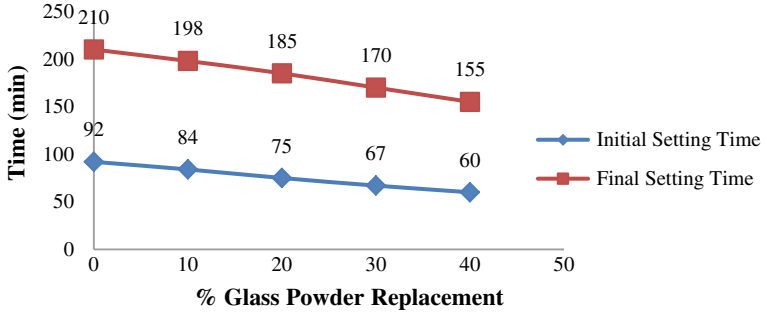

Fig. 2 Setting time for cement pastes altered by WGP as a cement substitute

Impact of utilization of WGP substituted to cement on the soundness method seems to be negligible. As per the provision of ASTM C150, the most significant permissible extensions are 10 mm, so all the tests with or without WGP fulfill the points of confinement of these benchmarks. This conduct affirms that no significant volume increased as an aftereffect regarding the nearness of WGP in the concrete paste. This conduct might occur because of a minimum value of chemicals like lime, magnesia, and sulfate percentage which is shown in Table 1.

3.2 Pozzolanic Effect on Mortar

The ASTM C 618 [20] mentioned some limits and conditions to use the WGP as a pozzolanic material. The requirements contain the addition of $SiO_2 + Al_2O_3 + Fe_2O_3$ higher than 70% and strength activity index (SAI) minimum of 75% of control mortar at curing of 7 and 28 days.

According to ASTM C 618 particular points of confinement, there are a few prerequisites for considering WGP as a pozzolanic material. These prerequisites incorporate physical and chemical properties. From Table 1, the chemical composition satisfies the points of confinement of ASTM C 618 of pozzolanic materials. Also, SAI is obligatory to use the WGP as pozzolanic materials. SAI at given age given by ASTM C 311 [21] is

$$\text{SAI} = \frac{\text{average compressive strength of blended cement mortar}}{\text{average compressive strength of control mortar bars}} \quad (1)$$

The SAI at ages of 7 and 28 days around 92 and 104% individually is presented in Fig. 4. From the result, it can be concluded that WGP of fineness 18 μm can be used as the pozzolanic material.

3.3 Flowability

The outcomes for the flow table test with different percentage variation of WGP mortar are presented in Fig. 3. The flow table test is performed as per the BIS code 1727:1967 [22]. In this test, keeping a constant flow of 110 mm is kept and the water content for a different variation of WGP is shown in the figure. It is understood that water content gets affected by the rise in the percentage of WGP in the mortar. Compared to the control mortar, the water content for 10 and 20% WGP mortar increases linearly by 4.76%, and for remaining each 10% increase in the percentage of WGP, it increases linearly around to 7%. The requirement of water content increases because of the smaller grain size and more surface area of WGP for the required flow.

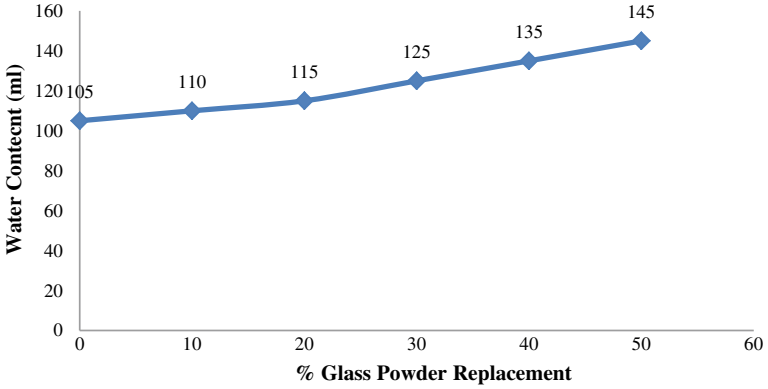

Fig. 3 Water content for mortar modified with WGP as a cement replacement keeping flowability of 110 mm

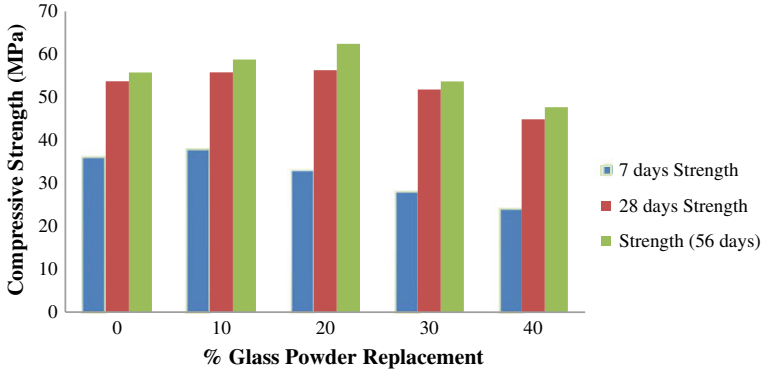

Fig. 4 Compressive strength of mortar mix grade 53 MPa

3.4 Compressive Strength Test

The test is performance of the test is as per ASTM C 109 [23] in which the individual compressive strength values are the mean of three specimens of size 50 × 50 × 50 mm, respectively. Figure 4 presents the outcomes of the compressive strength of various mixes having different percentage replacement of WGP as 0, 10, 20, 30, and 40%, respectively. It indicates that as the percentage replacement of WGP increases beyond 20%, the compressive strength of mortar decreases. Compared to control mortar, only 10% WGP mortar exceeded the compressive strength by 5.08% at seven days age. Similarly, for 28 and 56 days, just mortar containing 10 and 20% WGP had maximum strength compared to control mortar than 5.30 and 10.90%, respectively.

4 Conclusion

This research work evaluates the impact of WGP as a cementitious element on the fresh properties of the mortar. From the research, work conclusion can be drawn as:

- WGP material satisfies the points of confinement of pozzolanic material. The strength activity index is 92 and 104% at 7 and 28 days.
- Setting time of WGP goes on decreasing as the percentage of WGP level increases. Use of each 10% WGP decreases the initial and final setting time linearly about 10 and 7.5%, respectively. Soundness of WGP seems to be similar to unblended cement.
- Compared to the control mortar, the water content for 10 and 20% WGP mortar increases linearly by 4.76%, and for remaining each 10% increase in the percentage of WGP, it increases linearly around to 7%.
- The mortar containing 10 and 20% WGP had maximum compressive strength compared to control mortar than 5.30 and 10.90%, respectively. The remaining mortar had minimum compressive strength.

Acknowledgements The author would like to thank the help of Ambuja Cements Limited, Corporate Office, Andheri, Mumbai.

References

1. Brunauer S, Copeland LE (1964) The chemistry of concrete. Sci Am 210:80–93
2. Eisa A (2014) Properties of concrete incorporating recycled post-consumer environmental wastes. Int J Concr Struct Mater 8:251–258. https://doi.org/10.1007/s40069-013-0065-9
3. Tan KH, Du H (2013) Use of waste glass as sand in mortar: Part I—fresh, mechanical and durability properties. Cem Concr Compos 35:118–126. https://doi.org/10.1016/j.cemconcomp.2012.08.028
4. Shi C, Zheng K (2007) A review on the use of waste glasses in the production of cement and concrete. Resour Conserv Recycl 52:234–247. https://doi.org/10.1016/j.resconrec.2007.01.013
5. Shi C, Wu Y, Riefler C, Wang H (2005) Characteristics and pozzolanic reactivity of glass powders. Cem Concr Res 35:987–993. https://doi.org/10.1016/j.cemconres.2004.05.015
6. Shayan A (2002) Value-added utilization of waste glass in concrete. In: IABSE symposium, Melbourne, pp 1–11
7. Schwarz N, Cam H, Neithalath N (2008) Influence of a fine glass powder on the durability characteristics of concrete and its comparison to fly ash. Cem Concr Compos 30:486–496. https://doi.org/10.1016/j.cemconcomp.2008.02.001
8. Pereira-De-Oliveira LA, Castro-Gomes JP, Santos PMS (2012) The potential pozzolanic activity of glass and red-clay ceramic waste as cement mortars components. Constr Build Mater 31:197–203. https://doi.org/10.1016/j.conbuildmat.2011.12.110
9. Khatib JM, Negim EM, Sohl HS, Chileshe N (2012) Glass powder utilisation in concrete production. Eur J Appl Sci 4:173–176. https://doi.org/10.5829/idosi.ejas.2012.4.4.1102
10. Aliabdo AA, Elmoaty A, Elmoaty MA, Aboshama AY (2016) Utilization of waste glass powder in the production of cement and concrete. Constr Build Mater 124:866–877. https://doi.org/10.1016/j.conbuildmat.2016.08.016

11. Chikhalikar SM, Tande SN (2012) An experimental investigation on characteristic properties of fibre reinforced concrete containing waste glass powder as pozzolan a an experimental investigation on characteristic properties of fibre reinforced concrete containing. In: 37th conference our world concrete structures
12. Nassar RUD, Soroushian P (2012) Strength and durability of recycled aggregate concrete containing milled glass as partial replacement for cement. Constr Build Mater 29:368–377. https://doi.org/10.1016/j.conbuildmat.2011.10.061
13. Vandhiyan R, Ramkumar K, Ramya R (2013) Experimental study on replacement of cement by glass powder. Int J Eng Res Technol 2:234–238
14. Lu JX, Duan ZH, Poon CS (2017) Fresh properties of cement pastes or mortars incorporating waste glass powder and cullet. Constr Build Mater 131:793–799. https://doi.org/10.1016/j.conbuildmat.2016.11.011
15. BIS:650-1991 (1991) Standard sand for testing cement-specification. Bureau of Indian Standards, New Delhi, India
16. BIS:460 (Part 1)-1985 (1985) Specification for test sieves: wire cloth test sieves. Bureau of Indian Standards, New Delhi, India
17. 12269-1987, B. (1987) Specification for 53 grade ordinary Portland cement. Bureau of Indian Standards, New Delhi, India
18. ASTM C 150 (2018) Standard specification for Portland cement. Annual book of ASTM standards. https://doi.org/10.1520/c0150
19. BIS: 4031 (Part 5) (1988) Methods of physical tests for hydraulic cement part 5 determination of initial and final setting times methods of physical tests for hydraulic cement part 5 determination of initial and final setting times. Bureau of Indian Standards, New Delhi, IndiaTest
20. ASTM C 618 (2017) Standard specification for coal fly ash and raw or calcined natural pozzolan for use. Annual book of ASTM standards. https://doi.org/10.1520/c0618
21. ASTM C 311 (2017) Standard test methods for sampling and testing fly ash or natural pozzolans for use. Annual book of ASTM standards. https://doi.org/10.1520/c0311
22. BIS:1727-1967 (1967) Methods of test for pozzolanic materials. Bureau of Indian Standards. New Delhi, India
23. ASTM C 109 (2016) Standard test method for compressive strength of hydraulic cement mortars (using 2-in. or [50-mm] cube specimens). Annual book of ASTM standards. https://doi.org/10.1520/c0109

Characteristics of Concrete Prepared with Metakaolin and Recycled Coarse Aggregates

Rakesh Muduli and Bibhuti Bhusan Mukharjee

Abstract The study tries to demonstrate the effect of metakaolin to enhance the qualities of concrete prepared with natural coarse aggregates (NCAs) and recycled coarse aggregates (RCAs). Recycled aggregate concrete (RAC) mixes are made by substituting NCA with 100% RCA and ordinary Portland cement with 10, 15 and 20% metakaolin. The workability of fresh concrete mixes is evaluated by slump test. Mechanical properties of concrete are evaluated by means of compressive strength, splitting tensile strength and flexural strength after 28-day curing, and the corresponding results are collated with reference concrete. The outcomes of the study indicate that the compressive strength as well as splitting tensile and flexural strength decrease when natural aggregates are replaced with 100% RCA. However, the use of metakaolin up to 15% enhances the properties of both natural and recycled aggregate concrete. The recycled aggregate concrete mixes show optimum performance at 15% metakaolin replacement level and hence can be used in practical fields.

Keywords Compressive strength · Construction and demolition (C&D) · Flexural strength · Metakaolin · Recycled coarse aggregate · Split tensile strength

Acronyms

BIS	Bureau of Indian Standard
CS	Compressive Strength
CSH	Calcium silicate hydrate
FTS	Flexural Tensile Strength
MK	Metakaolin
NAC	Natural aggregate concrete

R. Muduli (✉) · B. B. Mukharjee
Veer Surendra Sai University of Technology, Burla 768018, Odisha, India
e-mail: babul.rakesh7@gmail.com

B. B. Mukharjee
e-mail: bibhuti.2222@gmail.com

S. Kumar Shukla et al. (eds.), *Advances in Sustainable Construction Materials and Geotechnical Engineering*, Lecture Notes in Civil Engineering 35,
https://doi.org/10.1007/978-981-13-7480-7_6

NCAs Natural coarse aggregates
NFAs Natural fine aggregates
OPC Ordinary Portland cement
RAC Recycled aggregate concrete
RCAs Recycled coarse aggregates
SEM Scanning Electron Microscope
STS Splitting Tensile Strength

1 Introduction

The extensive utilization of concrete as a construction material serves as the main reason for exhaustion of natural resources, since aggregates, which occupy a large volume of concrete, are derived from nature; therefore, several countries across the globe are confronting intense deficiency of natural aggregates. Again, enormous quantities of C&D wastes are produced due to the collapse or demolition of buildings, roads and various civil engineering structures. A large extent (approximately 40%) of these C&D wastes consists of waste concrete [1]. These wastes if not properly balanced may cause various issues like scarcity of landfill space, environmental pollution, vast resource dissipation and increase the transportation and disposal costs [2, 3]. Therefore, recycling of discarded waste concrete and generating RCA present a viable solution to the aforementioned issues. The RCA, which is obtained by crushing, screening and sieving of waste concrete, is composed of NCA and adhered mortar [4]. The concrete incorporating these RCAs is known to be RAC. Earlier research works have demonstrated that RCA possesses some inferior properties like high water absorption, low density, porous structure and lower strength than NCA as old mortar is attached to its surface [5]. Therefore, a substantial degradation in the properties of concrete is witnessed on using RCA in concrete [6]. Several techniques have been proposed by many investigators to enhance the qualities of RAC. Outski et al. [7] tried to improve the strength, carbonation resistance and chloride penetration resistance of RAC by adopting a double mixing method. Wang et al. [8] tried to modify the characteristics of RCA by soaking it in acetic acid initially and then by mechanical rubbing. Xuan et al. [9] adopted accelerated carbonation technique to strengthen RCA. Dilbus et al. [10] added 5 and 10% silica fume to upgrade the characteristics of concrete prepared with RCA. Kong et al. [11] adopted a triple mixing method in which the RCA surface is coated with pozzolanic materials. Another method to overcome drawbacks of RCA is the utilization of pozzolanic materials like metakaolin in RAC mix.

Limited research works have been undertaken to study the effect of metakaolin on RAC. Radonjanin et al. [12] stated that the CS and STS of RAC were enhanced by 13 and 6.5%, respectively, by replacing cement with 10% metakaolin. Kou et al. [13] detected an improvement in compressive as well as splitting tensile strength when 15% metakaolin was used in RAC containing 50 and 100% RCA. Singh and Singh [14] reported that use of 10% metakaolin in RAC showed better performance

in mechanical properties. Kapoor et al. [15] used 10% metakaolin with 20% fly ash in 100% RAC and observed that the shortcomings in properties of RAC can be compensated by using metakaolin.

Use of waste material like RCA in concrete production reduces the problems of waste management and facilitates the preservation of natural resources. The incorporation of metakaolin is very effective in improving the qualities of RAC, and the properties obtained are very close to that of NAC. Limited research works have been performed to demonstrate the behaviour of metakaolin in RAC. Moreover, the use of the only specified amount of metakaolin (10 or 15%) in RAC has been reported in the existing literature. The effect of different quantities of metakaolin on properties of RAC as well as the optimum percentage of metakaolin for better performance of concrete containing maximum quantity (100%) of RCA is yet to be addressed. Therefore, the present study aimed at determining the optimum percentage of metakaolin for production of concrete utilizing maximum quantity of RCA. Based on the above objective, a detailed experimental programme is carried out to examine the CS, STS and FTS of concrete containing RCA and metakaolin and hence popularize its use in practical field applications.

2 Experimental Programme

2.1 Materials

OPC of grade 43, sticking to the specifications of IS: 8112-1989 [16], was utilized for manufacturing concrete specimens. Metakaolin, utilized in the present experimental work, was procured from Kaomin Industries, Gujarat, India. The fineness and specific gravity of metakaolin were obtained as 12,600 cm^2/g and 2.64, respectively. The SEM micrograph of metakaolin is provided in Fig. 1, which indicates that metakaolin consists of fine particles of random size and geometry having rough surface texture. The chemical composition of metakaolin was determined and furnished in Table 1. From Table 1, it is seen that the major compounds present in metakaolin are silica and alumina which are responsible for the pozzolanic properties of metakaolin particles. Standard tests were performed in the laboratory to find out various physical and mechanical properties of cement like consistency, specific gravity, fineness, setting time and mortar strength at 28 days, according to BIS specifications, and the results of the same are provided in Table 2.

Table 1 Chemical composition of metakaolin

Compounds	SiO_2	Al_2O_3	Fe_2O_3	CaO	MgO	Na_2O	K_2O	TiO_2	Loss on ignition
Content (%)	53.56	41.5	1.38	0.03	0.02	0.18	0.76	1.54	0.8

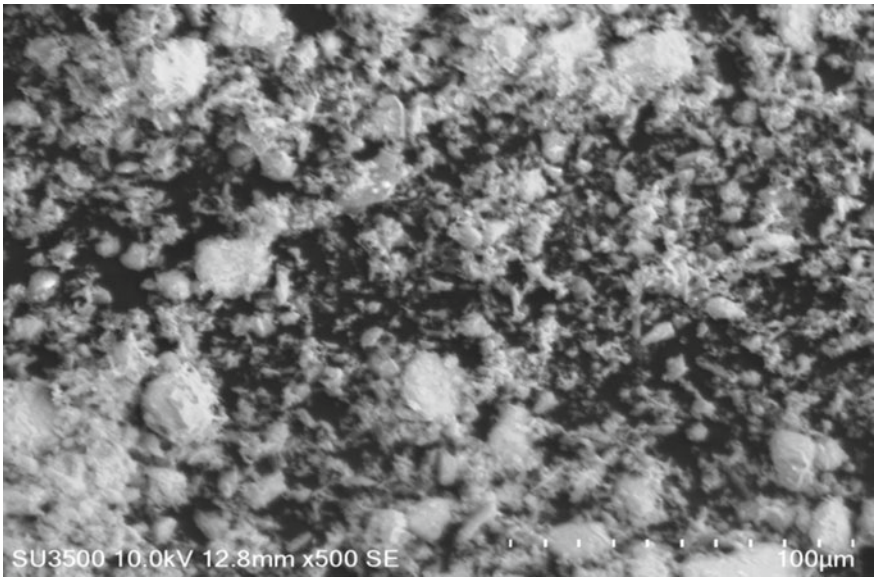

Fig. 1 SEM micrograph of Metakaolin

Table 2 Characteristics of cement

Consistency (%)	Specific gravity	Fineness (cm^2/gm)	Setting times (min)		Strength of mortar (MPa)		
			Initial	Final	3 days	7 days	28 days
32	3.15	3200	65	275	24.23	33.53	45.30

Clean river sand of grading zone II conforming to IS: 383-1970 [17] was utilized as NFA in the present investigation. The RCAs were collected by crushing the large concrete pieces obtained from the roof of a razed building near locality, and NCAs were collected from a local dealer. The nominal size of both RCA and NCA was maintained 20 mm. The grading analysis of coarse aggregates (NCA and RCA) and fine aggregate was carried out by following the procedures of IS: 2386-1963 [18], and the results are illustrated in Figs. 2 and 3, respectively, with the limits specified by IS: 383-1970 [17]. The other mechanical as well as physical properties of NFA, NCA and RCA were found out according to IS: 2386-1970 [19], and the results of the same are presented in Table 3. Normal tap water conforming to IS: 10500-2012 [20] was utilized for producing concrete specimens.

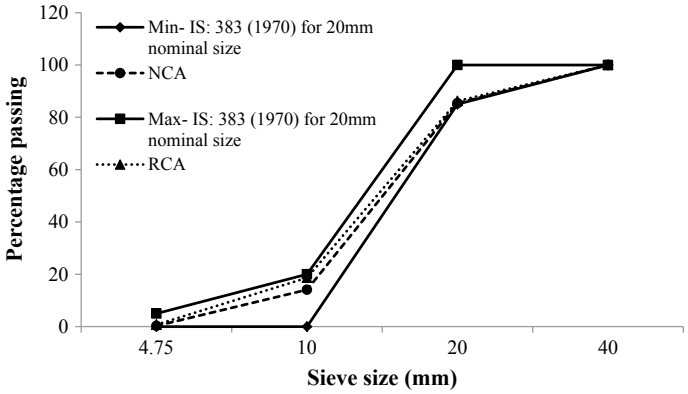

Fig. 2 Grading analysis curve of NCA and RCA

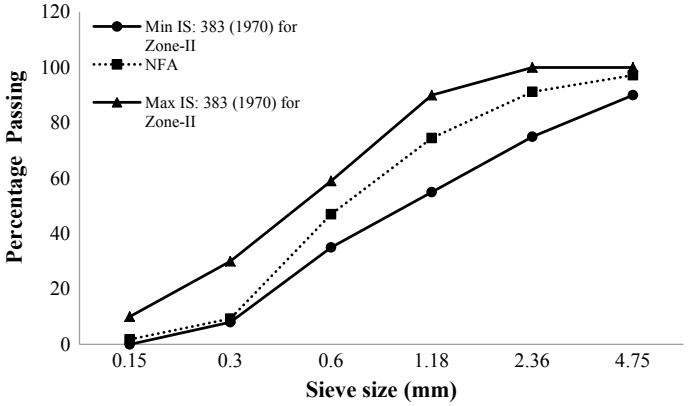

Fig. 3 Grading analysis curve of NFA

Table 3 Properties of aggregates

Type of aggregates	Specific gravity	Fineness modulus	Bulk density (kg/m^3)		Impact value (%)	Abrasion value (%)	Crushing value (%)	Water absorption (%)
			Loose	Compact				
NFA	2.63	3.21	1548	1666	–	–	–	0.8
NCA	2.85	6.95	1577	1792	17.28	14.3	20.5	0.36
RCA	2.35	7.00	1336	1505	32.4	20.23	29.2	4.32

2.2 Concrete Mix Proportion

The concrete mixes were prepared by substituting NCA with 100% RCA by volume and to study the influence of metakaolin, the OPC was partially substituted with 10, 15 and 20% metakaolin. The design of all concrete mixes was undertaken for M30 grade according to the procedures of IS: 10262-2009 [21]. The water-to-binder ratio was taken as 0.43, and slump of all concrete mixes was kept within 70–90 mm. The concrete mixes were designed by assuming the aggregates to be in surface saturated dry (SSD) condition. However, while casting air dried aggregates were used. Therefore, to compensate the water absorption of air dried aggregates and to bring these into SSD condition, additional water was added during mixing based on the water absorption as well as free surface moisture of the aggregates so that the slump is maintained within the desired range (70–90 mm). The quantities of various ingredients required per 1 m^3 of concrete are provided in Table 4.

2.3 Specimen Production, Curing and Testing

For each concrete mix, three 150-mm cubes, 150-mm-diameter cylinders and 100 × 100 × 500 mm prisms were casted and kept under water for curing at 27 ± 2 °C temperature for 28 days. The CS of cubes and STS of cylindrical specimens were tested in compressive strength testing machine of 2000 kN capacity after 28-day curing in accordance with BIS specifications. The FTS of prisms was determined in flexural strength testing machine of 1000 kN capacity. While carrying out flexural strength testing, the rate of loading was maintained according to IS: 516-1959 [22].

3 Results and Discussion

3.1 Workability

The workability of fresh NAC and RAC containing different quantities of metakaolin is evaluated in terms of slump and provided in Table 4. It is seen that the slump of concrete mix containing only NCA is 75 mm which rises to 88 mm when NCA is substituted by 100% RCA. The higher value of the initial slump for RAC mixes is because of the presence of extra water added during mixing to meet the water demand of RCA. However, later this water gets absorbed by RCA and hence does not affect the hydration and strength development of concrete. The incorporation of metakaolin at 10, 15 and 20% by weight of cement in NAC reduces the slump slightly to 72, 72 and 70 mm, respectively. Similarly, when 10, 15 and 20% metakaolin is used in RAC the slump value reduces to 86, 85 and 81 mm, respectively. The lower value of slump for metakaolin blended concrete mixes is due to the finer particles of metakaolin

Table 4 Mix proportions of concrete mixes per 1 m^3 of concrete

Mix	MK (%)	RCA (%)	Cement (kg)	MK (kg)	NFA (kg)	NCA (kg)	RCA (kg)	Water (kg)	Slump (mm)
NA1	0	0	420	0	668	1232	0	181	75
NA2	10	0	378	42	668	1232	0	181	72
NA3	15	0	357	63	668	1232	0	181	72
NA4	20	0	336	84	668	1232	0	181	70
RA1	0	100	420	0	668	0	1016	207	88
RA2	10	100	378	42	668	0	1016	207	86
RA3	15	100	357	63	668	0	1016	207	85
RA4	20	100	336	84	668	0	1016	207	81

possessing higher surface area. Since the reduction in slump is very less, the use of metakaolin in concrete does not have a significant effect on workability of concrete.

3.2 Compressive Strength

The cube CS of NAC and RAC with metakaolin after 28 days is furnished in Fig. 4. It is found that the CS of control mix (without RCA and metakaolin) is 40.43 MPa. When metakaolin is used at 10, 15 and 20% replacement level in NAC, the CS increases to 44.48, 45.36 and 43.82 MPa, respectively. This shows that the CS of NAC mixes is enhanced by 10, 12.2 and 8.4% with respect to control mix by using 10, 15 and 20% metakaolin in NAC, respectively. The CS of RAC mix containing only 100% RCA is 32.35 MPa which is 20% less than the CS of control mix. This strength degradation of RAC mix is generally associated with the lower properties of RCA like high water absorption, porous and week microstructure, and lower bond strength [23]. The reduced CS of RAC mixes is observed to be compensated by adding metakaolin. It can be seen that on adding 10, 15 and 20% metakaolin to fully RAC, the compressive strengths are increased to 36.22, 38.05 and 35.31 MPa, which are 12, 17.6 and 9.1% higher than RAC without MK, respectively. This enhancing effect of MK in both RAC and NAC is attributed to the pozzolanic and filler effect of MK. Again it can be visualized from the aforesaid figure that the strength-enhancing effect of MK is more pronounced in case of RAC than NAC. This trend may be because of the presence of huge amount of pores in RCA than NCA. When MK is added, the hydration products (CSH gel) resulting from the pozzolanic reaction of MK with $Ca(OH)_2$ enhance the strength and fills the micro-cracks to improve the properties of RAC. Again a part of fine particles of MK enters into the pores and causes pore refinement [24]. Moreover, significant strength development in RAC is achieved at 15% metakaolin replacement level, which is very close to the control mix. Hence RAC can suitably be used by completely substituting NCA with RCA at this percentage.

3.3 Splitting Tensile Strength

Figure 5 depicts the result of STS of cylindrical specimens of different concrete mixes. It is reported that the mix without RCA and metakaolin has a STS of 3.16 Mpa, which is enhanced by 8.5, 7.3 and 3.2% by replacing cement with 10, 15 and 20% MK, respectively. At 100% replacement, the STS of RAC mix is reduced to 2.68 MPa, which is 15.2% lower than the control mix. The decline in STS of RAC mix is caused by the lower properties of RCA, due to the existence of residual mortars on its surface [25]. However, when 10, 15 and 20% MK is incorporated into RAC mix, the STS is found to be enhanced by 10.4, 15.7 and 9%, respectively. This STS improvement of both NAC and RAC may be due to the strengthening of microstruc-

ture of ITZ and improvement in bonding of RCA with new cement paste caused by the pozzolanic effect of MK [24]. It can be noticed that the rate of strength improvement is more in RAC than NAC. The NAC mix attains maximum strength at 10% MK replacement percentage, whereas for RAC mix, the corresponding percentage is 15%. This behaviour may be because of the presence of more pores and micro-cracks in RCA which requires higher quantities of MK for its improvement. The STS at 15% replacement level is only 1.9% less than the control concrete, which confirms the suitability of use of RAC in concrete production with MK. At higher percentage of MK, the strength improvement is very poor, which may be due to the lack of $Ca(OH)_2$ for pozzolanic reaction of metakaolin and the presence of unhydrated MK particles inside concrete.

3.4 Flexural Strength

The development of FTS of both RAC and NAC at 28 days with MK percentage is illustrated in Fig. 6. The FTS of control mix is observed to be 4.59 MPa, which becomes 5.06, 4.98 and 4.78 MPa for 10, 15 and 20% MK replacement level, respectively. Again it is seen that the FTS is reduced by 15% to a value of 3.9 MPa when NCA is substituted with RCA. This decrease in FTS value is caused by poor bond strength and weak transition zone between RCA and new cement matrix [26]. Furthermore, the strength enhancement of RAC could be achieved by incorporating MK in RAC. The outcomes of the investigation show that on replacing MK at dosages of 10, 15 and 20%, the FTS is improved by 11.3, 13.8 and 10%, respectively. The strength improvement of both RAC and NAC is caused due to the strengthening of the

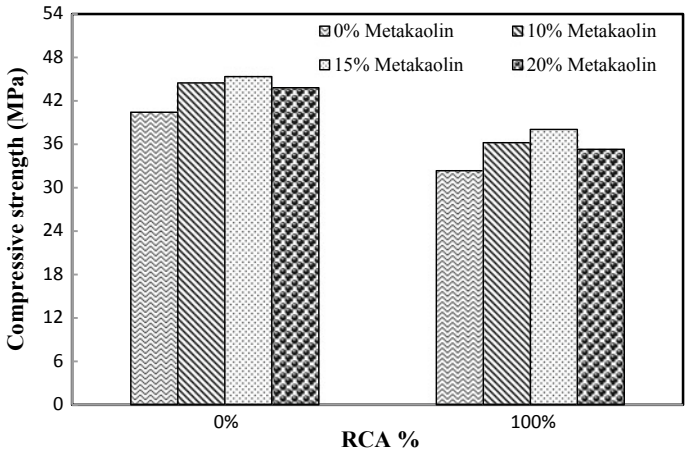

Fig. 4 CS of concrete mixes at 28 days

microstructure and the refinement of pore by the hydration products formed during the reaction of MK with $Ca(OH)_2$. Similar to STS, the rate of strength improvement is more for RAC than NAC. The maximum FTS for NAC is obtained at 10% MK, while for RAC it is obtained at 15% MK replacement level. The FTS of RAC at 15% MK is very close to that of control mix. For a higher percentage of MK, the rate of strength development decreases.

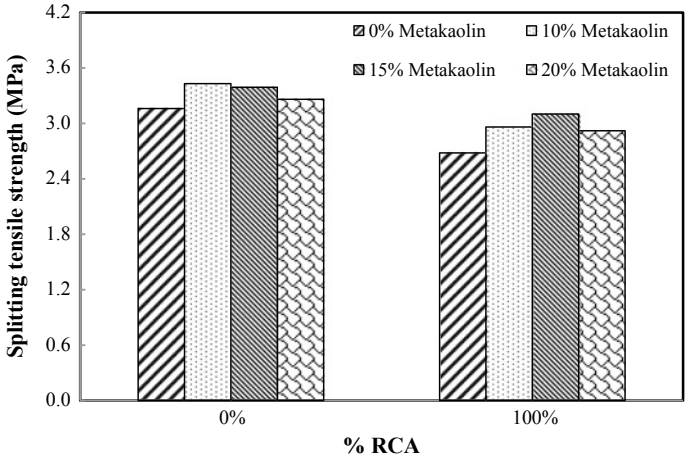

Fig. 5 STS of concrete mixes at 28 days

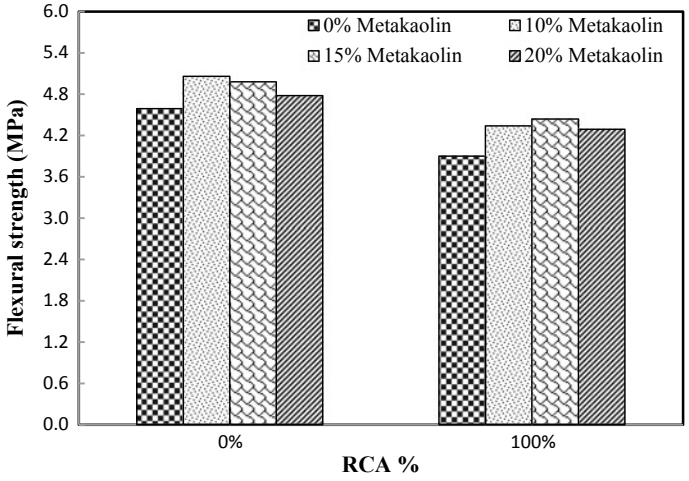

Fig. 6 Variation of 28-day flexural strength

3.5 *Comparative Study Between the Present Results and Previous Findings*

Though the research works incorporating RCA and metakaolin in concrete are limited, a comparative study has been conducted between the results of several available literature [12–15] and the present results. It is reported by Kou et al. [13] that the improvement in 28-day compressive strength of concrete containing 100% RCA and 15% metakaolin is 8.16% while the same for the present study is 17.6%. This shows that better performance in CS is observed for the present study than those of Kou et al. [13], which may be due to the use of high-quality RCA and metakaolin in the present study. Similarly, the improvement in CS of concrete mixes prepared with 100% RCA and 10% metakaolin, as reported by Singh and Singh [14], Kapoor et al. [15] and Radonjanin et al. [12], is 3.6, 11.46 and 13.12%, respectively, while the corresponding value for the present study is found as 12%. This indicates that the present result is consistent with the previous findings except for the results of Singh and Singh [14]. Similarly, the enhancement in STS of concrete mixes containing 100% RCA and 15% metakaolin is 17.3% for the work performed by Kou et al. [13] while it is 15.7% for the present study. This indicates that the STS results of the present study are comparable with the result of Kou et al. [13]. Moreover, for concrete mixes with 100% RCA content and 10% metakaolin, the improvement in STS is 6.45%, as reported by Radonjanin et al. [12] while better result (10.4%) is obtained for the present study.

4 Conclusion

The present investigation has been performed to access the effect of varying percentage of metakaolin on properties of both NAC and RAC. For this experimental work, 10, 15 and 20% MK are used as a partial substitution of cement in both NAC and RAC mixes. Workability and mechanical properties of the aforementioned mixes have been determined. The conclusions obtained after analyzing the experimental outcomes are stated as follows:

- The compressive strength as well as split and flexural tensile strength of concrete mixes decreases when NCA is replaced with RCA due to the lower properties of RCA like low density, high water absorption, higher porosity and lower crushing and impact value.
- The workability of RAC mixes is higher than NAC mixes due to the availability of extra water initially within the RAC mixture added to meet the water absorption of RCA. The use of metakaolin slightly reduces the slump value of both NAC and RAC due to higher surface area of metakaolin particles.
- The CS of NAC and RAC mixes is enhanced by replacing cement with 10–15% metakaolin. The use of 15% metakaolin enhances the CS of RAC to a maximum of 38.05 MPa which is very close to the CS of control mix.

- For NAC mixes, maximum enhancement in flexural and split tensile strength is observed at 10% metakaolin replacement level, whereas the same for RAC mixes is obtained at 15% metakaolin replacement level. Both the flexural and split tensile strength of RAC mixes at 15% metakaolin replacement level are close to the flexural and split tensile strength of the control concrete.
- The percentage of strength improvement is higher in RAC than NAC which may be due to the existence of more pores, micro-cracks and inferior properties of RCA which facilitates the strength development.
- The performance of RAC is improved greatly by including MK at a dosage of 15% in concrete. At higher doses of MK, the rate of strength enhancement decreases. Hence, 15% metakaolin replacement level is regarded as the optimum percentage for better performance of RAC, and the RAC mix incorporating 100% RCA and 15% MK can suitably be used for construction work in place of NAC.

References

1. Song X, Qiao P, Wen H (2015) Recycled aggregate concrete enhanced with polymer aluminium sulfate. Mag Concr Res 67(10):496–502. https://doi.org/10.1680/macr.14.00119
2. Tam VWY, Tam CM (2009) Parameters for assessing recycled aggregate and their correlation. Waste Manag Res 27:52–58. https://doi.org/10.1177/0734242X07079875
3. Coelho A, de Brito J (2011) Distribution of materials in construction and demolition waste in Portugal. Waste Manag Res 29:843–853. https://doi.org/10.1177/0734242X10370240
4. Mukharjee BB, Barai SV (2015) Development of construction materials using nano-silica and aggregates recycled from construction and demolition waste. Waste Manag Res 33:515–523. https://doi.org/10.1177/0734242X15584840
5. De Juan MS, Gutiérrez PA (2009) Study on the influence of attached mortar content on the properties of recycled concrete aggregate. Constr Build Mater 23:872–877. https://doi.org/10.1016/j.conbuildmat.2008.04.012
6. Chakradhara Rao M, Bhattacharyya SK, Barai SV (2011) Influence of field recycled coarse aggregate on properties of concrete. Mater Struct Constr 44:205–220. https://doi.org/10.1617/s11527-010-9620-x
7. Otsuki N, Miyazato S, Yodsudjai W (2003) Influence of recycled aggregate on interfacial transition zone, strength, chloride penetration and carbonation of concrete. J Mater Civ Eng 15:443–451. https://doi.org/10.1061/(ASCE)0899-1561(2003)15:5(443)
8. Wang L, Wang J, Qian X et al (2017) An environmentally friendly method to improve the quality of recycled concrete aggregates. Constr Build Mater 144:432–441. https://doi.org/10.1016/j.conbuildmat.2017.03.191
9. Xuan D, Zhan B, Poon CS (2016) Assessment of mechanical properties of concrete incorporating carbonated recycled concrete aggregates. Cem Concr Compos 65:67–74. https://doi.org/10.1016/j.cemconcomp.2015.10.018
10. Dilbas H, Şimşek M, Çakır Ö (2014) An investigation on mechanical and physical properties of recycled aggregate concrete (RAC) with and without silica fume. Constr Build Mater 61:50–59. https://doi.org/10.1016/j.conbuildmat.2014.02.057
11. Kong D, Lei T, Zheng J et al (2010) Effect and mechanism of surface-coating pozzalanics materials around aggregate on properties and ITZ microstructure of recycled aggregate concrete. Constr Build Mater 24:701–708. https://doi.org/10.1016/j.conbuildmat.2009.10.038
12. Radonjanin V, Malešev M, Marinković S, Al Malty AES (2013) Green recycled aggregate concrete. Constr Build Mater 47:1503–1511. https://doi.org/10.1016/j.conbuildmat.2013.06.076

13. Kou SC, Poon CS, Agrela F (2011) Comparisons of natural and recycled aggregate concretes prepared with the addition of different mineral admixtures. Cem Concr Compos 33:788–795. https://doi.org/10.1016/j.cemconcomp.2011.05.009
14. Singh N, Singh SP (2016) Carbonation and electrical resistance of self-compacting concrete made with recycled concrete aggregates and metakaolin. Constr Build Mater 121:400–409. https://doi.org/10.1016/j.conbuildmat.2016.06.009
15. Kapoor K, Singh SP, Singh B (2017) Permeability of self-compacting concrete made with recycled concrete aggregates and metakaolin. J Sustain Cem Mater 6(5):293–313. https://doi.org/10.1016/j.conbuildmat.2016.06.009
16. Bureau of Indian Standards (1989) Indian standard 43 grade ordinary Portland cement specification: IS: 8112, New Delhi
17. Bureau of Indian Standards (1970) Indian Standard specification for coarse and fine aggregates from natural sources for concrete: IS: 383, New Delhi
18. Bureau of Indian Standards (1963) Indian standard specification methods of test for aggregates for concrete: Part 1, particle size and shape: IS: 2386 (Reaffirmed in 2002), New Delhi
19. Bureau of Indian Standards (1963), Indian standard specification methods of test for aggregates for concrete: Part 4, mechanical properties: IS: 2386 (Reaffirmed in 2002), New Delhi
20. Bureau of Indian Standards (2012), Indian standard, drinking water—specification: IS: 10500, New Delhi
21. Bureau of Indian Standards (1982) Indian Standard recommended guide line for concrete Mix Design: IS: 10262, New Delhi
22. Bureau of Indian Standards (1959) Indian Standard methods of tests for strength concrete: IS: 516 (Reaffirmed in 1999), New Delhi
23. Mukharjee BB, Barai SV (2014) Influence of incorporation of nano-silica and recycled aggregates on compressive strength and microstructure of concrete. Comput Chem Eng 71:570–578. https://doi.org/10.1016/j.conbuildmat.2014.08.040
24. Kou SC, Poon CS, Agrela F (2011) Comparisons of natural and recycled aggregate concretes prepared with the addition of different mineral admixtures. Cem Concr Compos 33:788–795. https://doi.org/10.1016/j.cemconcomp.2011.05.009
25. Majhi RK, Nayak AN, Mukharjee BB (2018) Development of sustainable concrete using recycled coarse aggregate and ground granulated blast furnace slag. Constr Build Mater 159:417–430. https://doi.org/10.1016/j.conbuildmat.2017.10.118
26. Mukharjee BB, Barai SV (2014) Influence of nano-silica on the properties of recycled aggregate concrete. Constr Build Mater 55:29–33. https://doi.org/10.1016/j.conbuildmat.2014.01.003

A Relook on Dosage of Basalt Chopped Fibres and Its Influence on Characteristics of Concrete

Sanket Rawat, Rahul Narula, Nitant Upasani and G. Muthukumar

Abstract In the recent years, the need for the sustainable yet economically viable structural materials has drawn the special attention of the construction industry apart from the traditional parameters concerning safety and serviceability. One such material of interest gaining popularity in the twentieth century is the basalt fibre, due to its cost-effectiveness and desirable engineering properties, especially with respect to fire resistance. Basalt fibres are formed from basalt rocks and hence fulfil the concept of sustainable design and green building. Basalt can commonly be used as structural reinforcing material in the form of bars, sheets, chopped fibres, etc. Talking specifically about chopped basalt fibres, the dosage of fibre plays an important role in its case. This paper mainly highlights the existing studies on the optimum dosage of chopped basalt fibres with respect to strength aspect and points out several critical comments on relation of fibre content with workability through experimental testing.

Keywords Basalt fibres · Dosage · Strength · Workability

1 Introduction

The stride of technological advancement has also impelled the engineering fields to expand their horizon and develop new materials for real-time applications which not only satisfies the need of the day but also adapts to the ever-changing environment. Specifically, in civil engineering applications, the use of sustainable and energy efficient materials has become an important functional element of design along with the safety and serviceability aspects. Composite materials are an example of recently emerged materials in design due to their diversified advantages in terms of high mechanical properties, low specific weight, durability, etc. Carbon and Glass fibres are two of such materials which have gained significant attention due to excellent mechanical performance and durability. However, their use is still an environmen-

S. Rawat · R. Narula · N. Upasani (✉) · G. Muthukumar
Department of Civil Engineering, BITS Pilani, Pilani Campus, Pilani 333031, Rajasthan, India
e-mail: nitantupasani@gmail.com

S. Kumar Shukla et al. (eds.), *Advances in Sustainable Construction Materials and Geotechnical Engineering*, Lecture Notes in Civil Engineering 35,
https://doi.org/10.1007/978-981-13-7480-7_7

tal concern as incineration of discarded fibres generates plenty of smoke, unhealthy odours and can cause damage to the equipment [1]. To overcome such environmentally hazardous concerns, basalt has emerged as a suitable type of fibre, which has found multiple applications in many fields. In the 1990s, basalt found its way in multiple applications of civil engineering field and is now recognized as 'the twenty-first century non-polluting green materials' [1, 2]. The manufacturing process of basalt fibres is analogous to that of glass fibres; however, the former requires lesser energy and no additives, which is the main reason of its lower cost [3]. Basalt fibres are produced from natural volcanic basalt rocks, by putting them as raw materials into furnace for melting, which is further forced through suitable crucible bushings to produce the fibres. Moreover, recycling of basalt fibre resins also leads to the same, natural basalt powder, which can be used again [4]. Overall, basalt fibres are completely natural, inert and cost-effective and possess excellent mechanical properties, corrosion resistance, thermal resistance and sound absorption [1, 3, 5, 6]. Due to the aforementioned forte, basalt fibre-reinforced polymer composites are used in various infrastructural applications in different forms, viz. as basalt rebars, sheets, chopped fibres, fabrics and meshes. The present study is mainly aimed towards the recent developments in the use of chopped basalt fibres and the effect of its addition on the mechanical properties of concrete. One of the foremost concerns in the use of chopped basalt fibres is the dosage which can significantly affect the workability and strength of the concrete. Therefore, the assessment of optimum dosage is very important at which the strength and workability are as desired and do not adversely affect the concrete characteristics. To provide a better understanding of the optimum dosage, the present study briefly reviews the existing literature representing the effect of dosage of basalt fibre and highlights some critical inferences. Experimental testing results are also presented distinctly to check the effect of dosages on workability of concrete, and the same are compared with results available in the existing literature to reach to a conclusion which would benefit the future research in this area.

2 Performance of Basalt Chopped Fibres in Structural Members

Chopped basalt fibres are relatively new and have recently started being employed in several studies as reinforcements for the concrete. The first use of the basalt fibres was reported in 1998 for the Highway Innovations Deserving Exploratory Analysis (IDEA) Project 45 [7], and it was found that basalt fibres can show encouraging outcomes. Thereafter, the possibility of its use in structural applications also acquired significant attention. Existing literature suggests that the use of basalt fibres undoubtedly led to a positive effect in case of flexural strength and splitting tensile strength; however, their effect on compressive strength is still under reservation due to dissimilar performance in different investigations. Kabay [8] demonstrated that the inclusion of basalt fibres in normal as well as high strength concrete can lead

to massive improvement in flexural strength (9–13%), fracture energy (126–140%) and reduction in abrasion wear (2–18%). However, the compressive strength of concrete generally decreases on addition of basalt fibres. Irine [9], on the other hand, showed that compressive strength of concrete also improves along with the splitting tensile strength and flexural strength with the use of basalt fibres. Jiang et al. [10] also showed the increase in concrete compressive strength of about 0.18–4.68% with 12 mm basalt fibres and approximately 0.55–5.72% with 24 mm length basalt fibres. Ayub et al. [11] demonstrated that with the inclusion of basalt fibres in high strength fibre-reinforced concrete, considerable increase in the strain is observed corresponding to ultimate compressive strength (4.85–12.24%) and toughness (3.8–47.45%). Ramakrishnan et al. [12] showed that the addition of chopped basalt fibres (13 mm in length and 12 μm in diameter) can decrease compressive strength and flexural strength of concrete however improve impact strength and flexural toughness. On the other hand, Borhan [13], who used basalt fibres, 25.4 mm in length and 13 μm diameter, showed that even compressive strength can increase up to 0.3% by volume addition of basalt fibres. The test results from an analogous research conducted by the Kyiv National University of Construction and Architecture [14] showed improvement in flexural and compressive strength on the addition of basalt fibres (24 mm long and 16 μm in diameter).

Dong et al. [15] also confirmed that the inclusion of basalt fibres enhances the mechanical properties, strength and ductility of recycled aggregate concrete by strengthening the interfacial transition zone. Meng et al. [16] and Lu et al. [17] showed that the use of basalt fibres in BFRP bar-reinforced recycled aggregate concrete can limit the contraction of concrete and hence can reduce the bond stress with BFRP bars. However, increase in basalt fibre content might lead to reduction in bond strength. Moreover, Jiang et al. [10] found the beneficial effects of basalt fibres, e.g. bond strength, started degrading after 28 days and diminished significantly after 90 days. This may imply that basalt fibres are susceptible to a similar degradation mechanism as of glass fibres in concrete due to the reactions between the silicate component in the fibres and alkali solution in the cementitious matrix [3]. Therefore, coating of basalt fibres with a polymeric or protective matrix may be necessary. Therefore, Mahmoud et al. [18] developed basalt fibre pellets (basalt fibre encapsulated by polyamide resin), and nano silica was added in the concrete reinforced with basalt pellets. It was observed that nanomodified basalt fibre pellets (36 mm length)-reinforced concrete showed significant enhancement in residual flexural strength, ductility, flexural toughness, post-cracking behaviour and bond strength to GFRP bars.

The performance of basalt fibres is found to be unfavourable under alkaline exposure condition. Therefore, attempts have been made to improve their performance through the use of surface coating agents, addition of cement and concrete additives or improving the composition by increasing the content of alkaline resistant constituents. It was found that the indirect tensile and flexural properties of basalt fibres can considerably be improved in the alkaline environment by modifying them with surface coating agent, e.g. silane [19]. Furthermore, Lipatov et al. [20] also showed that basalt fibres produced with appropriate zirconia content can signifi-

cantly improve its performance in alkaline environment and long-term mechanical properties by reducing fibre corrosion in the cementitious matrix. Therefore, it can be affirmed that basalt fibre can significantly affect the strength, displacement and bond characteristics of concrete, and though the behaviour of basalt fibres is established under various loading conditions, further research can be done to investigate the effect of properties of fibre surface on the bond performance with concrete.

3 Observations on Dosage of Basalt Fibres

It has been generally observed that workability of high strength concrete is negatively affected by the increase in basalt fibre content [21]. Kizilkanat et al. [22] also showed that the inclusion of basalt and glass fibres reduced the workability; however, relatively, the glass fibre-reinforced concrete had lower slump value than basalt fibre counterparts. Iyer et al. [23] also found the reduction in workability of concrete on increase in the fibre length and content.

To evaluate the optimal parameters for basalt fibres, Elshafie and Whittleston [24] after their comprehensive literature review to obtain the optimum length and content of basalt fibres concluded that for optimal performance in mechanical strength, basalt fibre of dosage between 0.1 and 0.5% should be used with length in between 12 and 24 mm. However, Revade and Dharane [25] and Ayub et al. [26] confirmed the optimum basalt fibre content value for compressive strength as 1.0 and 2.0% (for high-performance concrete), respectively. Katkhuda and Shatarat [27] also showed that the maximum compressive strength value is 1.0% fibre volume in recycled aggregate concrete. Generally, in the case of basalt fibres, the existing research shows its addition is beneficial up to approximately 0.3–0.5% by volume and detrimental thereafter [10, 13, 23]. However, it has been observed that the optimum content of fibre can differ for different types of concrete such as geopolymer concrete and concrete mixed with supplementary cementitious material. [26, 28]. Using higher length (50 mm) and content of fibres (12 kg/m^3) can lead to clumping of fibres [23]. Table 1 depicts a compilation of the adoption of dosage of basalt fibres by the existing literature and the respective effect on concrete characteristics.

4 Experimental Investigations on the Effect of Basalt Fibre Dosage on Workability of Concrete

It can be clearly observed from Table 1 that the percentage variation of the dosage of basalt fibre in the existing literature results in scattered perspective. Different researchers have presented different opinions about the effect of addition of basalt fibre on the characteristics of concrete. A general statement can be inferred that addition of basalt fibre will lead to reduction in workability of concrete. However, a con-

Table 1 Effect of dosage of basalt fibres as available in the existing literature

Authors	Details about fibre content	Comments (about performance, etc.)		
Dias and Thaumaturgo [28]	*Fibre dosage*—0, 0.5 and 1% by volume of concrete	The drop in compressive strength and splitting tensile strength of concrete was found to be approximately 26.4 and 12.0% on addition of 1% basalt fibre by volume of mix		
Kabay [8]	*Fibre dosage*—2 and 4 kg/m^3 (for two different w/c ratio, i.e. 0.45 and 6 and for two different lengths 12 and 24 mm)	The addition of basalt fibres resulted in decrease in compressive strength. Although it was found that as the fibre content was increased from 2 to 4 kg/m^3, the compressive strength was increased. However, in spite of the increase, the compressive strength was below the control specimens. Contrary to this, the flexural strength and fracture energy were found to increase with the addition of basalt fibres		
Ayub et al. [11], Ayub et al. [26]	*Fibre dosage*—1, 2 and 3% volume fraction (i.e. by volume of concrete) in high-performance concrete	Contrary to the results available in the existing literature, it was observed that even at a very high volume of basalt fibres, i.e. 3.0%, balling and segregation did not occur during mixing. Also, though the compressive strength increased up to only 4% it was noticed that the strain corresponding to the peak strength increased up to 12.24%		
Jiang et al. [10]	*Fibre dosage*—0.05, 0.1, 0.3 and 0.5% by volume of concrete	% Increase In	12 mm fibre length	24 mm fibre length
		Compressive strength	0.18–4.68%	0.55–5.72%
		Splitting tensile	14.08–24.34%	14.96–25.51%
		Flexural strength	6.30–9.58%	7.35–10.37%
Iyer et al. [23]	*Fibre properties*—16 μm diameter and three different lengths of 12, 36, 50 mm *Fibre dosage*—three dosages 4, 8 and 12 kg/m^3 (0.15—0.46% by volume of concrete)	The workability was found to decrease drastically on increase in the fibre length or the fiber content. Clumping of fibres was visibly observable at 12 kg/m^3 fibre content. This even increased further on increasing the fibre content to 50 mm. 36-mm-length basalt fibres at content of 8 kg/m^3 were found to show optimal results for both compressive strength and moment of resistance		
Kizilkanat et al. [22]	*Fibre dosage*—four different volume fractions i.e. 0.25, 0.50, 0.75, and 1%	A slight increase in compressive strength and fracture energy was observed on increasing the fibre content beyond 0.25%. However, the splitting tensile strength increased appreciably and the increase was up to 40%, maximum at 1% fibre volume		

(continued)

Table 1 (continued)

Authors	Details about fibre content	Comments (about performance, etc.)
Shafiq et al. [29]	*Fibre dosage*—1–3% by volume of concrete	It was concluded that improvement in strain exhibiting characteristics at 2% fibre volume in metakaolin concrete was better than at 1 and 3% fibre volume
El-Shafie et al. [30]	*Fibre properties*—12 and 24 mm length *Fibre dosage*—0.2–0.3% fibre volume (by volume of concrete)	24-mm-length basalt fibres at 0.2% fibre volume were found to show optimal results for mechanical properties
Branston et al. [31]	*Fibre properties*—36 and 50 mm length *Fibre dosage*—Three dosages 4, 8 and 12 kg/m^3 (0.15–0.46% by volume of concrete)	Despite the use of superplasticizer, it was observed that dosages beyond 12 kg/m^3 (0.46%) of basalt fibre led to fibre balling and difficulty in achieving properly compacted mix
Arslan [32]	*Fibre dosage*—0.5, 1, 2 and 3 kg/m^3	Though the splitting tensile and flexural strength were improved with increase in fibre content, minor reduction was observed in flexural strength for high fibre content. However, the effect of fibre addition was not noteworthy on the compressive strength and elastic modulus of concrete
Zhao et al. [33]	*Fibre dosage*—1.5 kg/m^3	It was observed that the creep of concrete is most affected by the modulus of elasticity of fibres Fibres with modulus of elasticity much higher than normal concrete can distinctly restrict creep (8.8% decrease with basalt fibre), while fibres with lower modulus of elasticity have the reverse effect
Dong et al. [15]	*Fibre properties*—15–19 mm length *Fibre dosage*—2 and 4 kg/m^3	2 kg/m^3 was found to be the optimum fibre content
Zhang et al. [34]	*Fibre dosage*—0.05, 0.1, 0.15, 0.2, and 0.25% by volume of concrete	It was found that optimal content of fibre to improve the toughness will vary for different grade of concrete. Moreover, it was observed that high strength concrete shows a better bonding interface between fibre and cement paste

clusion cannot be drawn about the most optimal amount of basalt fibre as the results available are fairly inconsistent. For instance, Ayub et al. [11] reported that even on the addition of 3% basalt fibre, the workability was not reduced much and no balling effect was observed. On the other hand, Iyer et al. [23] found that clumping of fibres was observed on 0.46% fibre content. With so much variation in a common observable fact, it becomes necessary for the future researchers to further analyse the available research data as well as in performing more experiments to come to a common consensus. Therefore, the effect of fibre dosage on workability is reanalysed in the present study to get a clear assessment of the workability relation with fibre content.

Five different fibre contents were chosen, i.e. 0.2, 0.3, 0.5, 0.7 and 1.0% by volume of concrete and mixed in normal strength concrete, M30 grade, to check its effect on workability. Basalt fibres were randomly mixed in concrete, and the method of mixing was referred from Jiang et al. [10] and Sarmah et al. [35]. Minimum target slump was chosen as 50 ± 10 mm as mentioned in Cl. 7.1 of IS 456 [36] for light-reinforced concrete structures. The mixing of concrete was done at Pilani, India. Fosroc Conplast SP430G8 grade of superplasticizer was used to achieve the target slump in case if the workability is reduced in trials.

It was observed that workability is adversely affected by the inclusion of fibre in concrete. Table 2 depicts a summary of the adopted superplasticizer dosage to achieve the required target slump with respect to different basalt fibre contents. Though at lower fibre content (0.2–0.5%), the use of superplasticizer was effective in countering the reduction in the workability, it was observed that the required percentage of superplasticizer by weight of cement has increased beyond 1% for higher fibre dosage. For 1% fibre content, even 1.5% superplasticizer content was not enough to reach to the target slump. Generally, it is not advisable to increase the superplasticizer content beyond 1.5% as the setting time is severely affected with it, which ultimately creates a challenge in demoulding of the specimens or removing the formwork at site conditions. Moreover, it was observed that beyond 0.5% fibre content, the mixing of concrete also becomes difficult as at higher content fibres act like a cushion in concrete which hinders the closer packing of its constituents. Figure 1 shows a comparison of finishing surface at 0.2 and 1% fibre content of 100 mm × 100 mm × 500 mm beams. It can be clearly observed that at 1% fibre content, the surface finish is relatively poor with lots of internal voids, due to the improper mixing of concrete. Therefore, it is recommended that fibre content should be kept below 0.5% to obtain the optimum results in cases where workability is acting as a design parameter.

Table 2 Effect of basalt fibre on superplasticizer dosage (target slump—50 ± 10 mm)

Basalt content (%)	Superplasticizer content (%)	Basalt content (%)	Superplasticizer content (%)
0	0.4	0.5	0.9
0.2	0.6	0.7	1.2
0.3	0.7	1	1.5

Fig. 1 Basalt fibre-reinforced concrete beam at **a** 0.2% and **b** 1% fibre content

5 Conclusion

The present study briefly highlights the existing findings about the behaviour of chopped basalt fibres on strength and workability of concrete. It was observed that the addition of basalt fibers does not significantly influence the compressive strength of concrete. However, the mode of failure was found to be improved from brittle to ductile mode. Moreover, basalt fibre can significantly increase the tensile strength, flexural toughness and energy absorption capacity. The existing literature also suggests that higher dosage of basalt fibre can negatively affect the workability of concrete. However, to identify about the corresponding dosage of basalt fibre, an experimental investigation has been conducted in the presented study and it is concluded that the basalt fibre content should be limited to 0.5% in cases where workability and setting time are given significance in the design.

Acknowledgements This work is fully supported by Birla Institute of Technology and Science, sponsored research project under Additional Competitive Research Grant scheme.

References

1. Jamshaida H, Mishraa R (2016) Green material from rock: basalt fiber—a review. J Text Inst 107(7):923–937
2. Raj S, Kumar VR, Kumar BHB, Iyer NR (2017) Basalt: structural insight as a construction material. Sadhana 42(1):75–84
3. Sim J, Park C, Moon DY (2005) Characteristic of basalt fiber as a strengthening material for concrete structures. Compos. Part B 36(6):504–512
4. Kamenny V (2015) Advanced basalt fiber, Basfiber. Retrieved from http://www.basfiber.com
5. Matko S, Keszei S, Csontos I, Anna P, Marosi G, Zsuga M, Borda J, Nagy G (2006) Fire retarded insulating sheets from recycled materials. Macromol Symp 233:217–224

6. Wang M, Zhang Z, Li Y, Li M, Sun Z (2008) Chemical durability and mechanical properties of alkali-proof basalt fiber and its reinforced epoxy composites. J Reinf Plast Compos 27(4):393–407
7. Ramkrishnan V, Tolmare NS, Brik VB (1998) Performance evaluation of basalt fibers and composite rebars as concrete reinforcement. NCHRP-IDEA Project 45, Transportation Research Board, NRC, Washington DC
8. Kabay N (2014) Abrasion resistance and fracture energy of concretes with basalt fiber. Constr Build Mater 50:95–101
9. Irine F (2014) Strength aspects of basalt fiber reinforced concrete. Int J Innov Res Adv Eng 1(8):192–198
10. Jiang C, Fan K, Wu F, Chen D (2014) Experimental study on the mechanical properties and microstructure of chopped basalt fibre reinforced concrete. Mater Des 58:187–193
11. Ayub T, Shafiq N, Khan SU (2016) Compressive stress-strain behavior of HSFRC reinforced with basalt fibers. Tech Note J Mater Civ Eng 28(4):06015014
12. Ramakrishnan V, Tolmare NS, Brik V (1998) Performance evaluation of 3-D basalt fiber reinforced concrete and basalt rod reinforced concrete. Innovations deserving exploratory analysis programs (IDEA) Program Final Report, pp 1–79
13. Borhan TM (2013) Thermal and mechanical properties of basalt fibre reinforced concrete. In: Proceedings of World Academy of Science, Engineering and Technology, World Academy of Science, Engineering and Technology (WASET), pp 712–715
14. KNUCA (Kyiv National University of Construction and Architecture) (2011) Protocol no. 64-1-11: On control testing of fibre-concrete samples to determine their compression and tensile strength at bending. Technobasalt-invest, LLC, Kyiv, Ukraine
15. Dong JF, Wang QY, Guan ZW (2017) Material properties of basalt fibre reinforced concrete made with recycled earthquake waste. Constr Build Mater 130:241–251
16. Meng W, Liu H, Liu G, Kong X, Wang X (2016) Bond-slip constitutive relation between BFRP bar and basalt fiber recycled-aggregate concrete. KSCE J Civil Eng 20(5):1996–2006
17. Lu H, Yang J, Wang X (2017) Bond behavior between BFRP bar and recycled aggregate concrete reinforced with basalt fiber. Constr Build Mater 135:477–483
18. Mahmoud K, Ghazy A, Bassuoni MT, El-Salakawy E (2017) Properties of nanomodified fiber reinforced cementitious composites. J Mater Civ Eng 29(10):04017173
19. Afroz M, Patnaikuni I, Venkatesan S (2017) Chemical durability and performance of modified basalt fiber in concrete medium. Constr Build Mater 154:191–203
20. Lipatov YV, Gutnikov SI, Manylov MS, Zhukovskaya ES, Lazoryak BI (2015) High alkali-resistant basalt fiber for reinforcing concrete. Mater Des. 73:60–66
21. El-Shekh AEA, Shafiq N, Nuruddin MF, Fathi A (2014) Evaluation of effectiveness of chopped basalt fiber on the properties of high strength concrete. J Appl Sci 14(10):1073–1077
22. Kizilkanat AB, Kabay N, Akyuncu V, Chowdhury S, Akca AH (2015) Mechanical properties and fracture behavior of basalt and glass fiber reinforced concrete: an experimental study. Constr Build Mater 100:218–224
23. Iyer P, Kenno SY, Das S (2015) Mechanical properties of fiber-reinforced concrete made with basalt filament fibers. J Mater Civ Eng 27(11):04015015
24. Elshafie S, Whittleston G (2015) A review of the effect of basalt fibre lengths and proportions on the mechanical properties of concrete. Int J Res Eng and Tech 4(1):458–465 eISSN: 2319-1163
25. Revade A, Dharane S (2015) Study the effects of short basalt fibers on mechanical properties of concrete. J Civ Eng Environ Technol 2(12):1–6
26. Ayub T, Shafiq N, Nuruddin MF (2014) Mechanical properties of high-performance concrete reinforced with basalt fibers. Proc Eng 77:131–139
27. Katkhuda H, Shatarat N (2017) Improving the mechanical properties of recycled concrete aggregate using chopped basalt fibers and acid treatment. Constr Build Mater 140:328–335
28. Dias DP, Thaumaturgo C (2005) Fracture toughness of geopolymeric concretes reinforced with basalt fibers. Cem Concr Compos 27(1):49–54
29. Shafiq N, Ayub T, Khan SU (2016) Investigating the performance of PVA and basalt fibre reinforced beams subjected to flexural action. Compos Struct 153:30–41

30. El-Shafie S, Boulbibane M, Whittleston G (2016) Mechanical performance of reinforced concrete with different proportions and lengths of basalt fibres. J Mater Sci Eng. https://doi.org/10.4172/2169-0022.1000271
31. Branston J, Das S, Kenno SY, Taylor C (2016) Mechanical behaviour of basalt fibre reinforced concrete. Constr Build Mater 124:878–886
32. Arslan ME (2016) Effects of basalt and glass chopped fibers addition on fracture energy and mechanical properties of ordinary concrete: CMOD measurement. Constr Build Mater 114:383–391
33. Zhao Q, Yu J, Geng G, Jiang J, Liu X (2016) Effect of fiber types on creep behavior of concrete. Constr Build Mater 105:416–422
34. Zhang H, Wang B, Xie A, Qi Y (2017) Experimental study on dynamic mechanical properties and constitutive model of Basalt fiber reinforced concrete. Constr Build Mater 152:154–167
35. Sarmah M, Roy B, Mozumder RA, Laskar AI (2017) Effect of chopped basalt fibers on the cyclic behavior of RCC beam–column subassemblies. Arab J Sci Eng. https://doi.org/10.1007/s13369-017-2801-y
36. IS 456 (2000) Plain and reinforced concrete—code of practice, Bureau of Indian Standards, New Delhi, India

Influence of Nano-modification on Strength Parameters of Concrete

Himanshu Sharma, Basit Majeed and Sanjay Sharma

Abstract Production of cement results in the release of carbon in the atmosphere resulting in degradation of environment. Involvement of nanotechnology in concrete production can decrease the consumption of cement in concrete. In this study, an effort has been made to analyze the influence of nano-modification on the workability and strength parameters of concrete. For the purpose of nano-modification, nano $CaCO_3$ (NC) was utilized. Concrete mixes were prepared with 1 and 2% content of nano $CaCO_3$ with respect to the weight of the binder. As per the study, when cement was replaced with NC, the strength properties of concrete were significantly improved. Compressive strength results of NC-added mix after a curing period of 28 days show the highest improvement in strength of about 60% in comparison with a controlled mix. Addition of NC reduces the pores and capillaries in the concrete making the concrete more durable. Addition on NC also increases the flowability of the mix making the mix more workable.

Keywords Nano concrete · Nano $CaCO_3$ · Nano calcium carbonate · Strength properties · Durability · High-strength concrete

H. Sharma · B. Majeed (✉)
Department of Civil Engineering, Maharaja Agrasen Institute of Technology, Maharaja Agrasen University, Baddi 174103, India
e-mail: aaabasit62@gmail.com

H. Sharma
e-mail: Himanshu1027@gmail.com

S. Sharma
Department of Civil Engineering, National Institute of Technical Teachers Training and Research, Chandigarh 160019, India
e-mail: sanjaysharmachd@yahoo.com

S. Kumar Shukla et al. (eds.), *Advances in Sustainable Construction Materials and Geotechnical Engineering*, Lecture Notes in Civil Engineering 35,
https://doi.org/10.1007/978-981-13-7480-7_8

1 Introduction

Concrete is one of the dynamic products of the construction industry always remains in high demands. Concrete is preferred above all building materials for its versatile properties like strength, plasticity, elasticity modulus, and workability. These properties of conventional concrete were satisfactory for the early 1950s. In early 1960's with the growth of construction industry and demand of new and unique designs, concrete with a load-carrying capacity of 50–95 MPa was required [1, 2]. To fulfill the requirement, a new type of concrete with the name of high strength concrete (HSC) was introduced to withstand a load of 50–90 MPa [3, 4]. The development of HSC is done by proper mix designing ratio and using various mineral admixtures [5]. For the development of concrete with high strength, i.e., HSC the content of cement and aggregates required is too high as compared to conventional concrete. To compensate this concern, a large number of supplementary materials like fly ash, metakaolin, and silica fume were introduced for the development of HSC [6–8]. Silica fumes were introduced in HSC; it increases the strength of the mix [8–12]. Studies [13–16] have shown the feasibility of replacement of large quantity of cement with fly ash which not only makes the mix economical but also increases the flowability of the mix. With the advancement in the technology, nano concrete has been introduced to fulfill the requirements of HSC and ultra-high performance concrete (UHPC).

Any concrete mix utilizing nanoparticles of size less than 500 nm is termed as nano concrete [3, 17–21]. It is believed that nanoparticles increase the strength of the concrete mix by packing model structure. The nanoparticles also perform as fillers as they possess the ability of making the concrete mix dense by fill up the pores. Adding nanoparticles not only increases the strength properties of the mix but also accelerates the hydration reaction, as the water trapped in the pores of the concrete mix is utilized as free water for the hydration process [2, 22, 23]. Besides the utilization of fly ash, metakaolin, silica fumes, etc., in the concrete mix, limestone powder has also been utilized. A blend of cement, fine aggregate, and limestone fines can considerably increase the packing density [24]. It is believed that the addition of limestone powder accelerates the hydration process increasing the strength properties of concrete and also improves other properties of fresh concrete mix like flowability etc. The presence of limestone acts as filler, increasing early age hydration of OPC by providing supplementary surface area for the precipitation of hydration products [25–29]. The utilization of limestone is not restricted to filler effect; it also provides some chemical reactions. Some studies [25, 30–36] have shown that calcium monosulfoaluminate remains inactive whenever calcium carbonate is present, but the existence of $CaCO_3$ in limestone powder reacts with the aluminate hydrates which are formed by the hydration of cement. So calcium monocarboaluminate and calcium hemicarboaluminate hydrate will be formed, which will result in the increased quantity of total hydration product. This increased quantity of hydration products will lead to dense mix and increased strength. This chemical reaction is, however, not very noticeable as there is limited content of aluminate in anhydrous clinker. The high strength of concrete can be achieved by using microparticles as the grains are closely packed

[37]. Addition of nanoparticles can improve several properties of concrete including strength properties. The incorporation of nanoparticles in concrete has shown much more positive results as compared to microparticles. In recent years, a limited amount of research has been conducted on nano $CaCO_3$. Therefore, the aim is to analyze the workability and strength parameters of concrete by incorporating nano $CaCO_3$ in concrete.

2 Experimental Details

2.1 Materials

OP cement was used for the preparation of all concrete mixes. Powdered nano $CaCO_3$ (NC) with a particle size of 15–60 nm was used for preparing nano concrete. Some of the properties (physical and chemical) of cement and NC are given in Tables 1 and 2.

Table 1 Chemical composition of cement and nano $CaCO_3$

Chemical analysis	Cement (wt%)	Nano calcium carbonate (wt%)
SiO_2	19.88	–
Al_2O_3	5.2	0.01
Fe_2O_3	3.1	0.03
MgO	0.85	0.46
$CaCO_3$	–	95.6
CaO	62.7	–
K_2O	0.42	–
SO_3	2.30	–
Na_2O	0.13	–

Table 2 Physical properties of cement and nano $CaCO_3$

Properties (%)	Cement (wt%)	Nano calcium carbonate (wt%)
Particle size	–	15–60 nm
Surface area (m^2/g)	–	25–40
Loss of ignition (%)	1.92	–
Bulk density (g/cm^3)	–	0.7
Insoluble residue (%)	1.84	–

Table 3 Mix proportions of various concrete mixes (kg/m^3)

Designation	Cement	NC	Sand	Course aggregate	Water
PC	420.0	–	580	1210	177
NC1	415.8	4.2	580	1210	177
NC2	411.6	8.4	580	1210	177

2.2 Mix Proportions

Tests were conducted on various concrete mixes with and without the addition of NC. The work was separated into two parts. In the first part, a concrete mix with the incorporation of 1% NC as a restricted replacement of cement was developed and evaluated. In the second part, the concrete mix with 2% NC as a restricted replacement of cement was developed and evaluated. Both the mixes were evaluated in comparison with the nominal mix. Table 3 shows the mix proportions of various concrete mixes. NC, cement, fine aggregate, and course aggregate were mixed dry before adding water.

2.3 Method

All concrete mixes were prepared using a pan mixer. Three types of mixes, i.e., PC, NC1, and NC2 as discussed above were prepared. Some of the strength and durability properties were studied.

2.3.1 Compressive Strength

The cubes of 150 mm size were cast from all the concrete mixes and were tested for the compressive strength at 7, 14, 28, and 90 days of curing with normal water. The water-to-binder ratio for all the mixes was taken as 0.42. The compressive strength test was conducted as per Indian standards.

2.3.2 Early Age Strength

The cubes of 150 mm size for all mentioned concrete mixes were prepared and tested. The test was conducted to analyze the early age effect of NC on compressive strength of concrete. The test was conducted for a curing period of 8, 12, and 24 h for all mix proportions.

2.3.3 Flowability

The flowability of the concrete mix was calculated as per flow table test. This test method is proposed to find the flow rate of hydraulic cement mortars or other mortar mixes containing cementitious materials. This test is required to evaluate a standard water requirement of the mix for any particular flow rate.

2.3.4 Water Sorptivity

Water sorptivity or absorption can be explained as the amount of water that enters the concrete surface due to capillary suction. The phenomenon is dependent upon the volume of pores present in the concrete and the connectivity of pores within the concrete surface. The term sorptivity can also be related to permeability of concrete. One side of the concrete sample (50 mm from base) was immerged in water, while all the other sides were sealed. The rate of water absorbed by the concrete specimen can be evaluated by measuring the weight of the concrete sample before and after water absorption.

3 Results and Discussion

3.1 Later-Age Compressive Strength

The results for compressive strength of various concrete mixes, i.e., PC, NC1, and NC2 with NC 0%, NC 1%, and NC 2%, respectively, are described in Table 4. The study shows a remarkable increase in concrete's compressive strength by adding NC particles as a replacement to cement. The best results were obtained by NC1 concrete sample, i.e., replacement of cement by 1% NC. The incorporation of 1% NC has increased 28 days and 90 days compressive strength of about 60 and 55% as compared to nominal concrete mix. Addition of 2% NC has slightly increased the 28 days and 90 days compressive strength by about 13 and 5%, respectively. The reason for this can be, as the NC particles being very small in size, acted as filler in the concrete. These particles fill the excess pores in the concrete matrix, releasing the water trapped in the pores. This free water is utilized to accelerate hydration reaction of concrete, resulting in the formation of additional C–H–S gel. Also, the surplus surface area created by NC particles acts as nucleation spots for the formation of hydration products which increases the hydration reaction further increasing the compressive strength of concrete. On adding 1% NC in concrete mix, compressive strength increased due to the development of additional C–H–S gel, however, increasing the quantity of NC to 2% the increased compressive strength drops as excessive cementitious material has been replaced. Similarly, on addition of 1% NC the 28 days compressive strength increases by 62% [38]. As per another study

Table 4 Compressive strength and slump results of various concrete samples

Designation	Compressive strength (MPa)			
	7 days	14 days	28 days	90 days
PC	24.80	34.48	45.30	52.02
NC1	56.29	60.60	72.50	81.21
NC2	36.56	42.81	51.34	55.44

Table 5 Early-age compressive strength results of various concrete samples

Designation	Early-age compressive strength (MPa)		
	8 h	12 h	24 h
PC	2.00	6.56	19.85
NC1	3.68	8.66	24.00
NC2	6.10	11.82	29.25

[39], the best result for 28 days compressive strength was obtained at 1% addition of NC, further the compressive strength decreased with the increase in the content of NC.

3.2 Early-Age Compressive Strength

The outcomes for the early-age compressive strength of various concrete proportions are mentioned in Table 5. The early-age compressive strength of various concrete mixtures improved with the rise in the quantity of NC. An increase of 26 and 52% was seen at 24 h of curing by concrete sample NC1 and NC2 as compared to plain concrete mix. The addition of NC particles acts as nucleation sites for the hydration products. This chemical reaction gives birth to additional C–H–S gel. The NC particles which are not able to participate in this chemical process act as fillers. Combined effect of the presence of additional C–H–S gel and filler effect increases the compressive strength of concrete in early age. As per another study, the early-age compressive strength increased with the incorporation of NC [40].

3.3 Flowability

Addition of NC at both the percentage increases the flowability of the mix. The incorporation of NC1 as well as NC2 increases the flowability to about 15–25% as compared to conventional concrete. Nanoparticles being very small in size possess a very high surface area. On addition of NC up to 15%, the flowability of the mix increased till the addition of 5% and then decreased with higher percentage of NC [40]. This property of nanoparticles increases the flowability of the mix as it provides

a lubricating effect in cement particles. As on the other hand, NC also provides a filler effect, excessive addition of NC may lead to decrease in the flowability as by filling the pores of the concrete mix matrix it may increase the viscosity of the mix.

3.4 Water Sorptivity

The amount of water absorbed by concrete samples containing NC particles was much less as compared to water absorbed by conventional concrete. The amount of water absorbed by concrete sample NC1 at 28 days and 90 days was 15 and 25%, respectively, less than conventional concrete. The quantity of water absorbed by NC2 sample was 17 and 30% less as compared to conventional concrete at 28 and 90 days, respectively. This is due to the development of supplementary C–H–S gel by the reaction of CH in concrete matrix with NC particles and also due to fineness and high pozzolanic reactivity of NC particles. Further, the rate of absorption of water also decreased with the escalation in curing time. This is due to increased formation of supplementary C–H–S gel during long curing period, which fills the small holes of concrete matrix reducing the porosity and capillaries.

4 Conclusion

As per the work done on the incorporation of nano $CaCO_3$ in concrete, following conclusions can be made:

- Replacing cement with 1% NC can increase the compressive strength of concrete by 52% at 90 days. NC particles react with CH to form additional C–H–S gel which further improves the compressive strength properties of concrete. Replacing cement with 2% NC slightly increases the compressive strength of concrete as excessive cementitious material is replaced.
- Replacing cement with 1–2% of NC upturns compressive strength of concrete in early ages up to 52% as NC particles act as nucleation sites for hydration products further hastening the hydration reaction which imparts an upgraded early age compressive strength.
- Replacement of cement with 1–2% of NC increases the flowability of the concrete mix up to 25%. Fine NC particles act as lubricants in between cement particles increasing the flowability of concrete.
- The presence of NC particles up to 2% also reduces the water absorption capacity of the concrete. The presence of additional C–H–S gel and filler effect of nanoparticles plugs the pores and capillaries of the concrete.

High-strength concrete of 70 MPa (28 days) or 80 MPa (90 days) can be achieved by the replacement of cement with 1% nano $CaCO_3$, with strength gain of 52% in relation to controlled mix.

References

1. Ganesan KA (2012) Strength and water absorption properties of ternary blended cement mortar using rice husk ash and metakaolin. Scholar J Eng Res 1(4):51–59
2. Zhao S, Sun W (2014) Nano-mechanical behavior of a green ultra-high performance concrete. Constr Build Mater 63:150–160
3. Maholtra VM and Mehta PK (1996) Pozzolanic and cementitious materials. Taylor & Francis
4. Wang C, Yang C, Liu F, Pu X (2012) Preparation of ultra-high performance concrete with common technology and materials. Cem Concr Compos 34(4):538–544
5. Parande AK (2013) Role of ingredients for high strength and high performance concrete—a review. Adv Concr Constr 1(2):151–162
6. Rashad AM (2013) Metakaolin as cementitious material: history, scours, production and composition—a comprehensive overview. Constr Build Mater 41:303–318
7. Sobolev K (2004) The development of a new method for the proportioning of high performance concrete mixtures. Cem Concr Compos 26(7):901–907
8. Güneyisi E, Gesoğlu M, Karaoğlu S, Mermerdaş K (2012) Strength, permeability and shrinkage cracking of silica fume and metakaolin concretes. Constr Build Mater 34:120–130
9. Hassan AAA, Lachemi M, Hossain KMA (2012) Effect of metakaolin and silica fume on the durability of self-consolidating concrete. Cem Concr Compos 34(6):801–807
10. Matte V, Moranville M (1999) Durability of reactive powder composites: influence of silica fume on the leaching properties of very low water/binder pastes. Cem Concr Compos 21:1–9
11. Mazloom M, Ramezanianpour AA, Brooks JJ (2004) Effect of silica fume on mechanical properties of high-strength concrete. Cem Concr Compos 26(4):347–357
12. Kumar M, Singh SK, Singh NP, Singh NB (2012) Hydration of multicomponent composite cement: OPC-FA-SF-MK. Constr Build Mater 36:681–686
13. Brooks JJ, Johari MAM, Mazloom M (2000) Effect of admixtures on the setting times of high-strength concrete. Cem Concr Compos 22(4):293–301
14. Yazici H, Aydin S, Yiğiter H, Baradan B (2005) Effect of steam curing on class C high-volume fly ash concrete mixtures. Cem Concr Res 35(6):1122–1127
15. Akkaya Y, Ouyang C, Shah SP (2007) Effect of supplementary cementitious materials on shrinkage and crack development in concrete. Cem Concr Compos 29(2):117–123
16. Khatib JM (2008) Performance of self-compacting concrete containing fly ash. Constr Build Mater 22(9):1963–1971
17. Aïtcin PC (2000) Cements of yesterday and today: concrete of tomorrow. Cem Concr Res 30(9):1349–1359
18. Balaguru P, Chong K (2006) Nanotechnology and concrete: research opportunities. ACI Special Publication 254:15–28
19. Pellenq RJM, Lequeux N, Damme HV (2008) Engineering the bonding scheme in C–S–H: the ion covalent framework. Cem Concr Res 38(2):159–174
20. Sahin MOR (2008) New materials for concrete technology: nano powders. In: 33rd Conference on our world in concrete and structures, 25–27 Aug, Singapore
21. Hou P, Qian J, Cheng X, Shah SP (2015) Effects of the pozzolanic reactivity of nanoSiO_2 on cementbased materials. Cem Concr Compos 55(250–258):2
22. Birgisson AKMB, Geary G, Khan M and Sobolev K (2012) Nanotechnology in concrete materials. Transportation Research Circular E-C170, ISSN 097-8515
23. Nik AS (2012) Nano-particles in concrete and cement mixtures. Appl Mech Mater 110–116:3853–3855
24. Kwan AKH, McKinley M (2014) Packing density and filling effect of limestone fines. Adv Concr Constr 2(3):209–227
25. Weerdt KD, Kjellsen KO, Sellevold E, Justnes H (2011) Synergy between fly ash and limestone powder in ternary cements. Cem Concr Compos 33:30–38
26. Soroka I, Stern N (1976) Calcareous fillers and the compressive strength of Portland cement. Cem Concr Res 6(3):367–376

27. Soroka I, Setter N (1997) The effect of fillers on strength of cement mortars. Cem Concr Res 7(4):449–456
28. Bonavetti V, Donza H, Rahhal V, Irassar E (2000) Influence of initial curing on the properties of concrete containing limestone blended cement. Cem Concr Res 30(5):703–708
29. Bonavetti V, Donza H, Menéndez G, Cabrera O, Irassar EF (2003) Limestone filler cement in low w/c concrete: a rational use of energy. Cem Concr Res 33(6):865–871
30. Kuzel HJ, Pollmann H (1991) Hydration of C3A in the presence of $Ca(OH)_2$, $CaSO_4.2H_2O$ and CaCO. Cem Concr Res 21(5):885–895
31. Kakali G, Tsivilis S, Aggeli E, Bati M (2000) Hydration products of C3A, C3S and Portland cement in the presence of $CaCO_3$. Cem Concr Res 30(7):1073–1077
32. Bonavetti VL, Rahhal VF, Irassar EF (2001) Studies on the carboaluminate formation in limestone filler-blended cements. Cem Concr Res 31(6):853–859
33. Lothenbach B, Saout GL, Gallucci E, Scrivener K (2008) Influence of limestone on the hydration of Portland cements. Cem Concr Res 38(6):848–860
34. Hirao H, Yamada K, Hoshino S and Yamashita H (2007) The effect of limestone addition on the optimum sulphate levels of cements having various Al_2O_3 contents. 12th ICCC, Montreal
35. Matschei T, Lothenbach B, Glasser FP (2007) The AFm phase in Portland cement. Cem Concr Res 37(2):118–130
36. Matschei T, Lothenbach B, Glasser FP (2007) The role of calcium carbonate in cement hydration. Cem Concr Res 37(4):551–558
37. Murthy AR, Iyer NR, Prasad BKR (2013) Evaluation of mechanical properties for high strength and ultra high strength concretes. Adv Concr Constr 1(4):341–358
38. Shaikh FUA and Supit SWM (2015) Chloride induced corrosion durability of high volume fly ash concretes containing nano particles. Constr Build Mater 99(2015):208–225
39. Supit SWM and Shaikh FUA (2014) Effect of nano-$CaCo_3$ on compressive strength development of high volume fly ash mortar and concrete. J Adv Concr Tech 12:178–186
40. Jessica Camiletti J, Nehdi ML (2013) Effect of nano-calcium carbonate on early-age properties of ultrahigh-performance concrete. Mag Concr Res 65(5):297–307

Relevance and Assessment of Fly Ash-Based Sintered Aggregate in the Design of Bricks, Blocks and Concrete

Dhriti. R. Pal, J. P. Behera and B. D. Nayak

Abstract This paper presents the investigation carried out to evaluate the relevance and assessment of bricks, blocks and concrete using sintered aggregate. The main advantages regarding the use of lightweight aggregate concrete in construction are primarily to reduce the self-weight structures besides attaining better thermal insulation performance. Materials can thus be used for producing lightweight solid or hollow concrete blocks as well as bricks for walling purpose. The granular sintered fly ash is found to be best with use of powder fly ash while making bricks and blocks. For making concrete, mixes have been prepared with 20, 30 and 40% replacement of natural aggregate with sintered fly ash aggregate, keeping all in the aggregate grading was unchanged. Concrete with sintered fly ash aggregates up to 40% replacement by volume. The percentage increase of fly ash aggregate decreases the strength of concrete but these are well above the target strength. Research is carried out to evaluate the aggregate samples for evaluations of specific gravity, water absorption, bulk density, particle size, mechanical properties and soundness of aggregate as per relevant Indian standards to assess its suitability in use of sintered aggregate in making bricks and blocks, mixes for concrete with sintered aggregate. To reduce the drying shrinkage in brick, we can use calcinated gypsum instead of cement. The presence of lime in the absence of cement increases the drying shrinkage in brick.

Keywords Specific gravity · Water absorption · Bulk density · Particle size · Soundness of aggregate · Compressive strength · Young's modulus

Dhriti. R. Pal (✉) · J. P. Behera
ITER, Bhubaneswar, India
e-mail: ranjanaa.dhriti@gmail.com

J. P. Behera
e-mail: jpbehera52@gmail.com

B. D. Nayak
CSIR—IMMT, Bhubaneswar, India
e-mail: bansidharnayak55@gmail.com

S. Kumar Shukla et al. (eds.), *Advances in Sustainable Construction Materials and Geotechnical Engineering*, Lecture Notes in Civil Engineering 35,
https://doi.org/10.1007/978-981-13-7480-7_9

1 Introduction

Sintered fly ash lightweight aggregate is one of the different alternative building materials that can be produced by utilising the waste material fly ash from thermal power plants. The manufacture of this aggregate was started in the UK on 1957 and in the USA going ahead in 1963 [1–7]. In India, this product is commercially manufactured and utilised. The awareness to utilise fly ash in bulk to meet the disposal challenges faced by thermal power plants which otherwise may lead to an environmental hazard, health hazard affecting the well-being of the habitants living in close vicinity of thermal power plants. Up to 100% fly ash is used making of the mixture and then formed the sintered aggregate synthetically. The chacterization of physical, chemical and sintering properties of fly ash samples. Utilisation of thermal power plant ash (fly ash and bottom ash) in the area of building construction, cement, concrete, roads, embankments, wasteland development, mine filling, extraction of alumina and other metal values has been attempted in different parts of the world. Many processes have been developed, and further R&D investigation is in progress in the aspects for fruitful utilisation of thermal plant ash. Investigation on direct utilisation of fly ash or in the form of artificial aggregate in manufacture of building blocks, tiles blocks, concrete and other building materials has been made by a number of concrete, and other building material components have been made by a number of workers. The sintered aggregate is prepared by using the laboratory set up of sintered machine from the fly ash samples of Indian thermal power plants is evaluated to explore the possibilities for use in making building bricks, blocks, concrete and other masonry materials.

2 Literature Review

It has been well established that the advantageous application of lightweight structures, structural application in seismic zones, structures built in arctic climates, acoustic and thermal insulation structures and other severe environmental conditions [1–3]. When the experiments on the production of ash containing fly ashes containing lightweight aggregate of strengths were below 55 N-mm^2 which is measured when sintered aggregate FAI ash aggregate was used it was observed after 28 days of curing [8]. The microstructures revelled the solid cementitious matrices do not react with products, metakaolin and fly ash. Energy dispersive spectroscopy and X-ray diffraction showed the formation of amorphous silicoaluminate reaction products. The compressive and flexure strength reduces with the degradation of the density concrete and curing at high temp then the strength increased with the lesser densities. The source of the thermal conductivity was an existence of humidity, and quartz standards were better than those accounted for lightweight concrete [9]. With increase in binder content, the strength and specific gravity of all aggregate decreased at high temperatures and also the water absorption is reduced both at low, medium

and high temperatures. The aggregate with high strength and high specific gravity and with low water absorption can be endorsed to the intense structure with irregular and small pore structures.

3 Materials and Methods

The sintered aggregate pellet which is prepared from different ash samples is used to manufacture bricks and blocks. Fly ash, sand cement, limes and calcined gypsum as admixtures in different proportions are used for manufacturing of bricks and blocks. The sintered aggregate of size 12.5 mm down and 20 mm down has been mixed with the admixtures for casting of standard bricks and blocks in order to evaluate the use of sintered aggregate as building materials, and the test procedures were adopted according to various Indian standard codes. The specific gravity, water absorption, bulk density and particle size analysis of sintered aggregate samples are determined by as per IS: 2386—1963 (Part-1) [10]. The mortar making properties of fine aggregate are determined as per IS: 2386—1963 (Part-V). The soundness of sintered aggregate is assessed according to IS: 2386—1963 [4]. The impact value and 10% fines value are according to the methods specified in IS: 5640—1970 [11], and the properties of bricks such as compressive strength, water absorption and bulk density are determined by according to IS: 4139—1989 [12]. The brick, blocks and concrete were prepared by following methods and procedure.

3.1 "Bricks," "Blocks" and "Concrete"

3.1.1 Bricks

The bricks were shaped in BRICK shaping machine and steam cured for 6 h at one atmospheric pressure. When lime is used as a binder, the steam curing is done. And using cement as binder conventional moist curing can be adopted. In summer season, 28-day moist curing gives an equivalent strength of 6 h of steam curing time which is longer in winter months as the average atmospheric temperature drops down.

3.1.2 Blocks

The production of hollow or solid blocks, using sintered fly ash aggregate as course and natural sand as fines, has been successfully tried using a commercially available standard block making machine producing blocks of nominal size (20 cm × 20 cm × 40 cm). The manual method of produced on a smooth concrete platform, with the help of simple moulds and a surface vibrator. These blocks are instantly demoulded, and mould is reused for next casting. A continuous production is possible with the

help of 10–12 individual moulds. The nominal size of blocks is (15 cm × 20 cm × 30 cm), however the dimensions of the can be different from this, if so desired. The vibrocompaction moulding method was for casting condition and for curing condition steam curing was done at normal pressure for 6 h have been adopted in all cases to manufacture the bricks and blocks.

3.1.3 Concrete

The sintered aggregates prepared from fly ash 1 is being utilised in design of concrete mixes by % replacement of volume to natural granite aggregates. Design mixes have been prepared for M20 and M25 grade of concrete according to Indian Standard Guide Lines (SP-23, 1982) [13]. Mixes have been prepared with 20, 30, 40% replacement of natural aggregates by sintered aggregate, keeping all the aggregate in grading unchanged. The strength of concrete with the above mixes along with their values of Young's modulus of elasticity confirms to the requirement of the Indian standard values.

4 Properties and Results of Sintered Aggregate Pellet

Different properties of sintered aggregate prepared fly ash samples 1, 2 and 3, respectively, are given in Table 1. Tables 2, 3 and 4 show the admixture percentage and different properties of bricks made from aggregate pellets of fly ash 1, fly ash 2 and fly ash 3. The listings of properties of blocks are shown in Table 5. The strength of concrete (prepared from natural aggregate and sintered aggregate on replacement) is shown in Table 6.

The moulding conditions were vibrocompaction, and curing conditions were steam at normal pressure for 6 h for fly ash 1, 2 and 3. The determined results of Tables 2, 3 and 4 show that the more percentage of sintered fly ash aggregate in the absence of hydraulic lime gives the lesser results of drying shrinkage that is 0.22, 0.26 and 0.26%, respectively, among all the composition. Similarly, in the absence of cement, the presence of fly ash, sand and lime gives the bulk density 1410, 1415 and 1445 kg/m^3.

It is clearly shown that in Table 5 in the absence of cement, the compressive strength of blocks is decreased. In the absence of hydrated lime, the compressive strength increases, i.e. 112 and 102 kg/m^3 in fly ash 1 and 2. On the other hand, the flexural strength of the fly ash 1 and 2 also increased, i.e. 23 and 21.60 kg/m^3.

Table 6 and Fig. 1 show the graphical representation of compressive strength of concrete mixes at the age of 7 days and 28 days of curing period. The M25 grade of concrete Mix 1 gives the highest compressive strength 24.30 and 35.40 N/mm^2, and the M20 grade of concrete mix 4 offers the lowest compressive strength 20.80 and 29.70 N/mm^2 at the age of 7 and 28 days of curing period, respectively.

Table 1 Properties of sintered aggregate prepared fly ash samples 1, 2 and 3

Properties	Fly ash 1	Fly ash 2	Fly ash 3
Bulk density (kg/m^3)	740	835	675
Specific gravity (apparent)	1.61	1.67	1.48
Specific gravity (true)	1.71	1.77	1.57
Water absorption (%)	18	12	14
Impact value (%)	30	29	34
10% fines value (tonne)	9.3	10	8.1
Soundness (% loss)	2.92	3.6	3
Particles + 20 mm (% by wt.)	4.2	7.8	4.75
Particle −4.75 mm (% by wt.)	5	1.35	2.45

For Tables 2, 3 and 4
SFAA Sintered fly ash aggregate; *CS* Compressive strength; *CG* Calcined gypsum; *BD* Bulk density; *EF* Efflorescence; *DS* Drying shrinkage; *WA* Water absorption; *FA* Fly ash; *C* Cement; *L* Lime (Hydrated); *S* Sand

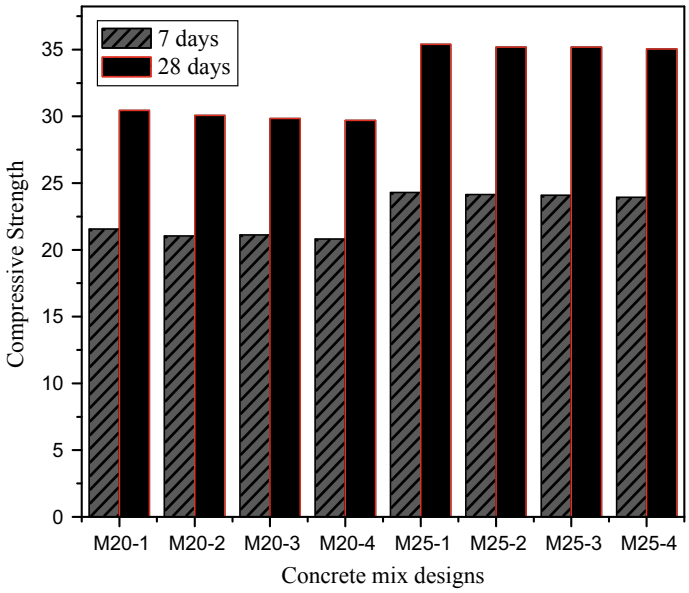

Fig. 1 Compressive strength versus concrete mix

Table 2 Properties of bricks (fly ash 1)

Mix composition by volume (%)							BD (kg/m^3)	WA (%)	CS (kg/cm^2)	DS (%)	EF
S.L.	SFAA (−12.5 mm + 10 mm)	SAFF (−10 mm)	FA	S	C	L					
1	20	30	20	20	–	10	1410	13.1	40	0.044	Nil
2	25	25	20	20	10	–	1525	10.1	112	0.022	Nil
3	25	25	20	20	5	5	1485	10.8	80	0.035	Nil
4	20	30	20	20	5	5	1420	10.8	82	0.030	Nil
5	20	20	25	25	+2CG	10	1465	10.5	84	0.032	Nil

Table 3 Properties of bricks (fly ash 2)

Mix composition by volume (%)							BD (kg/m^3)	WA (%)	CS (kg/cm^2)	DS (%)	EF
S.L.	SFAA −(12.5 mm + 10 mm)	SAFF (−10 mm)	FA	S	C	L					
1	20	30	20	20	–	10	1415	14.2	38	0.041	Nil
2	25	25	20	20	10	–	1530	10.4	108	0.026	Nil
3	25	25	20	20	5	5	1460	10.2	96	0.022	Nil
4	20	30	20	20	5	5	1440	12.8	84	0.030	Nil
5	20	20	25	25	+2CG	10	1450	13.8	88	0.032	Nil

Table 4 Properties of bricks (fly ash 3)

	Mix composition by volume (%)						BD (kg/m^3)	WA (%)	CS (kg/cm^2)	DS (%)	EF
S.L.	SFAA −(12.5 mm + 10 mm)	SAFF (−10 mm)	FA	S	C	L					
1	20	30	20	20	–	10	1445	9.5	48	0.035	Nil
2	25	25	20	20	10	–	1460	8.4	92	0.026	Nil
3	25	25	20	20	5	5	1460	8.5	66	0.032	Nil
4	20	30	20	20	5	5	1455	8.7	65	0.035	Nil
5	20	20	25	25	+2CG	10	1450	9.5	72	0.032	Nil

Table 5 Properties of blocks

Mark	SAFF (4.5 – 20 mm)	SFAA (−4.5 mm)	S	C	L	FS (kg/m^3)	CS (kg/m^3)
Fly ash 1							
1	50	20	20	–	10	18.90	75
2	50	20	20	10	–	23.00	112
3	50	20	20	5	5	20.13	90
Fly ash 2							
1	50	20	20	–	10	18.80	74
2	50	20	20	10	–	21.60	102
3	50	20	20	5	5	19.60	80

S Sand; *SFFA* Sintered fly ash aggregate; *C* Cement; *L* Hydrated lime; *CS* Compressive strength; *FS* Flexural strength

Table 6 Strength and Young's modulus of elasticity of concrete mixes (with natural aggregate and sintered aggregates on replacement)

Grades of concrete	Mix	Seven-day compressive strength in N/mm^2	Twenty-eight-day compressive strength in N/mm^2
M20	Mix 1	21.55	30.44
	Mix 2	21.03	30.07
	Mix 3	21.11	29.85
	Mix 4	20.80	29.70
M25	Mix 1	24.30	35.40
	Mix 2	24.15	35.18
	Mix 3	24.08	35.18
	Mix 4	23.93	35.03

Mix 1: Concrete with natural aggregates
Mix 2: Concrete with 80% natural granite aggregates and 20% sintered fly ash aggregates
Mix 3: Concrete with 70% natural granite aggregates and 30% sintered fly ash aggregates
Mix 4: Concrete with 60% natural granite aggregates and 40% sintered fly ash aggregate
Mix design stipulations: The maximum size of aggregate—20 mm; The degree of quality control—good; Compaction factor—0.95; Type of exposure—moderate

Table 7 Strength and Young's modulus of elasticity of concrete mixes (with natural aggregate and sintered aggregate)

Grades of concrete	Mix	Twenty-eight-day compressive strength in N/mm^2	Theoretical Young's modulus of elasticity, IS: 456—2000 N/mm^2	Calculated Young's modulus of elasticity N/mm^2
M20	Mix 1	30.44	27,586	29,600
	Mix 2	30.07	27,418	29.550
	Mix 3	29.85	27,317	28,800
	Mix 4	29.70	27,248	28,680
M25	Mix 1	35.40	29,748	32,520
	Mix 2	35.18	29,656	31,640
	Mix 3	35.18	29,656	31,445
	Mix 4	35.03	29,593	31,200

Table 7 shows the compressive strength of blocks after 28 days of curing, theoretical Young's modulus of elasticity, as per IS: 456—2000 N/mm^2. Comparing theoretical Young's modulus with actual Young's modulus, the M25 grade of concrete mix 1 gives the highest values that are 29,748 N/mm^2 and 32,520 N/mm^2, while the M20 grade of concrete mix 4 gives the lowest value 27,248 N/mm^2 and 28,680 N/mm^2. The theoretical Young's modulus was calculated by using formula 1 with multiplying the value of compressive strength of each concrete blocks. Formula for theoretical Young's modulus of elasticity, as per IS: 456—2000 N/mm^2, is given as, [8]. The theoretical values are less than the actual values of Young's modulus. The M25 design concrete mixes have the highest value while comparing with the M20 design concrete mixes.
Where

$$E_c = 5000\sqrt{\sigma_{ck}}$$

E_C short-term modulus of elasticity of concrete in N/mm^2,
$_{ck}$ 28-day characteristics strength of concrete in N/mm^2,
$_{ck}$ 28-day characteristics strength of concrete in N/mm^2.

5 Conclusion

1. It has been observed that the aggregate produced from fly ash 1, fly ash 2 and fly ash 3 samples pass all the requirements of properties except for water absorption as per IS standard.
2. Bricks which made from the cement, cement–lime or lime–gypsum binder aggregates give the adequate strength.
3. The strength brick is adequate to produce by substitution of the sintered aggregate pellet is up to 50 and 10% of cement, cement–lime or lime–gypsum.
4. Sintered aggregate pellets of below 20 mm size are suitable for the manufacture of normal size (20 × 20 × 40 mm) blocks.
5. The compressive strength of blocks (fly ash 1 and fly ash 3) is from 75 to 112 kg/cm^2 produced by 70% of sintered aggregate, 20% of sand and 10% of the binder of cement, cement–lime and lime–gypsum.
6. The sintered aggregate of various size fractions (0–20 mm) will be supple to use in replacement of natural stones, gravels and sands in making bricks, blocks and concretes.
7. The granular sintered fly ash is found to be best with the use of powder fly ash while making bricks and blocks.
8. Concrete with sintered fly ash aggregates up to 40% replacement by volume to natural aggregates maintains their characteristics parameter.
9. The M25 grade of concrete mix 1 gives the highest compressive strength 24.30 and 35.40 N/mm^2, and the M20 grade of concrete mix 4 offers the lowest compressive strength 20.80 and 29.70 N/mm^2 at the age of 7 and 28 days of curing period, respectively.

Acknowledgements The author wishes to acknowledge the CSIR—IMMT, Institute of Minerals and Materials Technology, Bhubaneswar, Odisha, for their support and to conduct the experimental work in the laboratory.

References

1. Bobrowski J (1980) Outstanding application of in lightweight concrete and an appreciation of likely future developments in light weight concrete, the concrete society. The construction Ltd., Lancaster, England, pp 239–260
2. Bomhard H (1980) Lightweight concrete structures, potentialities, limits and realities in light weight concrete, the concrete society. The Construction Press Ltd., Lank aster, England, pp 277–307
3. Roberts JE (1992) Lightweight concrete bridges for California high way system. In: Structural light weight aggregate concrete performance. In: Holm TA, Vaysburd AM (eds) ACI, SP-136, Detroit, pp 255–272
4. Jindal BK (1964) Properties of structural Lightweight concrete using sintered fly ash aggregate. India Concr J 38:413–418
5. Jindal BK (1996) Behaviour of reinforced lightweight concrete in flexure and shear. Indian Concr J, 1–8

6. Jindal BK (1996) Design and testing of precast reinforced lightweight concrete slabs. Indian Concr J, 1–6
7. Jindal BK, Bhise NN, Kishan Lal, Sharma KN (1974) Use of lightweight concrete in precast construction. Indian Concr J, 1–3
8. Cerny V, Kocianova M, Drochytka R (2017) Possibilities of lightweight high strength concrete production from sintered fly ash aggregate. In: 18th international conference on rehabilitation and reconstruction of building 2016, CRRB. Procedia Engineering, pp 9–16. https://doi.org/10.1016/j.proeng.2017,04.517
9. Aguilar R, Diaz O, Garcia JI (2010) Light weight concretes of activated metakaolin—fly ash binders, with blast furnace slag aggregate. Constr Build Mater 24:1166–1175. https://doi.org/10.1016/j.conbuildmat.2009.12.024
10. IS: 2386 (Part 1)—1963, Indian standard, methods of test for aggregates for concrete. Bureau of Indian standard, New Delhi, Indian
11. IS: 5640—1970 Indian standard, methods of test for determining aggregates impact value of soft coarse aggregates, Bureau of Indian standard, New Delhi, Indian
12. IS: 4139—1989 Indian standard, calcium silicate bricks specification. Bureau of Indian standard, New Delhi
13. SP 23: 1982, Indian stands, Handbook of concrete mixes

Influence of Microstructure of Geopolymer Concrete on Its Mechanical Properties—A Review

Amer Hassan, Mohammed Arif and M. Shariq

Abstract Geopolymer concrete (GPC) has been researched during the past few decades as a viable sustainable construction material, which can minimise CO_2 emission for its use of industrial by-products. Past research on GPC shows that GPC is best suited for structural application with workable slump and strength as compared to ordinary Portland cement concrete (OPCC). The microstructure of GPC and OPCC has been investigated to understand its influence on engineering properties. It has been observed that GPC contained more amorphous phases, less porosity and more pores in the mesopores range than OPCC. Review of the literature revealed that the production of geopolymer concrete requires great care and correct material compositions. During the activation process in making the geopolymer, high alkalinity also requires safety risk and enhanced energy consumption and generation of greenhouse gases. Furthermore, the production of GPC is also affected by the curing time and curing temperature. Few studies have also been carried out to observe the effect of curing temperature on the polymerisation reaction of GPC.

Keywords Geopolymer concrete · Geopolymer microstructure · Durability · Shrinkage

1 Introduction

The microstructure of geopolymers varies with the type of precursors used. An aluminium-replaced C-A-S-H, with cross-linked and non-cross-linked tobermorite-based structures is the fundamental reaction result of slag-based geopolymer [1],

A. Hassan (✉) · M. Arif · M. Shariq
Aligarh Muslim University, Aligarh 202001, UP, India
e-mail: ameralburay@gmail.com

M. Arif
e-mail: marifamu@gmail.com

M. Shariq
e-mail: mshariqdce@gmail.com

S. Kumar Shukla et al. (eds.), *Advances in Sustainable Construction Materials and Geotechnical Engineering*, Lecture Notes in Civil Engineering 35,
https://doi.org/10.1007/978-981-13-7480-7_10

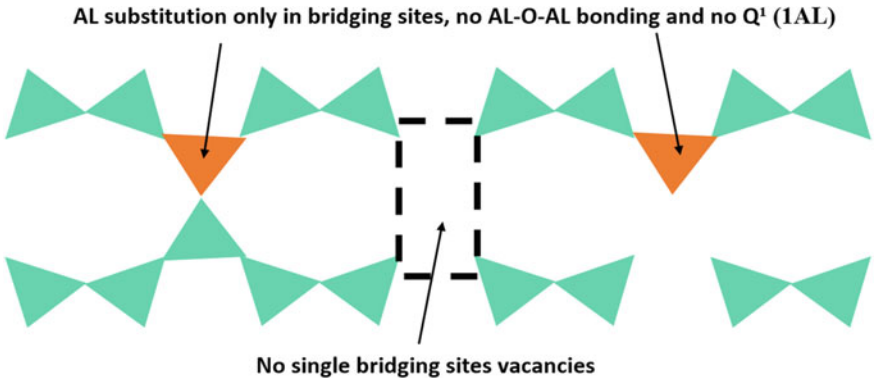

Fig. 1 Illustration of constraints in CSTM [1]

unlike the basic hydration result of OPC which is C-S-H gels with non-cross-linked structures [2]. The cross-linked structures of geopolymer result from the geopolymerisation. Myers et al. [1] proposed the model of cross-linked substituted tobermorite (CSTM) for C-A-S-H gel, which described the solid phases in geopolymer as a mixture of 14, 11 and 9 Å tobermorite structures as shown in Fig. 1.

In fly ash-based geopolymer, the primary reaction product is an alkaline silicoaluminate gel containing silicon and aluminium tetrahedral randomly distributed and cross-linked. When NaOH is used as activator to this type of geopolymer, the produced gel is identified as N-A-S-H gel. Furthermore, experiments done by Garcia-Lodeiro et al. [3] showed that in the presence of Ca, N-A-S-H would transform to C-A-S-H at high pH until available Ca is exhausted. Criado et al. [4] and Criado [5] studied the microstructure of N-A-S-H gel and proposed that it was an amorphous gel involving in a polymeric, cross-linked aluminosilicate network similar to C-A-S-H gel. The gel of N-A-S-H comprised two bonds types of Si-O, which were the terminal and bridge bonds. They found that the nature of this gel was influenced by the activator and curing method. When there was more soluble silica in the system, more bridge bonds were formed. Moreover, when it was under thermal curing, the structure became more arranged with a predominance of bridge bonds over terminal bonds and hence more stable.

2 Differences in Microstructure Between GPC and OPCC

Because of the cross-linked feature mentioned above, hardened GPC has a denser microstructure than hardened OPCC. The C-A-S-H matrix chains in geopolymer system were found longer than the C-S-H gel chains in OPCC system, due to the substitution of Al^{3+} for Si^{4+} in bridging positions. C-A-S-H gels had higher Al/Si ratio and lower Ca/Si ratio than C-S-H. It was found that Young's modulus was 77.3

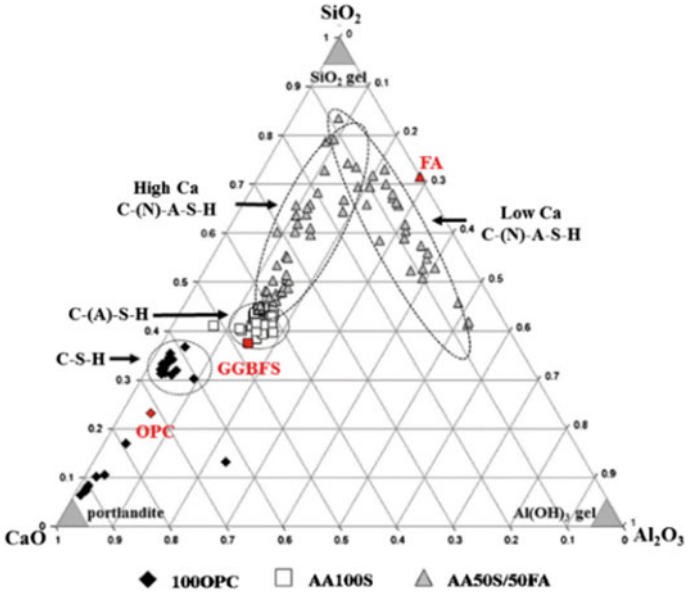

Fig. 2 Ternary plot of binder gel compositions of geopolymer [7]

and 49.9 GPa, for typical tobermorite 1.1 nm and tobermorite 1.4 nm, respectively [6]. This would be because of the higher interlayer cohesion presented by the linking between bridging tetrahedral of conservative layers [6].

Figure 2 portrays a ternary plot of gel composition of GPC and OPCC. The comparison of the gel compositions of GPC and OPC systems reveals that the C-S-H produced in OPCC has more Ca and less Al content than the C-A-S-H produced in slag-based GPC. When fly ash is presented in the system of geopolymer, N-(C)-A-S-H can be identified with low Ca content, but pure N-A-S-H is only stable at pH lower than 12 [3, 7].

Microstructure analysis of pore characteristic with the techniques such as (MIP) and gas adsorption revealed that the pore size distribution of slag-based geopolymer concrete showed more mesopores (pore size <50 nm) and also lower porosity than those of OPCC. A comparison of pore size distribution of slag-based geopolymer paste (GPP) and OPC paste (OPCP) is shown in Fig. 3. Most of the pores in OPCP were distributed in the range between 10 and 100 nm, while most of the pores in GPP were below 20 nm [8–12]. It was also found that when SCM, such as slag and silica fume, was used in OPCC, the pozzolanic reaction forms a denser microstructure which results in high strength and low permeability [13, 14]. Studies focusing on porosity can help in understanding the behaviour and properties of GPC and OPCC, as it encompasses the density of the microstructure, the presence of microcracks, the rate of diffusion of pore solution, etc. [15].

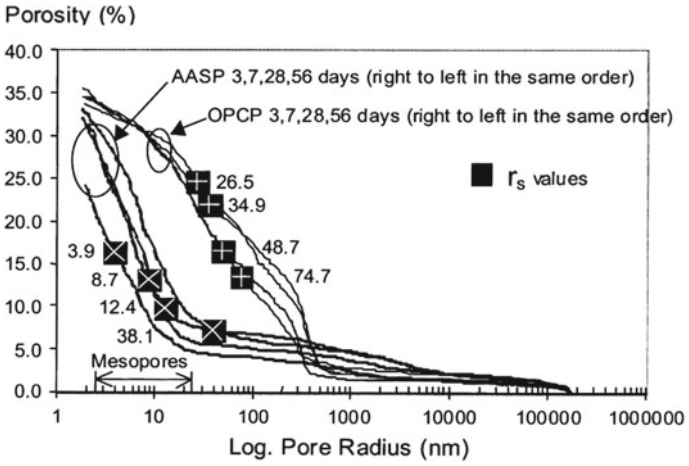

Fig. 3 Pore size distribution of GPC and OPC [11]

2.1 Relationship Between Microstructure and Properties of Concrete

It is believed that the microstructure has an influence on the characteristics and behaviours of the materials. The gels are the main strength giving component in geopolymer and OPC products. It was found that the pore structure has a certain effect on a range of properties for OPCC, such as strength and permeability. As pores are formed within the microstructure of C-S-H, size, shape, bonding and packing arrangement of the C-S-H would affect the pore microstructure. Prediction models, which include microstructure, or even nanostructure, can improve prediction of the properties of hydrated OPCC, which include strength, shrinkage, creep, permeability and diffusion [16, 17].

Compressive strength

The pore structure of concrete has an important effect on the strength of hardened paste and thus on concrete. Generally, strength decreases as total porosity increases. The relationships between porosity and strength of OPCP were summarised by Rößler and Odler [18] as follows:

Balshin's equation:

$$f_c = f_{c0}(1 - \phi)^n \tag{1}$$

Ryshkevitch and Duckworth's equation:

$$f_c = f_{c0}e^{-k_\gamma \phi} \tag{2}$$

Schiller's equation:

$$f_c = k_S \ln(\phi_{0S}/\phi) \tag{3}$$

Hasselman's equation:

$$f_c = f_{c0} - k_H \phi \tag{4}$$

where fc is the compressive strength (CS) at porosity ϕ, fc_0 is the CS at 0 porosity, ϕ_{0S} is the porosity at 0 strength, and n, k_r, k_S and k_H are the experimental constants.

Equations (1)–(4) predict the strength–porosity relationship in slag-based GPM and found that it followed different trend to OPCM due to the different nature of their pore structures. These equations yielded less accurate results for GPM as they were derived for OPCM primarily. However, he suggested that Eq. (4) was the most accurate to predict the strength–porosity relationship in both GPM and OPCM. The strength–porosity relationship in GPM and OPCM is shown in Fig. 4.

The compressive strength of slag-based GPM was found to be higher with increasing modulus and solution concentration. However, the flexural tensile strength of slag-based GPM did not show any improvement, that may attribute to the development of microcracks on the slag-based GPM gel. Baradan [20] assessed two types of heat treatment and found that autoclaving would be more efficient than steam curing in strength development and shrinkage reduction in slag-based GPM. This would be due to the development of a finer pore size distribution, lower Ca/Si proportion of C-S-H and compact structure of the product. However, autoclaving caused reduction in strength for OPCM. Under the condition of elevated temperature and pressure, the chemistry of hydration had been significantly changed. C-S-H form was transformed into a crystalline structure, α-calcium silicate hydrate (α-C-S-H), which caused porosity to increase.

Jambunathan et al. [21] suggested that the slow conversion of the hydration products (CAH10, C2AH8 and C4AH13) to a more stable structure (C3AH6) at room

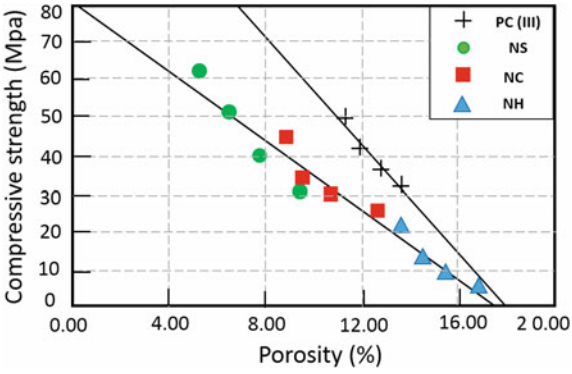

Fig. 4 Strength–porosity relationship in GPM and OPCM (PC denotes OPC, NS, NC and NH denote geopolymer with different activators) [19]

temperature had an effect on the loss of compressive strength in slag-based GPP. Since the latter structure has a greater density than the former structure, the conversion resulted in an increase in porosity and thus deterioration in strength.

Collinsand and Sanjayan [22] summarised the effect of curing on strength of slag-based GPC from a range of studies. The curing method mainly influenced the pore structure, and it can result in microcracks. For the GPC under exposed curing, a network of microcracks was indicated. These microcracks in the specimen increased the total porosity. The longer exposed specimens containing more microcracks showed a reduction in strength. Furthermore, the strength loss was larger in the smaller GPC-exposed specimen. The pore distribution showed coarser pore size towards the outer surface in the large specimen (150 mm dia.), so the higher loss in strength in the small specimen was due to larger portion of coarser pore size.

Brough and Atkinson [23] investigated the development of the paste/aggregate interfacial transition zone (ITZ) in slag-based GPM. The generated zone in the paste was filled up as hydration process showing an improved microstructure at ages after 14 days. Therefore, the slag-based GPM had much lower interfacial porosity than the OPCM, and the strength of slag-based GPM was higher than that of OPCM. Similar result was reported by San Nicolas and Provis [24].

Permeability and durability

Gas and water permeability are of interest in studying the durability of concrete, since they are related to the mass transport within concrete. There are two types of pore in the porous materials: open and closed. Open pores refer to pores with various size connected to each other and have an end open at the surface of the materials, but closed pores do not. Some porosimetry analysis methods, such as MIP and gas adsorption, can only be used in access to the open pores. Although there is such limitation, the analysis on these connected open pores is critical to the study of the permeability and diffusivity of concrete [15].

Durability of slag-based GPC has been studied in the past few decades, covering topics on sulphate attack, acid attack, chloride resistance, carbonation, corrosion resistance of reinforcement, elevated temperature and fire resistance, and freezing and thawing resistance. Immersing slag-based GPC in sulphate solution, acetic acid and seawater showed little negative effect on GPC, and GPC exhibited better performance than OPCC [25–29]. Thus, the degradation of strength of GPC was lower, and the resistance to corrosion of steel reinforcement was higher for GPC [30, 31]. Bakharev [32] and Byfors et al. [25] reported that carbonation resistance of slag-based GPC was lower than that of OPCC. However, this would be attributed to the relative humidity (RH) where the specimens were exposed. High RH in the saturated slag-based GPC would retard the carbonation in the early stage, and the carbonation is faster when slag-based GPC when drying occurs and proceeds from the surface [33]. The ASR in GPC was not well-known. Bakharev [34] found that GPC expanded more than OPCC under ASR, but Fernández-Jiménez [35] found the opposite way.

At a high temperature above 300 °C, OPCC chemically dehydrates while GPC remains chemically stable up to 800 °C. This makes geopolymer a potential option in

fireproofing for construction purposes. However, spalling was reported in some GPC under elevated temperature, and this was related to the size of the specimens and the size of aggregates [36–39]. On the other hand, GPC has excellence freeze–thaw durability but it is affected by the air entrainment in the concrete [25, 26, 40].

The rate of most of the above degradation processes is controlled by the rate of diffusion of the species of the penetrating chemical and the viscosity of the solution in the pores. Over the years, studies have been carried on investigating the relationship between pore characteristic and the permeability. Powers, Mann and Copeland [41] reported the relationship between the pore structure and the permeability of OPCP. Only the evaporable free water moved in the pore network. The viscosity of the fluid, as stated in Darcy's law, also influences the flow of fluid through the specimen. The viscosity of the pore solution is higher than water due to the presence of alkali, and it varied with the concentration and temperature. The more the alkali exists in the pore solution, the higher the viscosity it is. They also pointed out that the creep of concrete was a result of redistribution of evaporable water in the concrete member under change of stress.

Pore characteristic of concrete can be obtained through a number of methods. The most common methods are MIP and gas adsorption test. Damage would be induced to the sample during MIP. Experiment on OPC samples showed a higher connectivity, lower pores and greater average pore size after intrusion [42]. The analysis can also be done using image analysis method, but the range of pore sizes is limited by the resolution of the image conducted MIP on concrete broken chunks from the centre of specimen crushed with a hammer [43, 44]. The permeability was estimated through the porosity and the mean pore size by using model by Kondraivendhan et al. [44] and Pradhan et al. [45]. Their model predicted the hydraulic diffusivity from pore size distribution.

Nitrogen adsorption test has been used to examine the pore characteristic of OPCP at pore size around 1–40 nm [46]. Unlike MIP, gas adsorption test is more gentle to the sample when assessing the small pore sizes [15]. Therefore, gas adsorption test can be a better method to investigate the gel pores. However, the effectiveness of this method relies on the pretreatment method. It was pointed out that oven drying at 105 °C would increase the chance of pore collapsing and results in less surface area in measurement [46]. Solvent exchange with organic liquid is also an alternative in removing water from the pore structure by counter-diffusion process, but this process is slow and takes a long period [47]. It was found that the lower the porosity and the finer the pore structure, the lower the permeability. The rate of the degradation processes can be lower [8, 19]. The permeability can be determined based on Darcy's law:

$$Q = kA\eta \times \Delta PL \tag{5}$$

where Q (m^3/s) is the flow, κ (m^2) is the permeability of the medium, A (m^2) is the cross-sectional area of the pore, η (Pa·s) is the viscosity of the fluid and ΔP (Pa) is the pressure drop over the length L (m).

Besides Darcy's law, Hagen–Poiseuille law, as known as Poiseuille law, can also be used to analyse the flow through porous medium. It assumes that the Newtonian fluid flows through a cylindrical pipe of constant cross section. The Hagen–Poiseuille law is presented as the following equation:

$$Q = \pi r4\Delta P8\eta L \tag{6}$$

where r (m) is radius of the cylindrical pipe. Hagen–Poiseuille law was used in prediction of permeability of harden OPCP. However, the pores inside harden OPCP were not constant, but distributed in a wide range. Pan et al. [39] developed a model to investigate the relationship between pore size distribution and the permeability based on Hagen–Poiseuille law. In order to account the influence of pore size, he divided the pore size distribution into segments of $\log r = 0.05$:

$$Q = \frac{r^2 \Delta P \phi}{32 r^2 \eta h} \tag{7}$$

where r is expressed in Å, τ is the tortuosity factor and h (m) is the thickness of the specimen. With the assumptions of the pores within each interval forming a discrete package and no flow in pores size of less than 7.5 nm, the total flow was calculated as sum of flow in each interval.

Holly [48] proposed a model of two-dimensional network of tubes which took pore size distributions in account for permeability of OPCP based on Hagen–Poiseuille law. The network was of a square lattice arrangement.

$$\Delta P = \sum_{i=1}^{\mathrm{I}} \frac{8\eta b Q_i}{\pi r_i^2} \tag{8}$$

where b is the proportionality constant of length to radius of the tube, Q_i (m^3/s) is the flow corresponded to pore sizes of r_i (m). They pointed out the importance of pore size distribution in estimation of permeability, as it cannot be defined in terms of an average pore size and porosity. Different results were given by bimodal and unimodal log-normal distribution of pore size since flow through capillary pores was favoured.

Shrinkage

The pore structure and the diffusivity also play an important role in shrinkage of concrete. There are two major parts of shrinkage in concrete: autogenous shrinkage and dry shrinkage. Autogenous shrinkage occurs due to a capillary shrinkage related to water consumption through hydration, and drying shrinkage occurs as a reduction in volume due to loss of water from the pores to the external environment by the gradient of humidity [49, 50]. The size of the pores influenced the diffusion process because the resistance was larger for smaller pores. Thus, it takes longer time for the drying process [51]. Some researchers reported that the drying shrinkage of

slag-based GPC was higher than that of OPCC [11, 52]. However, the water loss in OPCC measured was higher than that in GPC after drying. They related this to the difference of pore size distribution between OPCP and GPP in concrete. Geopolymer paste (GPP) has a smaller pore size than OPCP and higher rate of pore size within the mesopore (1.25–25 nm) limits than OPCP. GPP was found to have the larger capillary tensile forces set up at the meniscus, resulting in higher shrinkage [53].

Drying generally induced microcracking in concrete and reduced both compressive and tensile strengths, but tensile creep reduced the risk of cracking in terms of stress relaxation [52]. Benboudjema [54] suggested that the effect of creep, effect of aggregate restraint, concrete mix and capillary pressure should be taken into account for more accurate prediction of microcracking and of the residual mechanical properties after drying.

The w/c ratio, paste volume, size effect and RH also influence the drying shrinkage of concrete. The shrinkage strain is directly proportional to the paste volume in concrete. Although the sample size does not have an effect on the ultimate drying shrinkage strain, it influences the strain rate. The drying shrinkage is approximately inversely proportional to the RH in the range from 48 to 100% [55].

3 Conclusion

To develop an advanced knowledge and better understanding of the process of GPC geopolymerisation, the microstructure and chemistry of GPC must be carefully understood and investigated. A better understanding will facilitate to get into the interactions between the microstructure of GPC on the one side and the alkaline activating solutions on the other side, which will offer significant insight into the mechanical properties of GPC with respect to the differences in microstructure of geopolymers used. This information will help very well in the analysis and design of geopolymer concrete.

References

1. Myers RJ, Bernal SA, San Nicolas R, Provis JL (2013) Generalized structural description of calcium-sodium aluminosilicate hydrate gels: the cross-linked substituted tobermorite model. Langmuir 29:5294–5306
2. Richardson IG (2008) The calcium silicate hydrates. Cem Concr Res 38:137–158
3. Garcia-Lodeiro I, Palomo A, Fernández-Jiménez A, Macphee DE (2011) Compatibility studies between N-A-S-H and C-A-S-H gels. Study in the ternary diagram Na2O–CaO–Al2O3–SiO2–H2O. Cem Concr Res 41:923–931
4. Criado M, Fernández-Jiménez A, Palomo A (2007) Alkali activation of fly ash: effect of the SiO2/Na2O ratio. Part I: FTIR study. Microporous Mesoporous Mater 106:180–191
5. Criado M et al (2008) Effect of the SiO2/Na2O ratio on the alkali activation of fly ash. Part II: 29Si MAS-NMR survey. Microporous Mesoporous 109:525–534

6. Puertas F et al (2011) A model for the C-A-S-H gel formed in alkali- activated slag cements. J Eur Ceram Soc 31:2043–2056
7. van Deventer JS et al (2015) Microstructure and durability of alkali- activated materials as key parameters for standardization. J Sustain Cem Mater 4:116–128
8. Garboczi EJ (1990) Permeability, diffusivity, and microstructural parameters: a critical review. Cem Concr Res 20:591–601. https://doi.org/10.1016/0008-8846(90)90101-3
9. Lu S, Landis EN, Keane DT (2006) X-ray microtomographic studies of pore structure and permeability in Portland cement concrete. Mater Struct Constr 39:611–620
10. Häkkinen T (1993) The influence of slag content on the microstructure, permeability and mechanical properties of concrete Part 1 Microstructural studies and basic mechanical properties. Cem Concr Res 23:407–421
11. Collins F, Sanjayan JG (2000) Effect of pore size distribution on drying shrinking of alkali-activated slag concrete. Cem Concr Res 30:1401–1406
12. Häkkinen T (1993) The influence of slag content on the microstructure, permeability and mechanical properties of concrete. Part 2 technical properties and theoretical examinations. Cem Concr Res 23:518–530
13. Mokhtarzadeh A, French C (2000) Time-dependent properties of high-strength concrete with consideration for precast applications. ACI Mater J 97:263–271
14. Roy DM, Idorn GM (1982) Hydration, structure, and properties of blast furnace slag cements, mortar, and concrete. J Am Concr Inst 79:444–457
15. Aligizaki KK (2006) Pore structure of cement-based materials. Taylor & Franics, New York
16. Beaudoin JJ, Feldman RF, Tumidajski PJ (1994) Pore structure of hardened portland cement pastes and its influence on properties. Adv Cem Based Mater 1:224–236
17. Jennings HM et al (2008) Characterization and modeling of pores and surfaces in cement paste: Correlations to processing and properties. J Adv Concr Technol 6:5–29
18. Rößler M, Odler I (1985) Investigations on the relationship between porosity, structure and strength of hydrated portland cement pastes I. Effect of porosity. Cem Concr Res 15:320–330
19. Shi C (1996) Strength, pore structure and permeability of alkali-activated slag mortars. Cem Concr Res 26:1789–1799
20. Aydın S, Baradan B (2012) Mechanical and microstructural properties of heat cured alkali-activated slag mortars. Mater Des 35:374–383
21. Jambunathan N et al (2013) The role of alumina on performance of alkali-activated slag paste exposed to 50 °C. Cem Concr Res 54:143–150
22. Collins F, Sanjayan JG (2001) Microcracking and strength development of alkali activated slag concrete. Cem Concr Compos 23:345–352
23. Brough AR, Atkinson A (2002) Sodium silicate-based, alkali—activated slag mortars: Part I. Strength, hydration and microstructure. Cem Concr Res 32:865–879
24. San Nicolas R, Provis JL (2015) The interfacial transition zone in alkali-activated slag mortars. Front Mater 2:70
25. Byfors K et al (1989) Durability of concrete made with alkali activated slag. In: Malhotra VM (ed) 3rd international conference proceedings fly ash, silica fume, slag, and natural pozzolans in concrete. Trondheim, Norway, pp 1429–1466
26. Douglas E, Bilodeau A, Malhotra VM (1992) Properties and durability of alkali-activated slag concrete. ACI Mater J 89:509–516
27. Bakharev T, Sanjayan JG, Cheng YB (2002) Sulfate attack on alkali-activated slag concrete. Cem Concr Res 32:211–216
28. Dellinghausen LM et al (2012) Total shrinkage, oxygen permeability, and chloride ion penetration in concrete made with white Portland cement and blast-furnace slag. Constr Build Mater 37:652–659
29. Bakharev T, Sanjayan JG, Cheng YB (2003) Resistance of alkali- activated slag concrete to acid attack. Cem Concr Res 33:1607–1611
30. Wang S-D, Pu X-C, Scrivener KL, Pratt PL (1995) Alkali-activated slag cement and concrete: a review of properties and problems. Adv Cem Res 7:93–102

31. Roy DM, Jiang W, Silsbee MR (2000) Chloride diffusion in ordinary, blended, and alkali-activated cement pastes and its relation to other properties. Cem Concr Res 30:1879–1884
32. Bakharev T, Sanjayan JG, Cheng YB (2001) Resistance of alkali-activated slag concrete to carbonation. Cem Concr Res 31:1277–1283
33. Bernal SA et al (2014) Durability and testing—degradation via mass transport. In: Provis JL, Van Deventer JSJ (eds) Alkali activated materials. Springer, London
34. Bakharev T, Sanjayan JG, Cheng YB (2001) Resistance of alkali-activated slag concrete to alkali–aggregate reaction. Cem Concr Res 31:331–334
35. Fernández-Jiménez A, Puertas F (2002) The alkali–silica reaction in alkali-activated granulated slag mortars with reactive aggregate. Cem Concr Res 32:1019–1024
36. Cheng TW, Chiu JP (2003) Fire-resistant geopolymer produce by granulated blast furnace slag. Miner Eng 16:205–210
37. Kong DLY, Sanjayan JG (2010) Effect of elevated temperatures on geopolymer paste, mortar and concrete. Cem Concr Res 40:334–339
38. Zhao R, Sanjayan JG (2011) Geopolymer and Portland cement concretes in simulated fire. Mag Concr Res 63:163–173
39. Pan Z, Sanjayan JG, Kong DLY (2012) Effect of aggregate size on spalling of geopolymer and Portland cement concretes subjected to elevated temperatures. Constr Build Mater 36:365–372
40. Fu Y, Cai L, Yonggen W (2011) Freeze-thaw cycle test and damage mechanics models of alkali-activated slag concrete. Constr Build Mater 25:3144–3148
41. Powers TC, Mann H, Copeland LE (1958) The flow of water in hardened-portland cement paste, Highway Research Board Special Report
42. Olson RA, Neubauer CM, Jennings HM (1997) Damage to the pore structure of hardened portland cement paste by mercury intrusion. J Am Ceram Soc 80:2454–2458
43. Neithalath N, Sumanasooriya MS, Deo O (2010) Characterizing pore volume, sizes, and connectivity in pervious concretes for permeability prediction. Mater Charact 61:802–813
44. Hu J, Stroeven P (2005) Size characterisation of pore structure for estimating transport properties of cement paste. Heron 50:41–54
45. Kondraivendhan B, Divsholi BS, Teng S (2013) Estimation of strength, permeability and hydraulic diffusivity of pozzolana blended concrete through pore size distribution. J Adv Concr Technol 11:230–237
46. Garci Juenger MC, Jennings HM (2001) The use of nitrogen adsorption to assess the microstructure of cement paste. Cem Concr Res 31:883–892
47. Feldman RF (1987) Diffusion measurements in cement paste by water replacement using Propan-2-OL. Cem Concr Res 17:602–612
48. Holly J, Hampton D, Thomas MDA (1993) Modelling relationships between permeability and cement paste pore microstructures. Cem Concr Res 23:1317–1330
49. Bažant ZP, Najjar LJ (1971) Drying of concrete as a nonlinear diffusion problem. Cem Concr Res 1:461–473
50. Ulm FJ, Coussy O (1995) Modeling of thermo chemo mechanical couplings of concrete at early ages. J Eng Mech 121:785–794
51. Xi Y, Bažant ZP, Molina L, Jennings HM (1994) Moisture diffusion in cementitious materials Moisture capacity and diffusivity. Adv Cem Based Mater 1:258–266
52. Collins FG, Sanjayan JG (1999) Workability and mechanical properties of alkali activated slag concrete. Cem Concr Res 29:455–458
53. Bažant ZP, Chern JC (1985) Concrete creep at variable humidity: constitutive law and mechanism. Mater Struct 18:1–20
54. de Sa C, Benboudjema F, Thiery M, Sicard J (2008) Analysis of microcracking induced by differential drying shrinkage. Cem Concr Compos 30:947–956
55. Bissonnette B, Pierre P, Pigeon M (1999) Influence of key parameters on drying shrinkage of cementitious materials. Cem Concr Res 29:1655–1662

Effect of Placement of Waste Tyre Fibres on Unconfined Compressive Strength of Clayey Soil

Mohit Mistry, P. Venkateshwarlu, Shruti Shukla, Chandresh Solanki and Sanjay Kumar Shukla

Abstract This paper presents the laboratory investigation on compaction and unconfined compression behaviours of clayey soil reinforced with waste tyre fibres. In the present study, waste tyre fibres (WTF) were mixed with the soil at optimum mixing moisture content (OMMC). The fibre-reinforced soil (FRS) was then compacted at a maximum dry density (MDD) into a cylindrical mould in alternate layers of virgin and fibre-reinforced clayey soils. It was found that if the top and bottom layers are kept as virgin soil, then the specimen achieves a better strength as compared to other combinations. The strength of fibre-reinforced soil (FRS) was found to be two times higher than the virgin soil. This study demonstrates that the placement of fibres in alternate layers is useful in increasing the strength properties of soil.

Keywords Discrete fibre-reinforced clay · Waste tyre fibre · Fibre distribution · Unconfined compressive strength

1 Introduction

The scrap tyre are the undesired waste, especially in urban areas. The disposal of scrap tyres has become a serious problem for the governments. The stockpiling a large mass of scrap tyre is also undesirable because of the potential fire hazard and environmental damage. One of the possible utilizations of waste tyre is using it as soil improvement material. In conventional reinforcement practice, the soil mass is reinforced with metal strips, steel bars, geosynthetics, etc., by placing them in predefined direction and in systematic pattern. Soil reinforcement with discrete fibre reinforcement has become very popular in the last few decades [1]. Within the fibre-reinforced soil, depending upon the adopted mixing technique and placement procedure, the

M. Mistry (✉) · P. Venkateshwarlu · S. Shukla · C. Solanki
Department of Applied Mechanics, SV National Institute of Technology, Surat, India
e-mail: Mohit.aryan1@gmail.com

S. K. Shukla
Discipline of Civil Engineering, School of Engineering, Edith Cowan University, Perth, Australia

S. Kumar Shukla et al. (eds.), *Advances in Sustainable Construction Materials and Geotechnical Engineering*, Lecture Notes in Civil Engineering 35,
https://doi.org/10.1007/978-981-13-7480-7_11

embedment of discrete fibres becomes random and three dimensional. In the present study, waste tyre fibres were mixed with the clay of Surat region and the strength behaviour of reinforced clay was studied in the laboratory. The effect of placement of fibres in layers within soil on its stress–strain behaviour was studied. In practice, reinforcing the soil with discrete fibres has not yet been utilized worldwide because of some difficulties that occur on construction site as well as the unavailability of codal provisions for the use of fibres in the soil. The engineering behaviour of FRS is materially controlled by the fibre concentration and distribution or placement. In most of the small-scale laboratory investigations [2–5], the fibre distribution was uniform throughout a small specimen. However, in the field, achieving a uniform distribution of fibres is a difficult task which is highly dependent on the method of mixing. Kumar and Gupta [3] have investigated the strength parameters and load-carrying capacity of the soil treated with polypropylene fibres. It was found that load-carrying capacity of the pavement soil enhances with an increase in the number of layers in subsoil strata.

2 Experiments

2.1 Soil Properties

The soil used in this study consists of 10% sand, 58% silt and 32% clay. All the basic properties of the soil are determined as per the relevant Indian Standards. Table 1 shows the various engineering properties of the soil.

Table 1 Properties of Soil

Soil properties	Values
Specific gravity (G)	2.64
Consistency limits	
Liquid limit (LL)	64%
Plastic limit (PL)	30%
Plasticity index (PI)	34%
Shrinkage limit (SL)	10%
Grain size analysis	
Sand	10%
Silt	58%
Clay	32%
Differential free swell index	72%
IS classification	CH

Table 2 Properties of fibres

Fibre properties	Values
Specific gravity	1.15
Fibre type	Single fibre
Water absorption capacity	3%
Length (*L*)	18.92 mm
Diameter (*D*)	4.36 mm
Thickness (*B*)	1 mm
Aspect ratio (*L*/*D*)	4.34

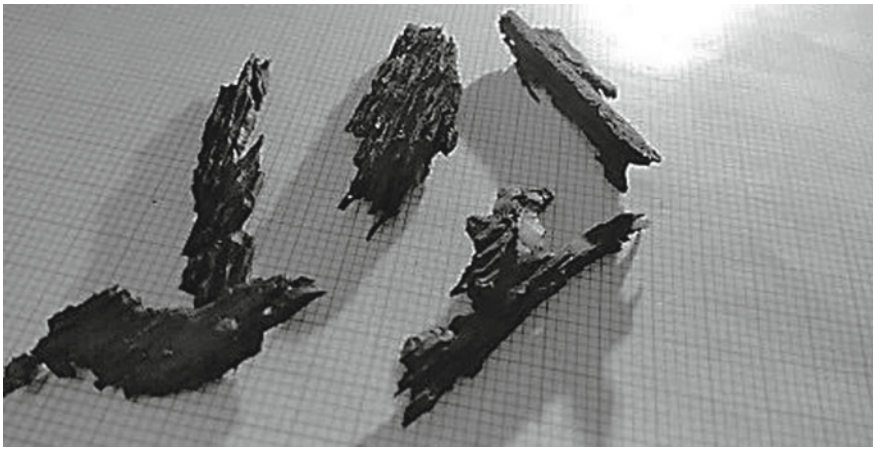

Fig. 1 Waste tyre fibre

2.2 Fibre Properties

The waste tyre fibres (WTFs) were used as the reinforcement material in this study. The fibres were pure rubber with no metal content inside. According to the ASTM D6270-08, fibres were falling into the category of tyre chips. In order to define the aspect ratio (length-to-diameter ratio) of fibres, they were separated through conventional sieve analysis by passing through 4.75-mm-IS sieve. Then the percentage of retained fibres on 4.75-mm-IS sieve by their weight was calculated. The aspect ratio followed by the mean particle diameter and length is presented in Table 2. In the present study, the specific gravity of the fibres is found to be 1.15 and the water absorption capacity is 3%. Figure 1 shows the waste tyre fibres used for the study.

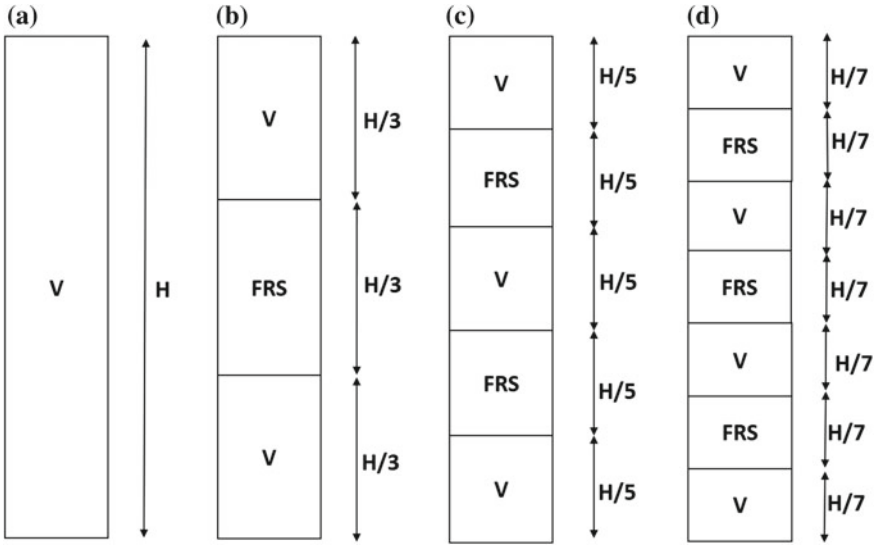

Fig. 2 Combination of different layers with top and bottom layers as the virgin soil

2.3 Specimen Preparation

To prepare the samples for tests, fibres were added into the soil in pre-moisture condition; i.e. fibres were added to the dry soil and then required amount of water is added to the mass. The optimum fibre content was determined from the compaction test. Fibre contents of 0.25, 0.5, 0.75 and 1.00% were added to the dry weight of soil mass for compaction test. The fibre content f_c is defined as

$$f_c = W_f / W_c \times 100\,(\%) \tag{1}$$

where W_f is the dry weight of fibres and W_c is the dry weight of clayey soil. For the unconfined compression tests, specimens were prepared in different combinations of layers where each layer is compacted at its MDD (maximum dry density) with OMMC (optimum mixing moisture content) obtained from compaction tests. The combination of different layers with top and bottom layers as virgin soil is illustrated in Fig. 2.

The combination of different layers with top and bottom layers as FRS soil is illustrated in Fig. 3. In Figs. 2 and 3, virgin soil is represented as "V" and fibre-reinforced clay is represented as "FRS" and H is the height of UCS mould, 100 mm.

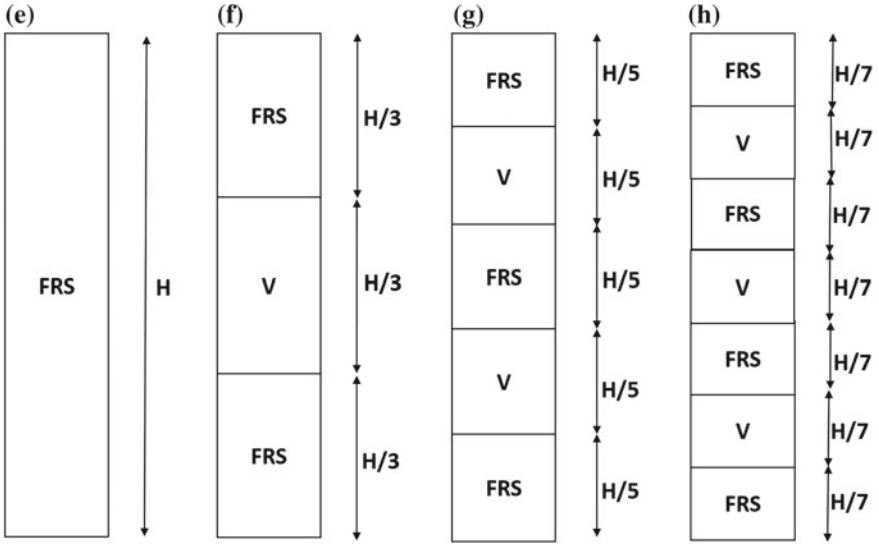

Fig. 3 Combination of different layers with top and bottom layers as the virgin soil

3 Experimental Testing

The standard Proctor compaction tests were performed as per IS 2720-07 on oven-dried soil sample with different fibre content. The optimum fibre content was determined from the MDD and OMMC obtained from trials of compaction test. The compaction mould of 127.30 mm height and 100 mm diameter was used by considering 1000 cm^3 volume capacity. The soil samples were compacted with 25 numbers of evenly distributed blows using 2.6 kg rammer with the free fall of 310 mm in three equal layers.

In order to examine the effect of placement of alternate FRS layers on compressive strength, the unconfined compression tests were conducted as per IS 2720-10. All the alternate layers were compacted on OMMC and MDD achieved from the standard compaction tests. The strength values of virgin soil and fibre-reinforced clayey soil were compared with the six different combinations of fibre inclusion layers. The alternate layers of virgin soil and fibre-reinforced soils in 3, 5 and 7 layers with different combinations are as follows: VFV (Virgin-FRS-Virgin), FVF (FRS-Virgin-FRS), VFVFVF (Virgin-FRS-Virgin-FRS-Virgin), FVFVF (FRS-Virgin-FRS-Virgin-FRS), VFVFVFV (Virgin-FRS-Virgin-FRS-Virgin-FRS-Virgin) and FVFVFVF (FRS-Virgin-FRS-Virgin-FRS-Virgin-FRS) in order to check the efficiency of FRS.

4 Results and Discussions

4.1 Standard Compaction Test

Figure 4 shows the variation in optimum mixing moisture content with percentage variation of WTFs. It is observed that OMMC enhances with an increase in fibre amount. A similar observation was observed by researchers [4–6] with the use of tyre fibres in the clayey soils. In the present study, moisture content increased with an increment in fibre content, and this is probably because the rough surface of tyre fibres tends to hold more water in surface gaps and the large size of fibres (>clay particles) changes the gradation of the soil–fibre matrix with an increase in the void ratio, thus leading to an increased OMMC [4].

In the present study, initially the OMMC increases with fibre inclusion in the soil mass, but the further increment in fibre content leads to the reduction in OMMC. The OMMC of reinforced soil varies from 23 to 29%. It is also observed that the MDD decreases with an increase in fibre content. The reduction in MDD is mainly due to the low specific gravity of the fibres. The size of the fibre also plays an important role in reduction of MDD. The tyre fibres are larger in size which has more reinforcing effect and which provides sufficient resistance to the particles to slipover each other and it will not allow particles to come closer until the fibre get stretched. Therefore, an increase in fibre content will also reduce the MDD. In the present study, the MDD of reinforced soil varies from 13.5 to 15%.

4.2 Unconfined Compressive Strength (UCS) Test

Figure 5 presents the variation in deformation with a change in fibre content. The UCS value of FRS depends on dry density, moisture content and fibre content. All the fibre-reinforced soil specimens prepared at their representative MDD and OMMC show an increase in UCS value with an increase in f_c up to 0.75%, then it shows a reduction

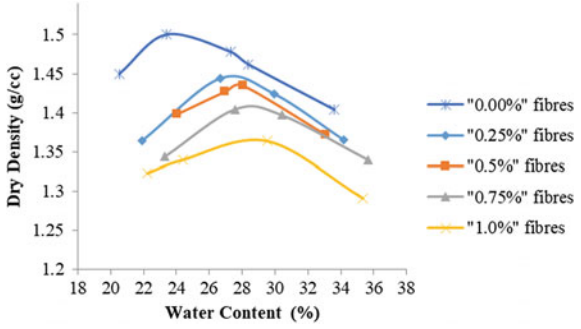

Fig. 4 Change in OMMC and MDD with an increase in fibre content

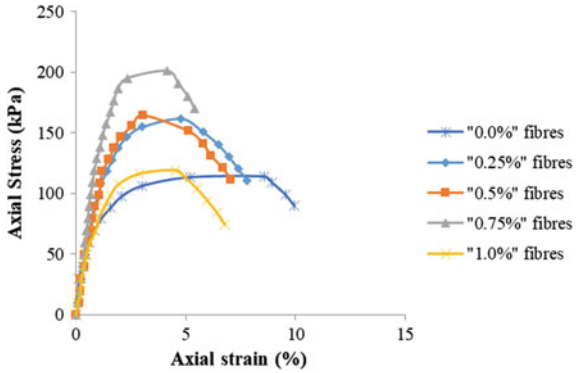

Fig. 5 Axial stress versus axial strain in unconfined compression tests

in UCS value for f_c of 1%. The decrease in strength might be due to increased flexibility of soil–fibre matrix and reduction in stiffness of clay. The maximum UCS value achieved at f_c of 0.75%, therefore, all the specimens for different combinations of alternate layers were prepared with 0.75% fibre content. The nonlinear increase in gain of axial stress with axial strain is observed in all the curves, which might be influenced by the heterogeneity of the soil–fibre matrix, which has number of weak planes across the stress path which leads to the different pick axial stress at different axial strain.

The addition of fibres has negligible effects on the initial stress–strain behaviour. It shows similar response at very low strains, but fibres in soil create the bridging effect in soil matrix which holds particles together and absorbs more energy at higher stress and hence exhibits less deformation. The inclusion of fibres restricts the propagation of the cracks and the bridging effect of the fibre effectively delays the development of the failure planes.

Figure 6 shows the variation in the UCS value of soil reinforced with alternate layers. Each layer is compacted at its maximum dry density. It is observed that strength value increases by two times in comparison with the strength of virgin soil. It is noted that with an increase in alternate fibre reinforcement layers, the strength increases up to a certain number of layers, and then the decrease in strength is observed. It is also observed that if FRS layers are sandwiched between the virgin soils then it gives better strength compared to the reverse combination of alternate layers (Table 3).

It is probably because, when the top and bottom layers are of FRS, the contact area of specimen becomes more flexible which leads to a decrease in strength and the gripping capacity is less due to fibres protruding out of the system. It also reduces the load-carrying capacity with virgin soil at top and bottom, the gripping capacity of the system enhances, FRS layers can be easily compacted to their maximum density as with applied force, elastic fibres compress and allow higher load-carrying capacity, thus higher the UCS values.

Table 3 Peak values of UCS with an increase in the number of alternate layers of FRS and virgin soil

FRS layers in between virgin soil		Virgin soil in between FRS soil	
Number of layers	Unconfined compressive strength q_u (kPa)	Number of layers	Unconfined compressive strength q_u (kPa)
3	213.038	3	186.411
5	264.702	5	192.69
7	219.409	7	162.698

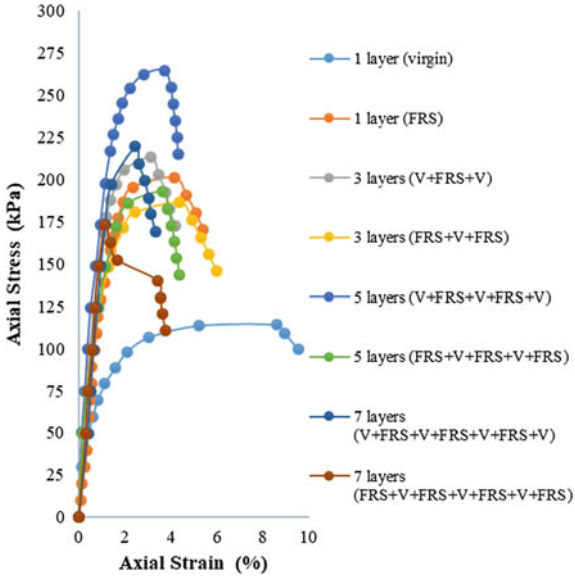

Fig. 6 Unconfined compressive strength of layered soil

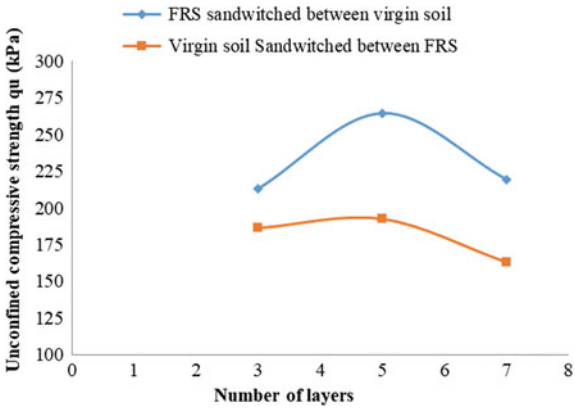

Fig. 7 Change in unconfined compressive strength of FRS with number of placement layers

It is clearly seen in Fig. 7 that the UCS value increases only up to five alternate layers after that decrease in strength is observed with an increase in alternate layers. It is probably because when the number of layers increases after certain numbers, it will start behaving like more or less virgin soil or entire specimen reinforced with fibres. In both cases, strength is observed lower as compared to alternate stratified soil layers.

5 Conclusions

The effects of fibre reinforcement in alternate layers on clayey soil were studied by conducting a series of unconfined compressive strength tests. The optimum fibre content was determined based on the compaction test results. The following points can be concluded from the results and discussion presented earlier:

- If the top and bottom layers in the specimen are kept as virgin soil and FRS layers are sandwiched between them, the soil–fibre matrix achieves a higher strength as compared to other combinations where the top and bottom layers in the specimen are kept as FRS and virgin soils are sandwiched between them.
- If the fibre placement layers are increased, after a certain number of layers, the strength starts decreasing in both the type of combinations. The use of fibres in clay soil improves the strength by almost two times the virgin soil.

In construction practice, many times a very thick layer of expansive soil is found near the ground surface. In such cases, this study can be helpful as a partial replacement of clay layer as reinforced clay soil.

References

1. Shukla SK (2017) Fundamentals of fibre reinforced soil engineering. Springer Nature, Singapore
2. Tang C, Shi B, Gao W, Chen F, Cai Y (2007) Strength and mechanical behavior of short polypropylene fibre reinforced and cement stabilized clayey soil. Geotext Geomembr 25(3):194–202
3. Kumar D, Gupta A (2014) Effects of fibres on strength properties of soil at different depth of soil layers. Int J Sci Res 3(10):657–661
4. Mistry M, Shukla T, Venkateswalu P, Solanki CH, Shukla SJ, Shukla SK (2018) A new mixing technique for randomly distributed fibre-reinforced expansive soil. In: Proceeding of international conference on environmental geotechnology, recycled waste materials and sustainable engineering. Springer Nature, Singapore, NITJ, Jalandhar, India, March 29–31, 2018
5. Tiwari B, Ajmera B, Moubayed S, Lemmon A, Styler K, Martinez JG (2014) Improving geotechnical behavior of clayey soils with shredded rubber tires-preliminary study. Geo-congress. 3734–3743. https://doi.org/10.1061/9780784413272.362
6. Park S-S (2009) Effect of reinforcement and distribution on unconfined compressive strength of fibre-reinforced cemented sand. J Geotext Geomembr 27:162–166

Numerical Investigation of Uplift Behaviour of Bell-Shaped Anchor in c-ϕ Soil

Arya Das and Ashis Kumar Bera

Abstract This paper depicts a detailed numerical study on bell-shaped anchor inserted in soil (c-ϕ soil) carried out using the finite element (*FE*) software 'ABAQUS'. Bell-shaped anchors with varying bell diameters (0.125–0.3125 m) have been analysed to investigate the influence of its different governing parameters such as H/D ratio (depth of embedment/bell diameter of anchor), bell diameter (D) on the uplift capacity of the anchor inserted in soil. A 2D axisymmetric model has been considered for the analysis, where the anchor has been considered as linear elastic material and soil mass as elasto-plastic material. Data obtained from the laboratory experiments performed on *CL* types of soil have been used in the analysis. Results of the analysis indicate that the ultimate uplift capacity (*UUC*) of bell-shaped anchor increases proportionately with the bell diameter and also with an increase in the H/D ratio of the anchor. It has also been observed that beyond H/D values of 4, there is a reduction in the rate of increase in ultimate uplift capacity (*UUC*).

Keywords Bell-shaped anchor · Uplift capacity · Axisymmetric · CL-type soil · FEM

1 Introduction

Many civil engineering structures like transmission towers, guyed towers, coastal structures and offshore structures are often subjected to huge uplift or pull-out forces. To resist these forces, anchor foundation plays an important role. With the help of self-weight of the anchor and the soil mass within the failure zone and also friction force surrounding the failure surface, anchor foundation counters the pull-out forces.

A. Das (✉) · A. K. Bera
Department of Civil Engineering, Indian Institute of Engineering Science and Technology Shibpur, Howrah 711103, India
e-mail: aryanbesu@gmail.com

A. K. Bera
e-mail: ashis@civil.iiests.ac.in

S. Kumar Shukla et al. (eds.), *Advances in Sustainable Construction Materials and Geotechnical Engineering*, Lecture Notes in Civil Engineering 35,
https://doi.org/10.1007/978-981-13-7480-7_12

Many researchers [3, 4, 9, 11, 12, 15] have investigated the uplift capacity of anchors inserted in sand. There are very few literatures available on the behaviour of a bell-shaped anchor in cohesive and cohesive-frictional soils. Liu et al. [10], Jesmani et al. [8], O'Kelly et al. [13], Perazzelli and Anagnostou [14], Singh et al. [16] have experimented on plate anchors, strip anchors and granular anchors in the soil mass. It can be said that comprehensive investigation on the *UC* of anchor, particularly the bell-shaped anchor inserted in *c*-ϕ soil, is very limited. Hence, in this paper, an effort has been made to study the behaviour of the bell-shaped anchor inserted in homogenous *c*-ϕ soil using ABAQUS. It has also been attempted to investigate the influence of various parameters on *UUC* of the bell-shaped anchor inserted in soil.

2 Statement of the Problem

A numerical simulation based on *FE* analysis has been carried out to investigate the response of the bell-shaped anchor inserted in *c*-ϕ soil. Using ABAQUS, a 2D axisymmetric model of soil, bell-shaped anchor system, has been considered for the investigation purpose. For analysing the uplift capacity (*UC*) of the anchor inserted in homogeneous *c*-ϕ soil, the bell diameters of the anchors are considered as 0.125, 0.250, 0.187 and 0.3125 m. The dimensions of the anchors have been chosen based on earlier work [3]. In the present investigation, the above anchors are designated as Anchor 1, Anchor 2, Anchor 3 and Anchor 4 for bell diameter 0.125, 0.1875, 0.2500 and 0.3125 m, respectively. Figure 1 represents the schematic diagram of the soil–anchor system considered in the study.

3 Assumptions and Analysis Procedure

In view of the symmetry of the anchor–soil system and to save time cost, a half model of the system has been considered for the current numerical study. Soil strip has been considered as 6 times and 10 times the bell diameter in the horizontal and the vertical directions, respectively. The anchor has been considered as an elastic material and *c*-ϕ soil as a linear elastic and perfectly plastic, viz. Mohr–Coulomb material. Between the anchor and soil, friction has been considered as interaction criterion. The model has been discretized by *CAX4R* (continuum axisymmetric 4 noded reduced integral) 4-noded bilinear elements. The analysis has been carried out in two steps. Hibbett et al. [7] showed that by assigning a displacement boundary condition, the limit load of granular materials like soil can be computed through *FE* analysis. In the first step, static analysis has been carried out to consider equilibrium condition and limit load analysis to find the uplift response in the second step. In this present study, the upward displacement of 30 mm has been applied to all the model analyses. From the result of the analysis, reaction forces have been calculated corresponding to the settlement of the anchor.

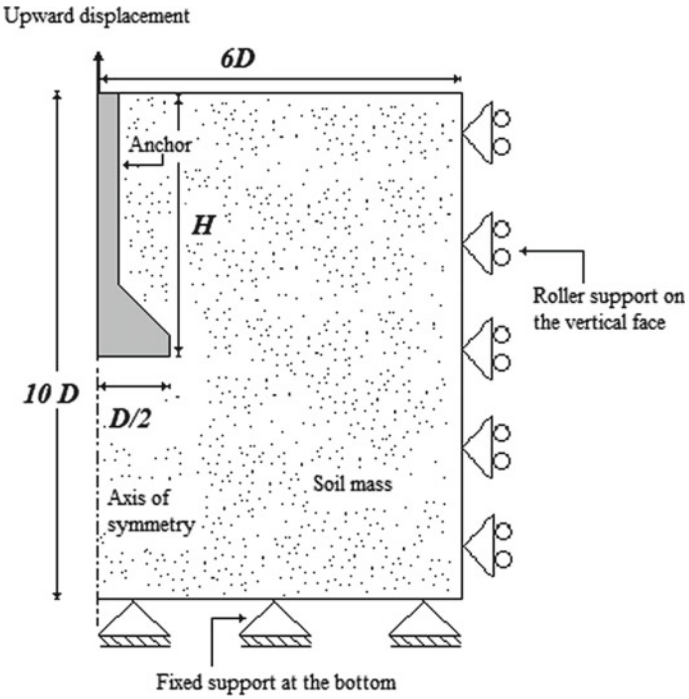

Fig. 1 Schematic diagram of the soil anchor system considered for modelling (not to scale)

4 Foundation Materials

In this study, one type of c-ϕ soil has been collected from Agarpara, Kolkata, West Bengal, India, used as foundation material. The grain size analysis, liquid limit (*LL*) and plastic limit (*PL*) of the soil has been performed in the Geotechnical Engineering Laboratory, IIEST, Shibpur, West Bengal, India. The values of sand size particle, silt-size particle and clay particle are 3, 65 and 32%, respectively. The specific gravity (ρ) of the soil is found as 2.68. The values of *LL* and *PL* of the particular soil obtained from the test are as 42.25 and 24.65%, respectively. According to ASTM 2487 [1], the soil may be classified as *CL*. The compaction tests of the soil have been performed in accordance with ASTM D698 [2] in the Geotechnical Laboratory. Dry unit weight versus moisture content curve is shown in Fig. 2. Maximum dry unit weight (*MDU*) and optimum moisture content (*OMC*) values as obtained from the curve (Fig. 2) are 15.5 kN/m^3 and 22.5%, respectively.

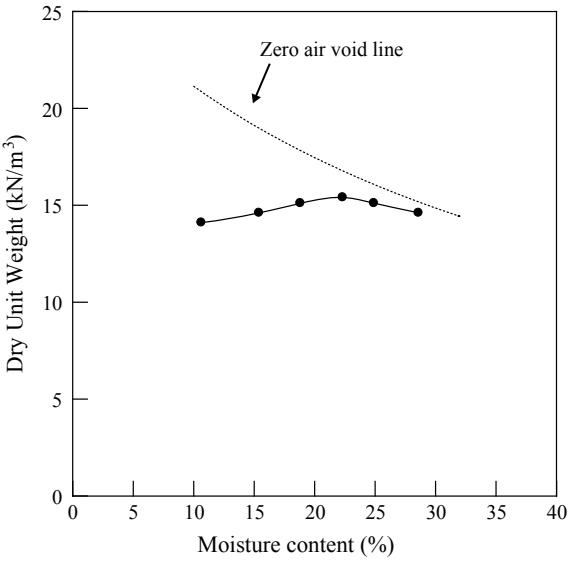

Fig. 2 Dry unit weight versus moisture content curve for soil

Table 1 Input parameter used in the ABAQUS analysis

Parameters	Values	
Dry unit weight (kN/m^3)	15.5	14.2
E (MPa)	17.69	5.99
Angle of internal friction (°)	25.5	10.42
Cohesion (kN/m^3)	86.87	79.7

5 Input Parameters

In the present work, bell-shaped anchors are considered to made of concrete and have been inserted in the soil bed. Density, Young's modulus and Poisson's ratio of concrete has been considered as 25 kN/m^3, 25,000 MPa and 0.15, respectively. The input parameters for foundation materials are dry unit weight (γ_d), elastic modulus (E), angle of internal friction (ϕ) and cohesion (c). The values of the respective parameters as obtained from the laboratory tests are presented in Table 1.

6 Convergence Study

Meshing of the geometric model is essential for the accuracy of the numerical analysis. Hence, a convergence study has been carried out with a typical model Anchor 3 with H/D ratio 2, and mesh size has been determined. The input parameters for foundation medium considered as 15.5 kN/m^3, 17.69 MPa, 25.5° and 87.5 kPa for

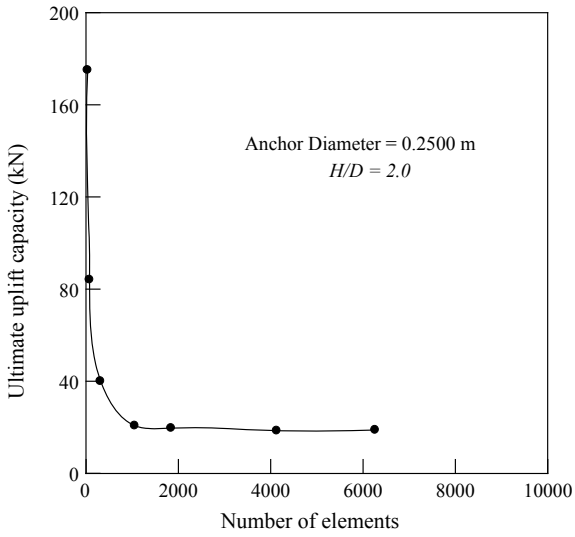

Fig. 3 *UUC* versus number of element curve for anchor in clay (Anchor 3, $H/D = 2.0$)

γ_d, E, c and ϕ, respectively. Figure 3 presents the *UUC* of anchor versus the numbers of elements. From the figure, it is found that 4132 no. of element quite sufficient to analyse the model anchor in soil efficiently. Now 4132 numbers of *CAX4R* elements have been generated by the meshing of the anchor soil model for each case.

7 Verification of the Model

Due to non-availability of past research data on the *UC* of anchor in c-ϕ soil, the results of the current ABAQUS analysis have been verified with available data of *UC* of anchor in sand represented by the previous author [3]. To verify the above ABAQUS analysis results, anchor with bell diameter 0.250 m and sand type S1 (relative density = 50%) have been considered. Figure 4 represents the *UUC* versus H/D ratio curve. It can be observed from Fig. 4 that the results obtained from ABAQUS analysis are quite close to the results of Bera and Banerjee [3].

8 Plan of the Numerical Analysis

To investigate the behaviour and the influence of the governing parameters, viz. (H/D), anchor diameter (D) and dry unit weight (γ_d) of c-ϕ soil on *UC* of bell-shaped anchor, three different series (A, B and C) have been chalked out for numerical analysis. In the series A, analysis has been performed with variable H/D ratios of 0.5–10.0 (0.5, 1.0, 1.5, 2.0, 2.5, 3.0, 3.5, 4.0, 4.5, 5.0, 6.0, 7.0, 8.0, 9.0, 10.0)

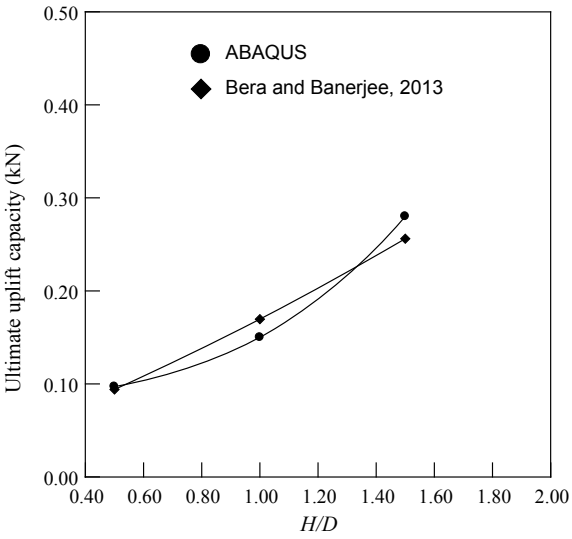

Fig. 4 *UUC* versus *H*/*D* ratio curve for anchor in sand ($D_r = 50\%$)

for Anchor 1. Series B has been carried out for investigating the influence of bell diameter (*D*) on *UC* of anchor with the variation of *H*/*D* values. In the series B, *H*/*D* is varying from 0.5 to 5.0, whereas bell diameter is varying from 0.125 to 0.3125 m. To distinguish the influence of the dry unit weight of soil on *UC* of anchor, series C has been planned. In this series, two different soils of dry unit weight 15.5–14.20 kN/m^3 have been considered with varying *H*/*D* ratios.

9 Results and Discussions

After performing the numerical analyses with the help of the ABAQUS, the results obtained are plotted. Figure 5 represents a contour plot for the vertical displacement of Anchor 1 for *H*/*D* ratio of 3. The load versus displacement curve for Anchor 4 (bell diameter = 0.3125 m) with the variable '*H*/*D*' ratio is presented in Fig. 6. Plots of *UUC* versus bell diameter (*D*) curves are presented in Fig. 7. The *UUC* versus *H*/*D* ratio curves for different anchors inserted in soil are presented in Fig. 8. Figure 9 represents the plots of *UC* versus *H*/*D* ratio (up to 10) curve for Anchor 1. The *UC* versus *H*/*D* ratio curves for Anchor 4 by varying the dry unit weight of soil are represented in Fig. 10.

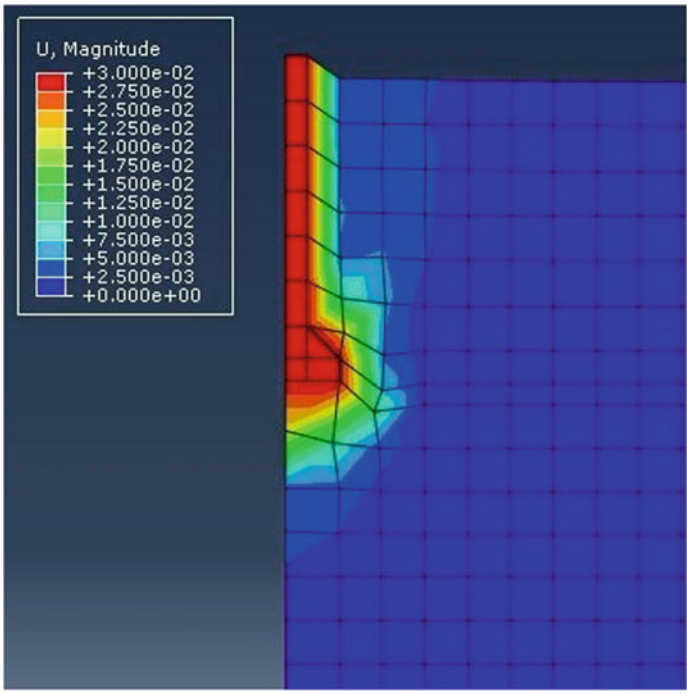

Fig. 5 Contour plot for vertical displacement for Anchor 1 for $H/D = 3$ (values are in 'm')

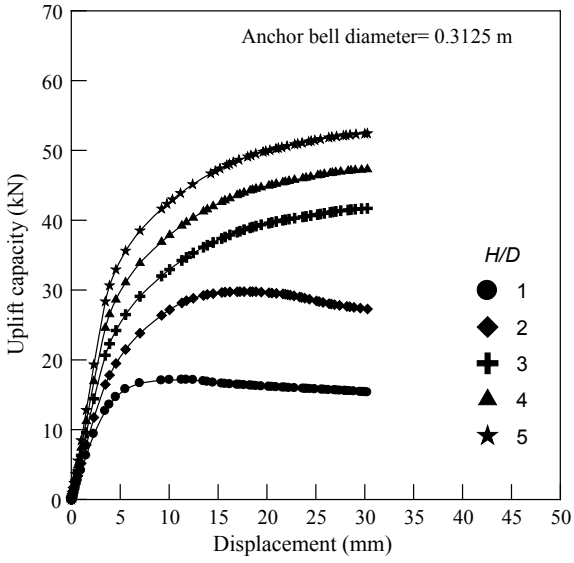

Fig. 6 Typical *UC* versus upward displacement curve for Anchor 4

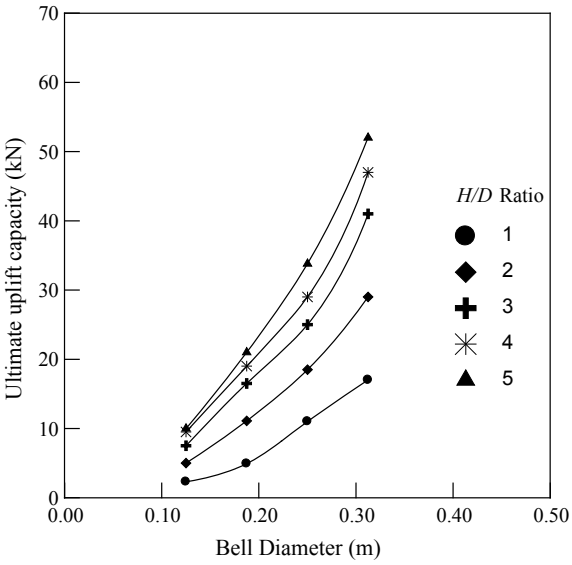

Fig. 7 *UUC* versus bell diameter curve

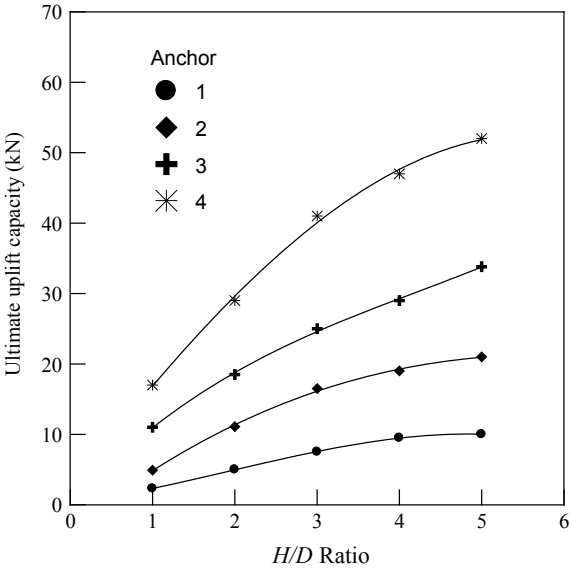

Fig. 8 *UUC* versus *H*/*D* ratio curve with varying anchor bell diameter

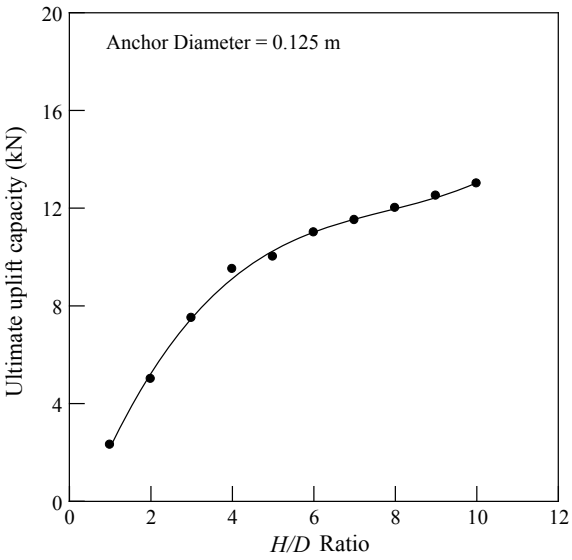

Fig. 9 Typical *UUC* versus *H*/*D* ratio curve for Anchor 1

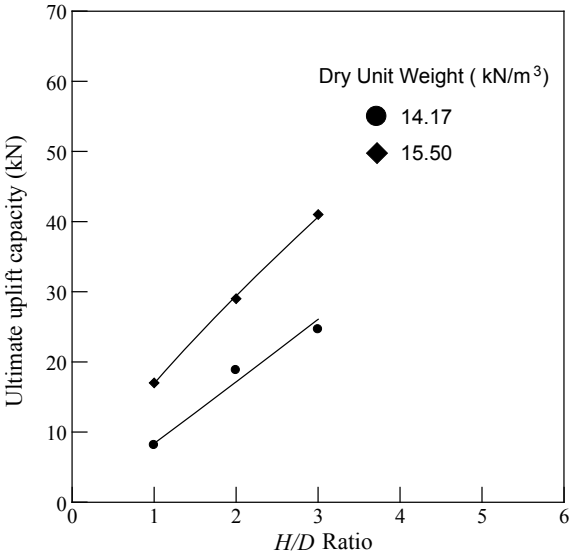

Fig. 10 *UUC* versus *H*/*D* ratio curve with varying the dry unit weight of soil (Anchor 4)

9.1 *Effect of Bell Diameter (*D*) on UC of Anchor*

Bell diameter of bell-shaped anchor is one of the governing parameters for determining *UC* of anchor. Figure 7 represents the plotting of *UUC* of anchor versus bell diameter curves. The curves depict that with the increase in the value of *D* (0.125–0.3125 m), the value of *UUC* increases for the entire *H*/*D* ratio under study. It can also be found that the rate of increase in *UC* for bigger bell diameter anchor is much greater than the small diameter anchor. It may be that due to the increase in the values of *D*, the size of failure zone increases. Hence, the weight of the soil mass inside the zone becomes larger, and as a result, the uplift capacity increases.

9.2 *Influence of* H/D *Ratio on* UC *of Anchor*

H/*D* ratio is a significant parameter for determining the *UC* of anchor. Figure 8 presents the *UUC* versus *H*/*D* ratio curves for different anchors (varying bell diameter 0.125–0.3125 m). The curve (Fig. 8) displays that the increment in the values of *H*/*D* ratio proportionately increases the value of *UUC* of anchor regardless of the value bell diameter. Figure 9 represents the *UUC* of anchor versus *H*/*D* ratio up to 10. The curve also showed that at certain *H*/*D* ratio ($H/D = 4$), the rate of increase in *UUC* of anchor has become smaller. Das [5] opined that the critical *H*/*D* ratio is in between 3 and 7 in case of the clay. Das and Sukhla [6] also reported in case of square and circular plate anchor in sand that the critical *H*/*D* ratio varies between 3 and 4 for friction angle, and ϕ ranges between 25° and 30°. In the present investigation, the critical *H*/*D* ratio may be of 4 in case of *c*-ϕ soil under study.

9.3 *Influence of Dry Unit Weight of Soil on* UC *of Anchor*

The dry unit weight of the soil is an important parameter in the calculation of the *UC* of anchor inserted in the soil. The plots of *UUC* of anchor versus *H*/*D* ratio curve with varying dry unit weight (dry unit weight of 15.5 and 14.2 kN/m^3) are displayed in Fig. 10. From the plots, it can be observed that the higher the dry unit weight of the soil, higher in the *UUC* of anchor irrespective of *H*/*D* ratio. Higher value of dry unit weight of soil implies higher strength of the soil, and as a result, higher is the *UC*.

10 Conclusions

Based on the results obtained from the present numerical analysis, the following conclusions may be drawn:

- The increment of the *UC* of bell-shaped anchor is proportional to the bell diameter under the study for *c*-ϕ soil irrespective of *H*/*D* ratio.
- Increase in the value of *H*/*D* ratio leads to an increase in the value of *UUC* of anchor regardless of the anchor diameter. The critical value of *H*/*D* has been found to be 4 in case of *CL* types of soil.
- The *UUC* of anchor inserted in *c*-ϕ soil increases with the increase in the dry unit weight of the soil regardless of the *H*/*D* ratio under consideration.

References

1. ASTM 2487 (1992) Classification of soils for engineering purposes (Unified soil classification system). Philadelphia, PA, American Society of Testing Materials
2. ASTM D698 (1992) Test method for laboratory compaction characteristics of soil using standard effort. Philadelphia, PA, American society of Testing Materials
3. Bera AK, Banerjee U (2013) Uplift capacity of model bell shaped anchor embedded in sand. Int J Geotech Eng 7(1):84–90
4. Bhattacharya P, Kumar J (2016) Uplift capacity of anchors in layered sand using finite-element limit analysis: formulation and results. Int J Geomech ASCE 16(3):04015078(1–14)
5. Das BM (1999) Shallow foundations: bearing capacity and settlement. CRC Press, Florida
6. Das BM, Shukla SK (2013) Earth anchors, 2nd edn. J. Ross Publishing, Florida
7. Hibbett, Karlsson, Sorensen (2012) ABAQUS/standard, User's Manual
8. Jesmani M, Kamalzare M, Nazari M (2013) Numerical study of behaviour of anchor plates in clayey soils. Int J Geomech 13(5). ASCE. ISSN 1532-3641/2013/5-502–513
9. Kumar J, Kouzer K (2008) Vertical uplift capacity of horizontal anchors using upper bound limit analysis and finite elements. Can Geotech J 45:698–704. https://doi.org/10.1139/t08-005
10. Liu HX, Su FM, Li Z (2014) The criterion for determining the ultimate pullout capacity of plate anchors in clay by numerical analysis. Am J Eng Appl Sci 7(4):374–386
11. Merifield RS, Sloan SW (2006) The ultimate pullout capacity of anchors in frictional soils. Can Geotech J 43(8):852–868
12. Meyerhof GG, Adams SI (1968) The ultimate uplift capacity of foundations. Can Geotech J 5(4):225–244
13. O'Kelly BC, Brinkgreve RBJ, Sivakumard V (2014) Pullout resistance of granular anchors in clay for undrained condition. Soils Found. The Japanese Geotechnical Society. http://dx.doi.org/10.1016/j.sandf.2014.11.009
14. Perazzelli P, Anagnostou G (2017) Uplift resistance of strip anchors in cohesive frictional mediums of limited tensile strength. Int J Geomech. ASCE. ISSN 1532-3641
15. Seider GL (2015) Bearing and friction design capacity software for helical anchors and piles. In: (*IFCEE 2015*). ASCE, pp 851–867
16. Singh V, Maitra S, Chatterjee S (2016) Generalized design approach for inclined strip anchors in clay. Int J Geomech ASCE 17(6):04016148(1–15). ISSN 1532-3641

Improving the Soil Subgrade with Plastic Waste Reinforcement—An Experimental Study

Alka Shah and Hiral Modha

Abstract The subgrade soil is an integral part of pavements which provides support to the pavement. The behaviour of road surface depends on the strength of filling material and the subgrade below it. The pavements are vulnerably affected by the change in subgrade soil properties due to water-table fluctuation, overloading, flooding, etc. This study focuses on improving the strength of soil subgrade using plastic waste soil reinforcement technique in pavement construction, looking to the current environmental issue related to the utilisation of waste plastic, as plastic is a non-biodegradable material. In this study, geocell and geogrid were prepared from plastic waste and used as soil reinforcement. The plastic waste geocell and geogrid were placed at different depths from the top of the CBR mould. The CBR test was performed for unsoaked condition of virgin soil and reinforced soil, and the behaviour of load versus penetration was observed. The results show that by placing plastic waste reinforcement at different depths, the strength of the reinforced subgrade soil considerably increased with respect to virgin soil. The confined structure of plastic waste geocell shows significant strength improvement compared to plastic waste geogrid. The result shows that the significant improvement in strength of soil using geogrid and geocell was effective at a particular depth. This study reveals that the use of plastic waste for improving subgrade soil strength is a good option. The plastic waste can be utilised in pavement construction as well as it can be the cost-effective solution.

Keywords CBR · Plastic waste · Geogrid · Geocell · Subgrade soil

A. Shah (✉) · H. Modha
Nirma University, Ahmedabad, India
e-mail: alka.shah@nirmauni.ac.in

H. Modha
e-mail: hiral.modha@nirmauni.ac.in

S. Kumar Shukla et al. (eds.), *Advances in Sustainable Construction Materials and Geotechnical Engineering*, Lecture Notes in Civil Engineering 35,
https://doi.org/10.1007/978-981-13-7480-7_13

1 Introduction

Infrastructure development is playing a major role in the Indian economy. This sector emphasising on major infrastructure sectors such as power, road, bridges and urban infrastructures. India has the second largest road network in the world. There are a lot of challenges against the construction of new road network like source material availability, quality of materials and type of subgrade soil. Infrastructure projects of highways or railways which are vulnerably affected by the change in subgrade soil properties due to water-table fluctuation, overloading, flooding, etc. Subgrade soil strength is one of the reasons for pavement failure. To improve engineering properties of soil subgrade, well-defined techniques are widely used by the addition of cementitious agents like lime, Portland cement and fly ash. Soil confinement by providing reinforcement through natural or synthetic fibres is also used. Use of geosynthetic material to reinforce the soil is, nowadays, the major field of research which alter the subsoil property effectively. As by introducing geosynthetics, relatively thinner layer of pavement is required compared to untreated soil subgrade which results in cost saving. On the other side, infrastructure development and urbanisation lead to high rate of municipal solid waste generation and cause problems of disposal of this type of waste. Out of all types of municipal solid wastes, disposal of plastic waste is one of the big issues all over the world, because recycling of some type of plastic waste is uneconomical as well as non-environmental friendly. According to the general survey report, 1500 plastic bottles are thrown in an ambient environment every second. In India, usage of different plastic products per year per person is 1 kg averagely and in the world, the same is 18 kg [1]. In India, it is observed that average plastic waste generation is about 6.29% of total MSW and 25,940 tons per day. Out of total plastic waste, around 94% plastic waste of which recycling or reuse can be carried out; because, it comprises of thermoplastic content (CPCB 2016). Hence, there is a need to reuse plastic waste as it will solve the problem of plastic waste disposal and reduce the impact on environment. Choudhary et al. [2] denoted the use of waste plastic strip as a reinforcement to improve soil subgrade in flexible pavement through California bearing ratio (CBR) test. The study carried out to investigate CBR behaviour of waste plastic strip reinforced soil for different amounts of strip percentage by weight (0, 0.25, 0.5, 1, 2, 4%) and aspect ratio (0, 1, 2, 3, 4). From the results, it can be said that there is a significant increase in CBR value. Also, the extent of CBR value improvement with the inclusion of plastic strip has been given with ratio known as California bearing ratio index (CBRI) defined as the ratio of CBR value of reinforced soil to the CBR value of virgin soil. Data shows that CBRI increment is 50–70% at 0.25% strip content and 80–90% at 2% strip content but when reaches to 4% CBRI started showing decrement [2]. Nair and Gali [3] carried out experimental analysis using geocell and geogrid as a reinforcing material to observe behaviour of soil subgrade through modified CBR test, model test in steel tank of 750 mm × 750 mm × 620 mm and field test in a stretch of 1 m × 2 m [3]. In this study, geocell (aspect ratio 0.4) was made from strong biaxial geogrid (ultimate tensile strength 38 kN/m). Test results show that pressure sustained by unreinforced is more than

reinforced section and also geocell is more effective than the planner reinforcement due to its confining action. Bala et al. [4] have concluded the results using plastic waste with red mud, fly ash and mixture of fly ash and red mud. The compaction and strength behaviour were analysed using compaction and CBR test. The maximum dry density of red mud and fly ash increased with increase in waste plastic up to 2%, further increase in waste plastic reduces the maximum dry density. OMC value remains same in each case. The addition of plastic waste in the proportion of 0.5, 1.0, 2.0% increases the CBR value, which reduces with 3% of waste plastic. Increase of CBR value indicates that the thickness of pavement can be reduced by the addition of waste plastic content up to 2% [4].

Use of plastic waste to alter the soil properties is an emerging research area [5]. Geosynthetics, which are made from different synthetic polymeric materials, have been used since early 1970 by the civil engineers to perform different functions like separation, drainage, reinforcement, protection, filtration and barrier [6]. To perform different functions, many products are available in different forms like geotextile, geomembrane, geogrid, geonet, geocell, geofoam and geocomposite materials. Geogrid is a stiff or flexible polymer-grid-like sheets with large aperture used primarily as reinforcement of unstable soils or waste masses as per the geosynthetics research institute (GRI). Geocell is known as cellular confinement system. Network of geocell forms a cellular soil confined system which result in to strong and stable mattress like layer in soil. Plastic is made up of synthetic or semi-synthetic polymers which are solid and non-biodegradable materials. Looking at the similar basic raw materials in this research work, effort has been made to reuse plastic waste bottles to solve the environment-related issues by reusing and/or recycling the materials. The main objective of present study is to analyse the behaviour of reinforced and unreinforced subgrade soil through CBR test by using plastic waste as a reinforcement which is converted into geogrid (by strips of plastic waste bottles) and geocell (by connecting neck of bottles) [7].

2 Experimental Study

In the present study, experimental investigation was carried out to analyse CBR behaviour of silty sand with the inclusion of plastic waste as a reinforcement in the form of geogrid and geocell which is made from plastic water bottle (PET or polyester—Polyethylene terephthalate). Geogrid was made by cutting the strips from plastic water bottles of 1.5 cm width and aperture size maintained as 1.5 cm × 3.0 cm. Geocell was made from the circular neck of the plastic bottle which is having a dimension of 1 cm height and 2 cm diameter. The geocell mat was prepared by connecting geocell (circular neck of bottle). The geogrid and geocell mat have the same dimension as of CBR mould, i.e. 15 cm diameter which is shown in Figs. 1 and 2, respectively. The plastic water bottles used in the present study were collected from the canteen of institute. Silty sand was procured from nearby site for experimental work, in which properties are given in Table 1. CBR specimens were prepared

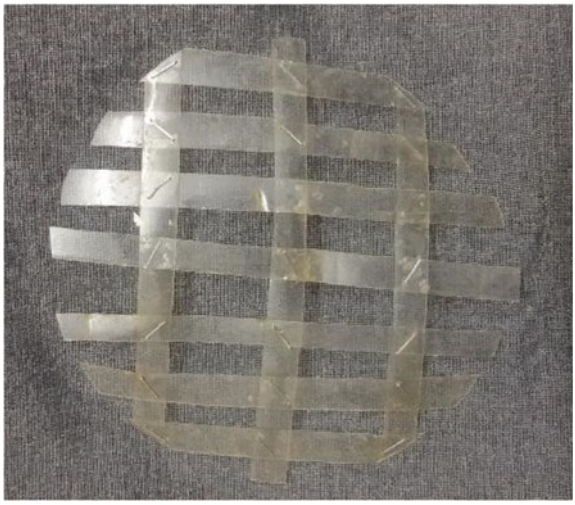

Fig. 1 Plastic waste geogrid (PWG)

Fig. 2 Plastic waste geocell (PWGc)

according to MDD, 19.12 kN/m^2 and OMC, 12% which found from standard proctor test as per IS 2720-Part VII (1980) [8]. The CBR test was carried out as per the procedures described in IS 2720-Part XVI (1987) [9]. The unsoaked CBR test was performed by the inclusion of plastic waste geogrid (PWG) and plastic waste geocell (PWGc) placed at different heights, i.e. 2.5, 5 and 7.5 cm from top of the CBR mould as shown in Fig. 3.

Table 1 Index properties of soil

S. No.	Index properties	Values
1	Specific gravity	2.67
2	Liquid limit (%)	15%
3	Plastic limit (%)	NP
4	Plasticity index (%)	N.A.
5	Soil classification	SM

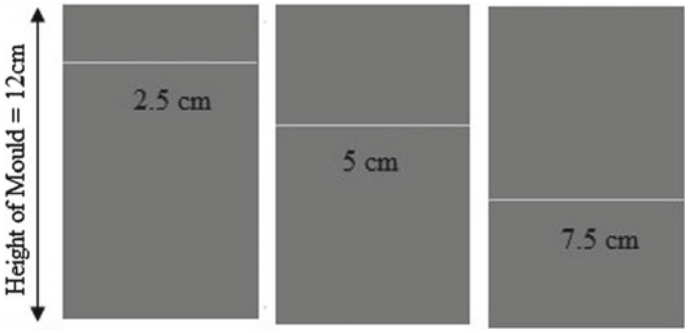

Fig. 3 Reinforcement at different layers of CBR mould

3 Test Result and Discussion

Load versus penetration curve was plotted after performing laboratory CBR test (unsoaked) for virgin soil and confined soil with plastic waste geogrid (PWG) and plastic waste geocell (PWGc) which were placed at different heights from top of CBR mould.

3.1 Effect of Plastic Waste Geogrid (PWG) Used as a Reinforcement

From the observation of load versus penetration curves for PWG and soil as shown in Fig. 4, it is clear that reinforcement inclusion in the form of PWG increases the load-carrying capacity of soil compared to virgin soil. This is may be due to the fact that plastic waste geogrid performs the same function that as of conventional geogrid. It is evident that plastic waste can be used as a reinforcement. From the result of CBR test, it can be concluded that as depth of PWG decreases from top of mould, the behaviour of soil is changing. From unreinforced soil to reinforced soil, reinforcement at 7.5 and 5 cm depth, the load-carrying capacity increases, but the capacity reduces after this depth, i.e. at 2.5 cm. This behaviour shows that the inclusion of reinforcement is effective at 5 cm depth from top of the CBR mould.

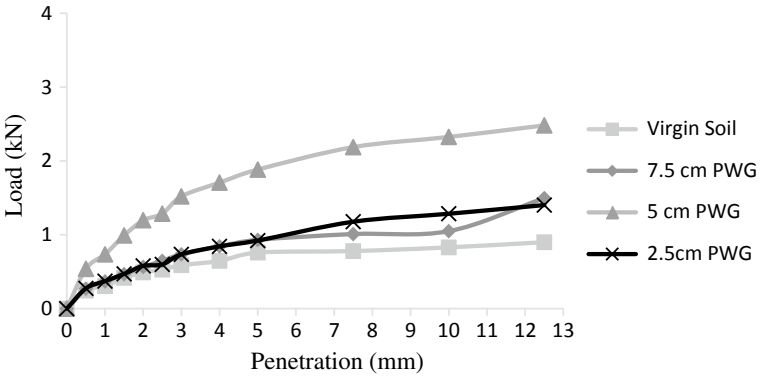

Fig. 4 Load versus penetration curve (PWG)

3.2 Effect of Plastic Waste Geocell (PWGc) Used as a Reinforcement

From the observation of load versus penetration curves for PWGc and soil is shown in Fig. 5, it is clear that reinforcement inclusion in the form of PWGc also showing the same behaviour as of plastic waste geogrid (PWG) that increases the load-carrying capacity of soil compared to virgin soil. Here, the load versus penetration behaviour is different from that of PWG. From virgin soil to PWGc at 7.5 cm depth, load-carrying capacity increases significantly but after that PWGc at 5 and 2.5 cm depth the same decreases; so, PWGc shows good response at 7.5 cm depth from top of the CBR mould.

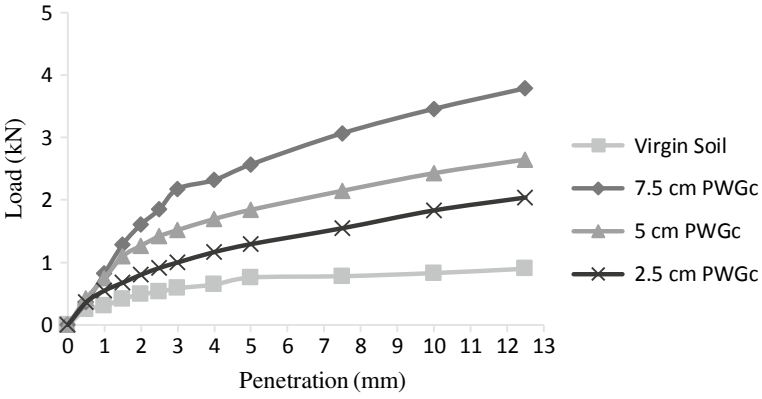

Fig. 5 Load versus penetration curve (PWGc)

3.3 *Comparison of PWG and PWGc as a Reinforcement in Soil*

Comparing PWG and PWGc as a reinforcement, PWGc shows significant load-carrying capacity, i.e. maximum 13.76 kN at 7.5 cm depth while in PWG, it is 9.56 kN at a 5 cm depth. CBR value is a parameter to express the strength of subgrade soil. CBR value of virgin and reinforced soil at different depth is shown in Fig. 6. CBR value is greater for all depth in case of PWGc as a reinforcement compared to PWG. There is a 250% increase in CBR value at 7.5 cm for PWGc and only 22% for PWG. There is an increase in CBR value 168 and 72% for PWGc at 5 and 2.5 cm depth, respectively. PWGc is effective at 7.5 cm depth from top of CBR mould. For PWG at 5 and 2.5 cm, 143 and 13% increase in CBR value, so PWG is effective at 5 cm depth. From these results, it can be concluded that PWG and PWGs show significant effect and considerable improvement in CBR values of silty sand at particular depth, i.e. 5 and 7.5 cm, respectively. Here in CBR test, the plunger acted as foundation which has 5 cm width. With the consideration that shear zone depth below foundation is less than the width of foundation, so looking to the shear zone, CBR value is effective at 5 cm depth in case of PWG while in case of PWGc due to its three-dimensional structure effective depth is more, i.e. 7.5 cm. Moreover, significant behaviour of geocell reinforcement is due to interconnected and cellular-type, honeycomb-like structure of geocell. The geocell-type reinforcing mechanism provides all-round confinement to the soil, which prevents the lateral spreading of material on the application of load. Because of this type of structure of geocell, soil composite system can be formed where geocell layer transfers the load over the layers beneath it and thus increasing the capacity of parent material.

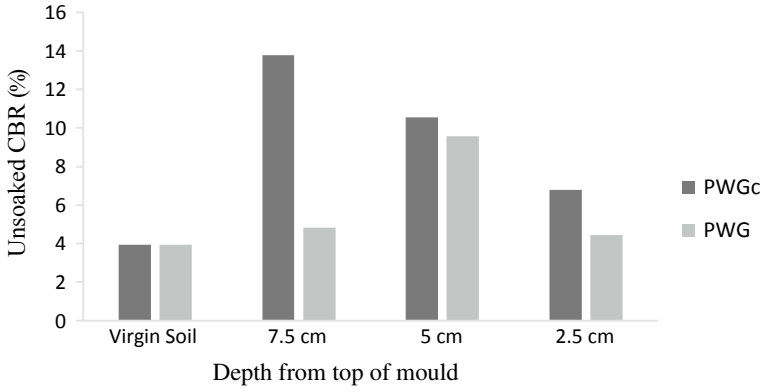

Fig. 6 CBR variation of PWG and PWGc

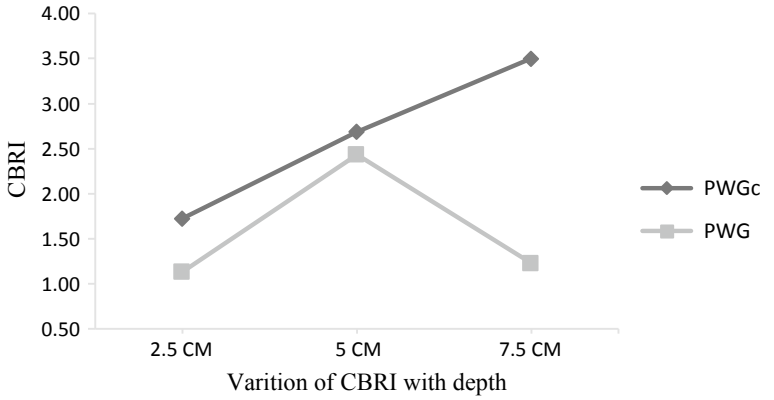

Fig. 7 CBRI variation of PWG and PWGc

3.4 CBRI Variation

The improvement in CBR value can also be shown by the ratio called California bearing ratio index (CBRI) [2]. CBRI is defined as the ratio of CBR value of reinforced soil to the CBR value of virgin soil. The value of CBRI with respect to the depth of the inclusion of PWGc and PWG is shown in Fig. 7. The maximum value of CBRI for PWGc is 3.50 at 7.5 cm and for PWG is 2.43 at 5 cm while at other depth improvement is not effective. CBRI variation with depth is significant in PWGc compared to PWG. CBRI is also representing the same behaviour as reinforcement is effective at particular depth only.

3.5 Application of PWG and PWGc in Field

PWG and PWGc show significant behaviour change in soil subgrade. So, it can be used in field with proper dimension and laying. Here in this study, the ratio of width of geosynthetics (W_g) to width of foundation/plunger (W_f) is 3 ($W_g/W_f = 15/5 = 3$). So, according to width of foundation, proper dimension of reinforcement can be taken.

4 Conclusions

Following are the conclusions drawn from the experimental investigation carried out to analyse CBR behaviour of soil subgrade with the inclusion of plastic waste in the form of geogrid and geocell made from waste plastic water bottle:

1. The addition of plastic waste bottle in the form of geocell and geogrid appreciably increases the load-carrying capacity, unsoaked CBR value and CBRI of virgin soil; so, it can be used for the improvement of soil subgrade as a geosynthetic material.
2. Reuse of plastic waste in the form of geogrid and geocell solves the problem of dumping of plastic waste.
3. Maximum improvement in unsoaked CBR is achieved by plastic waste geocell-type reinforcement (PWGc) compared to plastic waste geogrid reinforcement (PWG) due to its cellular type of structure which provides confinement to the soil.
4. Placing of reinforcement in soil material in the form of geocell and geogrid is effective at particular depth due to shear zone effect.

References

1. Mahali KP, Sinha AK (2015) Utilization of stone dust with plastic waste for improving the subgrade in highway pavement construction. Int J Res Eng Technol 4(6):29–35
2. Choudhary AK, Jha JN, Gill KS (2010) Utilization of plastic wastes for improving the subgrades in flexible pavements. In: GeoShanghai 2010 international conference proceeding, ASCE, pp 320–326
3. Nair AM, Gali ML (2014) Use of geocell as a reinforcing material for unpaved road section. Golden jubilee conference of the IGS Bangor Chapter, Geo-Innovation, pp 1–8
4. Paramkusam BR, Prasad A, Arya CS (2013) A study on CBR behavior of waste plastic (PET) on stabilized red mud and fly ash. Int J Struct Civ Eng 2(3):232–240
5. Consoli NC, Montardo JP, Prietto PDM, Pasa GS (2002) Engineering behavior of a sand reinforced with plastic waste. J Geotech Geoenviron Eng ASCE 128(6):462–472
6. Nsaif MH (2013) Behavior of soils strengthened by plastic waste materials. J Eng Dev 17(4):182–194
7. Carlos DM, Pinho-Lopes M, Lopes ML (2016) Effect of geosynthetic reinforcement inclusion on the strength parameters and bearing ratio of a fine soil. In: Advances in transportation geotechnics 3. The 3rd international conference on transportation geotechnics (ICTG 2016), vol 143, pp 34–41
8. IS 2720-Part VII (1980) Methods of test for soils: determination of water content-dry density relation using light compaction. Bureau of Indian Standards, New Delhi, India
9. IS: 2720-Part XVI (1987) Laboratory determination of CBR. Bureau of Indian Standards, New Delhi, India

Numerical Analysis of Behavior of Single Pile in Layered Soil Against Lateral Load

Shahnwaz Ahmed, Md. Rehan Sadique, Mudassir Ali Khan and Vishwas A. Sawant

Abstract Pile foundations are often subjected to lateral loads along with vertical loads. In this paper, the behavior of a single pile is determined using finite element analysis. The P-Y curve is generated by using finite element modeling which was used for comparison to investigate the behavior of soil. The analysis was performed for free headed pile as allowing for rotating. The analysis has been performed for the single pile in soil layering profile. Drucker–Prager and Mohr–Coulomb models have been used to simulate the medium dense sand and clay, respectively. Layering effect on lateral deflection was plotted for the different case. It has been observed that lateral deflection of single pile in uniform clay layer is greater than that in uniform sand layer.

Keywords Pile foundation · Lateral loading · Layered soil · Lateral bearing capacity · Lateral deflection

1 Introduction

Pile foundation is the most versatile method to transfer a load of superstructure through the deep problematic soil to hard strata. Pile foundations were frequently used to transfer not only the vertical load but also the lateral (lateral). High rise buildings, offshore platforms, bridges, defense structures, dams, metro projects, transmission towers, earth retaining structures, wharves, and jetties were few important structures,

S. Ahmed (✉) · Md. Rehan Sadique · M. Ali Khan
Department of Civil Engineering, ZHCET, Aligarh Muslim University, Aligarh, India
e-mail: shahnwazahmad100@gmail.com

Md. Rehan Sadique
e-mail: rehan.sadique@gmail.com

M. Ali Khan
e-mail: mudassir290@gmail.com

V. A. Sawant
Department of Civil Engineering, IIT Roorkee, Roorkee, UK, India

S. Kumar Shukla et al. (eds.), *Advances in Sustainable Construction Materials and Geotechnical Engineering*, Lecture Notes in Civil Engineering 35,
https://doi.org/10.1007/978-981-13-7480-7_14

where pile foundation was frequently used to support vertical and lateral loads. Analysis of the behavior of single pile under lateral loading, as far as load distribution and displacement along the pile are concerned, has been analyzed through various methods [1–3, 12, 13]. Under lateral loading, the pile foundation transfers the load to the surrounding soil mass by using the lateral resistance of soil. When a lateral load applied on the pile, a part or whole of the pile tries to shift laterally in the direction of the applied load, producing bending, rotation or translation of the pile [1]. For the purpose of design, the assessment of the load transfer mechanism of a single pile is of utmost important [5]. Nevertheless, the numerical methods are very versatile and worthwhile tools for analysis and design of geotechnical problems. However, it should be carefully used and calibrated with the appropriate tests. They also constitute a valuable way of performing a sensitivity analysis of the soil parameters. There have been extensive studies for laterally loaded pile in a single layer [6–9, 14, 16] but in the literature very less work on layered [10, 11, 13]. This work presents four three-dimensional finite element models single pile embedded in uniform and layered soil profiles subjected to the lateral load.

2 Methodology Adopted

In the present work, finite element analysis-based software Abaqus is used to model single pile behavior subjected to lateral load, Fig. 1. Soil layer has been considered as uniform sand, clayey soil, and their combination stratum, while the pile has been considered as free head reinforced concrete pile. The lateral load has been applied at the top of pile as a concentrated point load. Medium size element has been used for mesh as this will give us first insight into the problem. Fine mesh of element size 0.016 m has been used for the soil surrounding the pile, while rest of the soil, is provided with coarser mesh (i.e. element size 0.05 m). Linear hexahedron type element has been used for pile and soil modeling. The number of elements generated in soil modeling was 50,000, while 2500 elements have been generated in pile.

2.1 Geometric Modeling

In the present analysis, the geometric model has been scaled down to optimize the computational efficiency of the available workstation Dell Precision Tower 7810. A rectangular soil model having dimension of 900 mm in length, 700 mm in width, and 65 mm in height has been generated using Abaqus/CAE. However, the piles have been considered as reinforced cement concrete pile having a circular section. The diameter of the pile has been assumed as 15.88 mm and the length 0.5 m similar to pile studied by Khari et al. [7]. The geometric model of pile and soil has been kept constant for all the four cases considered in the present study.

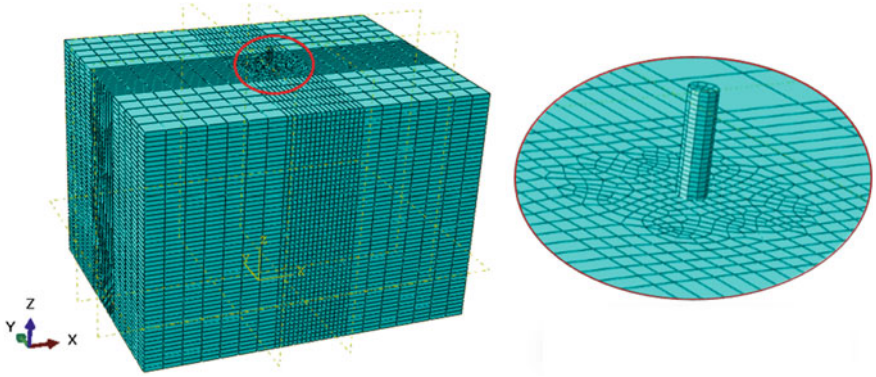

Fig. 1 Pile and soil modeling

Table 1 Material properties of sand and clay used in FEM analysis

Soil	E (KPa)	ν	γ (kg/m^3)	Φ	Ψ	Cu (KPa)
Medium dense sand	17,400	0.35	1444	37.1	0	–
Clay	11,000	0.47	1180	–	0	–
Concrete	25,000,000	0.15	2500	–	–	–

2.2 Constitutive Modeling

In this numerical study, the two simple models were used. Soil is modeled as non-linear elastoplastic. Sand is modeled as Drucker–Prager, and clay is modeled as Mohr–Coulomb model. Table 1 shows the various parameters used in FEM analysis [11].

3 Results

A number of analyses had been done to assess the comparative behavior of deflection of pile in different combination of soil. The results are expressed in terms of P-Y curve for various combination of soil layer system. Deflection of pile in uniform sand is shown in Fig. 2. The maximum value of deflection at the top of pile has been observed as 15.42 mm, while at base is 1.64 mm in the direction opposite to load directions showing the layer and Fig. 3 shows the same in multilayered soil. With the help of numerical analysis approach, the behavior of pile subjected to the lateral load in layered isotropic soils is investigated.

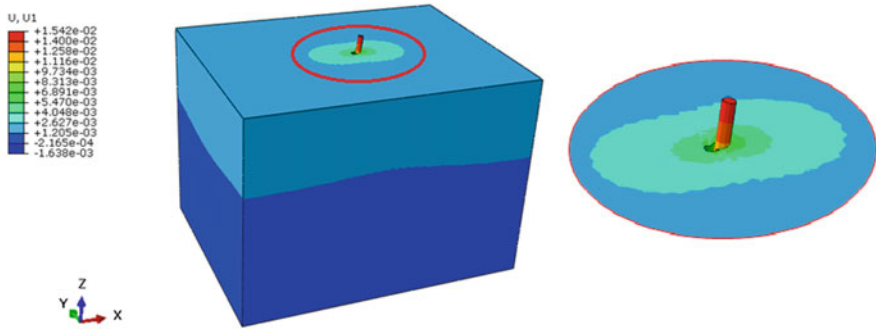

Fig. 2 Deflection contour of pile in single layer

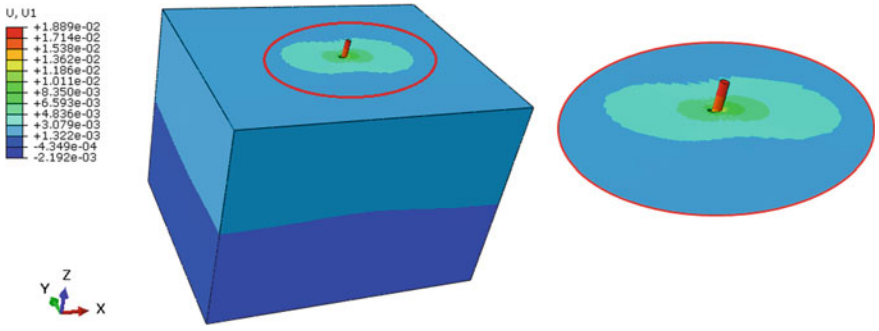

Fig. 3 Deflection contour of single pile in multilayered soil

4 Analysis

It has been observed that lateral deflection of single pile in clay layer is greater than that in the sand layer. It may be due to plastic behavior of clay. Figure 4 shows the deflection in uniform sand and uniform clay. The percentage of increment in deflection is about 30%. It is worth mentioning that uniform sand is stiffer than the uniform clay case, and therefore, displacement is lesser in sand as compared to clay.

4.1 Clay Layer in Sand Deposit

It is very interesting note that the difference of deflection of pile in sand deposit and sand deposit with clay layer is insignificant. Figure 5 shows comparative deflection. The percentage variation is about only 1.5%.

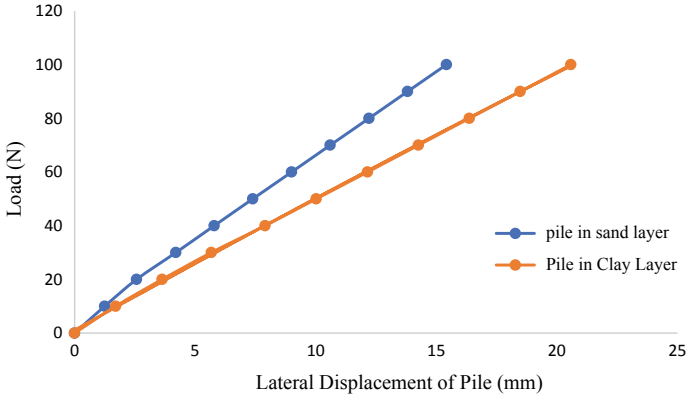

Fig. 4 Comparison of deflection of single pile in sand layer and clay layer

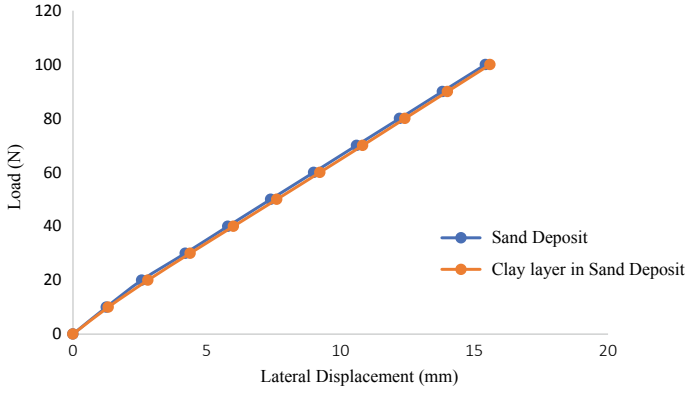

Fig. 5 Comparison of deflection of single pile in sand deposit and sand deposit with clay layer

4.2 Sand Layer in Clay Deposit

Figure 6 shows the comparison of single pile in clay stratum alone and pile in clay stratum when sand layer is present. There is little decrease in deflection when a layer of sand is present in clay deposit as compared to clay deposit only. It has been observed that the decrease in deflection of pile by introducing layer sand is about 4–5%. Also, it may be associated with the thickness of sand layer introduced.

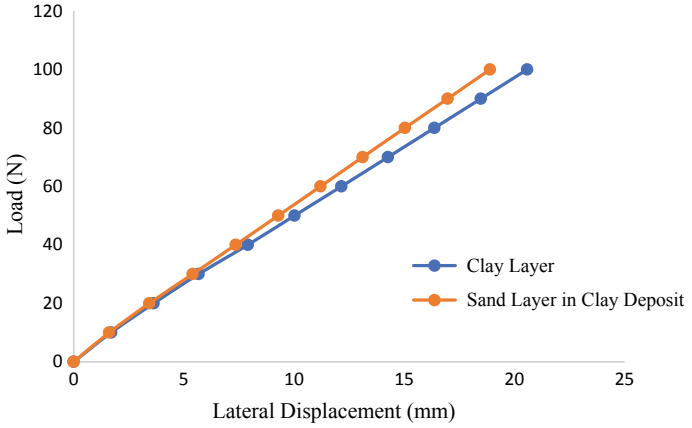

Fig. 6 Comparison of single pile in clay deposit and clay deposit with sand layer

5 Conclusion

This paper presents a series of FE analyses simulating the performance of reinforced concrete pile foundation against the lateral load. Assessment of the lateral displacement of pile due to lateral load has significant importance for the design aspect. Often bearing capacity of piles is attained for a displacement which is beyond the permissible limit for a structure. Since that, the experience is required in order to get reduced bearing capacity assuming full utilization of shaft friction. The numerical results showed that lateral displacement of pile in clay deposit is higher than that in sand deposit. A small decrease in deflection about 4–5% is observed when a layer of sand is introduced in clay stratum. This variation may be associated with the thickness of sand layer introduced. There was an insignificant effect of introducing of clay layer in sand deposit.

References

1. Ahmed S, Sadique MR, Sawant VA (2017) Response of pile foundation to lateral load: a review. In: One day national conference on recent innovations in science, technology and engineering, NIT Srinagar, India
2. Brown DA, Shie CF (1990) Numerical exploration into group effect response of pile to lateral loading. Comput Geotech 10(3):211–230
3. Elhakim AF, Khouly Mohamed AAE, Awad R (2014) Three-dimensional modeling of laterally loaded pile groups resting in sand. Hous Build Natl Res Cent J 12(1):78–87
4. Gandhi Shailesh R, Selvam S (1997) Group effect on driven piles under lateral load. J Geotech Geoenviron Eng 123(10):958–964
5. Hussien MN, Tobita T, Iai S, Karray M (2014) On the Influence of vertical loads on the lateral response of pile foundation. J Rock Mech Geotech Eng 55(1):392–403

6. Jeanjean P (2009) Re-assessment of p-y curves for soft clays from centrifuge testing and finite element modeling. Houston, Texas
7. Khari M, Kassim KA, Adnan A (2013) An experimental study on pile spacing effects under lateral loading in sand
8. Kishanrao WM, Prasad A (2016) Numerical modeling of single pile in a two-layered soil. Int J Mech Prod Eng
9. Meyerhof GG, Mathur SK, Valsangkar AJ (1981) Lateral resistance and deflection of rigid walls and piles in layered soils. Can Geotech J 18(2):159–170
10. Nichols NW, Rohani MJ, Mukherjee K, Ayob MSB, Clausen CJF, Luanne T (2014) Effect of lateral soil strength and stiffness on jacket foundation integrity and design for South China Sea sites. Kuala Lumpur, Malaysia, OTC-24842-MS: Offshore Technology Conference Asia
11. Pavlovec E (1985) Laterally loaded piles (in Croatian). Doctoral thesis, Faculty of Civil Engineering, University of Zagreb
12. Patra NR, Pise PJ (2001) Ultimate lateral resistance of pile groups in sand. J Geotech Geoenviron Eng 127(6):481–487
13. Reddy CRK, Padmakar KC, Manjari, Ekasaikumar C, Saikumar KPRK (2015) Numerical analysis of piles in layered soils: a parametric study. Int J Eng Technol (IJET) 7(2):482–489
14. Reese LC, van Impe W (2001) Single piles and pile groups under lateral Loading, 1st edn. Taylor and Francis
15. Taha A, Hesham M, Naggar EI, Turan A (2015) Numerical modeling of the dynamic lateral behavior of geosynthetics-reinforced pile foundation system Ahmed. Soil Dyn Earthq Eng 77(1):254–266
16. Yang Z, Jeremic B (2000) Numerical analysis of pile behavior under lateral loads in layered elastic plastic soils. Int J Numer Anal Meth Geomech 2(1):1–31

Determination of Liquefaction Potential of NCR Region

Sanjeev Mukherjee, Vardhman Jain, Akshay Gupta and Dev Anand Pandey

Abstract Evaluation of liquefaction potential of a region is useful in a variety of ways as it gives information on the geological characteristics of the region of interest and proves to be important when it comes to taking preventive measures before and after the occurrence of an earthquake. Study and analysis of liquefaction potential index involve criteria like the geotechnical characteristics, the historical criteria as well as the seismic vulnerability of the region. Region selected falls in both Delhi and Noida; hence, NCR region is taken in title. It was observed that the evaluation of LPI is of paramount importance. The aim of the present report is to evaluate potential of liquefaction of Noida and Greater Noida region by calculating factor of safety against liquefaction using simplified approach and comparison of the results with respect to the methods used; these results will extend its help in micro-zonation of the region. The total boundary of the study area falls within a radius of 20 km approximately. Standard penetration test was vital for the collection of SPT-*N* values. The field test was carried out at the specified location, and various soil characteristics were recorded for analysis using SPT. The project also consists of the effect of factor of safety due to the change in the peak ground acceleration by increasing or decreasing it as well as the change in the magnitude of the earthquake on the liquefaction potential sites. It was observed that, the MSF depends upon the resistance of the soil against the seismic activity and peak ground acceleration depends upon the seismic capacity of the earthquake against the soil. In our present study, 0.24g has been used.

S. Mukherjee (✉) · V. Jain · A. Gupta · D. A. Pandey
Department of Civil Engineering, Amity School of Engineering and Technology, Amity University, Noida, India
e-mail: smukherjee3@amity.edu

V. Jain
e-mail: vardhmanjain@hotmail.com

A. Gupta
e-mail: akshayg677@gmail.com

D. A. Pandey
e-mail: devpandey1994@gmail.com

S. Kumar Shukla et al. (eds.), *Advances in Sustainable Construction Materials and Geotechnical Engineering*, Lecture Notes in Civil Engineering 35,
https://doi.org/10.1007/978-981-13-7480-7_15

Keywords CSR · CRR · F.O.S · Standard penetration resistance · Liquefaction · MSF

1 Introduction

Liquefaction is a complex phenomenon that mainly occurs in saturated soils having undrained conditions as well as in cohesionless soils (such as sandy soil and clayey soil) in which the solid material of the soil transforms into the liquid state due to effect of an earthquake upon it which results into loss of the strength of the soil as well as the increase in the water pressure in the soil molecules. Earthquake persuaded liquefaction has been identified in the past, so many years such as the 1897 earthquake having magnitude of 8.1, initiated under the Shillong plateau caused into liquefaction phenomenon affecting mass destruction of the area.

Estimation of liquefaction is of paramount importance as it helps in the seismic micro-zonation of the city of Niigata earthquake of 1964 based on the study by Hamada [1].

While in our present study, the determination of the potential of liquefaction is by using the simplified procedure which was presented by Seed and Idriss [2]. Our aim is to determine the factor of safety as well as our study is confined in the Noida region spanning from Sector 72 to knowledge Park V.

2 Area of Study

Our study was primarily based upon the Noida region where most of the soils are sandy as well as silty. It was also observed that the Noida region is situated in zone IV according to the seismic zones as per IS 1893.9 boreholes data were collected stretching from Sector 72 to Knowledge Park V as shown in Fig. 1. In these Standard Penetration test were performed and the respective SPT-*N* values were determined for the calculation of CRR which in turn is known as the resistance of the soil against the liquefaction. The data for the SPT was taken from the consultancy which was further processed using the Excel worksheet to calculate the potential index.

3 Methodology

The methodology of the analysis of the liquefaction potential includes the following processes:

(i) Identification of the area based upon the historical criteria, geological characteristics, and the depth of the groundwater table.

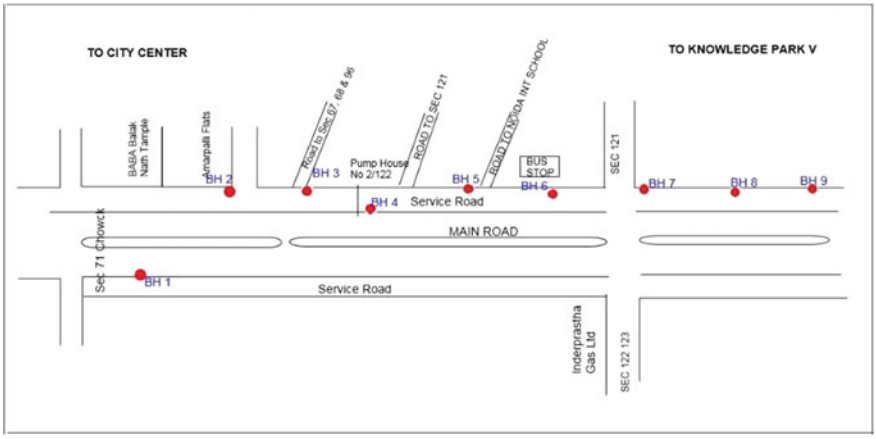

Fig. 1 Boreholes location

(ii) Determine the parameters such as CSR as well as CRR which is known as the seismic demand and resistance against liquefaction, respectively.
(iii) Lastly, the F.O.S which in turn is the ratio of resistance of the soil to seismic demand is determined.
(iv) The effect of the liquefaction potential which is the F.O.S [3] due to PGA as well as MSF [4] is also compared for generalizing the study.

It should be noted that Cyclic resistance ratio is to resist the effect of the increase of the pore water pressure due to the effect of the horizontal force of the earthquake or due to the presence of the dynamic loading.

4 Liquefaction Index of Boreholes

4.1 Cyclic Stress Ratio (CSR)

This is the seismic demand which can also be termed as the driving force for the flowing of the soil in the liquid form to occur. This is dependent upon the PGA [5] and is not dependent upon the magnitude scaling factor.

$$\mathrm{CSR} = \frac{\tau_{\mathrm{av}}}{\sigma'_{\mathrm{vo}}} = 0.65 \frac{a_{\max}}{g} \frac{\sigma_{\mathrm{vo}}}{\sigma'_{\mathrm{vo}}} r_{\mathrm{d}} \tag{1}$$

where

$a_{\max}$ peak level acceleration at the earth surface;
σ_{vo} total effective vertical;

σ'_{vo} overburden stresses;
r_d stress reduction coefficient.

Stress reduction factor is evaluated using the following equation and graph. While it has been assumed that the soil is layered in rigid form but due to the flexibility pertinent to it, the use of this coefficient comes into place. Here, z is the depth of the soil beneath the ground level.

$$r_d = \frac{1.000 - 0.4113z^{0.5} + 0.04052z + 0.001753z^{1.5}}{\left(1.00 - 0.4177z^{0.5} + 0.05729z - 0.006205z^{1.5} + 0.001210z^2\right)} \quad (2)$$

Liao and Whitman (1968) invented another formula to calculate r_d as given below.

$$r_d = 1.02 - 0.00765z \quad \text{for } z = 9.15 \text{ m}$$
$$r_d = 1.1742 - 0.0267z \quad \text{for } 9.15 \text{ m} < z < 23 \text{ m}$$

4.2 Cyclic Resistance Ratio (CRR)

This is primarily used for illustrating the resistance value of the soil in contradiction of soil to flow. Due to earthquake, there is the increase of the water pressure and it has been observed that the soil particles move with agility and start flowing the capacity of the soil to resist this motion is governed by the value of CRR. Hammer efficiency plays a major role in determining the CRR [6]. Here, the hammer efficiency is taken to be precise 65%. For standardization, the CRR is calculated for the magnitude of intensity at 7.5 Richter scale. While for the other intensity of magnitude, the MSF [7] is taken into consideration with it.

Here, it was observed that it was calculated for the corrected SPT-N value as shown in the formula.

In our project, we have made use of SPT and applied suitable correction for overburden for CRR calculation. N values obtained from standard test procedure is corrected for overburden pressure and hammer energy ratio of 60%. This value is restated as $(N_1)_{60}$

$$\text{CRR} = \frac{1}{34 - (N_1)_{60}} + \frac{(N_1)_{60}}{135} + \frac{50}{\left[10(N_1)_{60} + 45\right]^2} - \frac{1}{200} \quad (3)$$

$$\text{CRR} = \text{CRR}_{7.5} \times \text{MSF}$$

Hence, by Eq. (3) standardized value of CRR is calculated.

4.3 Factor of Safety (F.O.S)

Lastly, calculation of the factor of safety is done as shown below; it is given as the ratio of resistance pertinent to liquefaction to the seismic demand due to the driving force of the earthquake.

$$F_s = \frac{\text{CRR}}{\text{CSR}}\text{: If } F_s < 1.0\text{: Liquefaction}$$

The ratio less than unity governs the fact that the soil can undergo liquefaction. In most of the boreholes where the test was conducted, it was observed that most of the sites are not prone to liquefaction as the factor of safety was less than unity. A sample from the numerous boreholes data is indicated below. The experimental analysis of standard penetration test was explained as earlier. The data entirely focusses on index properties of the soil which are the specific gravity, plastic limit, liquid limit, SPT-*N* [8] value. It was observed that the value of SPT is larger as we go deeper the soil layer as compared near the ground level. While it has been observed if the soil layer consisting of SPT-*N* value more than 30, then the process of liquefaction won't occur. In situ test for the calculation of the term is primarily done (Fig. 2).

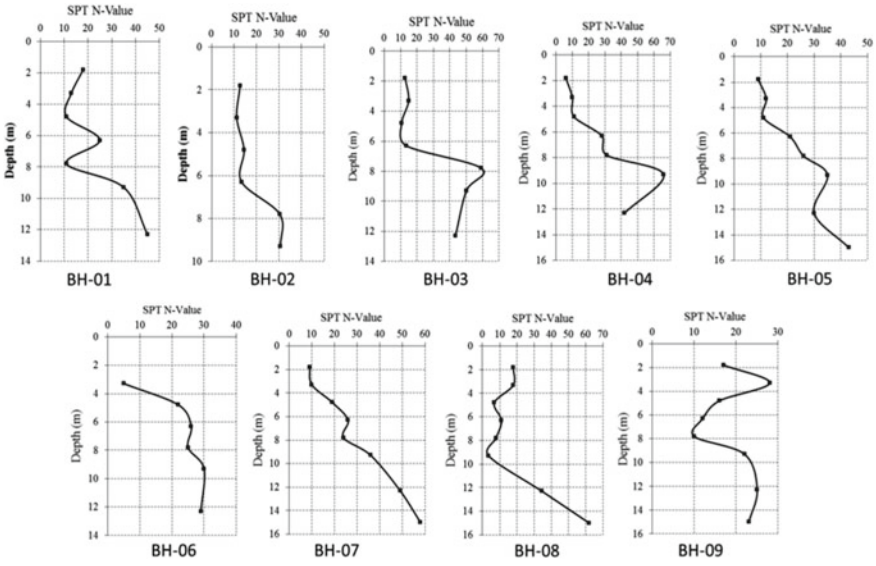

Fig. 2 SPT *N*-values with the depth all the nine sites in NCR region

5 Results and Discussion

5.1 Water Table at Actual Condition

In this case, the actual condition of the groundwater table is more effective. Here the soil characteristics were filled in the excel worksheet and the desired result was obtained. Most of the boreholes are susceptible to liquefaction at depths close to the ground. There is no general trend of liquefaction common to all boreholes, but one thing can be concluded that the region is susceptible to liquefaction if the ratio of CSR to CRR [8] is greater than unity as one can perceive from the graphs of the various bore log data. Since the graph of each of the bore log data follows a different trend, one cannot convey without conducting the experimental analysis whether the site will be prone to liquefaction or not. It can be observed that BH-7 is most liquefiable, while BH-2 is least liquefiable. This means that various ground improvement techniques would be of paramount importance of the site consisting of BH-7 in order to make it the normal working as well as sustainable condition for the numerous construction processes like the improvement techniques namely use of vertical drains, use of compaction techniques. It has been observed that BH-01, BH-03, BH-04, BH-06, BH-09 shows a similar trend while comparing the both the terms values. The rest of the bore log data shows the similar trend.

5.2 Water Table at Ground Surface

Here the soil characteristics were filled in the excel sheet and the desired result was obtained. The variation of CSR/CRR with depth (up to 16 m) for the first eight boreholes is shown in Fig. 3. Here the effect of the water table is not considered as it has been observed that during the monsoon reason the depth of the groundwater table fluctuates, so the water table is assumed to be near the ground level and then analysis is performed. The CSR/CRR is marked on *X*-axis, while depth is plotted on *Y*-axis. CSR is shown with thick lines, while CRR is shown with broken lines, it can be seen from the graph that for portions where CRR is less than CSR, liquefaction is likely to follow in those pockets. While in areas where CRR exceeds CSR, those pockets are permitted from liquefaction. Out of the eight boreholes, fifth is least vulnerable to liquefaction, while eighth is most liquefiable. In this case, water table is presumed to be at the ground surface and magnitude of earthquake is taken as 7.0.BH-01, BH-04, BH-06 shows a similar trend as is observed from the graphs as shown in Fig. 4.

While comparing both the cases, it is observed that the water table at the ground surface is more prone to the phenomena and the necessary measures to the boreholes should be applied to reduce the effect.

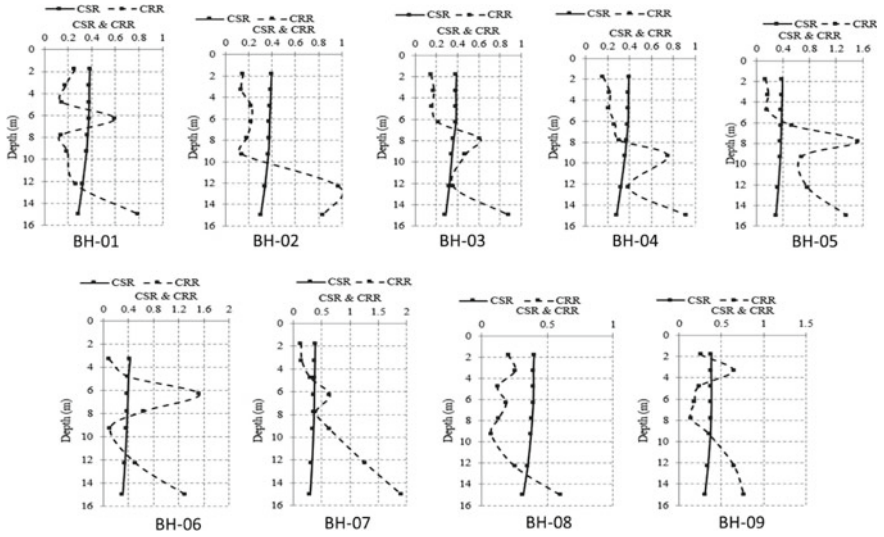

Fig. 3 CSR, CRR with the depth for all the sites when water table is at 5 m and magnitude of earthquake ($M = 7.0$)

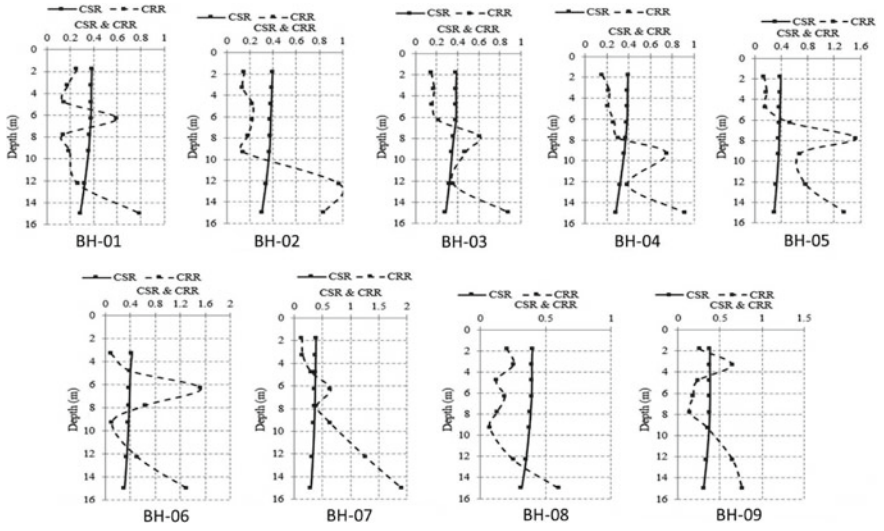

Fig. 4 CSR, CRR variation with the depth for all the sites when water table at ground surface and magnitude of earthquake ($M = 7.0$)

6 Effect of Magnitude Scaling Factor on Factor of Safety

In this leg of the project, the effect of the magnitude scaling factor on the liquefaction potential site was observed which are depicted as shown. Here the MSF is given as form the basis for the estimation of the effect of it on the F.O.S and water table situated at 5 m beneath the ground level. After analyzing it, we can conclude that when the magnitude of 7 and 6 is taken, there is hardly any change in the factor of safety. Therefore, we can also infer if we safeguard the site the extent of liquefaction for a site in which the magnitude of earthquake is relatively on the high side then the same site would be protected against the liquefaction even when the magnitude is relatively lower in case it was calculated earlier (Fig. 5).

It forms the basis for the estimation of the effect of it on the factor of safety. The water table at 5 m depth was located. It can be observed that BH-7 is most liquefiable, while BH-2 is least liquefiable. Various ground improvement techniques would be of paramount importance of the site consisting of BH-7 to make it the normal working as well as sustainable condition for the numerous construction processes.

$$\boxed{\text{MSF} = \frac{10^{2.24}}{M_{\text{W}}^{2.56}}} \tag{4}$$

In Fig. 6a, it can be inferred that with the decrease in the magnitude of the earthquake as shown in the graph the value of CRR increases by which the value of the factor of safety will increase enabling it to less prone to liquefaction. The similar

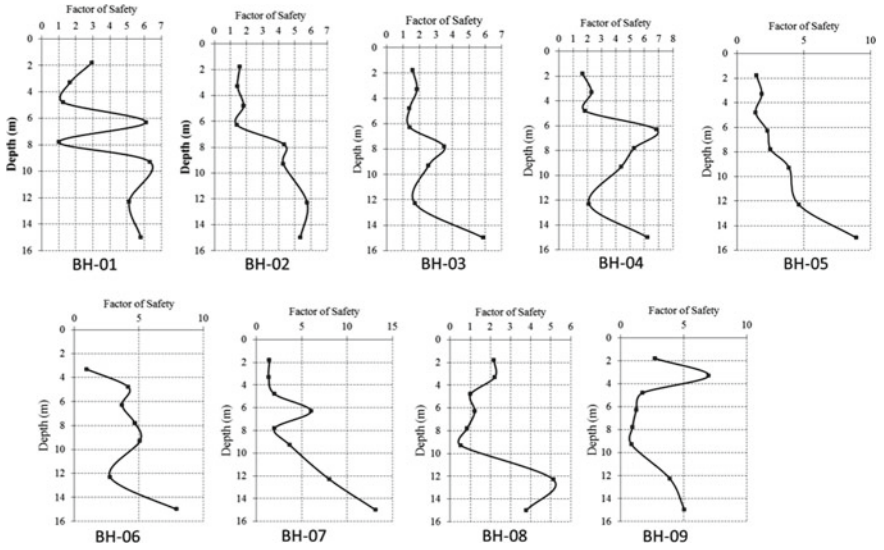

Fig. 5 FOS versus depth at all the sites (at $M = 6.0$ and WT 5.0 m)

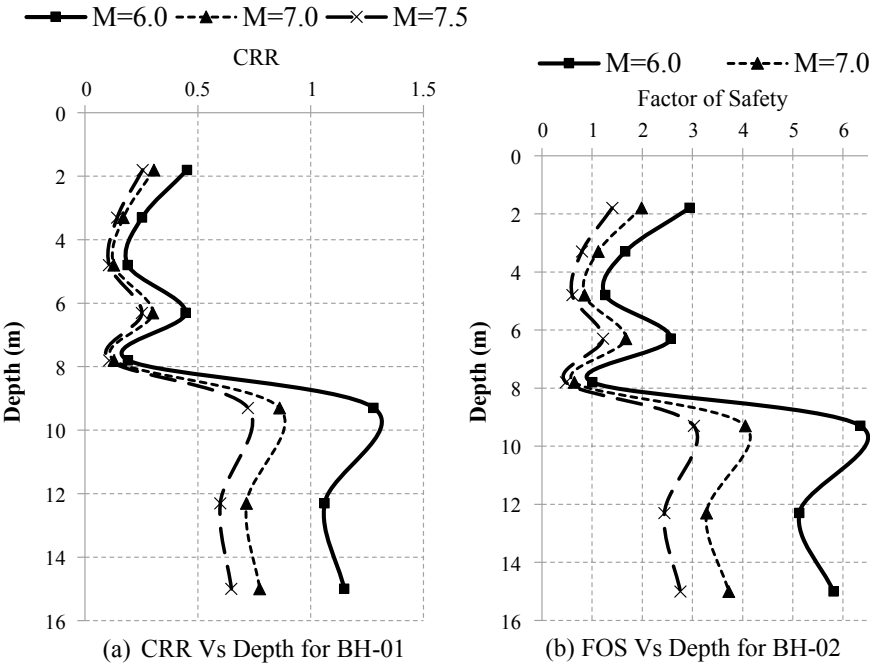

Fig. 6 Effect of magnitude on liquefaction potential of sites (WT = 5)

trend was observed with the remaining of the bore log data in which we can conclude that at lower magnitude of earthquake there would be less possibility of the soil vulnerable to liquefaction. Whereas in Fig. 6b, it was observed that with the increase in the magnitude of the earthquake the factor of safety decreases.

7 Effect of Acceleration on Liquefaction Potential

In the last leg of the project, the effect of acceleration on the liquefaction potential was observed. The peak ground acceleration was taken into consideration in the excel program from where the graph was generated. The peak ground acceleration depends upon the zone in which the region belongs. Consequently, in order to make the project universal, we went beyond the scope of the Noida region to analyze the effect of the acceleration onto the factor of safety which governs the liquefaction potential. Here a generalized approach is made effect here. Here the water table is considered at a depth of the 5 m below the ground surface.

From Fig. 7a, it was observed with the increase in the peak ground acceleration the value of CSR increases, and this similar trend was followed by all the remaining bore log sites. The peak ground acceleration is a function of CSR while calculating

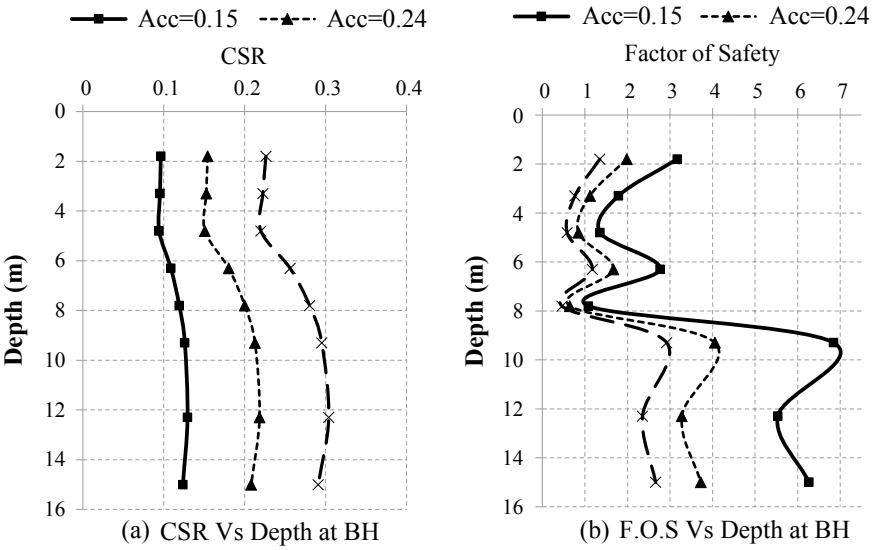

Fig. 7 Effect of acceleration (g) on liquefaction potential of sites (WT = 5.0)

CSR. While in Fig. 7b, we can conclude that with the increase in the peak ground acceleration the value of the factor of safety decreases significantly as shown in the graph which can be inferred from the fact that at higher peak ground acceleration the soil is more susceptible to liquefaction and vice versa. This trend was observed for all the bore log site. While it was also observed that for seismic zone IV, the value is taken as 0.24g, and for other boreholes, different PGA values are considered as shown in Fig. 7.

8 Conclusions

It was observed that the soil is susceptible to the phenomena depends upon the historical liquefaction pertinent to it as well on the geotechnical and geological characteristics. Our study engulfs the area of sector 62 to Knowledge Park V depicting nine boreholes data. In the study, SPT test was primarily done for the calculation of the coefficients to amount the degree of liquefaction. Some of the boreholes were prone to liquefaction and the initiation of the ground improvement techniques can be done such as the use of vertical drains or dewatering or the construction of the deep foundation.

- The factor of safety is dependent upon the geotechnical characteristics [9] and the intensity of earthquake; therefore, each borehole shows unique variation. While

for some the ratio is less than 1, therefore ground improvement technique should be applied to them.

- The F.O.S for entire sites vary as per CSR and CRR values, when the water table is close to the ground chances of liquefaction increases dramatically.
- The liquefaction occurs at all the boreholes but is not linear, some range of depth are free from liquefaction. It was observed that liquefaction of the boreholes enables for depths closer to the ground.
- The investigations specify that there is the presence of liquefaction at most of the bore log site in the measured depth when the water table at the ground and in actual field condition.
- Since the water table is located at shallow depths, there is the presence of peak earth acceleration values in the presence of silt and sandy soils.
- While in the bore log sites, it was predominantly observed with the increase in the magnitude of the earthquake the factor of safety decreases. MSF is a function of CRR and both of them shows inversely proportional behavior.
- It was observed that water table at ground level is more prone to liquefaction as compared to actual water condition.

References

1. Hamada M (1992) Large ground deformations and their effects on lifelines: 1964 Niigata earthquake case studies of liquefaction and lifelines performance during past earthquake. Technical Report: NCEER-92-0001, vol 1, Japanese case studies, National Centre for Earthquake Engineering Research, Buffalo
2. Seed HB, Idriss IM (1971) Simplified procedure for evaluating soil liquefaction potential. J Soil Mech Found Div ASCE 97(SM9):1249–1273
3. Seed HB, Idriss IM, Arango I (1983) Evaluation of liquefaction potential using field performance data. J Geotech Eng ASCE 109(GT3):458–482
4. Ishihara K (1993) Liquefaction and flow failure during earth-quakes: the 33rd Rankine Lecture. Geotechnique 43(3):351–415
5. Rao KS, Satyam DN (2007) Liquefaction studies for seismic micro zonation of Delhi region. Curr Sci 92(5):646–654
6. Muley P, Maheshwari BK, Paul DK (2015) Liquefaction potential of Roorkee region using field and laboratory tests. Int J Geosyn Ground Eng
7. IS 2131:1981 Indian standard method for standard penetration test for soils. 3rd Reprint Mar 1997. Bureau of Indian Standards (BIS), New Delhi
8. Noferesti H, Fallah H, Golabchi Y, Rezaee M (2015) Total risk rating and liquefaction analysis of Farrokhi Earth Embankment Dam, Eastern Iran. Indian Geotech J
9. Choudhary SS, Maheshwari BK, Kaynia AM (2010) Liquefaction resistance of Solani sand under cyclic loads. In: Proceedings of the Indian geotechnical conference, Bombay, pp 115–118

Pseudo-dynamic Approach to Quantify the Effect of Vertical Seismic Acceleration on Reinforced Retaining Wall for c-ϕ Soil Backfill

Ashish Gupta and Vishwas A. Sawant

Abstract The analysis of reinforced retaining walls in earthquake-prone regions is mostly performed by using the pseudo-static and pseudo-dynamic approaches for cohesionless soil backfill. For c-ϕ soil backfill, most of the researchers had used the pseudo-static approach to analyse the reinforced retaining walls situated in seismic regions those are still limited for the case of a pseudo-dynamic approach. In most of the earlier studies those had used pseudo-dynamic approach, vertical seismic acceleration was also not considered. The current study reflects a pseudo-dynamic approach to analyse the reinforced retaining walls in earthquake condition considering the propagation of primary and shear waves. Vertical seismic coefficients are also taken in the present study. A simplified formulation has been also presented here to obtain the maximum strength of reinforcements, critical angle of failure wedge and safety factor to analyse the reinforced retaining walls in earthquake condition. The effect of vertical seismic coefficients along with the soil cohesion, soil–wall adhesion and horizontal seismic coefficient on the maximum strength of reinforcements and safety factor has been carried out. For cohesionless backfill, numerical predictions are in good contract when compared with the existing studies for validation purpose.

Keywords Pseudo-dynamic approach · Maximum strength of coefficient · Cohesion · Adhesion · Horizontal and vertical seismic coefficient · Safety factor

1 Introduction

It is seen earlier that many historic earthquakes have caused permanent deformation of various concrete retaining walls. Sometimes, these deformations were very small, and sometimes the concrete retaining walls have collapsed during earthquakes. To

A. Gupta (✉) · V. A. Sawant
Department of Civil Engineering, IIT Roorkee, Roorkee, UK, India
e-mail: shi_g2000@rediffmail.com

V. A. Sawant
e-mail: sawntfce@iitr.ac.in

S. Kumar Shukla et al. (eds.), *Advances in Sustainable Construction Materials and Geotechnical Engineering*, Lecture Notes in Civil Engineering 35,
https://doi.org/10.1007/978-981-13-7480-7_16

support the soil backfills in various civil infrastructure projects, reinforced retaining (RR) walls have been used as the alternatives to conventional concrete retaining walls. Soil reinforcement has become extensively used earthwork construction technique due to its technical and economical advantages. Mononobe [1] and Okabe [2] did the pioneer work to determine the seismic earth pressure by the pseudo-static method without considering the time-dependent effect. Time-dependent effect was then incorporated by Steedman and Zeng [3] for analysing the retaining walls under earthquake condition, which is further known as pseudo-dynamic (PD) method. The only drawback of this study was the consideration of finite shear waves in soil backfill. Nimbalkar et al. [4] and Choudhury et al. [5] then improve the PD method incorporated by Steedman and Zeng [3]. Propagation of primary and shear waves is considered to act within the soil medium. Nimbalkar et al. [4], Choudhury et al. [5] and Reddy et al. [6] also studied the reinforced soil–wall considering PD method for cohesionless soil backfill. Ghanbari and Ahmadabadi [7] proposed PD approach considering horizontal slice method to analyse the RR walls under seismic conditions for c-ϕ soil backfill. Effect of vertical seismic coefficient was not taken in this study. Tafreshi and Rahimi [8] had noticed the effect of vertical seismic coefficient using PD approach to analyse the RR wall subjected to seismic loads for cohesionless soil backfill. Most of the literature presented in this study had not considered the effect of vertical seismic acceleration.

In the current study, a simplified limit equilibrium method has been taken to analyse the RR wall for c-ϕ soil backfill using PD method. Propagation of primary and shear waves has been taken to act within the soil. Vertical seismic coefficient is also taken in the present study. A parametric study showing the effect of vertical seismic acceleration along with the effect of cohesion and adhesion has been also reported in the present study.

2 Methodology

Figure 1 shows the RR wall system of height H. The retaining wall retained the soil backfill of cohesion c and soil friction angle ϕ, having unit weight γ. Reinforced retaining wall system is having n number of planar reinforcement of length L_r. Reinforcement layers are having the spacing $S_v = H/n$ except the reinforcements provided in the top and bottom. In the top and bottom, 0.5 S_v spacing is provided. On the base of wall, seismic acceleration is subjected in horizontal and vertical direction as $a_h = k_h.g$ and $a_v = k_v.g$, where k_h and k_v are the seismic coefficients in their respective direction. When the direction of k_v is upward, its value is assumed as positive. Failure plane AB is assumed as linear, which makes an angle α with the horizontal axis.

Various forces in the wedge ABC are shown in Fig. 2. The resultant of shear and normal force acting on this wedge is F. Shear and primary wave velocities are V_s and V_p. Ratio $V_p/V_s = 1.87$ is taken as given in most of the literature [4, 5]. The

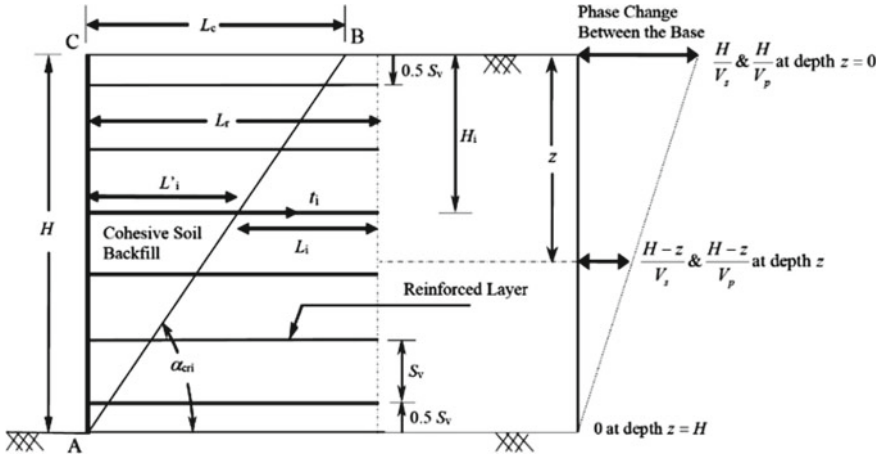

Fig. 1 Reinforced retaining (RR) wall system

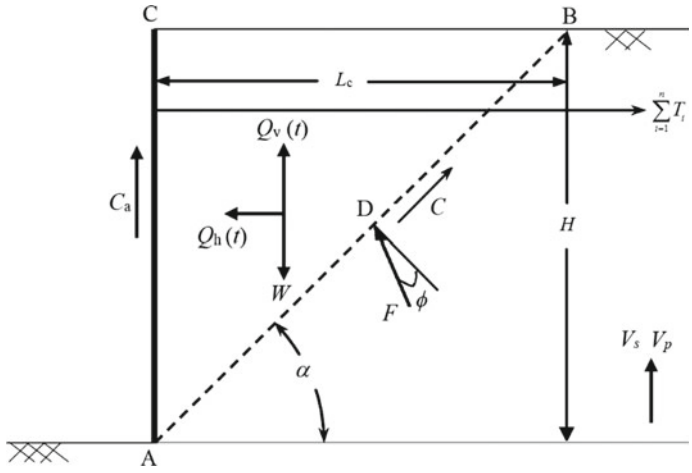

Fig. 2 Forces on the failure wedge ABC under seismic condition

analysis consists of the period of lateral shaking $T = (2\pi/\omega)$, where ω is the angular frequency.

2.1 Tensile Force Generated in the Reinforcement

For stabilizing the RR wall, $\sum_{i=1}^{n} T_i$ required a sum of the tensile forces, where T_i is the tension generated in the ith layer of reinforcement. Considering, dynamic

equilibrium of forces on RR wall system in horizontal and vertical directions and $\sum_{i=1}^{n} T_i$ can be expressed as:

$$\sum_{i=1}^{n} T_i = \begin{bmatrix} \{W - Q_{\mathrm{v}}(t)\}\tan(\alpha - \phi) + Q_{\mathrm{h}}(t) \\ -cH\{\tan(\alpha - \phi) + \cot\alpha\} - c_{\mathrm{a}}H\tan(\alpha - \phi) \end{bmatrix} \tag{1}$$

Total weight of the assumed failure wedge ABC is $W = 0.5\gamma H^2 \cot\alpha$. The required strength of reinforcement (K) can be stated as:

$$K = \frac{\sum_{i=1}^{n} T_i}{0.5\gamma H^2} = \begin{bmatrix} \tan(\alpha - \phi)\left\{\cot\alpha - \frac{Q_{\mathrm{v}}(t)}{0.5\gamma H^2} - c*(1 - a_{\mathrm{f}})\right\} \\ + \frac{Q_{\mathrm{h}}(t)}{0.5\gamma H^2} - c*\cot\alpha \end{bmatrix} \tag{2}$$

where $a_{\mathrm{f}} = c_{\mathrm{a}}/c$ and $c* = \frac{2c}{\gamma H}$.

2.2 Pseudo-dynamic Inertia Forces

At depth z, consider a small element of thickness $\mathrm{d}z$ with mass $m(z) = \frac{\gamma}{g}\frac{(H-z)}{\tan\alpha}\mathrm{d}z$. The seismic accelerations in horizontal and vertical directions at depth z and time t can be obtained as:

$$a_{\mathrm{h}}(z,t) = k_{\mathrm{h}} g \sin\omega\left(t - \frac{H - z}{V_{\mathrm{s}}}\right) \tag{3a}$$

$$a_{\mathrm{v}}(z,t) = k_{\mathrm{v}} g \sin\omega\left(t - \frac{H - z}{V_{\mathrm{p}}}\right) \tag{3b}$$

Total inertia force in horizontal direction, $Q_{\mathrm{h}}(t)$, can be derived as:

$$Q_{\mathrm{h}}(t) = \int_0^H m(z)a_{\mathrm{h}}(z,t) = \frac{\gamma k_{\mathrm{h}}}{\tan\alpha}(I) \tag{4}$$

Assuming,

$$\lambda = TV_{\mathrm{s}};\ \zeta = \left(t - \frac{H}{V_{\mathrm{s}}}\right);\ \eta = TV_{\mathrm{p}};\ \psi = \left(t - \frac{H}{V_{\mathrm{p}}}\right);$$

$$\theta_\lambda = 2\pi\left(\frac{t}{T} - \frac{H}{\lambda}\right);\ \theta_\eta = 2\pi\left(\frac{t}{T} - \frac{H}{\eta}\right) \text{and } \theta_t = 2\pi\frac{t}{T}$$

$$I = \frac{\lambda}{4\pi^2}[2\pi H\cos\omega\zeta + \lambda(\sin\omega\zeta - \sin\omega t)] \tag{5}$$

On simplifying Eq. (4), $Q_{\mathrm{h}}(t)$ can be obtained as:

$$Q_{\mathrm{h}}(t) = \frac{\gamma k_{\mathrm{h}}}{4\pi^3 H \tan\alpha}\left[2\pi^2 H^2 \lambda \cos\theta_\lambda + \pi H \lambda^2 \{\sin\theta_\lambda - \sin\theta_t\}\right] \tag{6}$$

Similarly, total inertia force in vertical direction, $Q_{\mathrm{v}}(t)$, can be stated as:

$$Q_{\mathrm{v}}(t) = \frac{\gamma k_{\mathrm{v}}}{4\pi^3 H \tan\alpha}\left[2\pi^2 H^2 \eta \cos\theta_\eta + \pi H \eta^2 \{\sin\theta_\eta - \sin\theta_t\}\right] \tag{7}$$

On substituting $Q_{\mathrm{h}}(t)$ and $Q_{\mathrm{v}}(t)$ in Eq. (2), K can be obtained as:

$$K = \frac{1}{\tan\alpha}\left[\begin{array}{l} \tan(\alpha-\phi)\{1 - c*(1-a_{\mathrm{f}})\tan\alpha\} - c* \\ +\frac{\lambda k_{\mathrm{h}}}{2\pi^3 H^3}\left\{\begin{array}{l} 2\pi^2 H^2 \cos\theta_\lambda + \pi H \lambda \sin\theta_\lambda \\ -\pi H \lambda \sin\theta_t \end{array}\right\} \\ -\frac{\eta k_{\mathrm{v}} \tan(\alpha-\phi)}{2\pi^3 H^3}\left\{\begin{array}{l} 2\pi^2 H^2 \cos\theta_\eta + \pi H \eta \sin\theta_\eta \\ -\pi H \eta \sin\theta_t \end{array}\right\} \end{array}\right] \tag{8}$$

2.3 Safety Factor, SF

On applying the load in the reinforced retaining wall system, the reinforcement axially pulled out, which causes shear resistance, and the tension fully mobilized in reinforcement layers. Hence, $\sum_{i=1}^{n} t_i$ can be obtained as:

$$\sum_{i=1}^{n} t_i = \sum_{i=1}^{n} 2(1+k_{\mathrm{v}})\gamma H_i L_i \tan\phi_{\mathrm{r}} \tag{9}$$

Using,

$$H_i = (i-0.5)S_{\mathrm{v}};\ S_{\mathrm{v}} = H/n;\ L_i = L_{\mathrm{r}} - (H - H_i)\cot\alpha_{\mathrm{cri}} \text{ and } \phi_r = 2\phi/3$$

In which ϕ_{r} is internal friction angle between soil and reinforcement. For the ith layer, H_i is the depth of embedment, L_i is the effective length and t_i is the tensile force mobilized.

$$\sum_{i=1}^{n} t_i = \gamma S_{\mathrm{v}} \tan\phi_{\mathrm{r}}(1+k_{\mathrm{v}})\left[n^2(L_{\mathrm{r}} - H\cot\alpha_{\mathrm{cri}}) + \cot\alpha_{\mathrm{cri}} S_{\mathrm{v}}\left(\frac{4n^3 - n}{6}\right)\right] \tag{10}$$

Hence, the safety factor can be expressed as:

$$\mathrm{SF} = \left(\sum_{i=1}^{n} t_i\right) / \left(\sum_{i=1}^{n} T_i\right) \tag{11}$$

Table 1 Variation of parameters taken in the present study

S. No.	Description	Values are taken
1	Unit weight of soil backfill (γ)	18 kN/m^3
2	The height of retaining wall (H)	5 m
3	Shear wave velocity (V_S)	100 m/s
4	Primary wave velocity (V_P)	187 m/s
5	Time period of lateral shaking (T)	0.3 s
6	Soil friction angle (ϕ)	30°
7	Horizontal seismic coefficient (k_h)	0.0, 0.1, 0.2 and 0.3
8	Ratio (k_v/k_h)	−1.0, −0.5, −0.25, 0.0, 0.25, 0.50 and 1.0

3 Results and Discussion

In the present study, required maximum strength of reinforcement and safety factor are presented for varying values of k_h for different k_v/k_h values. A parametric study has been performed to quantify the effect of k_v to analyse RR wall under seismic condition. Variation of parameters considered is reported in Table 1.

3.1 Required Maximum Strength of Reinforcement, $\mathbf{K}_{max}$

Figure 3a–d shows the variation in required maximum strength of reinforcement K_{max} with k_h varying from 0.0 to 0.3 for different k_v/k_h varied as −1.0, −0.50, −0.25, 0.0, 0.25, 0.50 and 1.0. The variation of K_{max} is shown for the values of (a) $c = 0.0$ and $a_f = 0.0$; (b) $c = 10$ kPa and $a_f = 0.0$; (c) $c = 10$ kPa and $a_f = 0.25$; and (d) $c = 10$ kPa and $a_f = 1.0$. It is clearly shown in Fig. 3a–d that the K_{max} value increases as the values of k_h increase from 0.0 to 0.3. When the ratio of k_v/k_h moves from its negative values to the positive values, the value of K_{max} increases continuously. It can also notice the more effect of the ratio of k_v/k_h from (−1.0 to −0.5) and (0.5 to 1.0) on the values of K_{max}. Effect of cohesion of soil and adhesion of soil–wall on the values of K_{max} also can be obtained from Fig. 3a–d. For the cohesive soil backfill without considering the value of soil–wall adhesion, the value of K_{max} decreases considerably, when comparing the K_{max} values for the cohesionless soil backfill.

For the cohesionless soil backfill without taking the soil–wall adhesion, when the ratio of k_v/k_h moves from its negative value (as −1.0) to the positive value (as +1.0), the value of K_{max} increases by 27.5% ($k_h = 0.2$) and 26.1% ($k_h = 0.3$). For the same set, when the k_h value is increased from 0.2 to 0.3, K_{max} increases by 22.31% ($k_v/k_h = -1.0$) and 20.97% ($k_v/k_h = 1.0$).

For the cohesive soil backfill ($c = 10$ kPa) without taking the soil–wall adhesion, on moving the ratio of k_v/k_h from −1.0 to +1.0, the value of K_{max} increases by 81.2%

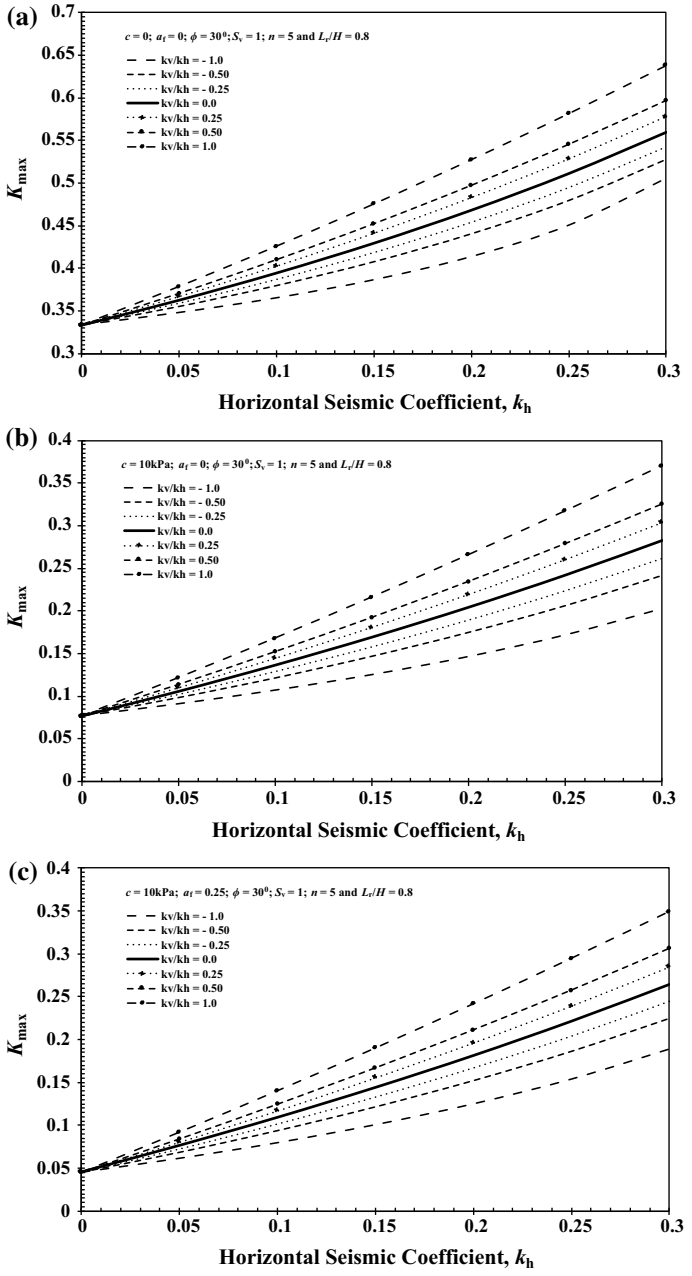

Fig. 3 K_{max} with k_h for different k_v/k_h for **a** $c = 0.0$ and $a_f = 0.0$,**b** $c = 10$ kPa and $a_f = 0.0$, **c** $c = 10$ kPa and $a_f = 0.25$ and **d** $c = 10$ kPa and $a_f = 1.0$

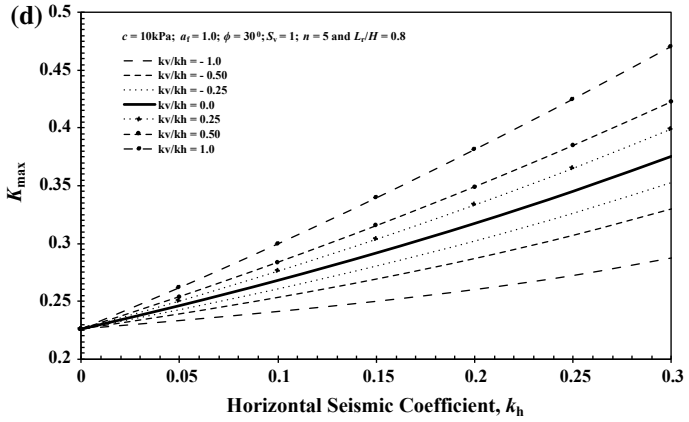

Fig. 3 (continued)

($k_h = 0.2$) and 82.1% ($k_h = 0.3$). For the same set, when the k_h value is increased from 0.2 to 0.3, K_{max} increases by 38.6% ($k_v/k_h = -1.0$) and 39.3% ($k_v/k_h = 1.0$).

For $c = 10$ kPa and $a_f = 1.0$, K_{max} increases by 46.7% ($k_h = 0.2$) and 63% ($k_h = 0.3$), when k_v/k_h varies from -1.0 to 1.0. The value of K_{max} increases by 10.5 and 10.1%, respectively, for $k_v/k_h = -1.0$ and 1.0, when k_h varies from 0.2 to 0.3.

3.2 Safety Factor, SF

The variation in safety factor, SF, with k_h is shown in Fig. 4a–d. The value of k_h is varying from 0.0 to 0.3 for different k_v/k_h varied as -1.0, -0.50, -0.25, 0.0, 0.25, 0.50 and 1.0.

Four sets ($c = 0.0$ and $a_f = 0.0$; $c = 10$ kPa and $a_f = 0.0$; $c = 10$ kPa and $a_f = 0.25$; and $c = 10$ kPa and $a_f = 1.0$) of cohesion and soil–wall adhesion values are taken to quantify the effect of vertical seismic coefficient as well as the effect of cohesion of soil and soil–wall adhesion. The behaviour is very evident that the SF values decrease as the values of k_h increase from 0.0 to 0.3, which can be noticed from Fig. 4a–d. As the ratio of k_v/k_h changes from its negative values to the positive values, the value of SF decreases constantly, except the more change is noticeable when k_v/k_h moves from -1.0 to -0.5 value. From Fig. 4a–d, the consequence of cohesion and adhesion values on the values of SF can be significantly noticed. It can also notice the significant increase in SF when cohesionless soil is replaced with the cohesive soil without considering the wall adhesion.

For c and a_f equal to 0.0, SF decreases by 74.9% ($k_h = 0.2$) and 32.7% ($k_h = 0.3$), when k_v/k_h changes from -1.0 to 1.0 value. The value of SF decreases by 96.8

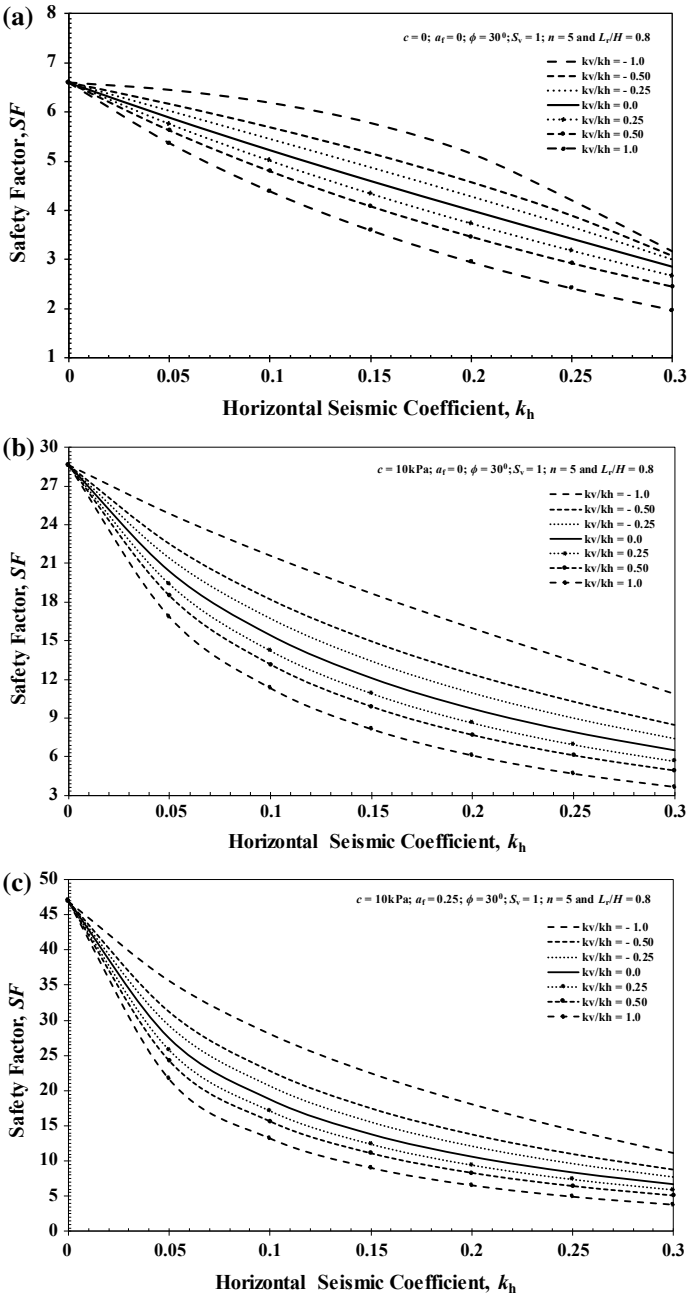

Fig. 4 Safety factor, SF with k_h for different k_v/k_h for **a** $c = 0.0$ and $a_f = 0.0$, **b** $c = 10$ kPa and $a_f = 0.0$, **c** $c = 10$ kPa and $a_f = 0.25$ and **d** $c = 10$ kPa and $a_f = 1.0$

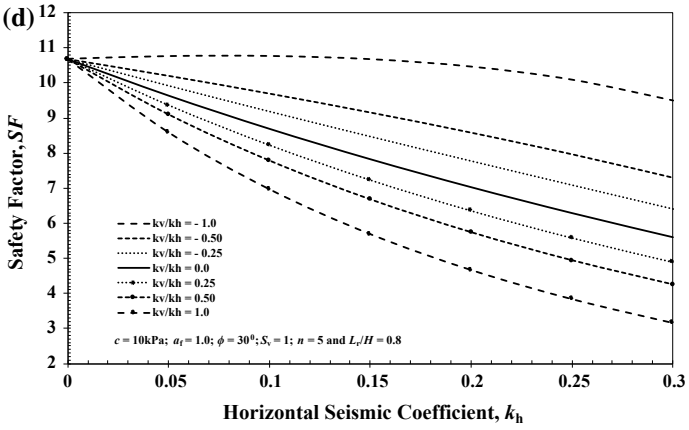

Fig. 4 (continued)

and 49.4%, when k_h value is increased from 0.2 to 0.3 for k_v/k_h equals to −1.0 and 1.0, respectively.

Considering $c = 10$ kPa and $a_f = 0.0$, SF decreases by 163.3 and 200.3% ($k_h =$ 0.2 and 0.3) for k_v/k_h changes from −1.0 to 1.0 value. The value of SF decreases comparatively lower as 46.7 and 67.3% for k_v/k_h equals to −1.0 and 1.0 (for k_h value varies from 0.2 to 0.3).

Taking $c = 10$ kPa and $a_f = 1.0$, SF decreases by 46.7 and 63% (for $k_h = 0.2$ and 0.3; k_v/k_h varies from −1.0 to 1.0). For k_h value varies from 0.2 to 0.3, the value of SF decreases by 23.5 and 47.6% (k_v/k_h equals to −1.0 and 1.0, respectively).

3.3 Validation of the Present Work

K_{max} and critical inclination of the failure angle (α_{cri}) have been compared with [7] as shown in Table 2. The results of K and α_{cri} obtained from the present study show a good agreement.

4 Conclusions

In the available literature, very limited solutions to analyse the reinforced retaining walls under seismic conditions are available considering c-ϕ soil backfills. The present formulation provides a solution in simplest form to analyse the reinforced retaining walls for calculating the required strength of reinforcements and safety factor under seismic loading condition. The main conclusions are as follows:

Table 2 Comparison between results obtained from the present study by Ghanbari and Ahmadabadi [7] for the case of ($k_v = 0$, $k_h = 0.2$, $\delta = 0$, $c = 0$, $\phi = 30°$, $\gamma = 20$ kN/m^3, $T = 0.2$ s, $V_s = 150$ m/s and $V_p = 1.87V_s$)

Time t (s)	0.0	0.02	0.04	0.08	0.10	0.12
K for ($H = 3$ m)						
Present method	0.29	0.36	0.43	0.45	0.38	0.31
Ghanbari and Ahmadabadi [7]	0.29	0.36	0.43	0.45	0.38	0.31
α_{cri} (°) for ($H = 3$ m)						
Present method	63.2	58.2	52.8	51.4	56.3	61.7
Ghanbari and Ahmadabadi [7]	62.5	58.2	54	53	57	61.8

- Required maximum strength of reinforcement K_{max} increases with a significant value increasing in k_h values for higher values of k_v/k_h (for more than 0.5 value).
- Required maximum strength of reinforcement K_{max} increases considerably with increase in k_h. For k_h value greater than 0.15, the effect is more prominent.
- Safety factor decreases very fast for the smaller values of k_h (less than or equal to 0.15) for both, cohesionless and cohesive soil backfill with or without considering the soil–wall adhesion.
- Effect of cohesion value is very significant for the design of reinforced retaining wall, which is clearly noticed in the present work.

References

1. Mononobe N (1924) Effects of vertical acceleration and theory of vibration. J Jpn Soc Civ Eng 10(5):1063–1094
2. Okabe S (1924) General theory on earth pressure and seismic stability of retaining wall dam. J Jpn Soc Civ Eng 10(6):1277–1324
3. Steedman RS, Zeng X (1990) The influence of phase on the calculation of pseudo-static earth pressure on a retaining wall. Geotechnique 40(1):103–112
4. Nimbalkar SS, Choudhury D, Mandal JN (2006) Seismic stability of reinforced soil wall by pseudo-dynamic method. Geosynthetics Int 13(3):111–119
5. Choudhury D, Nimbalkar SS, Mandal JN (2007) External stability of reinforced soil walls under seismic conditions. Geosynthetics Int 14(4):211–218
6. Reddy GVN, Choudhury D, Madhav MR, Reddy SE (2009) Pseudo-dynamic analysis of reinforced soil wall subjected to oblique displacement. Geosynthetics Int 16(2):61–70
7. Ghanbari A, Ahmadabadi M (2010) New analytical procedure for seismic analysis of reinforced retaining wall with cohesive-frictional backfill. Geosynthetics Int 17(6):364–379
8. Tafreshi SNM, Rahimi M (2012) A simplified pseudo-dynamic method of reinforced retaining-wall subjected to seismic loads. In: Proceedings of 15th world conference on earthquake engineering (15WCEE), Lisbon, Portugal, vol 27, 24–28 Sept 2012

Effect of Slope Angle and Edge Distance on Laterally Loaded Flexible Pile Embedded in Sandy Ground

Bhishm Singh Khati and Vishwas A. Sawant

Abstract There are many circumstances in which piles have to be provided on slopes. The present study involves laboratory model tests to explore single pile response for varies gradients of soil slopes. The experimental study was carried out on level ground and two different slopes ($1V$:$1.5H$) and ($1V$:$2H$). A relative density of 25% was achieved after pile installation. Pile length-to-diameter ratio is 30. The study examines the effect of edge distance, s, from the crest of slope on lateral pile capacity by varying (s/D = 0.0, 6.0 and 12.0). For different edge distance to pile diameter ratio (s/D) values, lateral pile capacity, maximum bending moment and lateral displacement are determined. It is established that lateral load capacity reduced significantly changing ground surface profile from horizontal to slope. Significant increase in lateral load capacity was observed with increase in pile distance from crest of slope. The maximum bending moments increase significantly with a decrease in distance of pile from the slope crest, when compared with horizontal ground.

Keywords Aluminium pile · Lateral load · Sloping ground · Edge distance · Lateral pile capacity

1 Introduction

When shallow foundations lead to unsatisfactorily low value of the factor of safety against shear failure or excessive settlement, pile foundations are the best replacement of shallow foundation. Piles are often subjected to axial loads, lateral loads and

B. S. Khati (✉) · V. A. Sawant
Department of Civil Engineering, IIT Roorkee, Roorkee, UK, India
e-mail: bhishmkhati007@gmail.com

V. A. Sawant
e-mail: sawntfce@iitr.ac.in

S. Kumar Shukla et al. (eds.), *Advances in Sustainable Construction Materials and Geotechnical Engineering*, Lecture Notes in Civil Engineering 35,
https://doi.org/10.1007/978-981-13-7480-7_17

moments. Further, there are many circumstances in which piles have to be provided near slopes. This in turn adversely reduces the lateral load capacity offered by the soil because of the reduction in confining pressure coming from surrounding soil. The capacity of pile foundation placed in the direction of slope reduces drastically in comparison to pile foundations that are laid on horizontal ground surface. Depending upon structure types and type of supporting piles, different causes are there to produce the lateral forces. The major causes of the development of the lateral forces are wind gusts, water current, waves and earthquake. During earthquakes, the shaking of the level ground develops the horizontal forces that the piles have to endure. Vehicle and wind movement are the major causes of the horizontal force generation in the bridge abutments and piers. Water pressure transfers the horizontal forces on the supporting piles in the dam structure. In all these cases, the reason for major failure is the development of the lateral forces, those acts in the supporting structures. Piles are mostly used to resist the pressure exerted by the soil mass behind retaining wall system, which is one of the major causes in the case of earth retaining structures. To support open excavations, no axial force is resisted by the piles. In that case, only role of the piles is to resist lateral forces. So in many circumstances, the external horizontal loads act at the pile top.

Mezazigh and Levacher [1] investigated the effect of edge distance in the sloping ground. The reported edge distances were $8B$ (B is diameter of pile) (for slope $1H{:}2V$) and $12B$ (for slope $1H{:}1.5V$). For the different sloping ground with different relative density, Muthukkumaran et al. [2, 3] had reported the effect of surcharge load on pile. With the obtained results for the different sloping ground condition, p–y curves were also developed. Muthukkumaran and Begum [4] extended the experimental study to report the effect of embedment length of pile along with the development of p–y curves.

Buildings in many hill regions may be supported on pile foundations considering stability of slope into consideration. The piles near slopes are subjected to lateral loads from superstructure and unbalanced earth pressure which are more predominant than vertical loads. Limited experimental studies have been carried out to analyse the behaviour of pile subjected to the horizontal load near slopes. Very few studies have considered the effect of pile distance from slope crest and slope gradient on lateral pile load capacity. In the present study, experimental model tests have been conducted in laboratory to investigate pile response for various gradients of soil slopes. Initial experiments were carried out on levelled ground condition. Then to determine the effect of sloping ground, two different slopes are used. In this parametric study, the effect of edge distance on pile response to lateral load was examined. A comparison was made with pile response in levelled ground condition to highlight the effect of ground slope.

Table 1 **a** Physical properties of soil. **b** Pile performance according to Matlock and Reese [5]

(a)

Parameters	Values
Specific gravity (G_s)	2.60
Percentage of fine sand	96.7%
IS classification	SP
Effective diameter, D_{10} (mm)	0.11
Uniformity coefficient, C_u	2.73
Curvature coefficient, C_c	1.60
Minimum density, ρ_{min} (g/cm^3)	1.40
Maximum density, ρ_{max} (g/cm^3)	1.59
Maximum void ratio, e_{max}	0.86
Minimum void ratio, e_{min}	0.64
Loose sand	$\rho = 1.44$ g/cc, $D_r = 25\%$, $\phi = 34.5°$

(b)

D_r (%)	η_h (Soil) MN/m^3	T (mm)	L/T	Remarks
25	2.5	165.46	4.53	Long pile

2 Experimental Procedure

Proposed work is aimed to be carried in a concrete tank of dimensions 2.5 m × 1.22 m × 1.12 m. The experimental set-up, i.e. the cable and pulley arrangement to provide lateral load on the embedded piles, is shown in Fig. 1a. Apparatus of the test includes a loading frame connected by a pulley, LVDT, strain gauges, data acquisition system and computer which are shown in Fig. 1b. The schematic diagram of the model test pile along with the position of strain gauges is shown in Fig. 1c. The test is conducted on river sand in dry condition. Physical properties of dry sand are shown in Table 1a. The values of coefficient of horizontal subgrade reaction η_h, characteristic length of pile T and L/T ratio are reported in Table 1b. It is to be noted that the length of model pile L is equal or greater than $4T$, referring to as long flexible pile [5].

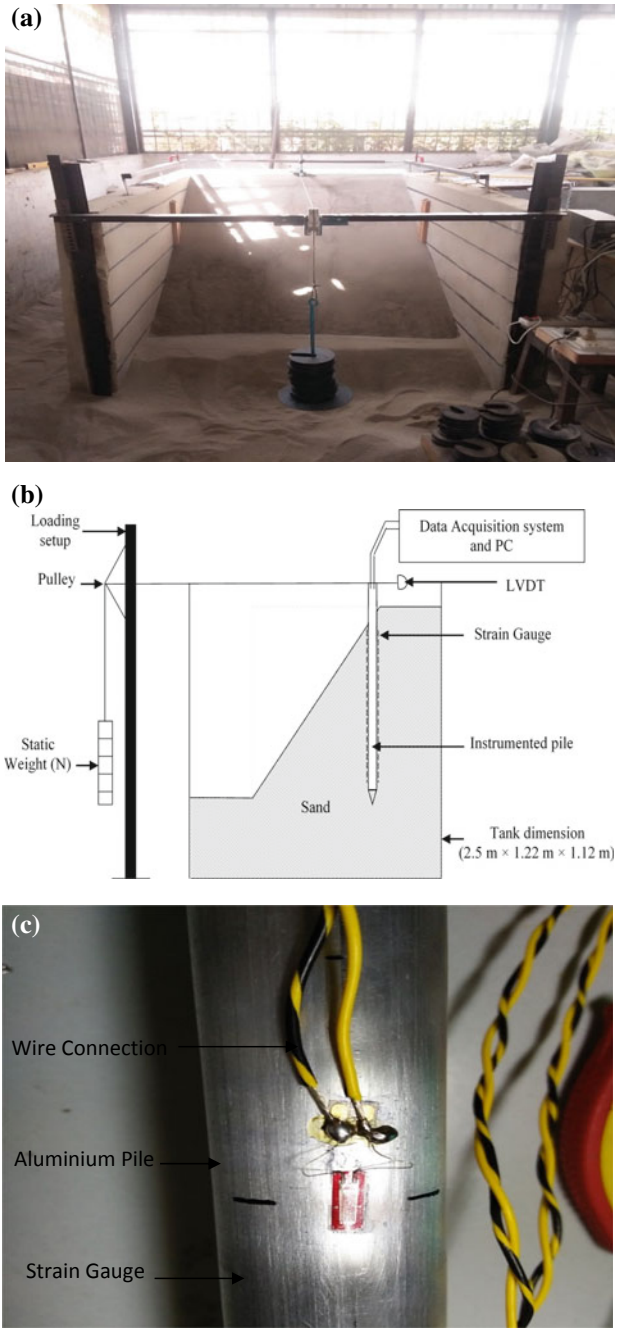

Fig. 1 **a** Concrete tank used for experiments in laboratory. **b** Actual laboratory set-up for sloping ground. **c** Pile instrumentation by strain gauges and wires

3 Results and Discussion

Pile is instrumented with electric resistance strain gauges for measurement of moment along the pile. With the increase of lateral load, strain value increases. For a particular load, the maximum value of micro-strain is obtained at the strain gauge located at a depth of $3L/8$ or $4L/8$ as shown in Fig. 2.

At the ground level, the value of applied lateral load and the respective displacement has been noted for each load increment. Figure 3a, b displays the typical horizontal load–displacement curves for various s/D ratios for both the slopes. Figure 3a, b shows clearly the effect of variation in ground condition from level to sloping ground and edge distance on pile lateral load capacity. The corresponding lateral pile capacity expressively reduced. The reduction of pile load capacity is due to the decrease in passive resistance of the soil in front of the pile. This results in the maximum displacement in the pile. However, the displacement is significantly reduced and the lateral pile capacity (LPC) is observed to increase with the increase of edge distance from the crest of slope. With a shift in pile from crest, passive resistance increase with edge distance. Pile tests have been carried out for $1V$:$1.5H$ slope ($D_r = 25\%$). On exceeding the lateral displacement of the pile 5 mm, the slope ($1V$:$1.5H$) crest has started to yield. Usually, the displacement-based criterion is adopted to estimate the ultimate load from load–displacement response observed in the pile load test. The permissible value can be fixed based on the tolerance level of the pile-supported structure. In the absence of specific criterion, the crucial load is taken at the capacity reported for the displacement of 20% of the pile dia, which is 5 mm in the present study [6].

Table 2 summarizes variation in lateral pile capacity ratio with edge distance respect to level ground. For level ground, ultimate lateral pile capacity is 56.14 N.

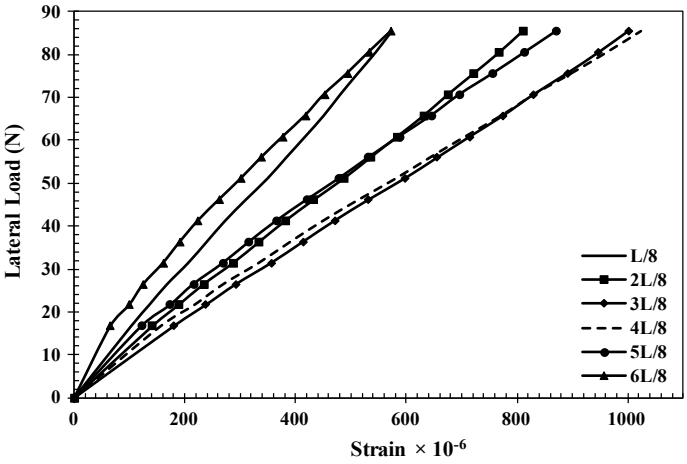

Fig. 2 Strain variation at different depth for slope $1V$:$1.5H$ and $s/D = 0$

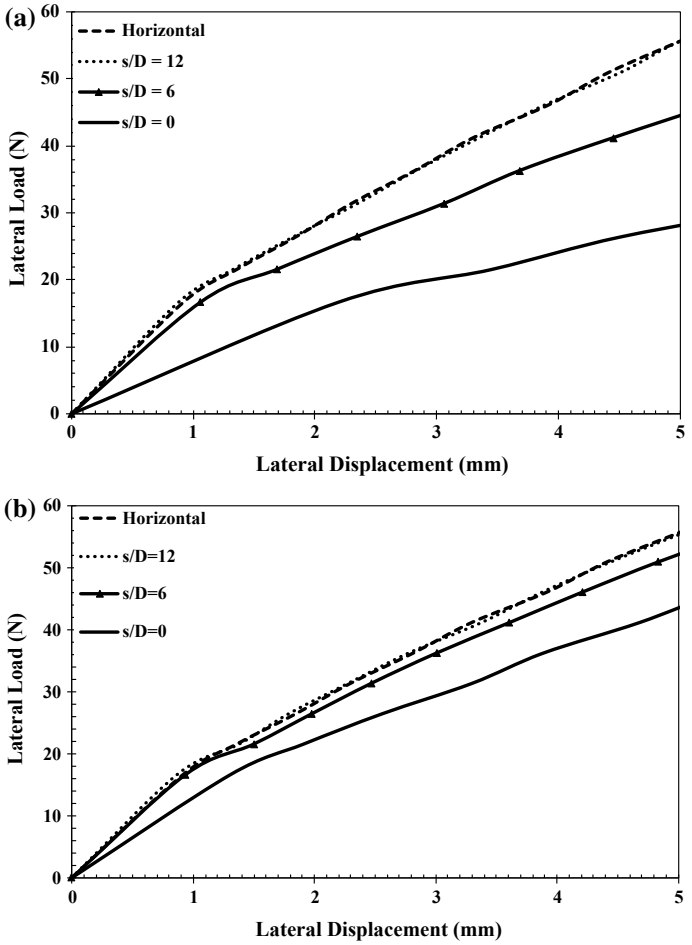

Fig. 3 **a** Effect of edge distance for slope 1*V*:1.5*H*. **b** Effect of edge distance for slope 1*V*:2*H*

Table 2 Variation in lateral pile capacity ratios

Slope	LPC in level ground (N)	LPC ratio with edge distance (*s*/*D*)		
		0	6	12
1*V*:1.5*H*	56.14	0.49	0.78	0.97
1*V*:2*H*		0.78	0.94	0.99

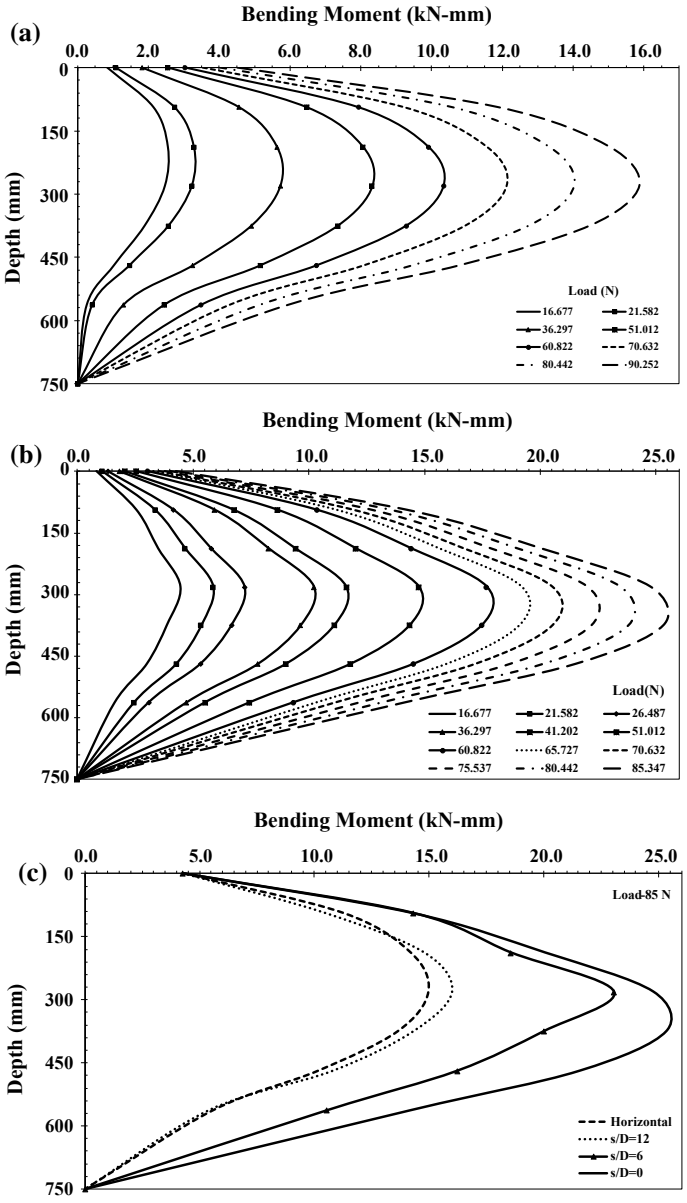

Fig. 4 **a** Bending moment versus depth for horizontal ground. **b** Variation in $BM_{\max}$ along the depth of pile for slope $1V{:}1.5H$ ($s/D = 0$). **c** $BM_{\max}$ versus depth for slope $1V{:}1.5H$. **d** $BM_{\max}$ versus depth for slope $1V{:}2H$. **e** $BM_{\max}$ versus depth for different slope and $s/D = 0$

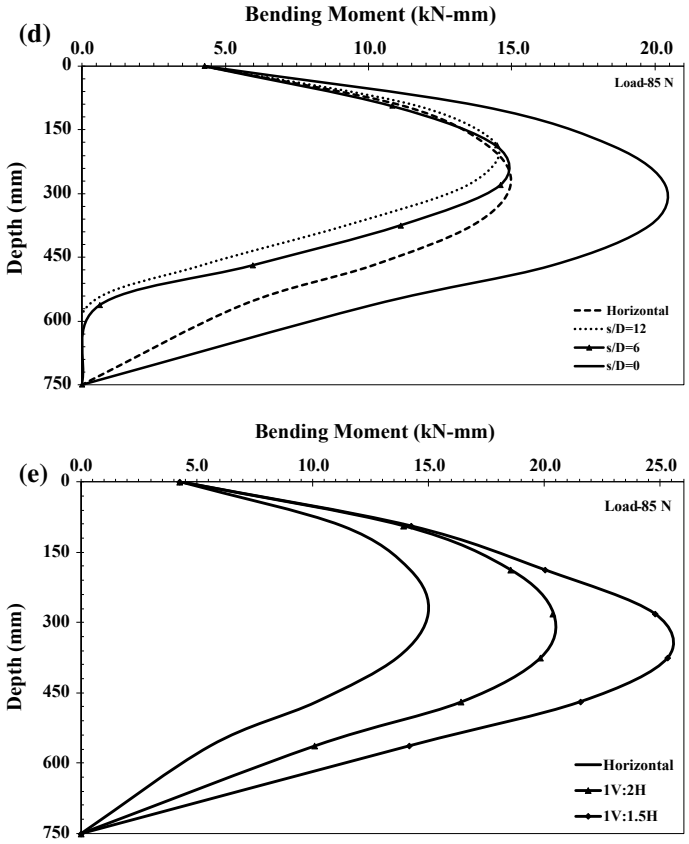

Fig. 4 (continued)

Lateral pile capacity ratio about 0.49 is observed for the slope 1*V*:1.5*H,* and location of pile is at crest of slope. This value is increased with an increase of edge distance. For $s/D = 12$, lateral pile capacity ratio is 0.97. For the same edge distance, the lateral pile capacity ratio is increased from 0.78 to 0.99 for the slope 1*V*:2*H*. As piles are moving away from crest, pile top displacement is decreasing at the same applied lateral load. It can be seen that for slope 1*V*:2*H*, load–displacement curve for the case of edge distance $s/D = 12$ is very close to horizontal response.

At the different locations of the strain gauges with the help of data logger, the bending moment values can be obtained by the strain measurement. The moment distribution along the pile shafts is shown against depth of pile. Shape of the bending moment distribution was noticed almost same value in all the cases. It is also noticed from Fig. 4a that $BM_{\max}$ increases with increase in the applied lateral load. The variation of $BM_{\max}$ magnitude for sloping (1*V*:1.5*H* and $s/D = 0$) ground surface is shown in Fig. 4b. The $BM_{\max}$ also decreases substantially with an increase in

the distance of pile from crest of slope as observed in Fig. 4c, d. It is clear that BM_{max} location moves downward as the pile moves towards crest of slope. Effect of ground slope on bending moments is compared in Fig. 4e with moments in level ground. From the discussed variations, BM_{max} of the pile as well as the depth of their occurrence (depth of fixity) noticed the considerable rise on increase in the ground slope. This happens generally due to the decrease of passive mass in the slopes, which results in the transfer of lateral load up to a deeper depth.

4 Conclusions

Present laboratory-based experimental study demonstrates the performance of a single pile mounted at a certain distance away from slope crest which is subjected to the horizontal load. The influence of sloping ground and edge distances on the lateral pile capacity, lateral displacement and BM_{max} along the pile is also reported in the present study. From the results obtained from the model pile laboratory tests, the following conclusions are drawn:

- When the distance of pile from slope crest increases, lateral displacement noticeably reduces, whereas pile load capacity increases.
- On changing ground condition from horizontal to sloped, the LPC reduces considerably. For the same changes in ground, i.e. from horizontal to sloped at the position of slope crest (s/D), the lateral pile capacity ratio reduces from 0.78 (for $1V$:$2H$) and 0.49 (for $1V$:$1.5H$). From the study, it has been observed that the slope effect is insignificant when the pile placed after $12D$ distance from the crest of slope.
- BM_{max} increases greatly with a decrease in distance of pile from the slope crest when compared with the horizontal ground.
- BM_{max} also increases significantly with increase in ground slope when compared with the horizontal ground. For pile at crest position increase is in the order of 36.11% and 69.18% (for slopes $1V$:$2H$ and $1V$:$1.5H$ individually).

References

1. Mezazigh S, Levacher D (1998) Laterally loaded piles in sand: slope effect on *p-y* reaction curves. Can Geotech J 35(3):433–441
2. Muthukkumaran K, Sundaravadivelu R, Gandhi SR (2004) Effect of sloping ground on single pile load deflection behaviour under lateral soil movement. In: Proceedings of the 13th world conference on earthquake engineering, Vancouver, BC, Canada, 1–6 Aug 2004
3. Muthukkumaran K, Sundaravadivelu R, Gandhi SR (2008) Effect of slope on *p-y* curves due to surcharge load. Soils Found Jpn Geotech Soc 48(3):353–361
4. Muthukumaran K, Begum NA (2015) Experimental investigation of single model pile subjected to lateral load in sloping ground. Geotech Geol Eng 33(4):935–946

5. Matlock H, Reese LC (1960) Generalized solutions for laterally loaded piles. Geotech Spec Publ ASCE 127(118):1220–1248
6. Narasimha SR, Ramakrishna VGST, Babu MR (1998) Influence of rigidity on laterally loaded pile groups in marine clay. J Geotech Geoenviron Eng ASCE 124(6):542–549

The Development of a New Low Carbon Binder for Construction as an Alternative to Cement

Ali Abdulhussein Shubbar, Monower Sadique, Hayder Kamil Shanbara and Khalid Hashim

Abstract The demand on cement in the construction industry has increased significantly due to the growth of industrial sectors. However, as the cement industry contributes to the emissions of 6–8% of CO_2 into the atmosphere, it becomes essential to develop alternative materials to reduce the usage of cement. This research aims at developing a new low carbon binder completely from waste materials to be used in construction industry. The performance of four different alkali-activated binary blended mortars made from ground-granulated blast-furnace slag (GGBS) and high-calcium fly ash (HCFA) was assessed using compressive strength test. The results indicated that the mixture made from (60% GGBS: 40% HCFA) and activated by sodium hydroxide (NaOH) with concentration of 4M and sodium silicate (Na_2SiO_3) solutions together with a Na_2SiO_3/NaOH ratio of 2 showed a comparable behaviour to the cement with a compressive strength of 39.8 MPa after 28 days of air curing. The findings in this study announced on the development of promising binder that can be used in different construction sectors as an alternative to cement and help in reducing the negative environmental impacts of cement industry.

Keywords Alkali-activated · Compressive strength · Ground-granulated blast-furnace slag · High-calcium fly ash · Low carbon binder

1 Introduction

Cement is the second most used material after water around the world as it can be used for all of the construction industry such as buildings, bridges, roads. The production of cement is responsible for almost 6–8% of all the CO_2 emissions worldwide [1]. This is because the production of one tonne of cement is associated with about one-tonne CO_2 emissions into the atmosphere, consumes around 5.6 GJ of energy and requires approximately 1.5 tonnes of raw materials [2]. The world cement production

A. A. Shubbar (✉) · M. Sadique · H. K. Shanbara · K. Hashim
Department of Civil Engineering, Liverpool John Moores University, Liverpool L3 2ET, UK
e-mail: alishubbar993@gmail.com; A.A.Shubbar@2014.ljmu.ac.uk

S. Kumar Shukla et al. (eds.), *Advances in Sustainable Construction Materials and Geotechnical Engineering*, Lecture Notes in Civil Engineering 35,
https://doi.org/10.1007/978-981-13-7480-7_18

in 2015 was approximately 4.6 billion tonnes, and this number is expected to increase and reach around 9 billion by 2050 as the world population is estimated to increase from 6 to 9 billion [3, 4].

The UK government have set strict legislations with the aim of moving the UK towards a low carbon economy and create a sustainable construction industry [5]. Therefore, looking for alternative materials, such as by-products and/or waste materials, to be used as cement replacement in construction industry might be an essential attempt as a sustainable solution towards reducing cement production and achieving an eco-friendly industry.

Extensive research has been carried out to fully or partially replace cement by inventing new supplementary cementitious materials (SCMs). The use of such materials can improve the characteristics of the generated products and comply with the strict environmental regulations.

Ground-granulated blast-furnace slag (GGBS) is a by-product material from manufacturing of steel which is one of the known viable alternatives materials to cement in different applications [6]. The employment of GGBS in different applications as an alternative to cement could help in reducing the cost of construction materials, solve landfill problems and address many of the environmental problems associated with cement production and slag despoiling [7, 8].

However, due to the expected reduction in iron consumption by industries, it is expected that there will be a reduction in the availability of GGBS in sufficient quantities to be used in the construction industry [9]. Therefore, there is a need for other cheap waste materials that could be used to replace the cement in addition to GGBS. High-calcium fly ash (HCFA), a waste material that is produced from the burning process in local power plants, could be used as this additional waste material.

HCFA is classified as class C fly ash. It has pozzolanic properties along with some self-cementing properties attributed to a high proportion of free lime [10, 11]. Therefore, HCFA is a promising material that could partially, or fully, replace the cement in different applications. Sadique et al. [11] have shown that mortar made by mixing 60% HCFA with 20% an alkali sulphate rich fly ash and 20% silica fume has better compressive strength than cement after 28 days of curing. Jafer et al. [10] found that HCFA could be used alone as a cement replacement in the stabilization of soft soil providing better results than cement. In addition, Dulaimi et al. [12] evidenced the efficacy of using HCFA as a filler in road construction.

This paper presents the results of the laboratory work to study the effect of combining GGBS and HCFA to produce a novel low carbon binder to be used in the construction industry as an alternative to cement.

2 Materials and Methodology

2.1 Materials

2.1.1 Sand

The sand used in this research was 100% building sand passed through a 3.35-mm IS sieve.

2.1.2 Cement

Ordinary Portland Cement (OPC)-type CEM-II/A/LL 32.5-N was used in this study. CEMEX Quality Department, Warwickshire, UK, has supplied the cement for this study.

2.1.3 Ground-Granulated Blast-Furnace Slag (GGBS)

The GGBS was provided by the Hanson Heidelberg Cement Group, Scunthorpe, UK.

2.1.4 High-Calcium Fly Ash (HCFA)

HCFA is a waste material generated by power generation plants through combustion between 850 and 1100 °C, using a fluidised bed combustion system.

2.1.5 Alkali Activators

Liquid sodium hydroxide (NaOH) was used with a concentration of 4M along with sodium silicate solution (Na_2SiO_3) as the alkali activators in this research. Both alkali activators were supplied by Fisher scientific.

2.2 Material's Characterization

The following techniques were employed to characterize, analyse and evaluate the raw materials.

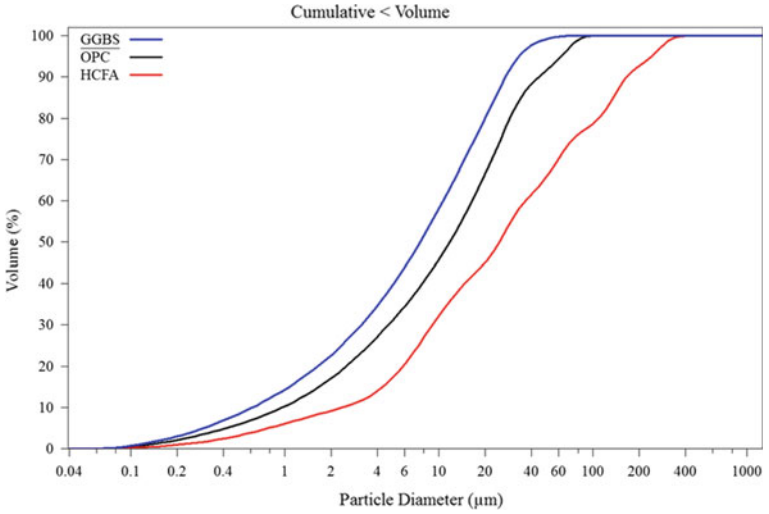

Fig. 1 Cumulative particle-size distribution of OPC, GGBS and HCFA

2.2.1 Particle-Size Distribution (PSD)

The PSD of raw materials were measured using a Beckman Coulter laser particle size analyser. Figure 1 shows the PSD curves for the OPC, GGBS and HCFA as obtained from the laser particle size analyser.

Figure 1 shows that GGBS has finer particles relative to the other materials. This means that the GGBS has higher pozzolanic reactivity [13]. In contrast, HCFA has larger particles relative to GGBS, which could retard the performance of the mortars during hydration reactivity [10].

2.2.2 Energy-Dispersive X-ray Fluorescence (EDXRF) Spectrometer

The chemical compositions of OPC, GGBS and HCFA were analysed by an energy-dispersive X-ray florescence spectrometer (EDXRF)-type Shimadzu EDX-720. Table 1 shows the chemical composition of OPC, GGBS and HCFA.

2.2.3 Scanning Electron Microscopy (SEM) Testing

The SEM tests were conducted on each raw material to identify the general shape of particles, thus helping to explain the performance of these materials during mixing. The SEM images for the raw materials shown in Fig. 2 show that both OPC and GGBS particles have an irregular shape and that OPC particles are coarser than

Table 1 Chemical composition of OPC, GGBS and HCFA

Item (%)	OPC	GGBS	HCFA
CaO	65.21	42.51	66.67
SiO_2	24.56	41.06	25.12
Al_2O_3	1.70	5.12	2.38
Fe_2O_3	1.64	–	0.03
MgO	1.30	4.25	2.57
Na_2O	1.34	3.09	1.72
K_2O	0.82	0.69	0.31
SO_3	2.62	1.27	0.26
TiO_2	–	0.98	0.41

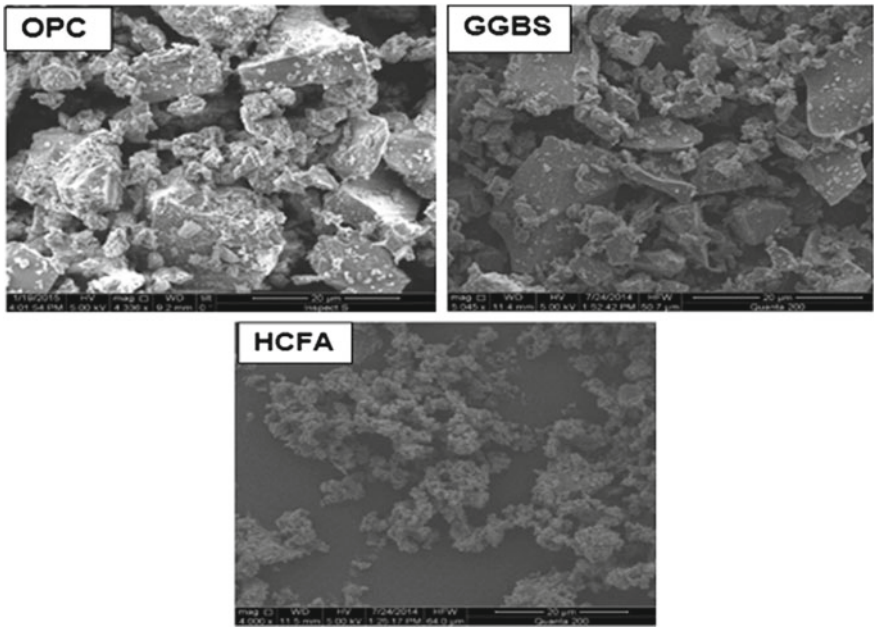

Fig. 2 SEM images of the raw materials

those of GGBS, this agreeing with the results of the PSD tests. HCFA can be deemed as coagulated particles with a high number of voids.

Table 2 Mixing proportions of raw materials

Mix ID	OPC (%)	GGBS (%)	HCFA (%)
R	100	0	0
M1	0	90	10
M2	0	80	20
M3	0	70	30
M4	0	60	40

2.3 Mixing Proportions and Testing Programme

2.3.1 Mixing Proportions

In this research, four mixtures with a different combination of GGBS and HCFA were casted to produce binary blended alkali-activated binder along with a mixture made with 100% OPC to be used as a reference for comparison purposes. Table 2 shows the mixing proportions of all the mixtures tested in this research. The binder-to-sand ratio for all mixtures was fixed as 1:2, while the activator-to-binder (A/B) ratios of the mixtures were adjusted in order to achieve a good workability for each mixture [14]. The alkali activator was made by mixing sodium silicate and sodium hydroxide solutions together with a Na_2SiO_3/NaOH weight ratio of 2.

2.3.2 Testing Programme

Compression testing was conducted in accordance with BS EN 196-1 [15]. Samples of each mixture were tested at two different curing periods: 7 and 28 days. The average compressive strength value of four mortar specimens was prepared for each mix proportions, and curing ages were taken to represent the final values for compressive strength. The mixture made with 100% OPC was tested for comparison purposes. The curing regime followed for the specimens made from GGBS and HCFA was air curing at temperature of 20 ± 2 °C; however, the reference mixtures were cured by placing them in water tank at 20 ± 2 °C.

3 Results and Discussion

The results of the compressive strength tests of all the mortars blended by mixing GGBS and HCFA along with the reference mixture made with 100% OPC at different ages of curing are shown in Fig. 3.

Figure 3 shows that the compressive strength values increased by increasing the curing period for all curing conditions. Figure 3 also shows that for the alkali-activated mortars, the compressive strength was decreased with increasing the HCFA content.

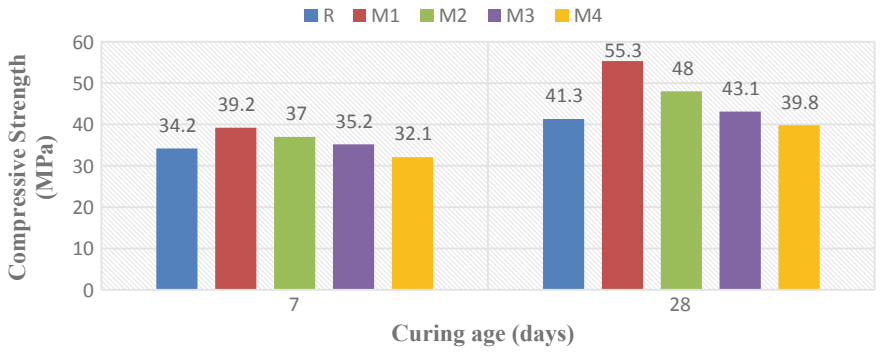

Fig. 3 Compressive strength results of mortars made from different blends

This can be attributed to the increased activator-to-binder ratio that was required to improve workability; increasing the percentage of HCFA increases the activator demand in the mixes.

The 7 days' compressive strength results indicated that the alkali activation of the binary mixtures made from different blends of GGBS and HCFA was higher than that for the reference mixture except the mixture with 40% HCFA that provided about 94% of the control mixture compressive strength.

At the age of 28 days, the results showed that the blends M1, M2 and M3 provided superior compressive strength than the reference mixture by 34, 16 and 4%. However, the mixture M4 has provided about 96% of the reference compressive strength. These results are well in agreement with the results obtained by Shubbar et al. [16].

In this study, the mixture M4 with 60% GGBS and 40% HCFA was chosen as the newly developed low carbon binder that can be used in the construction industry as an alternative to cement. It had comparable compressive strength to that of the control mixture, R, at the same time fully replaced the cement. Such a replacement can contribute significantly to reduce the CO_2 emissions of cement industry and contributes to the management of wastes by consuming two industrial wastes to produce an eco-friendly binder.

4 Conclusion

The aim of this research was to develop a new low carbon binder by fully replacing the cement with GGBS and HCFA. According to the results of laboratory work, the following conclusions have been drawn:

- Increasing the level of HCFA in the alkali-activated mortars led to increase the activator demand of the mixtures.
- The results indicated that with increasing the curing time, the compressive strength values increased for all curing conditions.

- At all curing ages, increasing the content of HCFA in the mixtures reduced the compressive strength of mortars.
- At all curing ages, the mixtures incorporating up to 30% HCFA have provided better performance than the reference mixture made from 100% cement.
- The mixture with 60% GGBS and 40% HCFA has provided 94 and 96% of the compressive strength of the control mixture after 7 days and 28 days of air curing, respectively.
- The mixture M4 (60% GGBS: 40% HCFA) was chosen as the newly developed low carbon binder that can be used in construction as a viable alternative to cement.

Acknowledgements The first author would like to acknowledge the financial support provided for this research by the Faculty of Engineering and Technology at Liverpool John Moores University (LJMU). The authors also would like to acknowledge the Hanson Heidelberg Cement Group for the free cost of supply of GGBS for this research.

References

1. Hawileh RA, Abdalla JA, Fardmanesh F, Shahsana P, Khalili A (2017) Performance of reinforced concrete beams cast with different percentages of GGBS replacement to cement. Arch Civ Mech Eng 17(3):511–519
2. O'Rourke B, McNally C, Richardson MG (2009) Development of calcium sulfate–ggbs–Portland cement binders. Constr Build Mater 23(1):340–346
3. Evi Aprianti S (2017) A huge number of artificial waste material can be supplementary cementitious material (SCM) for concrete production—a review part II. J Cleaner Prod 142:4178–4194
4. Department of Energy & Climate Change (2013) UK greenhouse gas emissions, final figures, in statistical release. 2015 National Statistics
5. MPA Cement (2013) The UK cement industry aims to reduce greenhouse gases by 81% by 2050. London
6. Grist ER, Paine KA, Heath A, Norman J, Pinder H (2015) The environmental credentials of hydraulic lime-pozzolan concretes. J Clean Prod 93:26–37
7. Aprianti E, Shafigh P, Bahri S, Farahani JN (2015) Supplementary cementitious materials origin from agricultural wastes—a review. Constr Build Mater 74:176–187
8. Karim MR, Zain MFM, Jamil M, Lai FC (2013) Fabrication of a non-cement binder using slag, palm oil fuel ash and rice husk ash with sodium hydroxide. Constr Build Mater 49:894–902
9. Heath A, Paine K, Goodhew S, Ramage M, Lawrence M (2013) The potential for using geopolymer concrete in the UK. Proc Inst Civ Eng Constr Mater 166(4):195–203
10. Jafer HM, Atherton W, Sadique M, Ruddock F, Loffill E (2018) Development of a new ternary blended cementitious binder produced from waste materials for use in soft soil stabilisation. J Clean Prod 172:516–528
11. Sadique M, Al-Nageim H, Atherton W, Seton L, Dempster N (2013) Mechano-chemical activation of high-Ca fly ash by cement free blending and gypsum aided grinding. Constr Build Mater 43:480–489
12. Dulaimi, A, Al Nageim H, Ruddock F, Seton L (2017) High performance cold asphalt concrete mixture for binder course using alkali-activated binary blended cementitious filler. Constr Build Mater 141:160–170
13. Zhao J, Wang D, Yan P, Zhao S, Zhang D (2016) Particle characteristics and hydration activity of ground granulated blast furnace slag powder containing industrial crude glycerol-based grinding aids. Constr Build Mater 104:134–141

14. Tangchirapat W, Jaturapitakkul C (2010) Strength, drying shrinkage, and water permeability of concrete incorporating ground palm oil fuel ash. Cement Concr Compos 32(10):767–774
15. BSI, Methods of testing cement–Part 1: Determination of strength. 2005, British Standard Institute, London
16. Shubbar A, Jafer HM, Dulaimi A, Atherton W, Al-Rifaie A (2017) The development of a low carbon cementitious material produced from cement, ground granulated blast furnace slag and high calcium fly ash. Int J Civ Environ Struct Constr Architect Eng 11(7):905–908

Developing a Premium Cementitious Filler Incorporating High Content of Sewage Sludge Fly Ash

Manar Herez, Hassan Al-Nageim, Clare Harris and Linda Seton

Abstract Cold bituminous emulsion mixture (CBEM) is a sustainable replacement to the conventional hot mix asphalt (HMA) due to environmental and safety issues associated with the use of the latter. However, CBEM experiences some drawbacks including long-term curing, low strength in the early days and high air voids content; thus, it needs from 2 to 24 months to reach its ultimate strength. Accordingly, the applications for CBEMs have been limited to low- /medium-trafficked roads, footways and reinstatements. This study aimed at developing a new cementitious material incorporating a high volume of sewage sludge fly ash (SSFA) with low ordinary portland cement (OPC) content and carbide lime waste (CLW), to replace the traditional limestone filler in CBEM. A significant improvement has been shown in the performance of the developed CBEM in terms of indirect tensile stiffness modulus (ITSM) and microstructure analysis compared to the conventional CBEM incorporating limestone filler. Furthermore, the developed mixture has being comparable to the mixtures including OPC and the conventional HMA. A considerable alteration in the microstructure components over the curing ages has been developed, which is confirmed by the creation of cementitious hydration products using scanning electron microscopy.

M. Herez (✉) · H. Al-Nageim · C. Harris
Department of Civil Engineering, Liverpool John Moores University, Byrom Street, Liverpool L3 3AF, UK
e-mail: M.H.Herez@2016.ljmu.ac.uk

H. Al-Nageim
e-mail: H.K.Alnageim@ljmu.ac.uk

C. Harris
e-mail: C.B.Harris@ljmu.ac.uk

M. Herez
Department of Civil Engineering, Kufa University, Kufa, Iraq

L. Seton
School of Pharmacy and Biomolecular Science, Liverpool John Moores University, Liverpool, UK
e-mail: L.Seton@ljmu.ac.uk

S. Kumar Shukla et al. (eds.), *Advances in Sustainable Construction Materials and Geotechnical Engineering*, Lecture Notes in Civil Engineering 35,
https://doi.org/10.1007/978-981-13-7480-7_19

Keywords Cold mix asphalt · Waste sewage sludge fly ash · Stiffness modulus · Scanning electron microscopy

1 Introduction

Cold bituminous emulsion mixture (CBEM) is considered to be a sustainable alternative to the conventional hot mix asphalt (HMA); because, there is no need for heating materials [1]. Although CBEM has many economic and ecological impacts, it is classified as a second class to the conventional HMA and the usage of the bitumen emulsion in the UK is generally restricted to surface treatment and reinstatement work on footways as well as low-trafficked highways [2]. This restriction using CBEM as a structural layer in the UK attributes to insufficient strength during the early life, long curing time due to the presence of water, and sensitivity to rainfall which handicaps the curing process.

Due to the shortfalls associated the performance of CBEM, many attempts have been implemented to upgrade its mechanical performance and make it comparable to the HMA. Incorporating traditional cement is the most commonly used technique to develop the performance of CBEM, which is resulting in producing sufficient strength in a short time period [3]. Oruc et al. [4] have been examined the performance of the asphalt emulsion mixture containing ordinary portland cement (OPC) in the range of 0–6%. Their finding demonstrated that with high addition of OPC, the properties of the mixtures have been improved significantly. Their conclusion was the addition of OPC leads to increase the modulus significantly and reduce susceptibility to temperature changes. Accordingly, they recommended to use the cement-treated asphalt emulsion mixtures as a structural pavement layer.

However, the cement industry has large environmental impact and consumed intensive energy. For instance, 5.6 GJ/ton energy and one and a half tons of raw materials required to produce 1 ton of cement. The cement production process in emissions about 0.9 tons of CO_2 which representing 5% of total anthropogenic CO_2 emissions [5].

With this in mind, several studies have been carried out to develop secondary cementitious materials (SCMs) from waste and by-product materials to work as replacements to the conventional limestone filler in the CBEM. The substitution of limestone filler in the CBEMs by fly ash and OPC has been studied by Al Nageim et al. [6]. A considerable enhancement in the mechanical performance has been achieved by the developed mixture compared to the conventional CBEM-incorporated limestone filler and CBEM-incorporated OPC. The water sensitivity and characteristics of cold rolled asphalt with filler comprising of cement and waste bottom ash (WBA) have been studied by Al-Hdabi et al. [7]. Their conclusion was that using WBA as an additive improves the mechanical characteristics in terms of strength, water sensitivity, and uniaxial deformation test. Furthermore, fluid catalytic cracking catalyst residue has been used as an activator to the fly ash to generate a new cementitious filler

in CBEMs [8]. Using waste and by-product materials in CBEM contribute to sustainable development by decreasing the need for waste disposal and save raw materials.

Sewage treatment plants around the world are producing huge quantities of sewage sludge every day. According to that and in order to reuse sewage sludge in a beneficial and economic way, many technologies have been developed which resulting in control of the environmental impact caused by sewage sludge disposal. Several studies have been investigated the usage of the incinerated residues of sewage sludge, i.e. sewage sludge fly ash (SSFA) in different construction applications. Such applications include the use of SSFA in manufacturing lightweight aggregates [9], in producing bricks and tiles [10], and in cement applications [11].

The usage of SSFA as an alternative to the cement or sand resulted in reducing the compressive strength of mortars and concrete [12]. It is agreed that the strength degradation of mortar does not affect when using a little amount of SSFA. Monzó et al. [13] stated that the strength of mortars cured in water bath at temperature 40 °C does not reduce when replaced cement by SSFA up to 30%. This could be referred to as the low pozzolanic action of SSFA compared to some common pozzolans. Thus, SSFA has not been fully accepted as a mineral additive to cement or concrete [14]. The literature roughly recommended to use SSFA as a cement component in the amount of up to 10% of the cement added to concrete [11].

Therefore, this study is the first one aimed at developing a new secondary cementitious material (SCM) incorporating high volume of SSFA, up to 70%, with low cement content and activated by carbide lime waste (CLW). Accordingly, a premium performance CBEM was developed using the developed cementitious filler instead of the traditional filler (limestone), which could remove the restrictions of the road engineers.

2 Materials

2.1 Mineral Aggregate

Carnsew Quarry located at Penryn, UK, supplied the author with coarse and fine-crushed granite aggregate. Table 1 presents the physical properties for coarse and fine aggregate along with the conventional limestone filler. Based on the standard BS EN 13108-1 [15], AC 10-mm gradation surface course was selected for this study. The aggregate gradation has shown in Fig. 1.

2.2 Bitumen Emulsion and Asphalt

In this study, the bitumen emulsion used for preparing the conventional and the developed CBEMs was slow-setting cationic (C50B4) containing 50% residual bitumen supplied by Jobling Purser, Newcastle, UK. This type of emulsion is

Table 1 Granite aggregate characteristics

Item	Characteristics	Values
Coarse aggregate	Bulk particle density, Mg/m^3 Apparent particle density, Mg/m^3 Water absorption, %	2.60 2.66 0.8
Fine aggregate	Bulk particle density, Mg/m^3 Apparent particle density, Mg/m^3 Water absorption, %	2.52 2.58 1.6
Conventional filler	Particle density, Mg/m^3	2.64

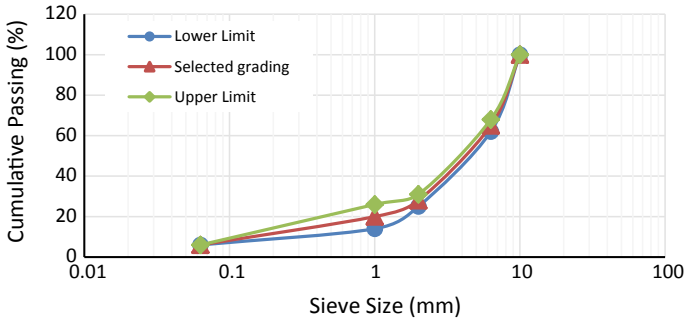

Fig. 1 AC-10 close-graded surface course gradation

recommended by many researchers such as Nikolaids [16] and Thanaya [17], because it is highly stable and highly adhesive.

Hot asphalt mixtures with two types of asphalt grades 100/150 and 40/60 were prepared for comparison purposes. Table 2 shows the characteristics of the chosen bitumen and bitumen emulsion.

2.3 Fillers

Sewage sludge fly ash (SSFA) was derived from an incinerator of the wastewater treatment plant in the UK. Flue gas desulphurisation gypsum (FGD) was collected from a coal-fired power station and used as a grinding aid for SSFA. Another by-product material produced from industrial production of acetylene called carbide lime waste (CLW), which is used as an activator for the binary blended filler.

The references mixtures were manufactured using 6% limestone fine filler and 6% OPC for the purpose of comparison.

Table 2 Bitumen and bitumen emulsion characteristics

Material	Property	Value
Bitumen emulsion	Type	Cationic
	Appearance	Black-to-dark-brown liquid
	Base bitumen, 1/10 mm	50
	Content of bitumen, %	50
	Boiling point, °C	100
	Relative density at 15 °C, g/ml	1.07
Bitumen 40/60	Appearance	Black
	Penetration at 25 °C	49
	Softening point, °C	51.5
	Density at 25 °C	1.02
Bitumen 100/150	Appearance	Black
	Penetration at 25 °C	131
	Softening point, °C	43.5
	Density at 25 °C	1.05

3 Samples Preparation

Marshall method for emulsified asphalt aggregate cold mixture design (MS-14) (Asphalt Institute [18] was adopted to prepare CBEMs). Different samples with different water contents (2.5, 3, 3.5, 4 and 4.5) % of the total aggregate were produced to conduct the coating test. This test was used to identify the less pre-moistening water content that achieving appropriate coating. Furthermore, optimum emulsion content was specified using indirect tensile stiffness modulus (ITSM), whereas the optimum content of total fluid during the compaction was indicated through density test. Accordingly, 3% pre-moistening water content, 12.5% optimum bitumen emulsion content, and 15.32% optimum total fluid content at compaction were used to prepare CBEMs.

Coarse aggregate, fine aggregate and mineral filler were mixed together with pre-wetting water content at low speed of Hobart mixer for 1 min. With keep blending for 2 min at the same speed, the bitumen emulsion content was poured progressively during the next 30 s of blending. Soon after that, the mixture was cast in the mould and directly compacted with 50 blow/face of the Marshall's hammer using Marshall's compactor. Then, the samples were extruded from moulds after 24 h and left them in the room temperature until the day of test.

4 Experimental Programme

4.1 Physical, Chemical and Mineralogical Analyses

In order to identify the similarity of the selected materials to OPC, the element composition of the materials under study was analysed using Shimadzu EDX 720 and energy dispersive X-ray fluorescence spectrometer. This analysis helps in understanding their behaviour in the CBEM. The physical properties of the chosen filler were studied in terms of particle-size distribution (PSD) using a Beckman Coulter laser diffraction particle size analyser LS 13 320.

4.2 Indirect Tensile Stiffness Modulus (ITSM) Measurement

This test has been used by many researchers as an indicative test to rank CBEMs [3, 8, 19, 20, 17]. Cooper Research Technology HYD-25 testing machine, Fig. 2, was used to carry out the stiffness measurements in accordance with the BS EN 12697-26 [21]. Table 3 summarises the test conditions summarised.

4.3 Scanning Electron Microscopy (SEM) Analysis

In this study, a high-resolution imaging technique was utilised to investigate the microstructure of the newly developed cementitious material paste. SEM images demonstrated the particle morphology and surface characterisation materials. Quanta 200 scanning electron microscope was used to depicting images to the materials under study.

Fig. 2 ITSM apparatus

Table 3 Characteristics of ITSM test [21]

Characteristics of test	Ranges
Diameter of specimen	100 ± 3 (mm)
Rise time	124 ± 4 (ms)
No. of conditioning pulses	5
Loading time	3–300 (s)
Transient peak horizontal deformation	5 (μm)
Poisson's ratio	0.35
No. of pulses	5
Temperature	20 ± 0.5 (°C)
Height of specimen	63 ± 3 (mm)
No. of blows (Marshall compactor)	50 blows/face
Time for temperature conditioning	4 h prior to test

5 Results and Discussion

5.1 XRF and PSD Analyses

The first stage of this study identified the physicochemical characteristics of the selected mineral filler which helps in evaluating their potential for developing cementitious materials. The chemical compositions for the conventional limestone filler and OPC along with SSFA, FGD and CLW are summarised in Table 4. The chemical analysis for of SSFA shows a significant silica content indicating pozzolanic reactive material. FGD gypsum used as a sulphate activation and grinding agent for SSFA. CLW has a high content of CaO which was used as a hydraulic activator for the

Table 4 Materials' chemical characteristics

Properties (%)	LF	OPC	SSFA	FGD	WLS
pH	9.12	12.85	8.29	12.29	13.1
CaO	73.712	65.488	10.538	34.036	90.031
SiO_2	16.937	27.862	30.233	14.409	15.939
Al_2O_3	0.029	2.247	3.071	–	–
MgO	0.977	1.519	2.498	0.520	0.954
Fe_2O_3	–	1.856	15.236	–	–
SO_3	0.100	2.805	0.079	33.335	0.619
K_2O	0.355	0.783	1.285	0.031	0.047
TiO_2	0.194	0.434	1.189	0.107	0.162
Na_2O	2.136	1.572	1.512	1.184	1.508

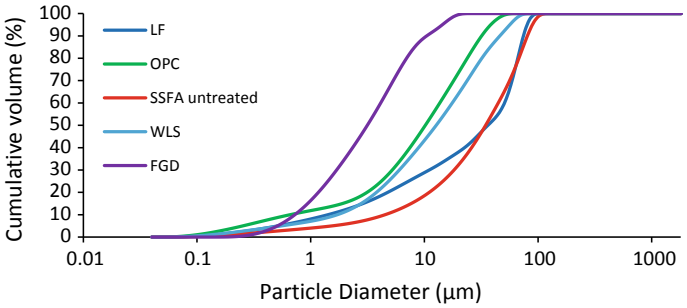

Fig. 3 PSD of the selected materials

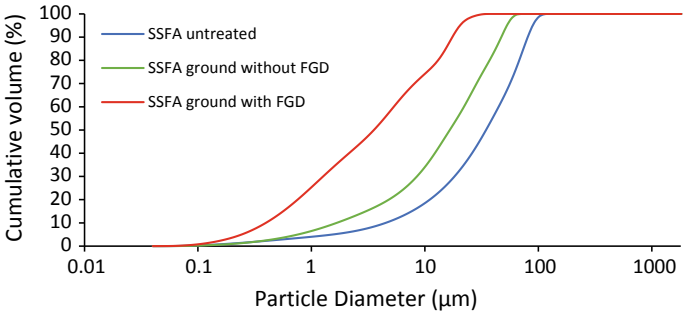

Fig. 4 PSD for grinding SSFA with and without FGD

new cementitious material. Figure 3 shows the overall particle-size distribution of all materials under study.

Mechanical activation for SSFA has been adopted to reduce the particle size and increase the surface area, hence increase the pozzolan reactivity. 5% FGD gypsum by the total mass of the binder was added to the SSFA and grinded together for 20 min. The PSD for SSFA after grinded with FGD has been shown in Fig. 4.

5.2 ITSM Performance

As this study is aiming at developing a new SCM with high volume of SSFA to be used as substitution to the conventional LF filler in CBEMs, therefore the replacement of the treated SSFA with OPC was selected to be 50, 40 and 30%. The performance of the mixtures was compared with CMA-LF, CMA-OPC and HMA. It is obvious from Fig. 5 that the ITSM of the tested samples decreased with the increase of percentage of OPC substitution by SSFA. This could be referred to the low content of CaO in the ash, which slows down the hydration process. However, the binary blended filler (BBF) containing 70% treated SSFA and 30% OPC was selected for further

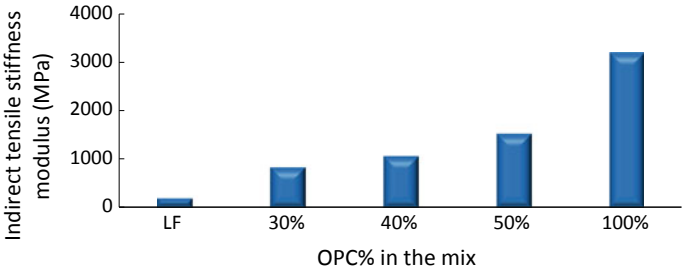

Fig. 5 Effect of replacing OPC with treated SSFA on the ITSM after 3 days

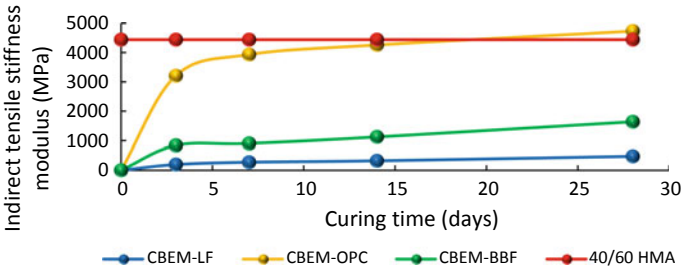

Fig. 6 Stiffness modulus of BBF with different curing times

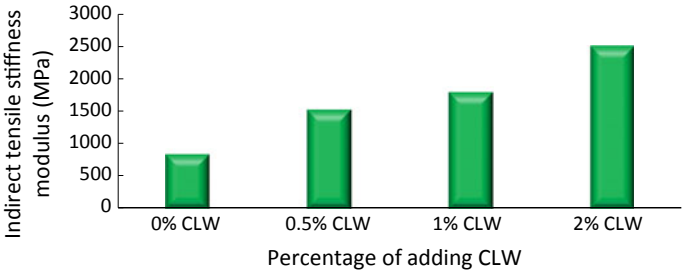

Fig. 7 Effect of adding CLW in different percentages on ITSM of BBF after 3 days

development using CLW, because this mixture involving high percentage of SSFA as well as still showing reasonable ITSM values compared to the conventional CBEM with LF. Figure 6 shows the ITSM for CBEM with BBF with different curing ages compared with references cold mixes with LF, and with OPC, and HMA.

CLW was added to the BBF in three percentages (0.5, 1 and 2%) as an additional filler. This technique has been adopted by several researchers to improve the performance of CBEM [22, 23]. Figure 7 reveals the effect of adding CLW on the ITSM of BBF.

From the results, it is clear that the addition of 2% CLW as an extra filler plus the BBF has been improved the performance of CBEM by 198.8% compared to the BBF

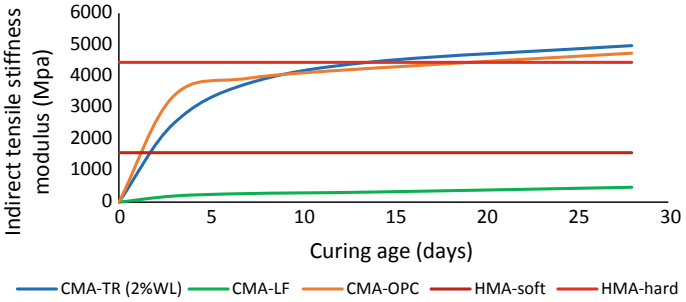

Fig. 8 ITSM for TBF with different curing times

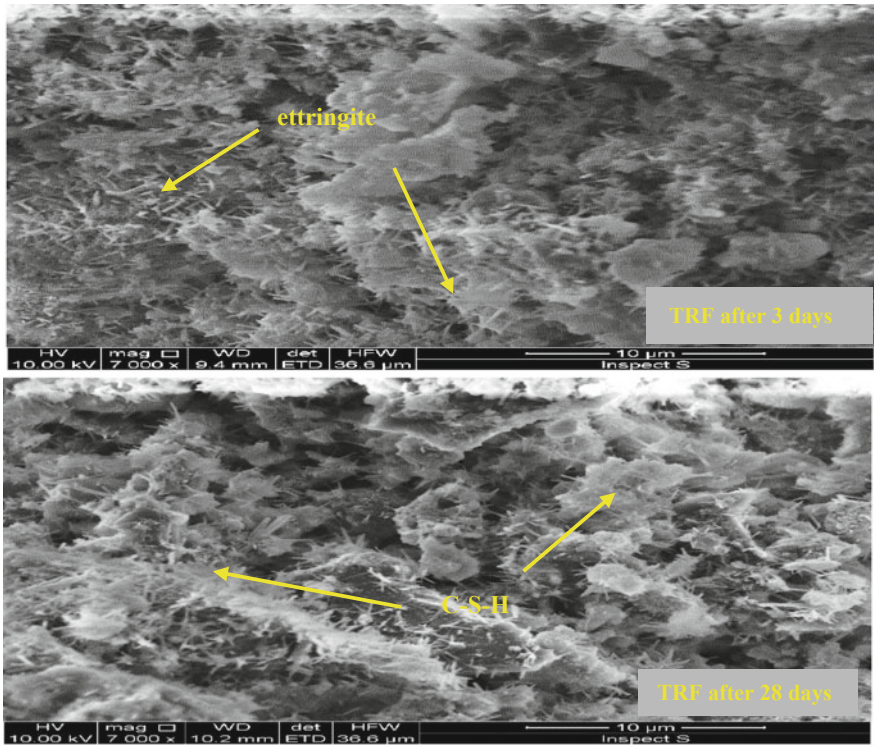

Fig. 9 SEM micrograph

after 3 days. The ITSM of the newly developed CBEM with ternary blended filler (TRF), containing 6% BBF + 2% CLW, with different curing times and compared with other reference mixtures has been shown in Fig. 8. It can be seen that the CMA-TRF after 14 days has performed better than CMA-OPC and HMA.

5.3 SEM Investigation

The SEM images for the TRB paste samples explain the reasons behind the improvement in the performance of the developed mixture. Figure 9 shows the micrograph of TRB paste after cured for 3 days and 28 days. It could be recognised a needle-shape hydration product, namely ettringite that developed at the early ages (3 days). After 28 days, the reaction process has been continued to produce more ettringite as well as the TRF particles' surfaces had altered to C–S–H gel. Accordingly, CBEM including TRF filler showed improvement in its properties.

6 Conclusions

The development of an eco-friendly cold asphalt mixture through developing a new cementitious filler from waste materials has been identified as the aim of this study. The investigation work included evaluation of the stiffness modulus which used as an indicator to the performance of the mixtures, while morphological characteristics were examined by SEM. The points below summarised the main conclusions:

1. The usage of SSFA in high volumes helps in reducing the impact on the environment.
2. CBEM incorporating BBF and activated by CLW can produce a filler with cementitious properties that is convenient to substitute the limestone fine filler in CMA.
3. SEM explains the reasons behind the improvement in the performance of CBEM containing the developed cementitious material by showing generated hydrated products.

As CLW appears to be very promising activating material, it is recommended to use this material for activating cement filler in asphalt mixture as future work.

Acknowledgements The corresponding author wishes to acknowledge with appreciation and gratitude the Ministry of Higher Education and Scientific Research and Kufa University in Iraq for supporting the first author morally and financially. Additionally, sincere thanks to Jobling Purser for supplying the bitumen emulsion and Colas for supplying the aggregate.

References

1. Gómez-Meijide B, Pérez I (2015) Nonlinear elastic behavior of bitumen emulsion-stabilized materials with C&D waste aggregates. Constr Build Mater 98:853–863
2. James A (2006) Overview of asphalt emulsions. Asphalt emulsion technology. Transportation research circular number E-C102, Washington DC (USA), Transportation Research Board
3. Al-Hdabi A, Al Nageim H, Seton L (2014) Performance of gap graded cold asphalt containing cement treated filler. Constr Build Mater 69:362–369
4. Oruc S, Celik F, Akpinar M (2007) Effect of cement on emulsified asphalt mixtures. J Mater Eng Perform 16:578–583

5. O'Rourke B, McNally C, Richardson MG (2009) Development of calcium sulfate–ggbs–portland cement binders. Constr Build Mater 23(1):340–346
6. Al Nageim H, Al-Busaltan SF, Atherton W, Sharples G (2012) A comparative study for improving the mechanical properties of cold bituminous emulsion mixtures with cement and waste materials. Constr Build Mater 36:743–748
7. Al-Hdabi A, Al Nageim H, Ruddock F, Seton L (2013) Enhancing the mechanical properties of gap graded cold asphalt containing cement utilising by-product material. J Civ Eng Archit 7(8):916–921
8. Dulaimi AF, Al Nageim H, Ruddock F, Seton L (2016) New developments with cold asphalt concrete binder course mixtures containing binary blended cementitious filler (BBCF). Constr Build Mater 124:414–423
9. Lau PC, Teo DCL, Mannan MA (2017) Characteristics of lightweight aggregate produced from lime-treated sewage sludge and palm oil fuel ash. Constr Build Mater 152:558–567
10. Lin D-F, Luo H-L, Cheng J-F, Zhuang M-L (2015) Strengthening tiles manufactured with sewage sludge ash replacement by adding micro carbon powder. Mater Struct 49(9):3559–3567
11. Piasta W, Lukawska M (2016) The effect of sewage sludge ash on properties of cement composites. Procedia Engineering 161:1018–1024
12. Pan SC, Tseng DH, Lee C (2002) Use of sewage sludge ash as fine aggregate and pozzolan in Portland cement mortar. J Solid Waste Technol Manag 28(3):121–130
13. Monzó J, Paya J, Borrachero MV, Peris-Mora E (1999) Mechanical behavior of mortars containing sewage sludge ash (SSA) and Portland cements with different tricalcium aluminate content. Cem Concr Res 29:87–94
14. Smol M, Kulczycka J, Henclik A, Gorazda K, Wzorek Z (2015) The possible use of sewage sludge ash (SSA) in the construction industry as a way towards a circular economy. J Clean Prod 95:45–54
15. European Committee for Standardization (2006) BS EN 13108: part 1. Bituminous mixtures materials specification-Asphalt Concrete. UK, British Standards Institution
16. Nikolaids A (1994) Construction and performance of dense cold bitumen mixtures as strengthening over layer and surface layer. In: The 1st European symposium on performance and durability of bituminous materials, University of Leeds, London
17. Thanaya INA (2003) Improving the Performance of Cold Bituminous Emulsion Mixtures Incorporating Waste Materials. Ph.D. thesis, University of Leeds
18. Asphalt Institute (1989) Asphalt cold mix manual. Manual series no. 14(MS-14) third edition, Lexington, KY 40512-4052, USA
19. Ojum CK (2015) The Design and Optimisation of Cold Asphalt Emulsion Mixtures. Ph.D. thesis, University of Nottingham
20. Oke O (2010) A Study on the development of guidelines for the production of bitumen emulsion stabilised RAPS for roads in the tropics. Ph.D. thesis, University of Nottingham
21. European Committee for Standardization (2012) BS EN 12697: Part 26. Bituminous mixtures-test methods for hot mix asphalt-stiffness. UK: British Standards Institution
22. AL-Hdabi A (2014) High strength cold rolled asphalt surface course mixtures. Ph.D. thesis, LJM University
23. Nassar AI (2016) Enhancing the performance of cold bitumen emulsion mixture using supplementary cementitous. Ph.D. thesis, University of Nottingham

Characterising the Performance of a Non-Portland Binder Using Analytical Techniques

Monower Sadique and Hassan Al-Nageim

Abstract The development and production of new materials require advanced analytical characterisation to explain the relation between the physicochemical structure of the material and its properties. Highly integrated microelectronic structure analysis of surfaces with laser beams and x-ray fluorescence-aided devices is found to be helpful for providing important information, including the interrelationships between physical, chemical, mechanical and durability characteristics of the new developed products. In most instances, no single technique provides all the needed information, and hence, simultaneous application of several techniques becomes necessary. This study was aimed for analysis, characterisation and evaluation of a new novel non-Portland cementitious binder in anhydrous and hydrated states using XRD, FT-IR and TG/DTA.

Keywords Non-Portland binder · FT-IR · TG/DTA

1 Introduction

One of the most significant current discussions in the construction sector is the reduction of carbon emission from its production and application process. The supplementary cementitious material (SCM) plays a key role in achieving this objective. Different types of additions other than the standard listed materials such as calcined clay, sewage sludge ash, rice husk ash, wood ash, sugar cane bagasse ash, corn cob ash, kaolin waste, perlite, diatomite and air pollution control residue have been studied as SCM. Much of the research up to now has been concluded by activating the additions with OPC and/or GGBS, and so far, there has been little discussion about cement and GGBS free systems [1–10].

M. Sadique (✉) · H. Al-Nageim
Department of Civil Engineering, Liverpool John Moores University,
Byrom Street, Liverpool L3 3AF, UK
e-mail: M.M.Sadique@ljmu.ac.uk

S. Kumar Shukla et al. (eds.), *Advances in Sustainable Construction Materials and Geotechnical Engineering*, Lecture Notes in Civil Engineering 35,
https://doi.org/10.1007/978-981-13-7480-7_20

Dramatic advancement has been achieved by using wet milled paper sludge ash (PSA) with GGBS (PSA: GGBS, 50:50) in cement-free systems [11]. However, attention should also be given concerning curing, reinforcement cover and carbonation when the GGBS level is more than 50% [12]. Moreover, GGBS is no longer classified as a waste, and hence, there is increasing concern regarding the replacement of GGBS with other waste/s such as SCM.

At the same time, the development and production of new materials require advanced analytical characterisation to explain the relation between the physicochemical structure of the material and its properties. Highly integrated microelectronic structure analysis of surfaces with laser beams and x-ray fluorescence-aided devices is found to be helpful for analysing substances at microlevel and molecular level [13]. In addition to characterisation, they provide important information, including the interrelationships between chemical and durability characteristics of the developed products. In most instances, simultaneous uses of several techniques become necessary. Different experimental techniques have been employed by researchers to investigate the chemical and morphological reaction upon hydration. This is because different techniques utilise different operating principles, and hence, a simultaneous application of them will be expected to provide multidimensional information of the hydration products of a binder. As a result, irrespective of the crystal or amorphous characteristics of the hydrates, chemical and morphological status can be obtained.

A new novel non-Portland binder (NPB) was developed through synergistic physicochemical composition by using PSA and blending it with another alkali sulphate-rich fly ash and silica fume and gypsum-aided grinding. This study was aimed for investigating the hydration mechanism, characterisation and evaluation of the new novel NPB using analytical techniques.

2 Experimental Technique and Materials Used

2.1 Materials

The chemical and physical properties of the new NPB and control cement have been provided in Table 1. For analysis and comparison with new NPB, a commercially available Portland composite cement-type CEM-II/A/LL 42.5-N has been used in this study which contains between approximately 6–20% limestone.

2.2 Fourier Transform Infrared Spectroscopy (FT-IR)

In this study, the spectrum of the specimen was studied by accumulating 16 scans at 4 cm^{-1} resolution between 515 cm^{-1} and 4000 cm^{-1} using a Fourier transform

Table 1 Properties of new NPB and control cement

	CEM II	NPB
D_{50}, μm	13.3	10.6
Fineness (BET), m^2/gm	6.78	9.67
Density, gm/cm^3	3.05	2.59
Soundness (mm)	1.3	2.0
Initial setting time (min)	150	70
Pozzolanicity (after 15 day)	Positive	Positive
Na_2O	1.5	1.8
CaO	62.58	45.15
SiO_2	25.06	31.19
Al_2O_3	2.26	3.49
SO_3	1.92	3.5
Cl	–	0.5
K_2O	0.75	4.00
Na_2O-equ [%]	2.0	4.2

infrared spectrometer (FTIR) equipped with a MIRacle ATR accessory (Specac, UK). The samples were finely ground, combined with pre-dried spectroscopic grade KBr (containing around 0.5% wt sample) and forced into a disc under 10 tonnes of pressure, following the process mentioned in previous studies [14–16].

2.3 Thermal Analysis

In this study, a Perkin Elmer TGA-7 analyser was used to analyse the binder paste and LOI of different materials by simultaneous TG/DTA. The samples were heated in a tungsten crucible at a constant rate of 5 °C/min using inert nitrogen gas in the temperature range from 24 to 960 °C. Commercial software Pyris was used to quantify the mass loss and identify the peaks from TGA and DTA. The changes in sample weight indicate material loss and phase transformation that occurs at particular temperatures.

2.4 Specimen for Analytical Analysis

For analysing hydration kinetics, phase development and microstructural analysis, the paste specimens of the NPB and control cement were prepared at a water/binder ratio of 0.50 and cured in 20 °C under water and analysed at designated ages. There are similarities between the approach followed in this study and those described by Singh [17] and Tkaczewska [18]. The mortar specimens of NPB using the optimised

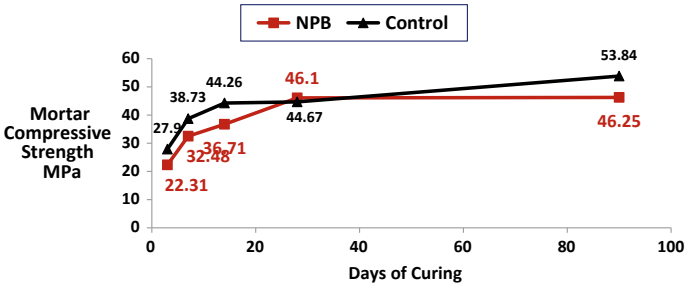

Fig. 1 Optimised strength development by NPB and reference cement mortar

design parameters (binder:fine aggregate ratio of 1:2.25, water/binder ratio of 0.45 with 1.5% SP) were prepared and cured for up to 90 days. The comparative strength development between NPB and the control cement (cement:fine aggregate ratio of 1:2.25 and water/cement ratio of 0.35) is displayed in Fig. 1. Though NPB shows slightly lower early strength than the control, however, its rate of hydration was more than that of the control between 7 and 28 days. However, the increase in strength after 28 days was very low in NPB compared to that of the control mortar.

3 Results and Discussion

3.1 Hydrates Under TG/DTA

The TG/DT analysis of NPB paste ranging from 7 days to 1 year was conducted, and a sample thermogram is shown in Fig. 2. To avoid interference by non-reacted residual water, at designated periods, the hardened paste was dried at 20 °C for four hours before TGA. Based on the suggestion provided by previous studies, the findings from the TG/DTA profile for NPB are summarised in Table 2. The absolute mass loss increases with age (up to 28 days) were evident from Fig. 1 and Table 2. This was an indirect indication of degree of hydration within the ternary blend and was in agreement with the result reported by Esteves [19] in the case of plain cement and silica fume modified cement.

Moreover, based on the findings presented in Table 2, it is evident that the mass loss in the temperature interval 0–150 °C with the first strong endothermic peak was attributed to dehydroxylation of CSH and found to be increasing until 28 days of curing. The mass loss at this phase was due to the loss of weakly bound water on the gel solid, which was adsorbed, and was taken at about 90–110 °C. Furthermore, the appearance of a new exothermic peak at 790 °C without a significant mass change was due to recrystallisation of C–S–H [15] and was found to be related to pozzolanic activity of silica fume within NPB [19]. The increased mass loss and shifting of DTA peaks towards higher temperature with increase of hydration age were due to

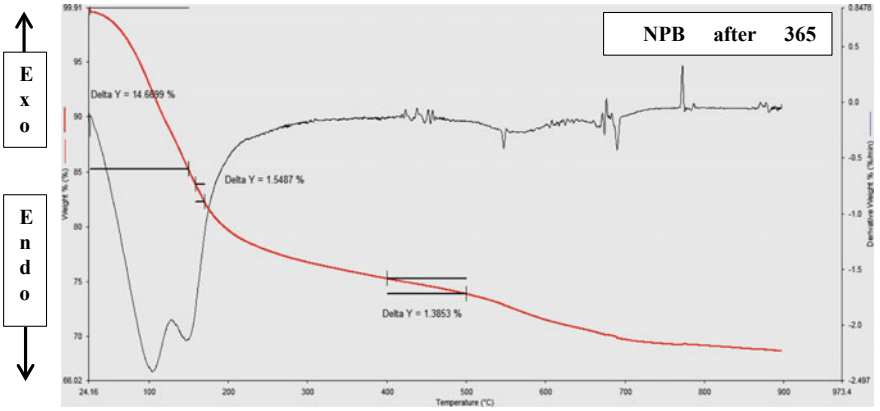

Fig. 2 Thermogram of NPB after 365 days curing

Table 2 Summary of TG/DTA curve for NPB paste

Temperature range	Comments	% Mass loss				
		7 day	14 day	28 day	90 day	365 day
0–150 °C	Endothermic peak is attributed to the dehydroxylation of CSH phase	6.17	22.43	25.49	23.30	14.6
150–170 °C	Mass loss is attributed to the dehydroxylation of Ettringite (AFm) phase	0.63	0.76	0.78	0.95	1.5
400–500 °C	Mass loss for dehydration of $Ca(OH)_2$ or portlandite (C–H)	1.0	0.78	0.98	1.6	1.3
Absolute mass loss (%)		20	35	37	35	32

the formation of C–S–H further, which supports the idea of Kourounis et al. [20]. The second major endothermic peak at 7 days of hydration and the corresponding mass loss in TG curve at 400–500 °C, as shown in Fig. 2, correspond to the dehydration of the C–H phase, formed for further hydration through the reaction of silicate with water. Similar thermal analysis was also reported in a recent work by Esteves [19] for a cement–silica fume system.

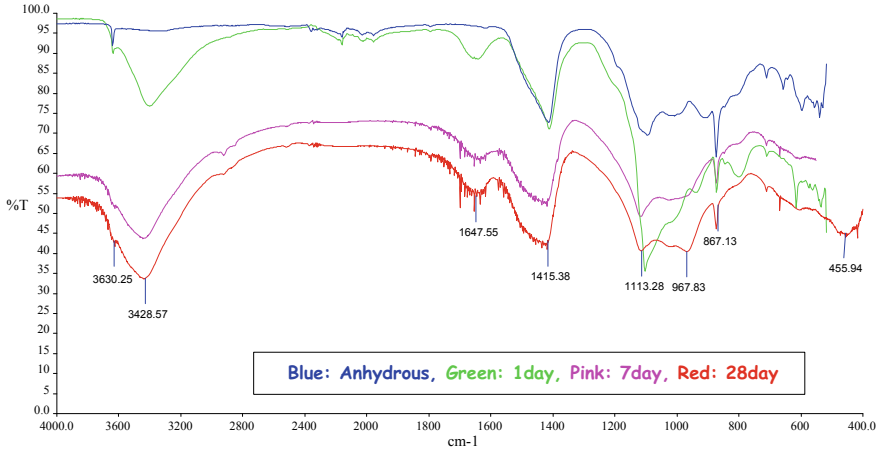

Fig. 3 FT-IR spectra for hydrated paste and anhydrous powder of NPB

3.2 Analysis of Hydrates by FT-IR

The identification of the main hydration product of blended cement [15] and pure cement [16] using FT-IR in association with IR spectral appearances during the progress of hydration has been studied previously. The progressive hydration was found to be supplemented by the increase of the intensities of C–S–H absorption bands and simultaneous decrease of absorption bands of constituent minerals [21]. The IR spectral studies of hydration of NPB paste with increasing ages have been plotted in Fig. 3. For identifying the successive changes in constituent materials and hydration products, the absorption band of anhydrous (powder) NPB has also been inserted in the IR spectrum of hydrated pastes in Fig. 3.

The IR spectra of ettringite presents a very strong band centred towards 1120 cm^{-1}. However, considerable difference between the spectra of two types of calcium sulfoaluminate hydrates AFm and AFt phases, in association with identification of a strong characteristic band at 1100 cm^{-1} and 1120 cm^{-1}, respectively, was reported by Bensted et al. [22]. At the same time, early formation of ettringite was detected by a change in the sulphate absorption to a singlet centred at 1120 cm^{-1}, and the subsequent replacement of ettringite by monosulfate by a further appearance to a doublet at 1100 and 1170 cm^{-1} was stated by Taylor. Hence, the strong singlet absorption peak for AFt at 1117 cm^{-1} after 1 day and initiation of return of doublet at 7 days and the subsequent appearance of a strong doublet for conversion of AFt to AFm at 1113 cm^{-1} and 967 cm^{-1} after 28 day (Fig. 3) in the case of NPB were in accordance with Taylor's observation. The appearance of a strong C–H absorption band at 3641 cm^{-1} and AFt band at 1118 cm^{-1} after 1 day of curing were the main early strength generating elements for NPB that have been confirmed by the observed compressive strength of 22.31 MPa after 3 days (Fig. 1).

Subsequently, progressive increases in the intensity of the absorption band of C–S–H with age at 1415 cm^{-1} and 1420 cm^{-1} (as shown in Fig. 3) played a dominating role for generating strength within the NPB and control mortar, respectively, which continued up to 90 days. The changes that occurred in the H_2O bending band around 1650 cm^{-1} and in the H_2O or OH stretching bands at 3100–3700 cm^{-1} also confirm the successful hydration within the ternary blend [23]. Moreover, the consumption of portlandite for progressive hydration and diminishing C–H band subsequently at 3630 cm^{-1} with age was also found to be in agreement with the TG/DTA observation of NPB paste.

4 Conclusion

The hydration kinetics within the NPB has been analysed utilising analytical approach and compared with the reference cement. The sulphate activation of PSA particles by alkaline fly ash was revealed in this analysis, where sulphate activation was found to be based on the reactivity of sulphates with the aluminium in generating ettringite (AFt). The ionic species of alkali sulphate (K^+, Na^+ and SO_4^{2-}) was found to influence the activation and subsequent hydration. During activation, the increased SO_4^{2-} concentration (from gypsum and alkali sulphate-rich fly ash) reacts with alumina phase of PSA and creates aluminosulphate that combines with Ca^{2+} and forms ettringite. This ettringite provides strength at early ages of hydration [24–26]. At the same time, the conversion of AFt to AFm phase was also established by TG/DTA and FT-IR analysis during the progression of hydration within the novel NPB.

References

1. Filho RDT et al (2007) Potential for use of crushed waste calcined-clay brick as a supplementary cementitious material in Brazil. Cem Concr Res 37(9):1357–1365
2. Rodriguez Largo O et al (2009) Novel use of kaolin wastes in blended cements. J Am Ceram Soc 92(10):2443–2446
3. Erdem TK et al (2007) Use of perlite as a pozzolanic addition in producing blended cements. Cem Concr Compos 29(1):13–21
4. Yilmaz B, Ediz N (2008) The use of raw and calcined diatomite in cement production. Cem Concr Compos 30(3):202–211
5. Bertolini L et al (2004) MSWI ashes as mineral additions in concrete. Cem Concr Res 34(10):1899–1906
6. Lampris C, Stegemann JA Cheeseman CR (2009) Comparison of the physical properties and leaching characteristics of apc residues solidified using portland cement and ground granulated blast furnace slag, In: Wascon conference 2009: France
7. Johnson A, Catalan LJJ, Kinrade SD (2010) Characterization and evaluation of fly-ash from co-combustion of lignite and wood pellets for use as cement admixture. Fuel 89(10):3042–3050
8. Udoeyo FF et al (2006) Potential of wood waste ash as an additive in concrete. J Mater Civ Eng 18(4):605–611

9. Adesanya DA, Raheem AA (2009) Development of corn cob ash blended cement. Constr Build Mater 23(1):347–352
10. Ganesan K, Rajagopal K, Thangavel K (2008) Rice husk ash blended cement: assessment of optimal level of replacement for strength and permeability properties of concrete. Constr Build Mater 22(8):1675–1683
11. Mozaffari E et al (2009) An investigation into the strength development of wastepaper sludge ash blended with ground granulated blastfurnace slag. Cem Concr Res 39(10):942–949
12. Osborne GJ (1999) Durability of Portland blast-furnace slag cement concrete. Cem Concr Compos 21(1):11–21
13. Grasserbauer M (1989) Materials analysis in high technology—from analytical chemistry to analytical science. TrAC Trends Anal Chem 8(6):191
14. Mollah MYA et al (2000) A fourier transform infrared spectroscopic investigation of the early hydration of Portland cement and the influence of sodium lignosulfonate. Cem Concr Res 30(2):267–273
15. Kaminskas R, Mituzas J, Kaminskas A (2006) The effect of pozzolana on the properties of the finest fraction of separated Portland cement—part 1. Ceram-Silik 50(1):15–21
16. Ylmén R et al (2009) Early hydration and setting of Portland cement monitored by IR, SEM and Vicat techniques. Cem Concr Res 39(5):433–439
17. Singh NB et al (2002) Effect of lignosulfonate, calcium chloride and their mixture on the hydration of RHA-blended Portland cement. Cem Concr Res 32(3):387–392
18. Tkaczewska E, Małolepszy J (2009) Hydration of coal–biomass fly ash cement. Constr Build Mater 23(7):2694–2700
19. Esteves LP (2011) On the hydration of water-entrained cement–silica systems: combined SEM, XRD and thermal analysis in cement pastes. Thermochim Acta 518(1–2):27–35
20. Kourounis S et al (2007) Properties and hydration of blended cements with steelmaking slag. Cem Concr Res 37(6):815–822
21. Ghosh SN (2001) 5—IR spectroscopy, in handbook of analytical techniques in concrete science and technology. In: Ramachandran VS, James JB (ed) William Andrew Publishing: Norwich, NY, pp 174–204
22. Bensted J, Varma SP (1974) Some applications of Infrared and Raman spectroscopy in cement chemistry. Cem Technol 5(4):378–382
23. Taylor HFW (1997) Hydration of Portland cement, in cement chemistry. In: Taylor HFW (ed) Thomas Telford: London
24. Qian JS, Shi CJ, Wang Z (2001) Activation of blended cements containing fly ash. Cem Concr Res 31(8):1121–1127
25. Xu AM, Sarkar SL (1991) Microstructural study of gypsum activated fly-ash hydration in cement paste. Cem Concr Res 21(6):1137–1147
26. Poon CS et al (2001) Activation of fly ash/cement systems using calcium sulfate anhydrite (CaSO4). Cem Concr Res 31(6):873–881

Predicting the Dynamic Properties of Plain Concrete Under the Impact Load

Islem Megdiche, William Atherton, Clare Harris and Glynn Rothwell

Abstract Materials subject to high strain exhibit an enhancement in its mechanical properties. High strain is caused by loads ranging from gas explosion and aircraft impact to hypervelocity impact. The dynamic increase factor (DIF) is a method used to take account of the strain rate. DIF is defined as the ratio of dynamic strength to static strength. Methods to determine the dynamic properties of a material are achieved via either conducting dynamic compressive and tensile testing or utilising formulae from the literature. CEB-FIP model code [3] presents the most comprehensive formulae for predicting the strain rate enhancement of concrete. Quasi-static flexural and compression tests of plain concrete were conducted using standard test machines on concrete cubes and prisms, respectively. CEB-FIP compression and tensile DIF models were then used to calculate the strength for the compression and tensile strain rates between 10^{-2} and 10^{0}, which are most relevant to common dynamic load cases in civil engineering structures.

Keywords Plain concrete · Dynamic properties · CEB-FIP model code

I. Megdiche (✉)
Department of Civil Engineering, Liverpool John Moores University,
15-21 Webster St, Liverpool L3 2ET, UK
e-mail: I.Megdiche@2015.ljmu.ac.uk

W. Atherton · C. Harris
Department of Civil Engineering, Liverpool John Moores University,
Peter Jost Enterprise Centre, 3 Byrom St, Liverpool L3 3AF, UK
e-mail: W.Atherton@ljmu.ac.uk

C. Harris
e-mail: C.B.Harris@ljmu.ac.uk

G. Rothwell
Department of Maritime and Mechanical Engineering, Liverpool John
Moores University, James Parsons Building, 3 Byrom St, Liverpool L3 3AF, UK
e-mail: G.Rothwell@ljmu.ac.uk

S. Kumar Shukla et al. (eds.), *Advances in Sustainable Construction Materials and Geotechnical Engineering*, Lecture Notes in Civil Engineering 35,
https://doi.org/10.1007/978-981-13-7480-7_21

1 Introduction

Above ground storage tanks are structures that contain many products such as chemicals, oil and water. For those which store hazardous materials, strict precautions have to be taken to prevent any sort of pollution or danger to the people and the environment in case of catastrophic failure of the primary containment. For instance, in the UK, all companies involved in the storage of hazardous materials are required by law to provide mitigation measures. These entail the construction of a structure surrounding the storage tank to retain any spillage in case of the release of small quantities of the inventory or the whole bulk of materials in the case of catastrophic failure. Such failures typically follow natural disasters such as hurricanes or accidental releases that might result from a human error [1]. This structure is referred to as a bund wall or secondary containment. In the UK, the bund wall is designed under the BS EN 1992-3:2006 [5] where it is only designed to withstand the static pressure of the fluid. However, in case of catastrophic failure, the bulk of material escapes the storage tank very rapidly and impacts the bund wall which implies that the structure is subjected to a dynamic load. The current project aims to study the behaviour of the bund wall under the impact load of the fluid numerically. Therefore, as part of the material calibration in the software, determining the dynamic properties of the concrete is of a paramount importance to model the behaviour of the structure accurately.

Impact loading involves the impactor and the target. Depending on the level of deformation occurring in the impactor, the impact loading can be classified into two main classes: they are hard and soft impacts. In the hard impact, the deformations occurring in the impactor are very negligible compared to the deformations in the target, such as a bullet hitting a concrete wall. In contrast, in the case of a soft impact, both the impactor and the target undergo significant deformations which necessitates considering the impactor in the analysis. An example of a soft impact is the fluid flow hitting the bund wall. Another characteristic of the impact loading is determined by the behaviour of the structure under the impact loading with various velocities. The structure tends to respond locally if the velocity of the impact load is more than 40 m/s according to Othman [7]. This is because the load is acting over a very short period of time which is smaller than the natural period of the structure, so the latter does not have time to respond globally. If the velocity is less than 40 m/s, then the structure responds globally and damage occurs everywhere in the structure. For civil engineering structures, they are mostly subjected to low velocity impact in case of dynamic accidental loading.

It is well recognised that materials subjected to high strain rates exhibit an enhancement in their mechanical properties. In particular, the compressive strength, tensile strength, the peak strain and the elastic modulus increase [4]. For example, the compressive strength of the concrete subjected to dynamic loading at the rate of 10 s^{-1} increased between 85 and 100% of the static compressive strength [2]. The degree of the increase in the dynamic properties depends on the strain rate, which itself depends

Fig. 1 Typical strain rate for different types of loading

on the load case. Figure 1 shows the typical strain rates occurring in different dynamic load cases.

Various tests exist to determine the dynamic properties of the concrete depending on the level of strain rate. The hydraulic test machine permits a strain rate between 10^{-2} and 10^{0}. The drop-weight impact test machine is capable of reaching a higher strain rate up to 10 s^{-1}. The split Hopkinson pressure bar (SHPB) permits the highest strain rate in the range of 10–10^{4} s^{-1} on small specimens according to Ross et al. [8]. Alternatively, it is possible to use codes in which formulae are derived from experimental tests in case of a lack of suitable experimental devices. CEB-FIP model code [3] contains the most comprehensive formulae to predict the strain rate performance of concrete. The code covers the dynamic properties of concrete up to 120 MPa in both compression and tension for a strain rate up to 3×10^{2} s^{-1} [3]. Therefore, it is appropriate to use this code to predict the dynamic properties of concrete under the impact load of fluid flow as the estimated strain rate is far below 3×10^{2} s^{-1}.

This paper presents the results of the compressive and flexural tensile strengths obtained from the quasi-static tests conducted at Liverpool John Moores University and the application of the relationships from CEB-FIP model code [3] to determine the dynamic properties of the plain concrete.

2 Materials and Sample Preparation

The materials used for the specimen preparation are Grade 35 Ordinary Portland Cement, silica sand, fine aggregate of a maximum size of 2 mm, superplasticiser and potable water. The mix proportions are given in Table 1.

In total, six specimens were prepared, three prisms for the flexural tensile test and three cubes for the compressive tests. Firstly, the dry constituents were mixed together using a Hobart mixer for 5 min, then water and superplasticiser were added to transform the mix into a paste, and this operation lasted 10 min. Then, the specimens

Table 1 Materials proportion of the concrete mix

Material	Proportion (Kg/m^3)
Cement	415
Aggregate	1200
Sand	624
Water	228
Superplasticiser	3.6

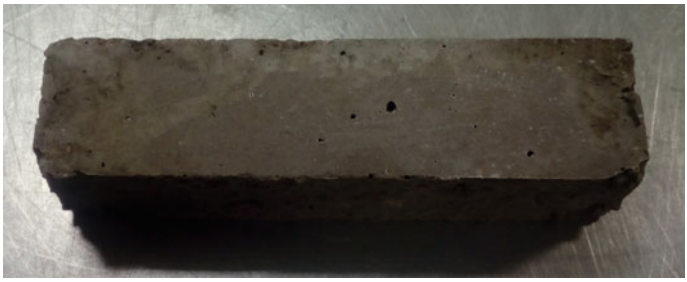

Fig. 2 Concrete specimen for flexural tensile testing

Fig. 3 Concrete specimen for compressive testing

were cast. After 24 h, they were demoulded and left to cure in water at 20 °C for 28 days. Figures 2 and 3 depict the specimens for the flexural tensile and compressive tests, respectively.

3 Experimental Results

3.1 Compressive Strength Test Procedure

Compressive strength of the plain concrete was determined from 150-mm concrete cubes using Controls Automax compressive test equipment depicted in Fig. 4. The compressive test was conducted according to BS EN 12390-3:2009 [6]. Table 2

Fig. 4 Compressive test machine

Table 2 Results of compressive strength test

	Compressive strength (MPa)	Load at failure (kN)
Specimen 1	34.48	775.8
Specimen 2	35.85	806.6
Specimen 3	33.66	757.4
Average	34.66	779.93

Fig. 5 Flexural test machine

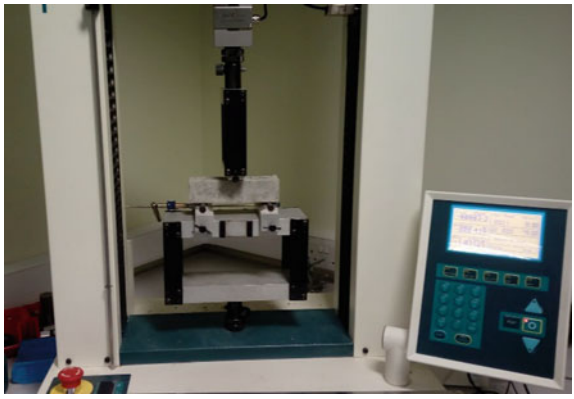

presents the results of the compressive strength and the load at failure obtained from the test.

3.2 Tensile Flexural Strength Test Procedure

The three-point bending test has been conducted on 40 × 40 × 160-mm prisms using a Tinius Olsen H25KS machine shown in Fig. 5.

Table 3 Results of flexural strength test

	Tensile flexural strength (MPa)	Load at failure (N)	Deflection at maximum load (mm)
Specimen 1	6.27	2230	0.742
Specimen 2	6.49	2310	0.891
Specimen 3	7.17	2550	0.54
Average	6.64	2363.3	0.724

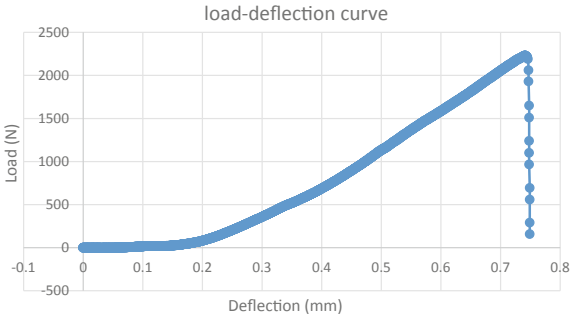

Fig. 6 Tensile load–deflection curve of specimen 1

The tensile flexural strength is equal to

$$\sigma = \frac{3FL}{2bd^2}$$

where

F is the load at the fracture point (N).
L is the length of the support span which is equal to 120 mm.
b is the width.
d is the thickness.

Table 3 indicates the tensile flexural strength, the load at failure and the deflection occurring at the maximum load for the three specimens and averaged values. The curve of load–deflection obtained from the flexural tensile test is presented in Fig. 6.

4 Dynamic Properties of Plain Concrete

The dynamic increase factor (DIF) is a method to take into account the increase in the mechanical properties of plain concrete. It is defined as the ratio of dynamic to static strength [7]. The formulae used to calculate the dynamic compressive strength and the dynamic tensile strength are given by Eqs. (1), (2), (3) and (4).

4.1 CEB-FIP Compression DIF Model

$$\mathrm{DIF}_{fc} = \frac{f_{\mathrm{cd}}}{f_c} = \left(\frac{\dot{\varepsilon}_c}{30 \times 10^{-6}}\right)^{0.014} \quad \text{for} \quad \dot{\varepsilon}_c \leq 30\ \mathrm{s}^{-1} \tag{1}$$

$$\mathrm{DIF}_{fc} = \frac{f_{\mathrm{cd}}}{f_c} = 0.012\left(\frac{\dot{\varepsilon}_c}{30 \times 10^{-6}}\right)^{\frac{1}{3}} \quad \text{for} \quad 30 \quad \leq \dot{\varepsilon}_c \leq 300\ \mathrm{s}^{-1} \tag{2}$$

where

f_{cd} the dynamic compressive strength corresponding to strain rate $\dot{\varepsilon}_c$.
f_c the static compressive strength corresponding to the static strain of 30×10^{-6} [7].

It is estimated that the strain rate induced by the impact of the fluid flow on the concrete bund wall is in the range of 10^{-1}–10^{0} which is the range of strain rate occurring in the case of pile driving and aircraft impact according to Fig. 1; therefore, the DIF is estimated from Eq. 1. Assuming that the strain rate is equal to 10^{0}, then $\mathrm{DIF}_{fc} = 1.15$ and $f_{\mathrm{cd}} = 40.10$ MPa.

4.2 CFB-FIP Tension DIF Model

$$\mathrm{DIF}_{ft} = \frac{f_{\mathrm{td}}}{f_t} = \left(\frac{\dot{\varepsilon}_t}{1 \times 10^{-6}}\right)^{0.018} \quad \text{for} \quad \dot{\varepsilon}_t \leq 10\ \mathrm{s}^{-1} \tag{3}$$

$$\mathrm{DIF}_{ft} = \frac{f_{\mathrm{td}}}{f_t} = 0.0062\left(\frac{\dot{\varepsilon}_t}{1 \times 10^{-6}}\right)^{\frac{1}{3}} \quad \text{for} \quad 10 \leq \dot{\varepsilon}_c \leq 300\ \mathrm{s}^{-1} \tag{4}$$

where

f_{td} the dynamic tensile strength corresponding to strain rate $\dot{\varepsilon}_t$
f_c the static tensile strength corresponding to the static strain of 1×10^{-6} [7].

Similar to the compression DIF model, the model given by Eq. 3 for the tensile DIF is chosen. For a strain rate of 10^{0}, $\mathrm{DIF}_{ft} = 1.282$ and $f_{\mathrm{td}} = 8.51$ MPa. The values obtained from the CFB-FIP DIF models for both tension and compression are in agreement with the experimental results presented in [2, 4, 8] for the range of the strain rate considered.

5 Conclusion

The aim of this study was to calculate the dynamic properties of the plain concrete under the impact loading. These values are to be utilised to calibrate the material model in the finite element analysis (FEA) model for subsequent numerical modelling of the bund wall. There are specific test machines that permit determination

the properties experimentally; however, these machines are very expensive and not always available or limited to a maximum rate of loading. Alternatively, the CEB-FIP model code presents formulae for plain concrete which are appropriate for the strain rate under investigation. The formulae are in agreement with other experimental studies. The quasi-static properties of the plain concrete were determined for compressive and flexural tensile tests. Then, the formulae for the appropriate strain rate range were utilised to calculate the dynamic compressive and tensile strength.

Acknowledgements The first author would like to thank Liverpool John Moores University for the financial support provided for this project.

References

1. Atherton W (2008) An Empirical investigation of catastrophic and partial failures of bulk storage vessels and subsequent bund wall overtopping and dynamic pressure. Ph.D. thesis, Liverpool John Moores University
2. Bischoff PH (1991) Compressive behaviour of concrete at high strain rates. Mater Struct 24:425–450
3. CEB-FIP (2010) Model code for concrete structures. Design Code, Comité EURO International du Béton, Lausanne, Switzerland, 350 pp
4. Cusatis G (2011) Strain-rate effects on concrete behaviour. Int J Impact Eng 38:162–170
5. European Committee for Standardization (2006) BS EN 1992: Part 3. Design of concrete structures. Liquid retaining and containing structures. UK, British Standards Institution
6. European Committee for Standardization (2009) BS EN 12390: Part 3. Testing hardened concrete. Compressive strength of test specimens. UK, British Standards Institution
7. Othman HAB (2016) Performance of ultra-high performance fibre reinforced concrete plates under impact loads. Ph.D. thesis, Ryerson University
8. Ross C, Tedesco J, Kuennen S (1995) Effects of strain rate on concrete strength. ACI Mater J 12:37

New Cementitious Materials for Sustainable Construction

Hassan Al-Nageim and Monower Sadique

Abstract The paper reports the mechanical and physical properties of new hydraulically bound cementitious materials made from environmentally friendly waste fly ash and chemical additives. The new products can be used for cement replacement material and need no burning process as the case with conventional cement manufacturing process. Two fly ashes generated from incineration of domestic and industrial wastes were blended and optimized to generate a new ternary blended cementitious material. The developed blended formulation showed versatility in terms of offering different grade mortar having properties like conventional cement. The early strength was comparable to the control mortar, but after the age of 14 days and in the new products, the crushing strength rate is higher than the crushing strength rate produced using ordinary Portland cement mortar. The influence of water content, alkali activation, synthesis by water dispersing agent has also been analyzed in addition to the new material compressive strength.

Keywords Alkali activation · Cementitious materials · Compressive strength · Fly ashes · XRD analysis

1 Introduction

In the process of manufacturing cement, intensive energy is used during the quarrying, heating, and crushing the materials to the required particle size. This creates a negative environmental impact. In 2016, 7.3 million ton CO_2 has been released by cement industry (Statistics on Emissions in the United Kingdom (UK)) [1]. The enormous CO_2 output from cement manufacturing process makes this industry as one of the top sources for greenhouse gases among other manufacturing industries. To reduce

H. Al-Nageim (✉) · M. Sadique
Department of Civil Engineering, Liverpool John Moores University, Liverpool, UK
e-mail: H.K.Alnageim@ljmu.ac.uk

M. Sadique
e-mail: M.M.Sadique@ljmu.ac.uk

S. Kumar Shukla et al. (eds.), *Advances in Sustainable Construction Materials and Geotechnical Engineering*, Lecture Notes in Civil Engineering 35,
https://doi.org/10.1007/978-981-13-7480-7_22

the energy consumption and CO_2 emission, at burning stage, natural pozzolana, steel slag, and limestone have been used by cement manufacturers for a long time. According to cement technology road map [2], one of the four identified technologies to minimize carbon emission was clinker substitution. BS EN 197-1:2000 describes the common 27 types of cement with mineral additives such as blast furnace slag (BFS), pulverized fuel ash (PFA), burnt shale (BS), and silica fume (SF). Irrespective of the mineral in addition to cement clinker, the specification allows in the range of 6–55% of clinker replacement. Based on 2006 GNR (getting the numbers right) data, globally 500 million tonnes of clinker substituting materials has been used for 2400 million tonnes of cement produced [2]. For lower reactivity, the supplementary materials were synthesized by OPC, and as a result, bulk utilization of the same was hindered.

In this study, a new hydraulically bound cementitious material made from environmentally friendly waste fly ash has been developed which offers analogous physical and chemical properties with cement and also shows strength development characteristics throughout the hydration process.

2 Materials Used in This Research Work

In this research study, the following materials have been used;

1. Fly Ashes: Biomass fly ash rich of CaO and fly ash with low contents of CaO named as FA1 and FA2, respectively.
2. Liquid sodium hydroxide alkali waste with less than 8% NaOH in water.
3. Dry silica fume and slurry silica fume, SF. With SF: water ratio of slurry was 50:50.
4. Gypsum (FGD) or commercially named flue gas desulfurization gypsum is the most widely used system in coal-fired power plants for removal of emitted sulfur. The process uses lime to absorb sulfur and produce GFD gypsum by-product. FGD has been collected from a coal-fired thermoelectric power plant.
5. Portland composite cement type CEM-II/A/LL 42.5-N. Used as a control cement for comparison with the new produced secondary cementations materials in this research work. As per the BS EN specification, this type of cement contains 6–20% limestone.
6. Sand: Local sand passing through 2-mm sieve has been used.

3 Physicochemical Activation of FA1 and FA2

Physical activation was achieved by grinding the fly ash in a laboratory using 1 horsepower grinder with a capacity of 2.5 l. The grinding was performed on the individual waste fly ash at the rate of 270 gm/batch for 15 min. About 5% FGD gypsum was added as grinding aid.

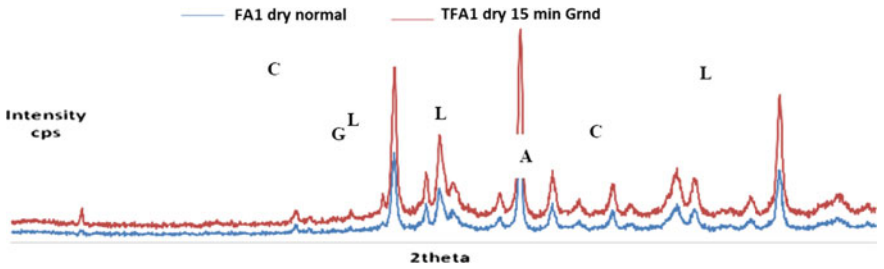

Fig. 1 XRD profile of FA1 before and after grinding XRD analysis (lime—L, calcite—C, anorthite—A, gehlenite—G)

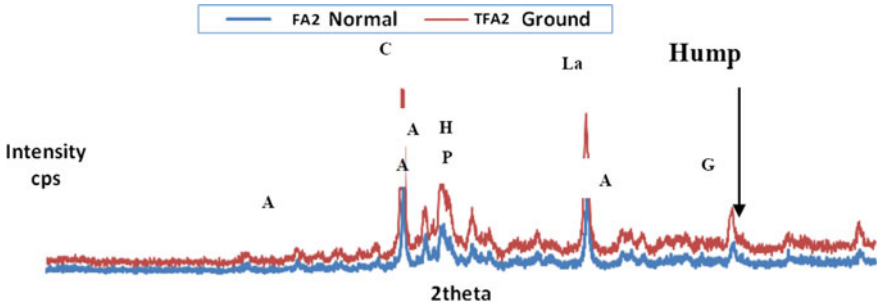

Fig. 2 XRD profile of FA2 before and after grinding (calcite—C, arcanite—A, larnite—La, hematite—H, perovskite—P, gypsum—G)

Particle size reduction due to elastic and plastic deformation of material during grinding is of obvious and mechanochemical amorphization. As a result, the XRD patterns show bands and humps rather than sharp lines and peaks, respectively [3]. As shown in Fig. 1, the hump and broadening of peaks for 15-min grounding (at the rate of 250 gm/batch with 5% FGF gypsum as grinding aid) of treated fly ash FA1 (TFA1) and treated TFA2 indicate its increase in amorphousness. Similar phenomena in terms of amorphousness of FA2 particles with the same charging rate in mortar pestle grinder has been identified in XRD analysis as shown in Fig. 2. Comparing the particle size distribution (PSD) of grounded materials, it can be recognized that the PSD of the new materials termed as HSC-3 approximately coincides with those of OPC. The change in this microstructural level can also be recognized in SEM view of the undisturbed and grounded materials in Figs. 4 and 5. The coagulation of very fine nanoparticles of silica fume (SF) is responsible for showing coarser PSD as shown in Fig. 3.

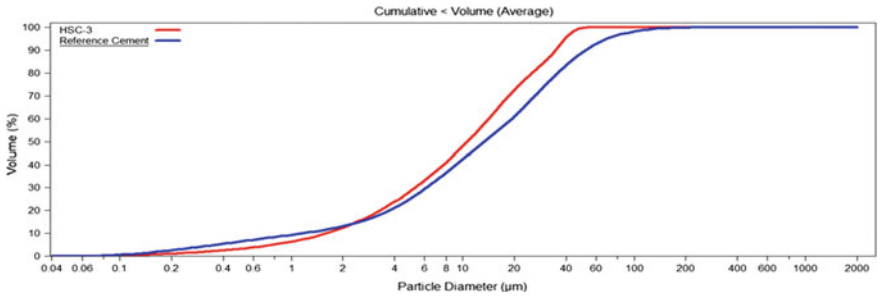

Fig. 3 PSD of the new materials, HSC-3, compared with reference cement OPC

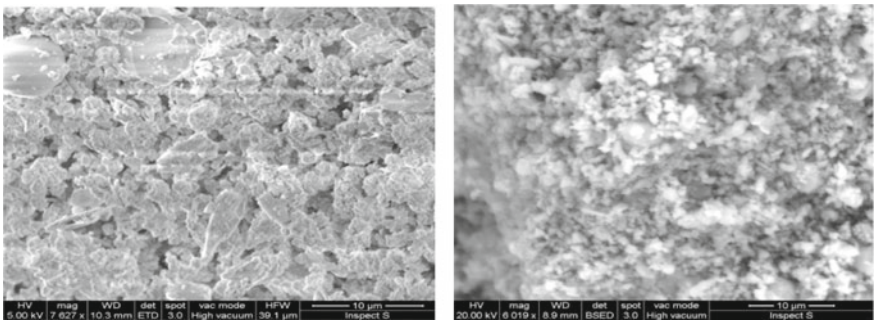

Normal TFA1Grounded

Fig. 4 SEM of normal and grounded TFA1

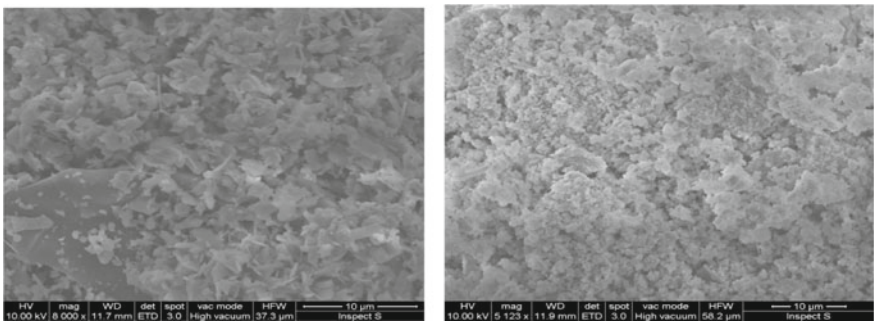

Normal FA2 Grounded TFA2

Fig. 5 SEM of FA2

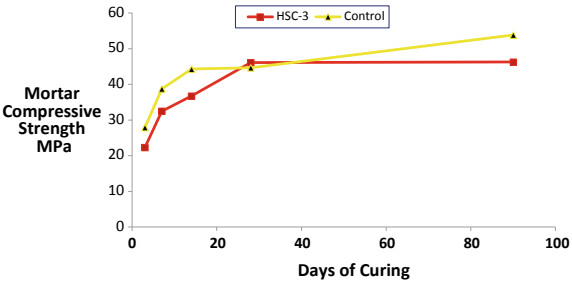

Fig. 6 Mortar compressive strength of HSC-3 compared with control mix

4 Blending—Developing LJMU Cementitious Material

A mix proportion for tertiary blended mixtures containing mechanically activated TFA1 and TFA2 in association with SF based on the analysis of blended of 3 part of TFA1 to one part by volume of TFA2 with 20% silica fume of the total weight was producing very good results as can be seen in Fig. 6. This cement, which has no OPC cement, was termed as LJMU-HSC-3, shows progressive strength gaining with respect to control paste confirms the increasing trends of pozzolanic reaction.

The figure also shows that the mortar containing the new cementitious materials possesses comparative crushing compressive strength to the mortar made from Portland composite cement type CEM-II/A/LL 42.5-N. Also interestingly, at age 3–28 days of curing at normal room temperature, the rate of crushing compressive is higher than the rate of gain of the control mortar at this early stage of strength development.

5 Conclusions

A new method of activating FA1 with FA2 and SF has been reported through this study. The characterization of undisturbed candidate waste materials and improvement in terms of higher reactivity through chemical and mechanochemical activation process has been confirmed by analyzing particle size distribution, powder diffraction pattern, microstructural, and thermal analysis of hydration product. The PSD, SEM, XRD analysis, and strength development profile and failure under the load of the developed composite blend show very similar characteristics with conventional cement. The method for producing the new cementations materials named as LJMU-HSC3 required no burning of the raw materials, low grinding energy, and minimum waste alkali activation. The new product can produce 86% cube compressive strength of OPC control mix. Based on this research study, following key findings could be summarized:

- The potentiality for supplementary cementitious material of FA1, FA2, FGD, and SF is promising,
- FA1, SF, and waste NaOH can be used for increasing the reactivity of FA1,
- FGD gypsum not only acts as grinding aid but also contributes toward strength development,
- Blending among the selected materials not only provides the analogous chemical composition of OPC but also shows remarkable reactivity during hydration.

Thus, a new method of producing supplementary cementitious materials with bulk usage of waste streams has been proposed through this study. The method will not only reduce the utilization of natural minerals and fossil fuel but also the omission of burning process (up to 1450 °C during OPC production) will drastically reduce CO_2 emission. Following issues have been scheduled for further development of the product:

- Optimization of the blending matrix
- Production of different grade strength mortar by optimized mix design
- The expansion, leaching, and freezing and thawing effect on the hydrated material of the proposed product.

References

1. United Kingdom (2016) Office for national statistics (UK), (2016) Ricardo-AEA; 1990 to 2016 UK emission statistics
2. WBCSD (2009) Cement technology roadmap 2009, carbon emissions reduction up to 2050. World Business Council for Sustainable Development and International Energy Agency, 2009, Paris
3. Juhasz ZA (1998) Colloid-chemical aspects of mechanical activation, Particulate Science and Technology

Influence of Texture on Mechanical Behaviour of Basalts

P. S. K. Murthy, Sukhdev Singh and S. L. Gupta

Abstract To understand the influence of texture on the mechanical behaviour of basalt, four variants each of vesicular basalt, four variants of amygdular basalt and two variants of porphyritic basalt were investigated in the laboratory. These basalts were obtained from different site locations of the Betwa River basin in central India. These basalts were investigated for uniaxial compressive strength, indirect tensile strength and shear strength parameters (cohesion and angle of internal friction). In addition to the above, wave velocities (compressive and shear), durability and density characteristics were also studied. And, mode of failure of basalts in compression has been discussed. The mineralogical composition of basaltic variants was quantified through an X-ray diffraction method. In comparison, vesicular basalts were inferior in all properties and parameters. And, it was observed that the failure propagated in vesicular and amygdular basalts along the chain of vesicles, whereas in porphyritic basalts, the failure is along the grain boundaries of phenocrysts.

Keywords Texture · Basalt · Laboratory study · Central India · Mode of failure

1 Introduction

Basalt is an igneous rock (extrusive type, occurs on or above the earth's surface) formed due to solidification of magma. It is generally formed as massive with 45–55% SiO_2; it has a high content of Fe, Mg, Ca and less of K and Na. Under different atmospheric conditions, basalt typically exhibits different textures. Texture depends mainly on crystallinity, granularity, shape of minerals and mutual relations of mineral grains. In some variants, small cavities are formed by the expansion of bubbles of gas or steam during solidification of the volcanic rock. Several researchers have observed that the strength of vesicles in basaltic flows was considerably affected by their porosity [1, 2]. These vesicles were sometimes filled by secondary minerals like calcite,

P. S. K. Murthy (✉) · S. Singh · S. L. Gupta
CSMRS, New Delhi, India
e-mail: pskmryiitd@gmail.com

S. Kumar Shukla et al. (eds.), *Advances in Sustainable Construction Materials and Geotechnical Engineering*, Lecture Notes in Civil Engineering 35,
https://doi.org/10.1007/978-981-13-7480-7_23

quartz or olivine depending on groundwater chemistry and underground physical conditions [3]. These are called amygdules. Another texture generally observed in basalts was porphyritic texture, in which large crystal or phenocryst was surrounded by fine-grained mass.

The knowledge of rock including its strength, deformation behaviour and their failure characteristics is important in geotechnical engineering. The textural differences in basalts greatly affect the geotechnical properties and parameters [4]. Hence, an attempt was made in the present study to understand the mechanical behaviour of three texturally varied basalts such as vesicular (VB), amygdular (AB) (with secondary mineral fillings) and porphyritic (PB) textures along with their failure characteristics. All the variants were collected from the Betwa River basin of central Indian region. The basaltic flows of these locations belong to Malwa Group of the Deccan trap complex comprising low lying hills, hill clusters, valleys and extensive plains.

2 Experimental Work

To meet the objective, four variants of vesicular basalt, four variants of amygdular basalt and two variants of porphyritic basalts collected from the Betwa basin of central India were investigated for uniaxial compressive strength, indirect tensile strength and shear strength parameters. X-ray diffraction (XRD) studies were performed to assess the minerals in the variants of basalt, to delineate the influence of intrinsic properties on the mechanical behaviour of basalt. Using CuKα radiation ($\lambda = 1.5404A°$), the representative powdered sample of rock is used for quantification of minerals. Figure 1 shows the diffraction patterns of vesicular basalt, amygdular basalt and porphyritic basalt (relative intensity vs. 2 THETA). Table 1 shows average mineral compositions of all variants of basalt.

For holistic analysis, physical, durability and wave velocity characteristics were also evaluated. All the investigations were carried out in saturated condition duly applying the procedures suggested by International Society of Rock Mechanics [5]. The test specimens were prepared for different sizes in regular shapes using cutting,

Table 1 Average chemical composition of basalts

Mineral	Au	Alb	O	La	Q	Ma	I	Mo
VB (%)	27.1	38.4	2.0	23.6	ND	ND	6.5	2.4
AB (%)	26.5	36.2	12.2	17.6	4.5	ND	2.5	0.5
PB (%)	40.5	18.8	22.7	8.5	6.2	3.3	ND	ND

Au augite, *Alb* albite, *O* olivine, *La* labradorite, *Q* quartz, *Ma* magnetite, *I* illite and *Mo* montmorillonite
ND Not detected

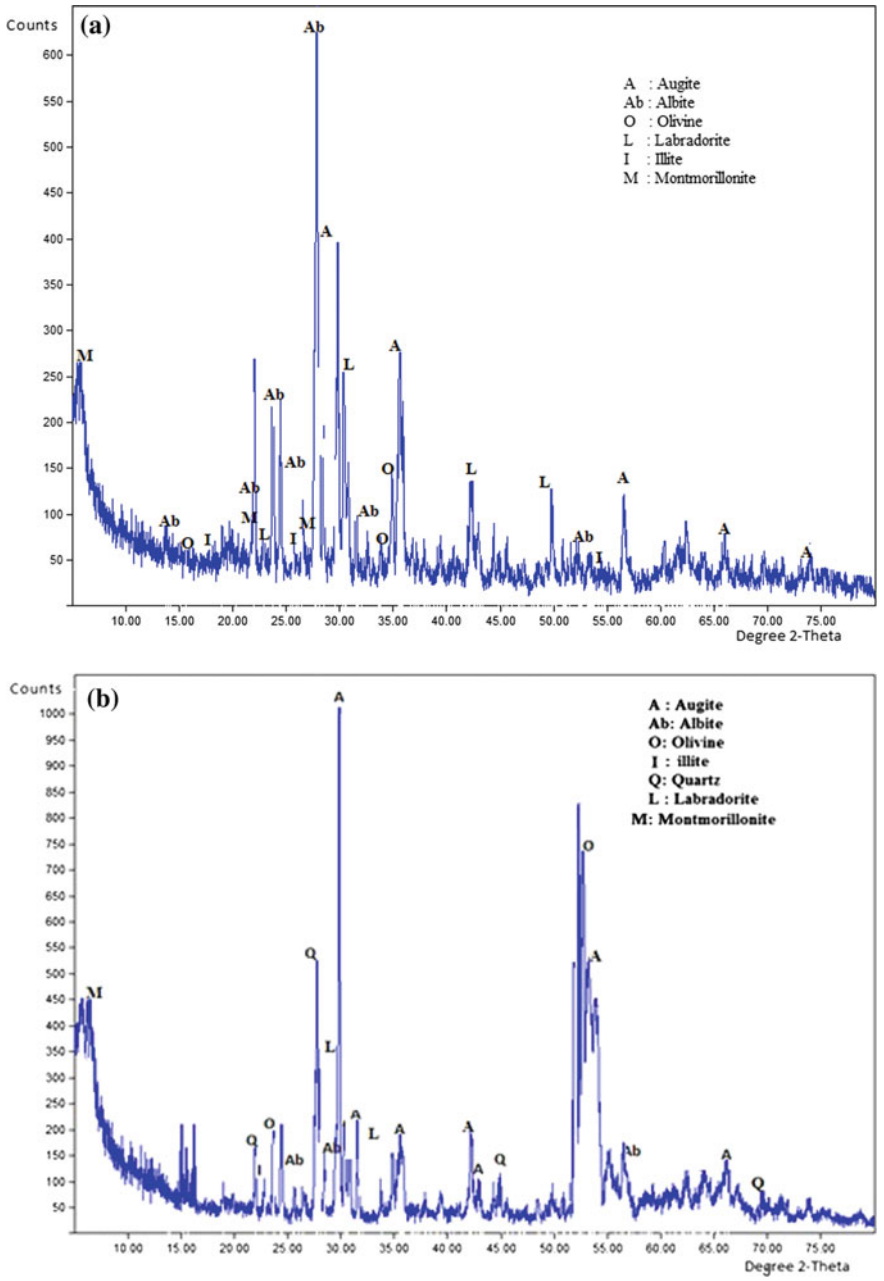

Fig. 1 Diffraction patterns for **a** vesicular basalt, **b** amygdular basalt and **c** porphyritic basalt

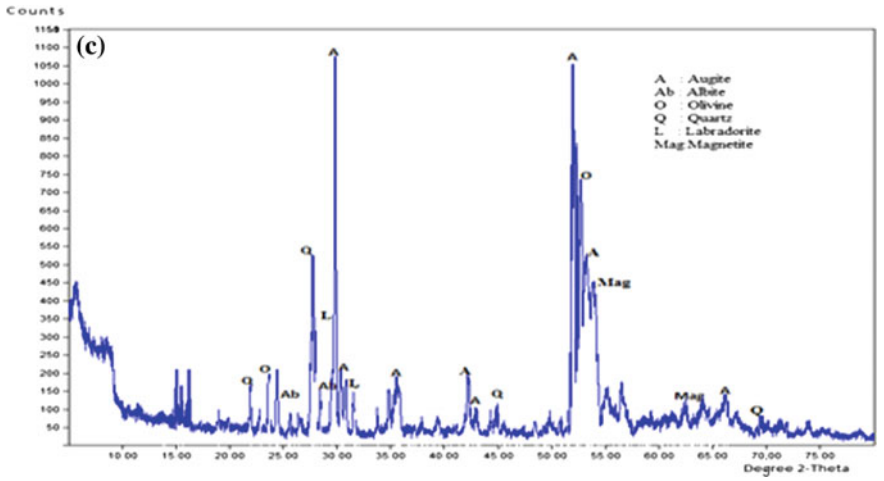

Fig. 1 (continued)

polishing rock cores. And, it was ensured that the dimension of the prepared specimens was within the tolerance limits suggested by ISRM [5]. Rock samples were saturated by immersing in water and applying a vacuum not less than 800 Pa for a period of at least one hour.

The results were discussed under the following major categories: (i) physical and durability properties, (ii) waves' velocities and (iii) mechanical behaviour and mode of failure. The uniaxial compressive strength (UCS) was evaluated for NX size cylindrical cores with length-to-diameter ratio of 2.5, under statically applied compressive load. The indirect tensile strength was assessed employing Brazilian test, and the NX size saturated specimens, with length-to-diameter ratio of 0.5, were tested under static loading. In Brazilian test, the loading is compressive. But, the failure takes place under tension because of the experimental fact that most of the rocks in biaxial stress fields fail in tension at their uniaxial tensile strength when one principal stress is tensile and the other finite principal stress is compressive with a magnitude not exceeding three times that of the tensile principal stress. The shear strength parameters, i.e. cohesion (c) and angle of internal friction (Φ) for three variants of basalt, were evaluated using conventional triaxial compression as per ISRM [5]. For triaxial compression test, Hoek cell was employed, and the saturated specimens, with length-to-diameter ratio of 2, were tested over the desired range of confining pressure 3–10 MPa. For all the samples tested in uniaxial compression, waves' velocities were evaluated, namely compression wave velocity and shear wave velocity. These were evaluated both in dry and saturated states also by employing two piezoelectric crystals of 200 and 33 kHz frequency for compression and shear wave, respectively. These velocities help in understanding scatter in the data and arriving at a representative value of parameters. Hence, velocities were evaluated for the samples subjected to the uniaxial compressive test.

3 Results and Discussion

3.1 Physical and Durability Properties

Figure 2 shows the variation of densities (dry bulk density, saturated bulk density and grain density) for three textures of basalt. It was observed that vesicular basalts have resulted in low densities both in dry and saturated conditions. In the case of amygdular basalts with the addition of secondary mineral fillings, these densities have increased substantially. However, in respect of grain content, there was marginal variation among the three textures. Due to phenocrysts in porphyritic basalts, an increase in grain density can be observed.

Figure 3 shows the variation of water content (at saturation) and apparent porosity in three textures of basalt. The retention capacity of water in vesicles (interconnected) was high. As such, water content at saturation in vesicular basalts was marginally higher (1.5–5%) than amygdular basalts (0.5–5%). Similar to water content, the variation in vesicular basalts resulted in higher apparent porosity (4–14%) than the rest of other textures.

Durability. Figure 4 shows the variation of slake durability indices (SDI) of three variants of basalt subjected to two cycles. It was observed that alteration of mineral fillings during the process of slaking has resulted in a substantial reduction in durability index of amygdular basalts. For VB and PB, the reduction in SDI was marginal.

3.2 Waves' Velocities

From Fig. 5, it was observed that the velocity data values (both compressive and shear) for VB were lower than AB and PB. And, most of the samples in vesicular basalts have shown the reduction in waves' velocities on saturation (Fig. 6). Normally, all rocks exhibit increase in waves' velocities on saturation [6, 7]. It was inferred that

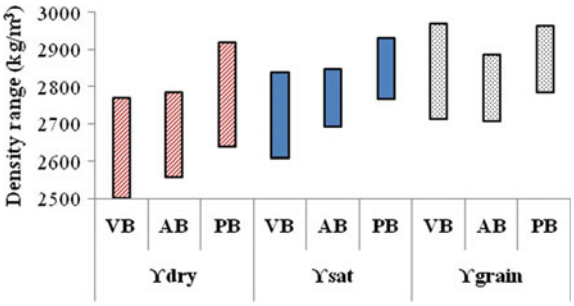

Fig. 2 Variation of densities

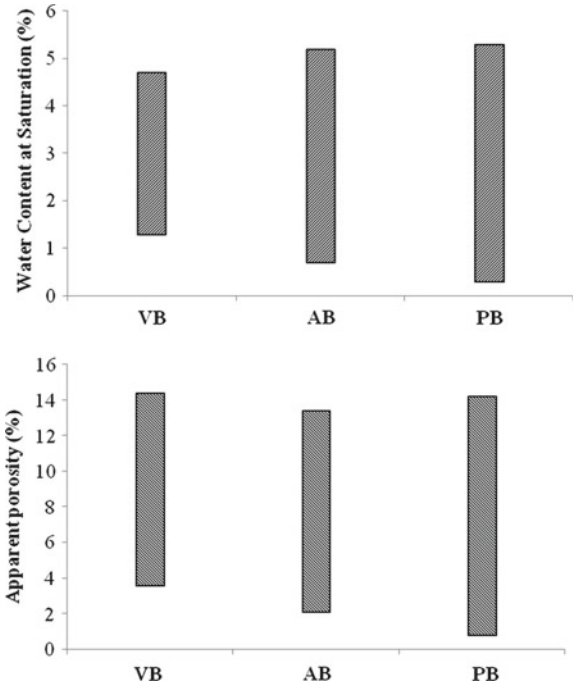

Fig. 3 Variation of water content at saturation and apparent porosity

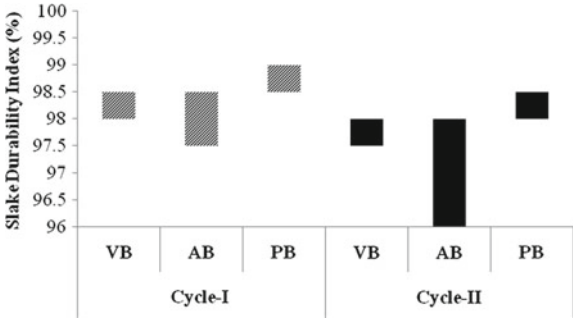

Fig. 4 Variation of durability indices

the marginal reduction in waves' velocities of VB was possibly due to alteration of clay mineral fillings on water saturation.

3.3 Mechanical Behaviour

Uniaxial compressive strength. It was observed from Fig. 7 that vesicular basalts were failed much lower strengths than the rest of variants of basalt possibly because of a vesicular structure. Most of the samples failed along the periphery of vesicles,

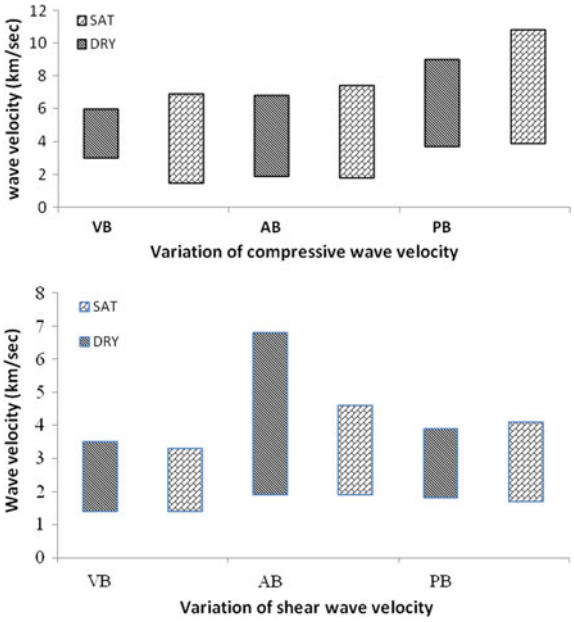

Fig. 5 Variation in waves' velocities (in dry and saturated states)

Fig. 6 Variation in waves' velocities in VB

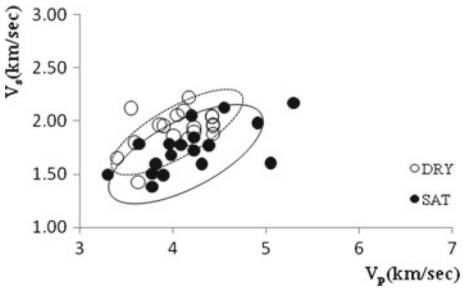

Fig. 7 Variation in UCS

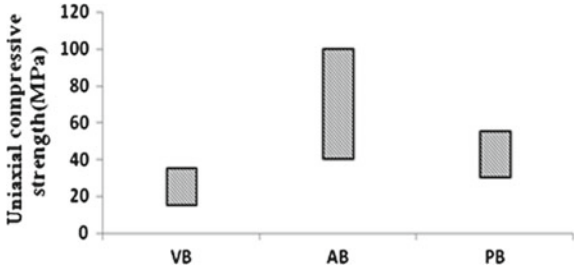

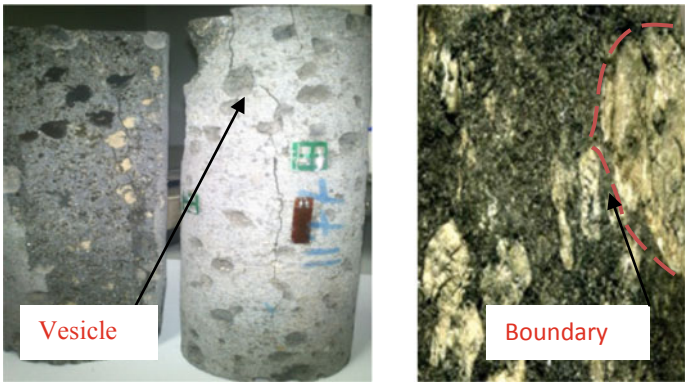

Fig. 8 Failure pattern of VB and PB in uniaxial compression

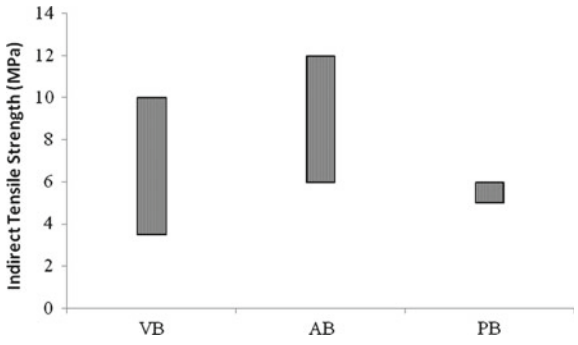

Fig. 9 Variation of indirect tensile strength in Brazilian test

and propagation of failure is along the chain of vesicles (Fig. 8). In the case of amygdales, secondary mineral fillings improve in much more compact rock and that has resulted in higher strengths than the rest of the variants. Hence, it can be inferred that as the amount of vesicles and foreign materials in basalt decreases, the responses of vesicular basalt approach that of massive basalt.

It can be observed that the strength of porphyritic basalt much lower than amygdular basalt. Porphyritic texture in volcanic rocks like basalt formed when slow cooling of magma is followed by faster cooling, resulting in the formation of a large crystal or phenocryst, surrounded by fine-grained mass. As such, in porphyritic basalts, failure was initiated and propagated along the boundaries of phenocrysts, resulting in lower strength than amygdular basalts.

Indirect tensile strength. Similar to UCS, vesicular basalts have failed (Fig. 9) at lower strengths than the other variants of basalt. In addition to the existence of vesicles over the surface area of rock cores, the clay minerals played a greater role in reducing the bond between rock's constituents. This has resulted in a reduction in strength of vesicular basalts on saturation.

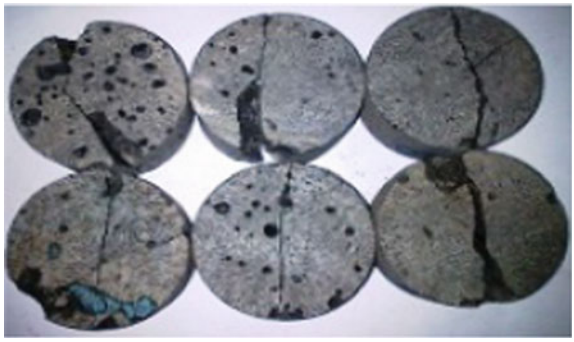

Fig. 10 Failure patterns of VB in Brazilian test

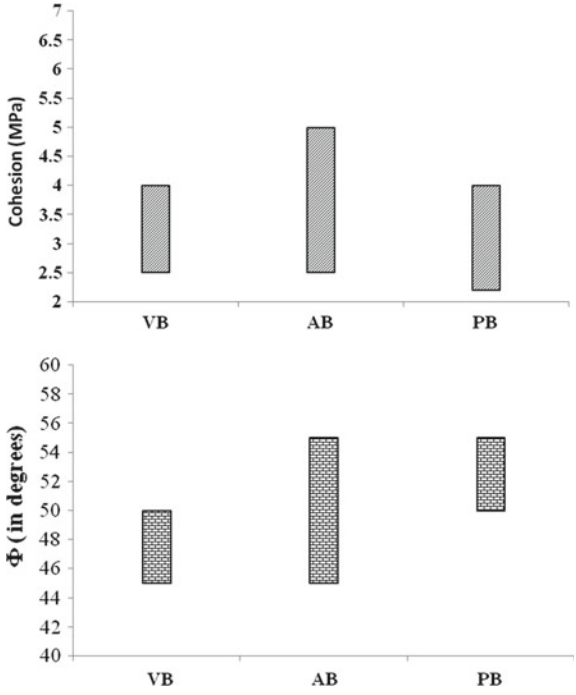

Fig. 11 Variation of cohesion and Φ under triaxial test

Figure 10 shows the mode of failure of vesicular basalts in Brazilian test. Similar to UCS, in Brazilian test also, vesicular basalts have failed along the periphery of vesicles. Moreover, the variation in data was substantial compared to porphyritic basalt. However, the detrimental effect of strength on saturation due to the existence of clay minerals in vesicular basalts cannot be ignored in the present case also.

Shear strength parameters. Figure 11 shows the variation of shear strength parameters, i.e. cohesion (c) and angle of internal friction (Φ) for three variants of basalt. The confining pressure was selected in the range of 3–10 MPa. In view of scatter in triaxial data, for all the variants upper and lower bound curves were plotted,

Fig. 12 Failed sample of VB under triaxial test

and the tangents drawn to these curves were considered to represent the range of shear strength parameters for the selected variant. The mode of failure of vesicular basalts under triaxial compression is shown in Fig. 12. Similar to UCS, cohesion in VB and PB was lower compared to AB. And, angle of internal friction in porphyritic basalts was higher than vesicular basalts. It is inferred that the presence of harder minerals such as augite, albite and labradorite in higher proportion has contributed to a higher angle of internal friction in PB than VB.

4 Conclusions

In the present study, the influence of basaltic textures (vesicular, amygdular and porphyritic) on its mechanical behaviour was investigated in the laboratory. Based on the results, it is inferred that

- The presence of vesicles in basaltic rocks has drastically reduced the strengths (UCS, indirect tensile strength, shear strength) in vesicular basalts. However, in amygdular basalts, due to secondary mineral fillings (olivine, calcite) in the vesicles, the strengths were increased substantially.
- On slaking, the reduction in durability indices observed.
- Most of the vesicular basalt samples were failed along periphery of vesicles, and the propagation of failure was along the chain of vesicles. In the case of porphyritic basalts, the strengths were reduced due to the failure of samples along the boundary of phenocrysts.
- Also, on saturation, the reduction in waves' velocities was observed in vesicular basalts possibly due to alteration of clay fillings with water.

Acknowledgements The authors are grateful to Director, CSMRS, for granting permission to publish this self-sponsored work. We thank our co-workers in CSMRS's Rock Mechanics Laboratory for their help during laboratory works. The cooperation of authorities in making available the rock samples is highly appreciated.

References

1. Saar MO, Manga M (1999) Permeability and porosity relationship in vesicular basalts. Geophys Res Lett 26(1):111–114
2. Bishop CW (1991) Hydralic properties of vesicular basalts. MS Thesis, University of Arizona
3. Abdullah H, Murthy PSK (2013) Laboratory study of four basalts. Water Energy Int, CBIP 70(3):48–56
4. Al-Harthi AA, Al-Amri RM, Shehata WM (1999) The porosity and engineering properties of vesicular basalt in Saudi Arabia. Engg Geo 54:313–320
5. Ulusay R, Hudson JA (2007) The blue book: the complete ISRM suggested methods for rock characterization, testing and monitoring
6. Abdullah H, Dhawan AK, Bandyopadhyay A (1999) Use of waves' velocities in laboratory investigation of rock. Proc. IGC-9, Calcutta, pp 20–23
7. Abdullah H, Murthy PSK (2013) Laboratory study of four basalts. Proc. Tunneling Asia' 2013, Delhi, pp 207–219

Experimental Investigation to Study the Properties of Concrete Incorporated with GGBS and GBS

Uday Bhanu Chakraborty, Sanjeev Bajaj and Sandeep Dhanote

Abstract In the present study, mix design ingredients viz. water, cement, ground granulated blast-furnace slag (GGBS), aggregate (fine and coarse), ground blast-furnace slag (GBS) and chemical admixture were collected, tested and the findings are presented in this paper for Joda and Khondbond Iron Mines Expansion Project, Orrisa for Tata Steel Limited. Tata Steel Group is implementing ground granulated BF slag (GGBS + GBS) in its entire construction project sites after preparing a proper mix design. Compatibility (complex interaction between cement [1–3] and chemical admixtures [4]) may be issued because of the large variation of fine contents during the trials. Due to incompatibility between cement and chemical admixtures, concrete may face various problems during the concreting works viz. late setting of concrete, fast slump loss/moisture loss, inadequate strength increase, cracking, etc. These problems may affect the properties of fresh and hardened concrete viz. primary strength and durability. Compatibility between GGBS blended cement and chemical superplasticizer (IS: 9103) was confirmed by Marsh cone test. Considering the compressive strength of cement mortar, setting time of concrete, workability, compressive strength and durability (measured in terms of rapid chloride penetration test (RCPT)) and the mix design for M30 grade of concrete were prepared with 40% replacement of cement by GGBS and 25% replacement of sand by GBS. During the course of trials/study, the main objective was to find the effect of fines (GGBS + GBS) content on the properties of concrete. Many research papers have been published pertaining to GGBS utilization/properties but GGBS + GBS concrete is rarely seen after recent advancement in IS 383 pertaining to the uses of aggregate from unconventional sources.

Keywords GGBS · GBS · Compatibility · Split tensile strength · Flexural strength · Ultrasonic pulse velocity · Activity index

U. B. Chakraborty (✉) · S. Bajaj · S. Dhanote
Central Soil and Materials Research Station, Government of India, New Delhi 110016, India
e-mail: uday401133@rediffmail.com; ub.chakraborthy@gov.in

S. Kumar Shukla et al. (eds.), *Advances in Sustainable Construction Materials and Geotechnical Engineering*, Lecture Notes in Civil Engineering 35,
https://doi.org/10.1007/978-981-13-7480-7_24

1 Introduction

In the world, there are numbers of significant structures that were made from a combination of Portland cement and GGBS. Some examples are World Trade Centre at New York (40% replacement of OPC), Three Gorges Dam in China (40% replacement of OPC), Detroit Metro Airport Terminal Expansion at Michigan, etc. (40% replacement of OPC). In various national and international journals, it was established that GGBS can be a sustainable and cost-effective material. The behaviour of GGBS and GBS blended concrete in various proportions has been reported by number of researchers viz [5–8]. They concluded that GGBS increases the compressive strength, workability and durability of the concrete and also significantly reduces the carbon footprint.

In the present research, GGBS was used as a partial replacement of ordinary Portland cement (OPC) in varying ratio of 0–70% for preparing a suitable concrete mix. From the various studies, it was found that concrete made with GGBS is stronger, durable and eco-friendly.

Following are the benefits of using GGBS in partially replacing ordinary Portland cement:

1. Concrete made with a mix of GGBS and OPC sets slowly as compared to concrete made by using only OPC.
2. Due to the lower heat of hydration and low temperature rise, this concrete can be used in mass concrete works.
3. Structure damages due to alkali–silica reaction (ASR) significantly reduces.
4. GGBS provides higher resistance from chloride attack,thereby reducing the risk of reinforcement corrosion.
5. Provides a low strength in early age and higher strength in later stage.
6. GGBS provides a cohesive mix due to its finer particle size and therefore permeability of concrete reduces.
7. Due to the crisis of natural virgin construction material like river sand, GBS can become a suitable alternative material.

2 Chemical Composition of GGBS and GBS

The chemical compositions of blast furnace slag are CaO, SiO_2, Al_2O_3 and MgO [9]. Out of these components, Cao is mainly responsible for enhancing of compressive strength. Therefore, increasing the CaO content in the slag, compressive strength of the concrete wall can be increased.

Granulated blast-furnace slag (GBFS) to be used as partial replacement of sand should conform the requirement given in Table 1 as per IS: 12089 and the chemical composition of GBS and GGBS should be same.

Additionally, granulated blast-furnace slag should also conform the requirements as mentioned in Table 2, as per IS: 383 [10, 11].

Table 1 Requirement of GGBS

Constituents	Limits (%)
Manganese oxide, percent, max	5.5
Magnesium oxide, percent, max	17.0
Sulphide sulphur, percent, max	2.0
$(CaO + MgO + 0.33Al_2O_3)/(SiO_2 + 0.67Al_2O_3)$	1.0
$(CaO + MgO + Al_2O_3)/SiO_2$	1.0
Insoluble residue, percent, max	5.0
Glass content, percent, min	85

Table 2 Additional requirements of GBS

Characteristics	Limits
Total alkali content as Na_2O equivalent, percent max	0.3
Total sulphate content as SO_3, percent max	0.5
Acid soluble chloride content, percent max	0.04
Water absorption, percent max	5
Specific gravity	2.1–3.2
Calcium oxide as CaO, percent, max	45
Total sulphur as S, percent, max	2.0
Total iron as FeO, percent, max	3.0

3 Results and Discussions

In the present study, replacement of GGBS by cement varies from 0, 20, 30, 40, 50, 60 and 70%, whereas GBS remains constant, i.e. 25% replacement of sand. Accordingly, all ingredient changes as per the IS: 10262 mix design process [12–15]. In this present study, Portland slag cement (PSC) [16–21] with 25% of GGBS was tested separately and the same was compared with GGBS blended with OPC.

It is a well-known fact that on altering the volume of GGBS/fine content, the properties of cementious material viz. setting time, activity index and compressive strength change. In the second phase, the properties of fresh concrete were observed by its workability, bleeding and segregation and setting time. The compressive strength of concrete was observed by casting large numbers of concrete cubes with varying proportion of GGBS, GBS and other ingredients in the mix design. The same were tested in laboratory and the results are also presented in. During trials, following tests were conducted:

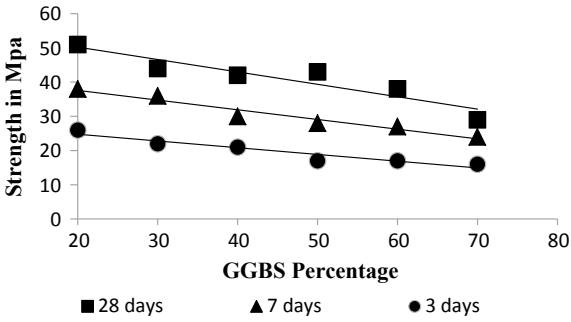

Fig. 1 Compressive strength of cement mortar

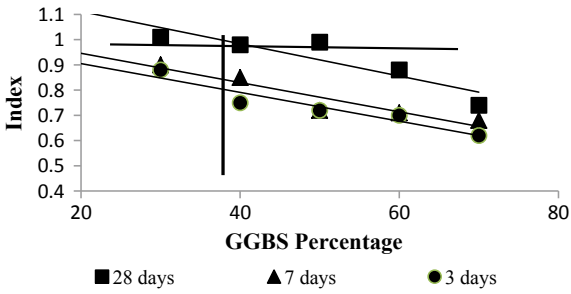

Fig. 2 Activity index of cement mortar w.r.t PSC

3.1 Cement Mortar Tests

3.1.1 Compressive Strength of Cement Mortar

Figure 1 shows that strength of OPC + GGBS cement mortar decreases with increase in GGBS replacement. As per IS4031 Part6, cement: standard sand 1:3 (by weight) mix was prepared and water content $\left(\frac{P}{4}+3\right)\%$ of combined weight of cement and sand where p stands for normal consistence.

3.1.2 Activity Index of Cement Mortar w.r.t Reference PSC

Activity index of OPC + GGBS cement mortar is determined as the ratio of cube strength of OPC + GGBS cement mortar to the strength of reference PSC 28 days cement mortar strength.

Up to 38% GGBS, the 28 days strength of OPC + GGBS cement is higher than the 28 days strength of reference PSC. 3 days and 7 days strength of OPC + GGBS cement is always lower than the strength of reference PSC at the same period as shown in Fig. 2.

Fig. 3 Slump test

3.2 Concrete Fresh Properties (Checks/Tests)

3.2.1 Bleeding of Concrete

GBS/GGBS is fine glassy and dense surface material. The water absorption capacity of GBS/GGBS is lesser than natural and manufactured aggregate and Portland cement. Therefore, extra/free water may rise at the surface of the concrete. In this study, it was observed that up to 40% replacement of OPC by GGBS + 25% replacement of fine aggregate by GBS concrete does not exhibit any bleeding characteristic but due to excess vibration or rotation it may have occurred.

3.2.2 Slump Loss

GGBS mix concrete may have shown bleeding characteristic due to its less water absorption capacity. Therefore, during summer, a higher slump loss may occur. To make the concrete workable, higher initial slump should be considered during mix design. Slump test at batching plant and site is shown in Fig. 3.

3.2.3 Setting Time

The setting time of concrete made with GGBS is higher than the same mix design of concrete made with Portland cement. Setting time of concrete will increase by adding of GGBS. The tendency of setting times initially up to 30% is a reduction but above 30%, it increased significantly. The same phenomenon was observed during mix design as shown in Fig. 4. As the batching plant is generally established outside of major project site/city due to area constraints, the lead of transportation of the concrete may increase, resulting concrete get time set if pouring time of concrete exceeds the design mix retention time. GGBS concrete reduces the risk of cold joints during mass concrete pours.

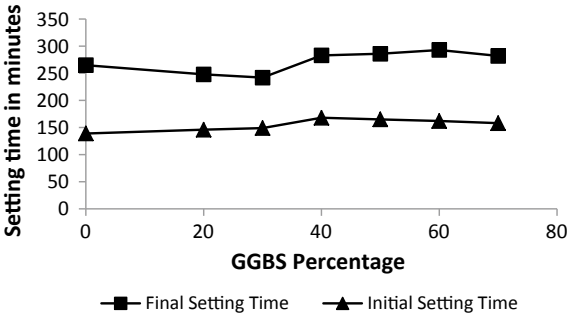

Fig. 4 Strength of cement mortar with % GGBS

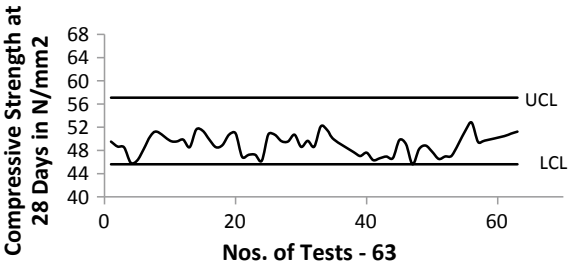

Fig. 5 Statistical analysis of cubes

3.3 Harden Properties (Checks/Tests)

3.3.1 Compressive Strength Test

15 cm × 15 cm × 15 cm size of concrete cubes were prepared (IS: 516 and IS: 1199) using standard cube moulds and the size of cube moulds were in confirmation to the latest Indian standard IS 10086. The cubes were unmoulded after setting and were placed in the curing tank. Compressive strength test was conducted at 28 days by compressive strength testing (CTM) machine under a constant rate of 140 kg/cm^2/min. Total 63 nos. of cubes were tested and are presented in this paper for mix of 40% replacement of GGBS and 25% replacement of fine aggregate. The statistical analysis of cubes test results of the design mix (60% OPC + 40% GGBS + 25% GBS partially replaced by fine aggregate) are shown in Fig. 5.

During compressive strength testing of all mixes from 0 to 70%, it has been observed that compressive strength of concrete up to 40% GGBS and 25% GBS has increased significantly.

3.3.2 Rapid Chloride Penetration Test (RCPT)

To maintain the slump and water–cement ratio for M30 grade of concrete, polycarboxylic ether-based superplasticizers was used with other ingredients of concrete viz. aggregates (IS: 383, IS: 2386, IS 456), cement (IS 455, IS 4032, IS 4634, IS

Table 3 Test results of RCPT

GGBS replacement level in %	Average of RCPT (in coulombs)
0	2196
20	1135
30	834
40	654
50	523
60	450
70	314

Table 4 Test results of split tensile strength

Specimens	GGBS	GBS	Average split tensile strength (N/mm^2)
A0	–	–	2.92
A20	20%	25%	3.19
A30	30%	25%	3.24
A40	40%	25%	3.38
A50	50%	25%	3.47
A60	60%	25%	3.53
A70	70%	25%	3.41

4925, IS 8112: 43 and IS 10262), GGBS and water. Concrete should be checked for chloride permeability whenever there is a potential risk of chloride induced from admixture/cement/aggregate/water or even from the surrounding soils. Seven combinations (by percentage of Cement and GGBS) of concrete were produced, casted and tested for RCPT as per technical standard ASTMC 1202-97and AASHTO T277. The results are tabulated in Table 3.

3.3.3 Split Tensile Strength Test

Splitting tension test was conducted to find out the tensile strength of concrete specimens. A dynamic compression load was applied at a constant rate of approximately 14–21 kg/cm^2/min on the specimen (size 15 cm × 30 cm) diametrically across the circular cross section (c/s). A tensile deformation was induced perpendicular to the loading direction, which may be the reason for tensile failure. The test results are shown in Table 4.

Calculation of split tensile strength of the specimen is as follows:

$$\text{Split tensile strength(MPa)} = \frac{2 \times \text{Max. applied load indicated by testing machine, } N}{\pi \times \text{Length of specimen, mm} \times \text{Dia.of specimen, mm}}$$

Table 5 Test results of Avg. flexural strength

Specimens	GGBS	GBS	Average flexural strength (N/mm^2)
A0	–	–	3.86
A20	20%	25%	4.35
A30	30%	25%	4.37
A40	40%	25%	4.58
A50	50%	25%	4.88
A60	60%	25%	4.74
A70	70%	25%	4.53

3.3.4 Flexural/Bending Strength Test

Concrete is weak in tension due to its brittle nature. Reinforcements are provided in concrete to enhance tensile strength of the concrete structure. Although little dependence laid found on concrete, the developed tensile stresses (due to drying shrinkage, cracks for low cover, cracks for substandard materials, temperature variation, rusting of steel bars or may be other reasons) in concrete are likely to be resisted. Flexural/bending strength was measured of an unreinforced concrete beam of specimen size 100 mm × 100 mm × 500 mm (confirmed by latest IS: 516) by universal testing machine (UTM) as per the technical specification of IS 1199. Specimens were casted, tested and 28th day test results for flexural strength of seven mixes are presented in Table 5.

Calculation of Flexural strength of the specimen is as follows:

$$\text{Flexural strength of beam(MPa)} = \frac{3 \times \text{Max. applied load indicated by testing machine, N} \times \text{Support Span, mm}}{2 \times \text{Width of Specimen, mm} \times \text{Thickness of the specimen}^2,\ \text{mm}^2}$$

3.4 *Ultrasonic Pulse Velocity (UPV) Test*

This test was conducted by Pundit UPV tester. The principle of this test is that by measuring the time of travel of an ultrasonic pulse passing from one transducer to another through the concrete is being tested and presented in this paper. Higher velocities indicate good quality of concrete in terms of density, homogeneity and uniformity. While lower velocities generally indicate that the tested concrete specimen may have the same cracks or voids. The test results are presented in Table 6.

$$\text{Pulse velocity} = \frac{\text{Path length}}{\text{Travel time}}$$

Table 6 Test results of UPV test

Mix	Average ultrasonic pulse velocity results (km/s)	General condition	Quality classification
A0	4.986	Excellent	Very good
A20	4.473	Excellent	Very good
A30	4.576	Excellent	Very good
A40	4.456	Excellent	Very good
A50	4.126	Excellent	Very good
A60	4.268	Excellent	Very good
A70	4.387	Excellent	Very good

4 Conclusion

Compressive strength of cement motor drastically decreases with increase in percentage of GGBS. On replacement of OPC with GGBS up to 38%, the 28 days strength of OPC + GGBS cement is higher than the 28 days strength of reference Portland slag cement (PSC). 3 days and 7 days strength of OPC + GGBS cement was, however, lower than the strength of reference PSC at the same period. Some samples of GGBS mix concrete has shown bleeding characteristic due to less water absorption capacity of GGBS particle. Setting time of concrete mixed with GGBS is higher than the concrete made with Portland cement. Compressive strength of concrete replaced with up to 40% GGBS and 25% GBS has increased significantly. Permeability of concrete decreases with the increase in GGBS content. Split tensile strength increases with the increase in GGBS content. Average flexure strength of concrete increases with the increase in GGBS content. Ultrasonic pulse velocity for all the specimens was found to be excellent and shows no crack or undulations inside the specimens. OPC mixed GGBS has shown higher setting time; therefore, it is that concluded de-shuttering period will be higher for OPC + GGBS concrete. So, the cycle time of concrete will increase. Slump loss is also higher for OPC mixed with GGBS concrete during summer. Therefore, the higher initial slump is to be considered during mix design. During winter, slump loss will be less.

Acknowledgements The author would like to thank Shri. S. L. Gupta, Director, CSMRS, Dr. R. Chitra, Group Head (Soil and RSD), CSMRS and Dr. N. P. Honkanadavar, Division Head (RF and SD) for their continuous support in carrying out the above study. Thanks are also to the staff of rockfill division, CSMRS for their help during the testing.

References

1. IS 269:33 Grade Ordinary Portland cement—specification
2. IS 8112: 43 Grade ordinary Portland cement—specification
3. IS 12269:53 Grade ordinary Portland cement—specification
4. IS 9103: Concrete admixtures—specification
5. Latha KS, Rao MVS, Reddy SV (2012) Estimation of GGBS and HVFA strength efficiencies in concrete with age. Int J Eng Adv Technol (IJEAT), 2(2), ISSN: 2249–8958, Dec 2012
6. Li C, Yoda A, Yokomur T (1998) Pore structure, strength and carbonation of cement pastes containing ground granulated blast-furnace slag. Fly Ash, Silica Fume, Slag and Natural Pozzolana in Concrete, SP 178, American Concrete Institute, Farmington Hills, Mich., pp 875–892
7. Arivalagan S (2014) Sustainable studies on concrete with GGBS as a replacement material in cement. Jordan J Civil Eng 8(3):2014
8. Pavia S, Condren E (2008) Study of the durability of OPC versus GGBS concrete on exposure to silage effluent. ASCE J Mater Civil Eng 20(4), Apr 2008
9. IS 4032: Method of chemical analysis of hydraulic cement
10. IS 383: Coarse and fine aggregates for concrete
11. IS 2386: Methods of test for aggregates for concrete
12. IS 456: Plain and reinforced concrete—code of practice
13. IS 4634: Batch type concrete mixers—method of test—performance
14. IS 4925: Concrete batching and mixing plant—specification
15. IS 10262: Recommended guidelines for concrete mix design
16. IS 455: Portland slag cement—specification
17. IS 12089: Specification for granulated slag for the manufacture of Portland slag cement
18. ACI Committee 233 report, slag cement in concrete and mortar ACI 233R-03 American Concrete Institute, Farmington Hills, March 2003
19. Duos C, Eggers J (1999) Evaluation of ground granulated blast furnace slag in concrete (Grade 120). Rpt. No. FHWA/LA-99/336, Louisiana Trans. Res. Center, Baton Rouge, Louisiana, Oct 1999, 45 p
20. Bijen J (1996) Blast furnace slag cement for durable marine structures. Stichting Beton Prisma, Netherlands
21. Malhotra VM (1987) Properties of fresh and hardened concrete incorporating ground granulated blast furnace slag. In: Malhotra VM (ed) Supplementary cementing materials for concrete. Canadian Government Publishing Centre, Ottawa, pp 291–331

Ground Improvement Using Municipal Solid Waste Ash

Darin Baruah, Shubham Goel, Chandan Gupta and Anil Kumar Sahu

Abstract Municipal solid waste (MSW) is heterogeneous in nature. As lands for disposal are not adequate, solid waste is becoming a major environmental problem. At present, incineration is one of the methods being used in the Ghazipur landfill for the treatment of municipal solid waste. An experimental investigation is performed to understand the effect on the unconfined compression strength of clayey soil mixed with different percentages of municipal solid waste. Usually, clayey soils have low-strength characteristics due to which they are unable to take excessive loads transmitted on them from the foundation structures. The study outlines the influence on the properties of soil and its engineering behaviour when ash is used in different proportions and hence proving it as soil stabilizing material for ground improvement. The tests results demonstrated good improvement in strength of soil and showed that MSW ash can be used for ground improvement. The increase in unconfined compressive strength exceeded 50% as compared to pure soil.

Keywords Municipal solid waste · Ash · Unconfined compressive strength

D. Baruah (✉) · S. Goel · C. Gupta
Department of Civil Engineering, Amity School of Engineering and Technology, Amity University, Noida, India
e-mail: baruahdarin01@gmail.com

S. Goel
e-mail: goelshubham919@gmail.com

C. Gupta
e-mail: cgchandan.gupta27@gmail.com

A. K. Sahu
Department of Civil Engineering, Delhi Technological University, New Delhi, India
e-mail: sahuanilkr@yahoo.co.in

S. Kumar Shukla et al. (eds.), *Advances in Sustainable Construction Materials and Geotechnical Engineering*, Lecture Notes in Civil Engineering 35,
https://doi.org/10.1007/978-981-13-7480-7_25

1 Introduction

The rapid modernization and urbanization are putting more and more stress on our natural resources, as a result of which we are consuming more of our resources and producing much more waste than what we used to produce several years ago. Safe and efficient disposal of waste substances has become a major task. These waste materials tend to degrade our environment and surroundings, thus leading to environmental pollution. The recent landfill failures have highlighted the urgent need for the disposal of municipal solid waste. At present, incineration is one of the methods being used in the landfill for the treatment of municipal solid waste. Every year, a significant amount of municipal solid waste is burned, thus leaving municipal solid waste incinerator ash (MSWI ash) as a by-product. Hence, the ash produced from this waste can be used for various civil building applications and furthermore to improve the quality attributes of soil. The qualities of the MSW ash are dependent on the configuration of municipal solid waste that is burned. Low-quality soils, for example, clayey soils and expansive soils, show unsuitable designing conduct, similar to high shrinkage, high dampness vulnerability, high swell potential and low bearing limit. These low-quality soils can be balanced out utilizing different added substances, for example, cement, lime and pozzolanic ash.

The longevity and firmness of the structures depend mainly on the strata of the soil. Since MSW incinerator ash is a waste material that shows pozzolanic characteristics, it is suggested that we should try to utilize this MSW ash for economical stabilization of poor quality soils.

In the past, several researches have been conducted to incorporate the utilization of the waste materials like fly ash along with several other additives like cement, lime, polyester fibres and bitumen for enhancing the engineering properties of soils. Sivapulliah et al. [1] showed that the pliancy of the black cotton soil decreases, upon the subsequent addition of fly ash. The degree of change relies on the free lime content, particle size distribution and pozzolanic reactivity of fly ash. Mirsa [2] examined the stabilization qualities of clayey soil utilizing class C fly ash and discovered that stabilization attributes are reliant on the soil mineral composition and the plasticity of soil. Temimi et al. [3] examined the impacts of incorporation of fly ash in clayey soil samples. It was concluded that on the addition of fly ash, various mechanical properties of clay got enhanced. Subsequently, properties like settlement and the compressibility decreased, whereas the consolidation increased.

Puppala et al. [4] treated two diverse expanding soils with fly ash and fibre reinforcement, to improve their quality. Both the strategies ended up being powerful in enhancing the unconfined compression strength values of the soils. Some researchers like Erdalcokca [5] and Nalbantoglu [6] conducted experiments and explored the utilization of fly ash (class C) as a soil stabilizer for heaving soils. It was discovered that fly ash was successful in enhancing the plasticity and structure by diminishing the swell potential and plasticity index of the expansive soil.

Prabhakar et al. [7] contemplated various impacts of fly ash upon the strength characteristics of soils. It was found that incorporation of fly ash enhances the bearing capacity, cohesion and shear strength of clayey soils, thus making it an economical soil stabilizer. Phani Kumar and Sharma [8] concluded that by adding fly ash, there was a decrease in swelling potential and plasticity, but strength and dry unit weight increased. Amu et al. [9] examined the potential of stabilization of fly ash and cement mixed with expansive soils. It was concluded that on accumulation of fly ash, the potential of stabilization of cement in expansive soils improved.

Parsons and Kneebone [10] assessed the field performance of fly ash balanced subgrades. It was found in their research that with increment in fly ash content, the soil potency and stiffness increased and a subsequent reduction in swell potential and pliancy was observed. Misra et al. [11] performed experiments on fly ash–clay samples and found that the addition of ash in the samples led to an increase in stiffness and compressive strength, also on the addition of fly ash the California bearing ratio (CBR) values and swell potential improved notably.

Kate [12] explored the likelihood of utilizing the fly ash as a stabilizer for soil with or without utilizing lime. It was found that swelling characteristics diminished as the content of fly ash was increased in the mix; furthermore, the addition of lime made the value changes more significant. Edil et al. [13] performed experiments to stabilize soft fine-grained soils using fly ash and concluded that introduction of fly ash improved the California bearing ratio value as well as the modulus of resilience of the inorganic soils. Senol et al. [14] tried stabilizing soft subgrades using fly ash. The results depicted that incorporation of fly ash improved the unconfined compression strength (UCS) and California bearing ratio (CBR) values of the soil.

Kumar et al. [15] examined the impact of fly ash, polyester fibres and lime on strength characteristics of mainly expanding soils. Zha et al. [16] contemplated how expansive soils react when they are introduced to fly ash. It was seen that when the content of fly ash was raised, the optimum moisture content (OMC) and maximum dry unit weight reduced. Bin-shafique et al. [17] analysed that the capability of fly ash in the long run that led to the stabilization of sub-bases of finely grained soil. It was observed that as fly ash content was raised, the measurements of unconfined compression strength (UCS) of soil samples also improved and led to the reduction of swell potential as well as the plasticity of the soil.

Bose [18] assessed the geotechnical properties when the fly ash was bended with soil. It was found that optimum moisture content (OMC), plasticity and swelling characteristics decreased on the addition of fly ash, whereas maximum dry density (MDD) and unconfined compression strength (UCS) values increased on increasing fly ash content. Sharma et al. [19] examined the usage of fly ash and lime as a clayey soil stabilizer. It was concluded that introduction fly ash and lime led to an increase in the overall strength of the soil sample.

Lin et al. [20] performed a structural study on the influence of fly ash on expansive soils and found that the addition of class C fly ash led to an increment in the unconfined compression strength (UCS) value of the soil, whereas the pliancy and swelling characteristics diminished. Calderon Vizcarra et al. [21] analysed the utility of MSW incinerator ash on foundation of pavement sand concluded that use of fly

ash enhanced the CBR value and resilient modulus value. Athanasopoulou [22] studied how introduction of fly ash and lime enhanced the highway subgrade soils and came to a conclusion that as we are increasing the lime–fly ash admixture, the pliancy is increasing and the liquid limit is decreasing. Further introduction of ash–lime mixture improved the California bearing ratio value (CBR).

As the composition of raw sewage is different in different places, it is imperative that the properties of the municipal solid waste ash would vary based on the geographic location. As such, the objective of undertaking this research is to understand the efficacy of the MSW ash of the waste-to-energy plant in Ghazipur as a suitable method of soil stabilization. In this study, the variation of unconfined compressive strength is analysed on the addition of different percentages of MSW ash.

2 Materials and Methodology

2.1 Materials

The argillaceous soil sample used in the project was gathered from surrounding area of Chhatarpur, New Delhi, India, and municipal solid waste ash was obtained from Ghazipur waste-to-energy plant, New Delhi, which receives more than 2000 tons of Delhi's municipal solid waste everyday and generates around 12 MW of green power.

2.2 Methodology

In order to find the strength of soil after mixing it with municipal solid waste ash, various experiments were conducted to stabilize it and use it for ground improvement. Initially, characteristics of the soil were determined by conducting experiments like proctor test, sieve analysis, specific gravity, plastic limit and liquid limit tests. The plastic limit and liquid limit were examined in which soil was blended with municipal waste ash at different proportions to observe the variation in consistency of the mix.

In the second stage, UCS values of the stabilized soil were determined by using unconfined compression strength testing machine. Firstly, we calculated the UCS values of the soil and then examine the UCS values of soil blended with certain percentage of MSW ash.

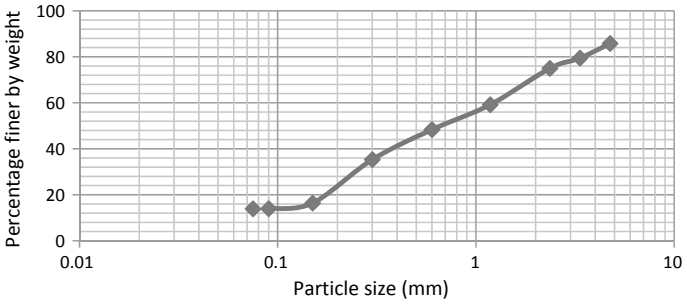

Fig. 1 Gradation curve of soil

3 Results and Discussion

Grain size distribution, specific gravity, plastic limit, liquid limit, maximum dry density, optimum moisture content and unconfined compression strength were founded on the soil sample. The particle sieve distribution curve below shows the grading of soil or the distribution of particles of different sizes (Fig. 1).

From the particle size distribution curve, we obtain the values as D10 = 0.043, D30 = 0.25 and D60 = 1.3. From the above values, we found that the coefficient of curvature equals to 1.18 which indicates that the soil is well graded.

Many index properties of the soil were listed out keeping in mind all the principles laid out by the Indian Standard Code of Practice. After the soil was collected, the moisture content of the soil was calculated by oven-drying method as per IS:2720 (Part 2). The specific gravity of soil was found out using pycnometer method and MSW ash using Le Chatelier's method. The specific gravity of soil blended with MSW ash was also calculated, and it was discovered that the specific gravity decreases as the amount of ash increases. The liquid limit was founded out by Casagrande's method and then simultaneously the plastic limit using IS:2720 (Part 5). It was observed through tests that the liquid limit decreases and plastic limit increases as the percentage of MSW ash increases.

The results of the tests performed are tabulated in the (Table 1):

The proctor compaction test tells about the optimum moisture content and the maximum dry density. It gives the range of moisture that allows minimum compactive effort to obtain better density (Fig. 2).

The unconfined compression strength (UCS) is the maximum axial compressive stress that a material can withstand or simply the strength of the material. It was observed that the unconfined compression strength increases as the percentage of MSW ash increases. The variation in compression strength at different percentages of ash is shown in Table 2 and Fig. 4 (Fig. 3).

Table 1 Index properties

Property	Value
Specific gravity	2.38
Plastic limit	22%
Liquid limit	38%
Plasticity index	16%
IS classification	CL
Optimum moisture content	18.75%
Maximum dry density	1.748 g/cc
Specific gravity of MSW ash	1.728

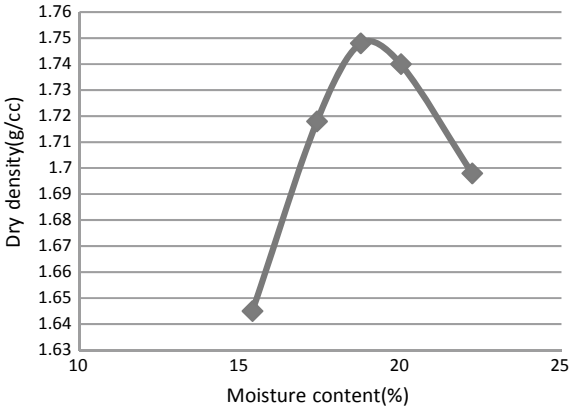

Fig. 2 Compaction curve

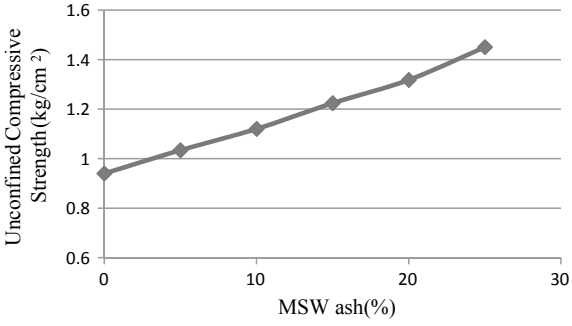

Fig. 3 Variation of compressive strength

Table 2 Unconfined compressive strength values at different percentages of ash

Sample	Unconfined compressive strength (kg/cm^2)
0% ash	0.940
5% ash	1.034
10% ash	1.120
15% ash	1.224
20% ash	1.318
25% ash	1.450

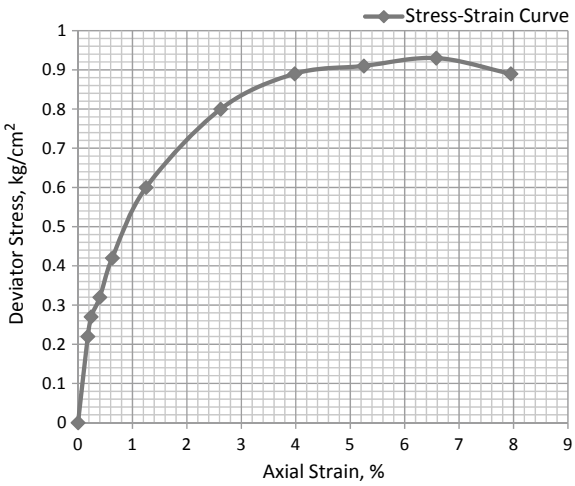

Fig. 4 Stress–strain characteristics of soil at 0% ash

Now, in order to examine the difference in the compressive strength of soil at 0% ash and 25% ash, unconfined compressive test was performed. For UCS test, mould is made in which moisture content is equal to the optimum moisture content of the given sample. With the help of above test, the stress–strain characteristics graph is obtained which helps to determine the variation in failure strain, initial tangent modulus, secant modulus and cohesion intercept. It has been indicated by several researchers earlier that the optimum percentage of ash is 25%, above which the unconfined compression strength of soil decreases. And it is not feasible to use more than 25% of MSW ash as we do not have mass production of ash. Therefore, we have used the percentage of ash up to 25%. The test was carried on the fresh samples of soil without any curing. The test has been performed in accordance with the guidelines of IS:2720 Part-10-(1991), RA-2010. The difference in the results is presented in Table 3 (Table 4 and Fig. 5).

Table 3 Unconfined compression strength of soil

Sample details	
Initial diameter (cm):	3.80
Initial length (cm):	7.60
Bulk density, g/cc	2.05
Dry density, g/cc	1.73
Moisture content, %	18.3
Results	
Unconfined compressive strength, kg/cm^2	0.94
Cohesion intercept, kg/cm^2	0.47
Failure strain, %	6.6

Table 4 Unconfined compression strength of 75% soil and 25% MSW ash

Sample details	
Initial diameter (cm):	3.80
Initial length (cm):	7.60
Bulk density, g/cc	2
Dry density, g/cc	1.68
Moisture content, %	19.1
Results	
Unconfined compressive strength, kg/cm^2	1.45
Cohesion intercept, kg/cm^2	0.73
Failure strain, %	3.9

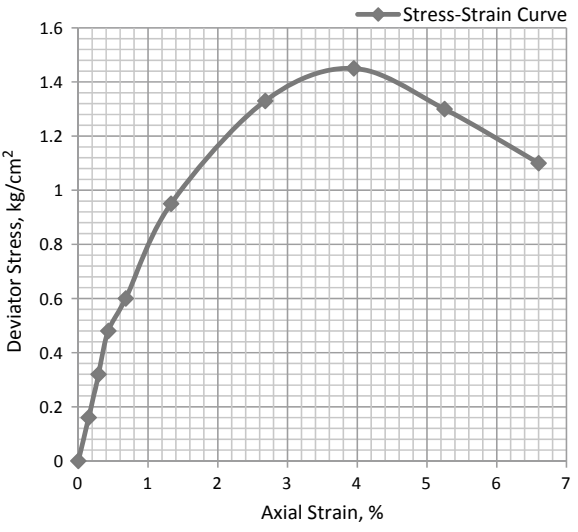

Fig. 5 Stress–strain characteristics at 25% ash

4 Conclusion

The study was successfully completed to examine the unconfined compression strength and other geotechnical properties of soil mixed with MSW ash. The UCS value increased from 0.94 to 1.45 kg/cm^2 by the addition of 25% ash. This is likely due to the pozzolanic reaction of municipal solid waste ash due to its chemical composition and physical characteristics. The use of MSW ash as an admixture in the stabilization of a clay resulted in stabilized samples with an improved strength more than 50% of the untreated clay. Hence, it shows that the quality of soil can be improved by adding ash to it which can further be used as base material for road, structural landfill or embankment construction. The addition of MSW ash has changed the physical and compaction characteristics of the soil. More tests are required to study the chemical composition of the MSW to understand the environmental impact of using an industrial waste.

References

1. Sivapullaiah PV, Prashanth JP, Sridharan A (1996) Effect of fly ash on the index properties of black cotton soil. Soils Found 36:97–103
2. Mirsa A (1998) Stabilization characteristics of clays using class C fly ash. Transp Res Rec 1611:98–1025
3. Temimi M, Rahal MA, Yahiaoui M, Jauberthie R (1998) Recycling of fly ash in the consolidation of clay soils. Resour Conserv Recycl 24(1):1–6
4. Puppala A, Hoyos L, Viyanant C, Musenda C (2001) Fiber and fly ash stabilization methods to treat soft expansive soils. In: Soft ground technology conference, March 2001
5. Çokça E (2001) Use of class C fly ashes for the stabilization of an expansive soil. J Geotech Geoenviron Eng 127(7)
6. Nalbantoglu Z (2004) Effectiveness of class C fly ash as an expansive soil stabilizer. Constr Build Mater 18(6):377–381
7. Prabakara J, Dendorkarb N, Morchhalec RK (2004) Influence of fly ash on strength behavior of typical soils. Constr Build Mater 18:263–267
8. Phani Kumar BR, Sharma RS (2004) Effect of fly ash on engineering properties of expansive soils. J Geotech Geoenviron Eng 1307:764–767
9. Amu O, Fajobi AB, Afekhuai SO (2005) Stabilizing potential of cement and fly ash mixture on expansive clay soil. J App Sci 5. https://doi.org/10.3923/jas.2005.1669.1673
10. Parsons RL, Kneebone E (2005) Field performance of fly ash stabilised subgrades. Ground Improv 9:33–38
11. Misra A, Biswas D, Upadhyaya S (2005) Physico-mechanical behavior of self-cementing class C fly ash–clay mixtures. Fuel 84:1410–1422
12. Kate JM (2005) Strength and volume change behaviour of expansive soils treated with fly ash. In: Geo frontiers 2005, ASCE. Geotechnical Special Publication
13. Edil TB, Acosta HA, Benson CH (2006) Stabilizing soft fine-grained soils with flyash. J Mater Civ Eng 18:283–294
14. Senol A, Edil TB, Acosta HA, Benson CH (2006) Soft subgrades' stabilization by using various fly ashes. Resour Conserv Recycl 46(4):365–376
15. Kumar A, Walia BS, Bajaj A (2007) Influence of fly ash, lime, and polyester fibers on compaction and strength properties of expansive soil. J Mater Civ Eng 19(3)

16. Zha F, Liu S, Du Y, Cui DK (2008) Behavior of expansive soils stabilized with fly ash. Nat Hazards 47:509–523
17. Shafiquea SB, Rahmanb K, Yaykirana M, Azfara I (2010) The long-term performance of two fly ash stabilized fine-grained soil subbases. Resour Conserv Recycl 54:666–672
18. Bose B (2012) Geo engineering properties of expansive soil stabilized with fly ash. Electron J Geotech Eng, Vol. 17, Bund J, pp. 1339–1353
19. Sharma NK, Swain SK, Sahoo UC (2012) Stabilization of a clayey soil with fly ash and lime: a micro level investigation. Geotech Geol Eng 30:1197–1205
20. Lin B, Cerato AB, Madden AS, Elwood Madden ME (2013) Effect of fly ash on the behavior of expansive soils: microscopic analysis. Environ Eng Geosci 19(1):85–94
21. Vizcarra GOC, Casagrande MDT, da Motta LMG (2014) Applicability of municipal solid waste incineration ash on base layers of pavements. J Mater Civ Eng 26(6)
22. Athanasopoulou A (2014) Addition of lime and fly ash to improve highway subgrade soils. J Mater Civ Eng 26:773–775